Wrocław University
of Science and Technology

FIELD OF SCIENCE: Engineering and Technology

DISCIPLINE OF SCIENCE: Environmental Engineering, Mining and Energy

---

DOCTORAL DISSERTATION

Data-Driven Insight into Ball Mill Scaling

Unveiling Differences Across Scales Through Computer Vision, Numerical Simulations, and Design of Experiments

Błażej Doroszuk, B.Eng.

Supervisor:
Prof. Robert Król, PhD, DSc, Eng.

Keywords:
Numerical Modeling, Simulations, DEM, SPH, Computer Vision, DoE, Mineral Processing, Scaling, Ball Mill

WROCŁAW 2024

Abstract

Although ball mills are important elements in the mineral processing industry, optimizing and scaling up their performance remains a challenge. This thesis aims to gain insights into ball mill scale-up by investigating the influence of selected operational parameters on milling performance and energy efficiency across different mill diameters. The research employs advanced modeling techniques, such as the Discrete Element Method (DEM) and Smoothed Particle Hydrodynamics (SPH), coupled with experimental methods and a Design of Experiments (DoE) approach.

This research proposes a systematic methodology for calibrating a digital twin of a laboratory ball mill by integrating DEM-SPH simulations with experimental data from video recordings. The calibrated digital twin is then used in a multivariate analysis of copper ore milling, with a focus on the impact of operational parameters such as mill diameter, filling degree, rotational speed, lifter size, lifter number, and slurry properties on main performance indicators.

A novel scaling constant is also proposed and evaluated as a potential parameter for maintaining similar milling performance across different mill scales. The results indicate that with the scaling constant maintained at a comparable level, the values of energy efficiency metrics in dry and wet milling conditions remain consistent across scales. The same is observed in the case of product size reduction for wet milling.

The main relationships between the studied factors and their effect on mill performance metrics for both dry and wet milling series are investigated with the Design of Experiments (DoE) approach. The DoE results provide information on the parameters which have the greatest impact on ball mill efficiency and product quality. The results of the DoE experiments are also used to identify and quantify correlations between mill diameter, operational parameters, and performance metrics in both dry and wet milling environments with an aim to inform the development of scale-up strategies.

The thesis also includes such recommendations for future research directions as further improvement of the scaling constant approach and potential tests that can be performed on industrial-scale copper ore mills to verify the actual efficiency gains.

The findings of this research can inform the design and operation of ball mills across different scales, ultimately leading to improved productivity, profitability, and environmental sustainability in the mining sector, with specific implications for the Polish copper mining industry.

Preface

This dissertation culminates an intense and rewarding study period in the Doctoral School at Wrocław University of Science and Technology. The journey towards completing this PhD has stimulated my both personal and academic growth. I have been trying to contribute to the body of knowledge in my field through peer-reviewed publications. The research presented in this thesis has been disseminated partially in the following articles:

- Doroszuk B, Król R. The influence of working parameters on ball mill performance and charge behavior. W: Intelligent mining: innovation, vision and value : Proceedings of the 41th International Symposium "Application of Computers and Operations Research in the Mineral Industry" : APCOM 2023, June 25-28, 2023, Rapid City, United States of America. Englewood : Society for Mining, Metallurgy, and Exploration (SME), 2023. s. 352-364.

- Doroszuk B, Bortnowski P, Ozdoba M, Król R. Calibrating the Digital Twin of a Laboratory Ball Mill for Copper Ore Milling: Integrating Computer Vision and Discrete Element Method and Smoothed Particle Hydrodynamics (DEM-SPH) Simulations. Minerals. 2024; 14(4):407. https://doi.org/10.3390/min14040407

- Doroszuk B, Bortnowski P, Ozdoba M, Król R. Scaling Energy Transfer in Ball Mills: A Scale-Agnostic Approach Through a Universal Scaling Constant. Energies. 2024; (under review)

These publications resulted from collaborative efforts with my advisor, Prof. Robert Król, and colleagues at the Department of Mining. I am deeply grateful for their guidance, support, and insights throughout this process.

The co-authors explicitly authorized the inclusion of these articles in this thesis. Each publication contributed significantly to the development of the thesis' overarching research questions and objectives.

At this point I would like to express my gratitude to the above co-authors for their critical and insightful reviews and to other employees of the Department for their support in conducting the experiments. I hope my research results will be a useful resource for future scholars and practitioners in the fields of Mineral Processing and Numerical Modeling.

Funding Statement: Scientific work funded from the state budget for science in the years 2019-2024, as a research project under the "Diamond Grant" (pl. "Diamentowy Grant") program.

Integrating Large Language Models: A Transparency Note

In the composition of this thesis, I have extensively employed Large Language Models (LLMs) and AI-supported tools, including but not limited to OpenAI's GPT, Anthropic's Claude, and Grammarly, which represented the state-of-the-art up to March 2024. My engagement with these tools was grounded in the belief that utilizing AI as an auxiliary instrument, akin to traditional tools enhancing the writing process, aligns with ethical standards. The deployment of such technologies was strictly limited to refining and articulating my original work more effectively, ensuring that the core research remained unequivocally under my direction and execution.

The utility of AI was particularly invaluable in achieving high-quality written English, addressing the challenges posed by my non-native proficiency in the language. This assistance was critical not only for basic grammar and spelling corrections but also for elevating the overall clarity and coherence of the text. Throughout this process, every AI-generated suggestion underwent rigorous review to ensure factual consistency and alignment with the original research notes and outcomes. However, it is imperative to note that the research—laboratory experiments, simulations, and data analysis—was conducted personally without AI intervention.

AI facilitated the careful reorganization of the text and thus has contributed to making the document more accessible and understandable. Moreover, translating extensive research notes, originally in Polish, into articulate English prose was instrumental in preserving the integrity and authenticity of my work.

By integrating AI tools in this manner, I aimed to uphold the highest ethical standards, ensuring that the essence of my research remained untainted by the technological assistance employed. The outcome is a thesis that not only adheres to academic rigors but also exemplifies the potential of AI to augment human capability in research.

Błażej Doroszuk
April, 2024

Contents

List of Figures

List of Tables

Nomenclature

Abbreviations

ANOVA Analysis of Variance

CFD Computational Fluid Dynamics

CoC Center of Circulation

CoG Center of Gravity

COR Coefficient of Restitution

CUDA Compute Unified Device Architecture

CV Coefficient of Variation

DBC Dynamic Boundary Condition

DCDEM Distributed Contact Discrete Element Method

DDT Density Diffusion Term

DEM Discrete Element Method

DoE Design of Experiments

GPU Graphics Processing Unit

GUI Graphical User Interface

LGPL GNU Lesser General Public License

PBM Population Balance Model

RPM Revolutions Per Minute

SAM Segment Anything Model

SPH Smoothed Particle Hydrodynamics

SSE Sum of Squared Errors

SSR Sum of Squared Residuals

Domain-Specific Words

Abrasion Gradual wearing down of particle surfaces due to sliding and rolling motion of the charge

Attrition Form of abrasion that occurs when particles are subjected to compressive forces, leading to chipping and rounding of edges

Autogenous grinding Grinding process where the ore itself acts as the grinding media

Breakage rate The rate at which particles are broken in the mill, typically modeled using a selection function in PBM

Calibration Process of tuning model parameters to match experimental results

Cascading Charge motion where the balls tumble down the free surface of the charge in a cascading pattern

Cataracting Charge motion where the balls are thrown from the shoulder and follow a parabolic trajectory before impacting the toe of the charge

Centrifuging Charge motion where the balls are pinned to the mill shell due to high rotational speed, reducing the effective grinding volume

Charge/Load The mixture of grinding media and material inside the mill

Critical speed The theoretical rotational speed at which the centrifugal force on the outermost balls is equal to the gravitational force, causing them to centrifuge

Digital twin A virtual representation of a physical system that is updated with real-time data

Dry milling Milling process in the absence of water or slurry

Filling degree/level The volume of the mill occupied by the charge, typically expressed as a percentage of the total mill volume

Fractional factorial design A type of experimental design that uses a subset of all possible combinations of factors and levels

Grindability A measure of how easily a material can be ground, typically assessed using standardized tests such as the Bond work index

Grinding efficiency The ratio of the energy used for size reduction to the total energy consumed by the mill

Impact breakage Breakage mechanism where particles are fractured by high-energy impacts with the grinding media or mill shell

Kernel Weighting function in SPH

Kernel support Region where the kernel function is non-zero

Lifter Protrusions on the inside of the mill shell that lift the charge and promote cascading and cataracting motion

Liner Wear-resistant material lining the inside of the mill shell, which protects the shell and promotes the desired charge motion

Rheology The study of the flow and deformation of matter, particularly relevant for the behavior of slurries in wet grinding

Shoulder The highest point reached by the charge before it falls

Slurry A mixture of finely ground solid particles suspended in a liquid, usually water in the context of wet milling

Smoothing kernel Term used synonymously to the kernel function in SPH

Smoothing length Radius of the kernel support

Soft sensor A virtual sensor that estimates a difficult-to-measure variable using other available measurements and a mathematical model

Specific energy The energy consumed per unit mass of the ground material, typically expressed in kWh/t, but here expressed in J/kg

Toe The accumulation point at the bottom of the mill charge where the cascading and cataracting material lands after falling from the shoulder

Tumbling mill A type of mill that uses the tumbling motion of the charge to achieve size reduction; the term here includes ball mills, rod mills, and autogenous mills

Wet milling Milling process in the presence of water or slurry

Chapter 1

Introduction

1.1 Background and Motivation

Ball mills have been used as a an important technology in the mineral processing industry since the mid-19th century. Their development has been motivated by the increasing demand for fine-grinding solutions, especially in the cement, gold, and sulfide mineral industries [107]. During the 20th century, the size and power demand of ball mills increased significantly, owing to advances in mechanical design, materials engineering, and the incorporation of autogenous grinding [107]. Ball mills still remain the most widely used type of fine-grinding equipment, accounting for a significant portion, often over 50%, of the total energy consumed in mineral processing plants [158, 84].

The performance of ball mills is influenced by many factors such as mill dimensions, operating speed, ball size and load, as well as ore properties and slurry density [72]. The optimization of these parameters is required for maximizing throughput and minimizing energy consumption [56]. Computer models and simulations have become important tools enabling a better understanding and the improvement of ball mill performance. They include such techniques as the Population Balance Model (PBM) for simulating the kinetics of the particle size reduction process and the Discrete Element Method (DEM) for detailed analyses of the charge motion, energy utilization, and wear processes inside the mill [12, 30]. Combining these models with in field measurements on the premises of the plant allows the simulation and optimization of full-scale milling circuits [172].

The optimization of the processes observed in the ball mill requires the development of accurate digital twins that integrate advanced numerical models, real-time data acquisition, and flexible simulation environments. Numerical modeling techniques like DEM, PBM, and Computational Fluid Dynamics (CFD) can now predict mill performance with considerable accuracy and provide valuable information on the milling-related processes. [148]. However, process control in mineral processing is hindered by problematic real-time measurements of some important ore properties, and by the complexities involved in the development of accurate fundamental models, especially for grinding [78]. The integration of different simulation and control tools via OPC servers and hardware-in-the-loop architectures provides flexible real-time environments for designing and testing control systems, thus bridging the gap between academic research and industrial practice [69, 105].

Computer vision and advanced simulation techniques, such as coupled DEM-SPH (Smoothed Particle Hydrodynamics) models, seem to be promising solutions enabling the development of digital twins of ball mills. High-speed video combined with image analysis can provide valuable data for validating models and developing advanced control strategies

based on direct visual measurement of the mill charge [88, 6, 141]. DEM-SPH models enable detailed investigations of the complex multi-phase dynamics inside the mill during wet milling, as well as predictions of charge motion, collision energy, product size, and slurry transport [31, 29, 32]. Integrated with data analytics and machine learning, these technologies may allow improved soft-sensors for monitoring key operating parameters and support dynamic optimization of the grinding process [165, 5].

The development of high-fidelity digital twins that would incorporate advanced computer vision and simulation is a promising approach to the optimization of ball mill performance and energy efficiency. However, such tools require further research on precise industrial vision systems, multi-sensor data fusion, and machine learning, as well as the validation of coupled DEM-SPH/CFD models for quantitative industrial applications.

1.2 Research Objectives

The primary goal of this research is to provide additional information on the process of ball mill scale-up (here referred to in terms of both the geometry and the operating parameters of the ball mill). Ball milling is of great significance to the comminution of ores in the mineral processing industry. The efficiency and performance of ball mills directly impact the overall productivity and profitability of mining operations. However, the complexity of the milling process and the challenges of moving from laboratory to industrial scale have long been identified as obstacles to the optimization of ball mill operations [55].

The above challenges are here addressed by developing a systematic methodology for calibrating a digital twin of a laboratory ball mill. This research task involves collecting experimental data from an actual laboratory mill operated under various conditions. The data include mill power draw [86, 149, 8], charge motion and trajectory [86, 109, 76], and product particle size distribution [77, 130, 157]. They may also include mill vibration, acoustic, and thermal signals [164, 10, 119, 54]. A DEM model of the laboratory mill is developed with such software as EDEM or Rocky DEM. Special attention is paid to ensuring that the geometry of the model accurately reflects that of the physical mill [30, 8, 139]. The DEM model parameters is calibrated in iterations to match the experimental data [8, 30], and the calibrated model is validated using additional experimental data [8, 45]. The validated DEM model can be integrated with 3D models of the mill and its elements in order to build a full digital twin of the laboratory mill [133, 168], and to simulate its operation under different conditions and optimize its performance metrics, such as energy efficiency and product size [73, 26].

An important aspect of this research is to integrate computer vision techniques into the processes of calibrating and validating the ball mill digital twin. High-speed video systems are used to record the charge motion inside the lab mill [88, 87], and image processing techniques are applied to extract quantitative information such as the dynamic angle of repose of the charge, enabling the DEM predictions to be validated against the actual mill behavior [6].

The complex multi-phase dynamics inside wet mills are accurately modeled with the use of purpose-developed coupled DEM-SPH models. The DEM component represents the mill grinding media [29, 181], while the SPH component models the slurry phase [31, 29]. The DEM and SPH solvers can be coupled using a bi-directional, in which the fluid exerts drag forces on the particles and the particles appear as a porous media resistant to the fluid [86, 32, 160]. Realistic size distributions and shapes of the grinding media, as well as slurry rheology models, are also incorporated [29], and the coupled model is used to

analyze charge performance metrics and forces acting on the grinding media in order to acquire additional information about mill performance [31, 34, 100, 135].

Another objective of this research is to develop and evaluate a scaling constant as a potential parameter for maintaining similar milling performance across different mill scales. The scaling constant is tested in order to verify whether its consistent level ensures a consistent size reduction degree, similar specific energy (energy per unit mass of ore), and comparable specific energy per rotation. These relationships are investigated in both dry and wet milling conditions.

The calibrated digital twin is applied to perform a multivariate analysis of copper ore milling, and the simulations are used for in-depth analyses of load dynamics and dominant types of forces within the mill. The investigations include the impact of operational parameters such as mill diameter, filling degree, rotational speed, lifter size, lifter numbers, and slurry properties on key performance indicators, including size reduction, energy consumption, and force distribution within the mill.

The development of scale-up strategies is informed by the identified and quantified correlations between mill diameter, operational parameters, and performance metrics in both dry and wet milling environments. Recommendations for future research directions provided in the final chapter include refinements of the scaling constant approach and potential tests that can be performed on industrial-scale copper ore mills to improve their efficiency.

A systematic approach to the above problems is expected to result in a better understanding and an improved optimization of ball milling processes, laying the foundation for energy-efficient and sustainable mineral processing strategies.

1.3 Thesis Structure Overview

1. **Introduction:** The introduction chapter provides an overview of the background, motivation, and objectives for research into ball mill operations in the mineral processing industry. It highlights the importance of ball mills, the challenges related to the optimizing of their performance, and the potential of integrating advanced modeling and simulation techniques. It also outlines the research objectives and the thesis structure.

2. **Literature Review:** This chapter reviews the current state-of-the-art in ball mill grinding, focusing on the evolution of modeling approaches, measurement and monitoring techniques, and emerging tools such as digital twins. It identifies knowledge gaps and defines the research questions to be addressed in the thesis.

3. **Theoretical Background of Numerical Environment:** The theoretical background chapter introduces the main components and methods used for simulating the behavior of charge in dry and wet milling. It presents such solutions as the DualSPHysics code, SPH formulation, and DEM methods for modeling solid-fluid and solid-solid interactions.

4. **Research Goal and Objectives:** The chapter defines the primary research goal, which is to acquire information on the process of laboratory ball mill scale-up. It also describes specific objectives such as to develop a calibration methodology, to define and evaluate the scaling constant, and to perform multivariate analysis using the calibrated digital twin.

5. **Materials and Methods:** This chapter describes the experimental setup, the materials and the methodologies employed in the research process, including the laboratory-scale ball mill, the slurry preparation procedure, and the experimental and simulation techniques used to investigate the process of ball mill scale-up and to develop a scaling constant.

6. **Results:** The results chapter presents key findings of this experimental study into ball mill scale-up, including the results of the calibration process and of test series performed for both dry and wet milling. It also provides an analysis of the experiments and their results, as well as statistical tests aimed at verifying the working hypotheses behind the proposed scaling process, and correlations across mill scales.

7. **Conclusions and Implications:** The final chapter offers an interpretation of the experiment results and an evaluation of the effectiveness of the developed scaling constant. It discusses the implications of the research results for ball mill optimization and scaling. It also provides recommendations for future research directions and potential applications of the methodology in other industries.

Chapter 2

Literature Review

Ball mills are extensively used in the mineral processing industry for reducing the size of ore particles and thus for facilitating the liberation and recovery of valuable minerals [70, 158]. Efficiently operating ball mills allow minimum energy consumption, maximum throughput, and desired product size distributions [45]. However, complex relationships between various design and operating parameters, such as mill geometry, speed, filling degree, media size, and slurry properties, cause the optimization of ball mill performance to be a difficult task [72, 162].

In traditional approaches, ball mill design and operation rely on empirical models and operator experience. Although they are effective in many cases, such approaches have a limited ability to adapt to changes in ore characteristics, identify optimal operating points, and predict the effects of design changes [45]. Over recent decades, much progress has been observed in the analyses of the basics of grinding mechanisms, the development of physics-based models, and the application of advanced measurement and control techniques to ball mills [29, 172, 168].

This literature review of the current state-of-the-art in ball mill grinding focuses particularly on the integration of advanced modeling, simulation, and measurement techniques for process optimization. The review begins with a discussion of the fundamental principles of ball mill operation and the influence of key operating parameters on grinding performance. It subsequently examines the evolution of modeling approaches, from early empirical models to modern DEM simulations coupled with PBM and SPH. The applications of these models for process understanding, scale-up, and optimization purposes are highlighted, along with current limitations and research gaps.

The review also discusses ball mill measurement and monitoring techniques, ranging from conventional methods based on power draw and product size analysis to advanced sensor-based methods employing vibration, acoustics, and vision. It investigates the potential application of data-driven models and soft-sensors (virtual sensors) in real-time optimization and control. It concludes with the exploration of emerging tools and future directions in ball mill research, including the development of digital twins, the integration of modeling and measurement, and the remaining significant challenges and opportunities in this research area.

By identifying the critical knowledge gaps in the area, this literature review is expected to allow the definition of the research question addressed in the subsequent chapters and to inform the development of integrated modeling, simulation, and measurement frameworks that can be used to optimize the design and operation of ball mills, improving energy efficiency, product quality, and process sustainability in the mineral processing industry.

2.1 Fundamentals of Ball Mill Grinding

Ball mills are extensively used in the mineral processing industry as tools for reducing the size of ore particles and liberating valuable minerals. Their performance is influenced by various design and operating parameters, e.g. by mill geometry, rotational speed, filling degree, ball size distribution, and slurry properties.

This section reviews the main components of a ball mill, the different grinding mechanisms and breakage modes, and the influence of the operational parameters on mill performance. They all have an important role in developing accurate models, optimizing mill operation, and improving the energy efficiency of the grinding process.

2.1.1 Operating Principles and Key Components

Ball mills (Figure 2.1) are cylindrical vessels that rotate around a horizontal axis and that are partially filled with grinding media (typically steel balls) and the material to be ground (the charge) [70, 158]. The basic principle of operation involves the transfer of kinetic energy from the moving balls to the ore particles, causing size reduction through impact, abrasion, and attrition [147]. As the mill rotates, the charge is lifted along the rising side of the shell until the dynamic angle of repose is reached, at which point the balls fall in a cascade or in a cataract, impacting the toe of the charge [70].

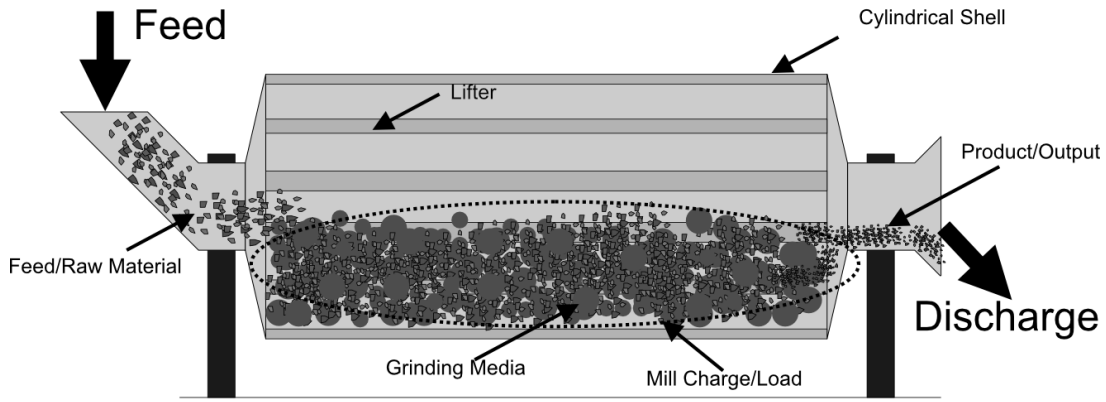

Figure 2.1: Simplified schematic diagram of a ball mill, with indicated main components

The main components of the ball mill include a cylindrical shell, grinding media, liners/lifters, as well as feed and discharge systems [70, 158]. The shell is typically made of steel and lined with wear-resistant materials such as manganese steel, rubber, or ceramic [70, 107]. The grinding media are usually steel balls, whose sizes range from 10 to 150 mm depending on the application [70]. The mill is driven by a motor, either through a girth gear or a wrap-around drive system [15, 107].

The feed material is introduced into the mill via a feed chute or conveyor (not shown in the figure), while the ground product is discharged through a grate or overflow system [70, 158]. The discharge grate (not shown) controls the maximum size of the particles that can leave the mill, while the overflow system (also not shown) allows finer particles to exit with the slurry [158]. The internal dynamics of the charge, influenced by the mill speed, filling level, and liner design, have a significant impact on the grinding efficiency and size distribution of the product [147, 158].

2.1.2 Grinding Mechanisms and Breakage Modes

The size reduction of ore particles in a ball mill is due to a combination of different grinding mechanisms and breakage modes, depending on the particle size, material properties, and the intensity of the stress events [172]. The main grinding mechanisms include impact, attrition, and abrasion (Figure 2.2) [30, 42].

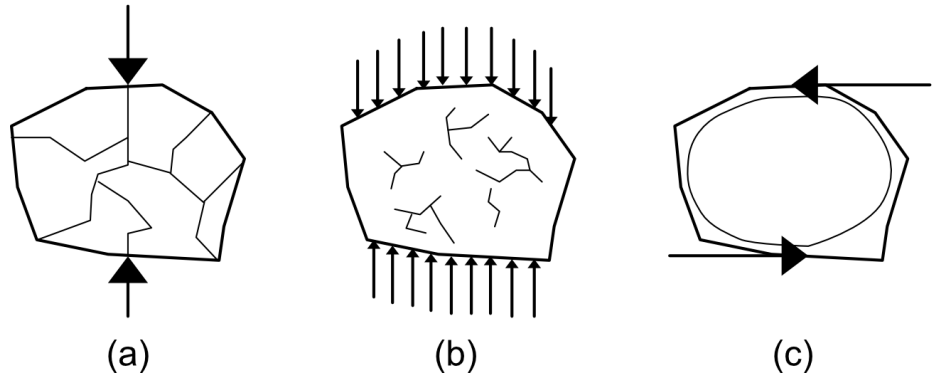

Figure 2.2: Particle breakage mechanisms; (a) impact breakage; (b) attrition; (c) abrasion

Impact breakage is the result of the grinding media or ore particles colliding with each other or with the mill shell at high velocities. In effect, particles rapidly fracture into daughter fragments having a wide range of sizes [30, 42]. This mechanism dominates in the case of coarser particles and higher mill speeds, as the kinetic energy of the impacts is sufficient to cause fracture [126].

Abrasion, on the other hand, results from the gradual wearing of particle surfaces due to the sliding and rolling motion of the charge [30, 42]. This mechanism is more prevalent for finer particles and at lower mill speeds, in which cases the stresses are insufficient to cause fracture but may lead to the generation of fine particles through surface wear [126].

Attrition is a form of abrasion that occurs when particles are subjected to compressive forces between the grinding media, causing the chipping and rounding of particle edges and corners [36]. This mechanism is important for the generation of very fine particles and the changes in particle shape during grinding [36].

The overall grinding behavior is also influenced by such factors as the accumulation of fatigue damage due to repeated low-intensity impacts and the preferential breakage of weaker particles [49, 172]. The relative importance of each of the above mechanisms depends on the specific operating conditions and ore characteristics, and can change during the grinding process as the particle size distribution changes [172].

The following sections explore how these mechanisms are influenced by various design and operating parameters, and how these can be manipulated to improve grinding efficiency and product quality.

2.1.3 Influence of Operational Parameters

The performance of a ball mill is highly dependent on a range of operational parameters that influence the grinding mechanisms and breakage rates. As already mentioned and discussed in detail below, these parameters include the mill rotational speed, filling degree (charge volume), ball size distribution, and slurry properties, among others. The

optimization of these parameters is crucial for achieving expected grinding efficiencies and desired product size distributions while minimizing energy consumption. In this section, we will discuss the effects of each key parameter on mill performance.

Rotational Speed

The rotational speed of a ball mill is a has a significant impact on the motion of the charge and on the energy input to the grinding process. As the mill speed increases, the charge transitions from a sliding to a cascading and then to a cataracting motion [70]. The optimal speed for grinding is typically between 65-80% of the critical speed, which is the theoretical speed at which the charge would centrifuge against the mill shell [158, 194].

At lower speeds, the grinding efficiency is reduced due to the absence of impact forces and the predominance of abrasion and attrition mechanisms [61, 162]. As the speed increases, the charge motion becomes more violent, with higher impact energies leading to improved grinding rates [26, 24]. However, beyond a certain speed, the efficiency decreases again as the charge begins to centrifuge, reducing the effective grinding volume and increasing the energy consumption [61, 194].

The mill power draw is also significantly influenced by the rotational speed, with higher speeds leading to increased energy consumption until critical speed is reached [26, 187]. The speed for optimal energy efficiency is often similar to that for optimal grinding efficiency, as the increased energy input is balanced with the improved breakage rates [26, 158].

Filling Degree

The filling degree, or charge volume, refers to the amount of grinding media and ore material inside the mill. The ball filling is typically in the range of 30-50% of the mill volume, while the ore filling (powder filling) degree is usually lower, around 15-30% [158, 26]. Higher filling degrees lead to increased power draw due to the greater mass of the charge, but also improve the grinding efficiency to a certain point [26, 70].

As the degree of the ball filling increases, the number of contact points between the balls and ore particles increases, leading to higher breakage rates [100]. However, beyond a critical filling degree, the motion of the charge becomes restricted, reducing the impact forces and leading to a decrease in grinding efficiency [100]. Similarly, increasing the ore volume can improve the throughput and energy efficiency, but excessive filling degree can lead to cushioning effects and reduced breakage rates [26].

The filling degree can be optimized by finding a balance between maximum grinding efficiency and minimum energy consumption. This optimal point depends on factors such as the mill dimensions, rotational speed and ore properties, and can be determined from experiments or models [26, 100].

Ball Size Distribution

The size distribution of the grinding media significantly influences grinding efficiency and product size distribution. Large-size balls are more effective for breaking coarser particles, while small-size balls are more optimal for producing finer particles [159, 132]. The optimal ball size distribution depends on the feed size distribution and the desired product size [26].

In practice, a mixture of ball sizes is often used to achieve a balance between coarse and fine grinding [20, 194]. Ball size distribution can be optimized to maximize the grinding efficiency and minimize the energy consumption, by adjusting such factors as mill dimensions, rotational speed, and ore properties [137, 77].

The breakage rates and energy utilization of the mill are also influenced by the ball size distribution. Larger balls have higher impact energies but lower surface areas, while smaller balls have lower impact energies but higher surface areas [30]. The optimal distribution balances these factors to achieve a desired breakage rate and energy efficiency [72].

Slurry Properties

In wet grinding, the properties of the slurry, such as the solids concentration and viscosity, have a significant impact on the grinding performance. As the slurry density increases, The viscosity increases as a result of an increase in the slurry density and produces a dampening effect on the charge motion, causing a reduction in the impact forces [162, 159]. As a result, the grinding efficiency may decrease and the energy consumption may increase [187].

The slurry also influences the transport of broken particles out of the mill, with higher densities and viscosities leading to reduced classification efficiency and increased overgrinding [59]. The optimal slurry density should be adjusted to such factors as ore properties, mill dimensions, and desired product size distribution [132, 187].

Modeling approaches, such as DEM coupled with SPH or CFD have been used to study the influence of slurry properties on the charge motion and grinding performance [29, 32]. These models can aid both the optimization of slurry properties for specific applications and the design of efficient wet grinding systems.

2.1.4 Charge Dynamics and Slurry Impact

This subsection explores the most common types of charge motion, as well as methods for measuring and quantifying these types of motion. It additionally examines the impact of slurry on charge dynamics and concludes with a discussion on the implications of this information for mill design and optimization.

Charge Motion in Ball Mills

The grinding efficiency and energy utilization of a ball mill is influenced by the type of charge motion. The main such types depend on the rotational speed of the mill [115, 158, 146] and include sliding, cascading, cataracting, and centrifuging (Figure 2.3).

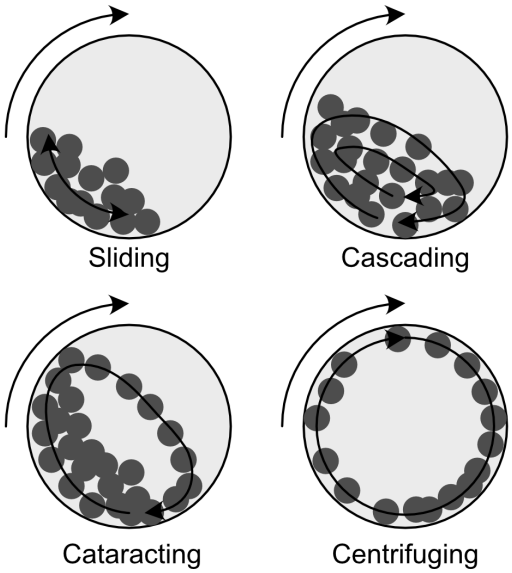

Figure 2.3: Charge motion types

Sliding occurs at low rotational speeds, at which the charge tends to slide downwards to the toe of the mill, and as a result it is subjected to primarily abrasive grinding [115]. As the rotational speed increases, the charge motion changes its type to cascading (also called rolling or tumbling), characterized by a continuous circulation of the charge with particles rolling downwards the free surface of the charge. This motion produces a combination of abrasion, attrition, and some impact breakage [115, 158, 146].

At higher rotational speeds, cataracting becomes the dominant type of motion, with particles being thrown in parabolic trajectories, away from the charge and into the free space above it. They then fall on the toe of the charge or mill shell, and thus cataracting leads to higher-energy impact breakage [115, 158, 146, 28]. However, at very high rotational speeds approaching the critical speed, particles cling to the mill shell and start to centrifuge (Figure 2.4). As a result, the grinding action is reduced [115, 158, 108].

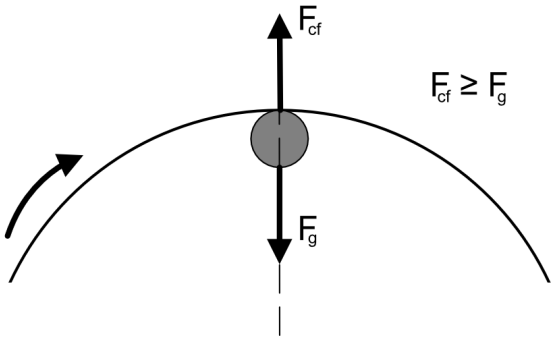

Figure 2.4: Forces acting on the ball during centrifuging at highest point inside the mill

The desired grinding action in ball mills is usually a combination of the cascading and cataracting types of motion which allow a balance of abrasion and impact breakage while preventing the inefficient centrifuging of the charge [158, 141]. The charge motion regime is influenced by such mill operating parameters as rotational speed, ball characteristics, and lifter design [8, 137].

The charge motion regime also influences the energy utilization in the mill. DEM simulations demonstrate that an increase in speed causes the part of energy dissipated by cataracting collisions to increase at the expense of the energy dissipated in the grinding zone by abrasion [34]. Cataracting collisions are associated with higher peak energies that promote impact breakage of coarser particles, while the shearing action in the cascading charge produces finer particles by attrition [30]. However, very high speeds lead to inefficient energy utilization, as a significant portion of the energy is wasted in cataracting impacts on the liners rather than used in grinding [146]. At an optimum speed, typically 70-80% of the critical speed, the grinding action can be maximized while avoiding excessive cataracting [158].

Charge Motion Analysis Techniques

Analyzing the charge motion in ball mills is important for the understanding and optimization of the grinding process. Some of the techniques for characterizing the behavior of the charge employ the center of gravity, center of circulation, toe and shoulder positions (Figure 2.5), and various experimental methods.

The center of gravity is a point that describes the circulation of the charge within a ball mill. It represents the effective mass of the entire charge reduced to a single point [8]. The center of gravity is an important descriptor of charge motion. Others include the head, shoulder, toe, and equilibrium surface [8]. While simplified models based on the moment of the center of gravity provide estimates of mill power, more advanced modeling is required to represent completely complex types of charge motion and their influence on mill performance.

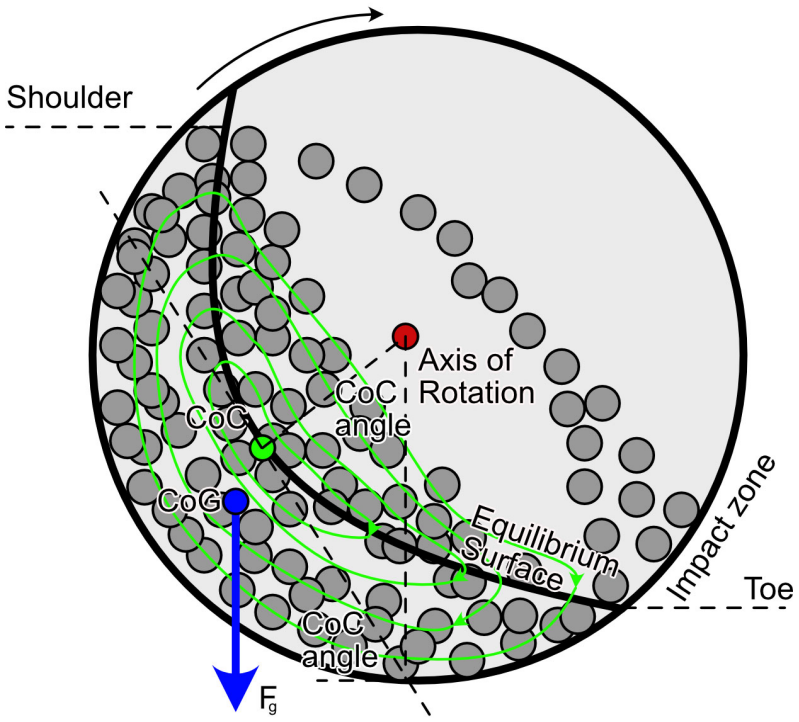

Figure 2.5: Characterization of mill charge dynamics; CoC – center of circulation; CoG – center of gravity

The center of circulation is another important descriptor, representing the rotational center about which the ascending and descending charge circulates [8]. It is located along the equilibrium surface, which differentiates the ascending en-masse charge from the descending charge [8]. The position of the center of circulation depends on the operating conditions of the mill and is directly related to the lifting and cascading action that enables the grinding of the ore.

The toe and shoulder positions are also important indicators of the charge shape and depend on the operating conditions and on the liner wear [140, 21]. The toe is the accumulation point at the bottom of the mill charge where the cascading and cataracting material lands after falling from the shoulder [63]. The shoulder, on the other hand, is the highest point reached by the charge before it falls [8]. The toe and shoulder positions recorded over time can provide information on the overall charge motion and grinding efficiency.

Various experimental techniques have been employed to measure and analyze charge motion in ball mills. High-speed video imaging is occasionally used in laboratory-scale tests, in which the motion of the charge inside the mill is observed through a transparent end wall or faceplate [76, 88]. Sensor-based methods, such as instrumented balls equipped with accelerometers and gyroscopes, can measure physical quantities like acceleration, impact forces, and rotational kinetic energy within the mill [112, 187]. Accelerometers mounted on the mill shell or on the bearing housings can also provide information about the charge motion by measuring the vibration response of the mill [10, 43, 119, 81].

Other experimental techniques include Positron Emission Particle Tracking (PEPT), which uses a radioactive tracer particle to track the charge motion [8, 128, 9], and laser profiling, which uses a laser distance meter to generate a point cloud of the charge surface [44]. These experimental methods are often used in conjunction with DEM simulations in order to gather more comprehensive information on the dynamics of the charge and to validate numerical models.

Impact of Slurry on Charge Dynamics

In wet grinding, the presence of slurry significantly influences charge motion and grinding performance in ball mills. The properties of slurry that most significantly affect charge dynamics include density and viscosity, which both depend on solids concentration.

Slurry density has a great influence on charge motion and energy dissipation. An increase in slurry density results in higher viscosity and packing density of the mill contents, and in considerably smaller impact forces [162]. Higher slurry density also increases the resistance to motion of the slurry [171]. As slurry viscosity increases, it acts as a damper, providing resistance to the ball motion and decreasing impact forces [162]. Higher viscosity slurries tend to cause charge particles to move along fluid streamlines rather than inertial trajectories [117].

Slurry pooling and rheology also have significant effects on the charge motion and grinding efficiency. As the slurry filling volume increases, a slurry pool forms inside the mill, exerting buoyancy forces on the charge and increasing the toe angle while decreasing impact forces [162, 132]. The slurry pool can decrease the speed of the cataracting particles and dampen their impacts in the toe region [43, 29]. The rheological properties of the slurry, such as its Newtonian or non-Newtonian behavior, influence the slippage between layers of charge particles and the resulting slurry shoulder position [147]. Higher viscosity increases the resistance to charge motion, lowering the slurry shoulder and limiting the cataracting effect [171, 117].

Wet grinding differs from dry grinding in several aspects due to the presence of slurry. Wet-ground particles tend to have more irregular shapes and smoother surfaces compared to dry-ground particles [17]. The slurry acts as a cushion, absorbing impact energy and reducing breakage rates, especially at higher solids concentrations [162, 43]. Wet grinding facilitates abrasion and attrition with lower impact energies, while dry grinding involves higher impact energies and facilitates the crushing of particles [136].

Understanding the complex interactions between slurry properties, charge motion, and breakage mechanisms is important for optimizing wet grinding efficiency. Advanced models like coupled DEM-SPH/CFD can aid in the analysis of these interactions and provide valuable information on the slurry flow patterns, energy dissipation, and particle breakage in wet grinding mills [117, 29, 32].

Implications for Mill Design and Optimization

Precise information on charge dynamics and slurry impact has a significant role in the design and optimization of ball mills. A holistic approach that integrates charge motion, slurry dynamics, and equipment design is necessary to improve grinding efficiency and energy utilization in wet milling operations.

Lifter design is an important aspect of mill optimization, as it influences charge trajectory, slurry transport, and energy transfer to the charge [110, 11]. The lifter face angle, height, and number of lifters can be optimized in simulations and experiments to enhance the milling performance [149]. The lifter design should ensure a good balance between the cascading and the cataracting motion while limiting the occurrence of centrifuging.

Mill speed is another parameter that controls charge dynamics, slurry flow, and energy consumption [26]. Within a certain optimal speed range, the breakage rate can be maximized and the energy waste due to cataracting and slurry pooling can be minimized. This optimal speed can be determined in a combination of simulations and plant experiments. In order to maintain efficient grinding, the mill speed should be adjusted to the particular ore properties, ball size distributions, and desired product sizes.

Ball size distribution and feed size distribution are also of considerable importance to the charge packing, segregation, and breakage rates within the mill [71]. In scale-up and optimization studies, a more realistic simulation is obtained with the use of a mix of ball sizes rather than with mono-size charges. The ball size distribution should be adjusted to the feed size distribution and the desired product size in order to ensure efficient energy transfer and breakage.

Coupled DEM models have emerged as powerful tools for representing the complex interactions between the slurry, the charge, and the mill structure in a computationally efficient manner [87]. These models can accurately predict the mill dynamics, allowing for slurry rheology and drag effects, and help optimize grinding operations in order to minimize energy consumption, maximize throughput, and achieve desired product characteristics [117].

Information on charge motion and slurry behavior allow advanced process control strategies and improved mill automation systems. Such information may include data provided by sensors on mill load, charge position, or slurry properties [171]. It may be also based on interpretations of vibration signatures from the mill, which can be used to predict charge dynamics and identify the state of grinding [10]. However, as such signals are significantly affected by wear processes of both the balls and the liner, their condition should be subjected to real-time, online monitoring and diagnostics [73].

The oscillatory movement of the central part of the mill charge against the shell occurs at certain filling degrees and speed values. Its proper control may cause an increase in mill efficiency by 6-8% and a decrease in energy consumption by 8-10% [73]. Such an optimal regime translates into both improved grinding performance and energy efficiency gains.

2.2 Modeling and Simulation of Ball Mills

Modeling and simulation techniques have become increasingly important tools used in the analyses predictions and optimization of ball mill performance. They may be both empirical models based on experimental data or advanced physics-based models that represent the complex interactions between the grinding media, ore particles, and slurry.

This section provides an overview of the different modeling approaches used for ball mills, with a particular focus on the Discrete Element Method (DEM) as coupled with Population Balance Models (PBMs) and Smoothed Particle Hydrodynamics (SPH). It also includes a discussion of the applications of these models in ball mill analyses, scale-up, and optimization. It also indicates the current limitations and research gaps observed in such approaches.

2.2.1 Overview of Modeling Approaches

The complex nature of the ball-mill grinding process, which involves the interaction of multiple phases (grinding media, ore particles, and slurry) and various physical phenomena (impact, abrasion, attrition, and transport), has led to the development of a wide range of modeling approaches. These approaches can be broadly classified into three categories: empirical models, Population Balance Models (PBMs), and Discrete Element Method (DEM) models [45].

Empirical models, such as the Bond work index and the Hardgrove grindability index, have been extensively used in the mineral processing industry for decades [45]. They rely on experimental data and statistical correlations to predict the energy consumption and product size distribution for a ball mill based on a limited number of input parameters [65]. Although empirical models are not complicated and can provide relatively accurate estimates for well-known ore types and mill designs, they demonstrate limited predictive capability when extrapolating to new conditions or optimizing mill performance [45].

Population Balance Models (PBMs) represent a more advanced approach that addresses the evolution of the particle size distribution in the mill as a result of breakage and transport processes [45]. PBMs are based on a set of differential equations that describe the rates of particle breakage and the distribution of daughter fragments, as well as the flow of particles into and out of the mill [45]. The parameters of the model, such as the breakage rate and breakage distribution functions, are typically estimated from experimental data or back-calculated from on-site measurements [45, 46]. PBMs have been successfully applied to predict the performance of industrial ball mills and optimize their operating conditions [45, 59]. However, they still require empirical relationships for calculating the breakage rates and do not provide detailed information on the internal dynamics of the mill [45].

DEM models represent the most advanced and fundamental approach to ball mill modeling [45]. DEM simulations produce reliable models the motion of and interactions between individual grinding media and ore particles, based on Newton's laws of motion

and the principles of contact mechanics [181, 172]. By precisely representing charge dynamics and energy distribution in the mill, DEM models provide information on the influence of various design and operating parameters on the grinding performance [45]. When coupled with PBMs and particle breakage models, DEM simulations can predict the product size distribution and the energy consumption of a ball mill based on equations offered in publications [45, 172]. However, DEM models are computationally intensive and require careful the calibration and validation process to be based on experimental data [181].

The following subsections focus in more detail on the formulation of DEM models and their application in ball mill simulations, as well as on their coupling with other methods such as PBMs and smoothed particle hydrodynamics (SPH) for modeling multi-phase flows.

2.2.2 Discrete Element Method (DEM)

The discrete element method (DEM) is used for numerical simulations of the motion and interactions of a large number of discrete particles, such as the grinding media and ore particles in a ball mill. DEM models are based on the integration of Newton's equations of motion for each particle, and they allow for the forces and torques arising from particle-particle and particle-geometry contacts [181].

In a typical DEM ball mill model, the grinding media (balls) and ore particles are represented as spherical or multi-spherical particles with specified sizes, densities, and mechanical properties (e.g., stiffness, damping, and friction coefficients) [172]. The mill geometry, including the shell and liners, is modeled as a set of fixed or moving walls with appropriate contact parameters [181]. The simulation proceeds by calculating the contact forces and torques acting on each particle at each time step. The calculations are based on the relative positions and velocities of the contacting particles and walls [181]. The resulting accelerations are then integrated to update the particle positions and velocities for the next time step [181].

DEM simulations can provide detailed information that would be otherwise difficult to measure experimentally, for example information on the charge motion, energy distribution, and particle interactions inside the mill [172]. Analyses of the collision forces, energy spectra, and particle trajectories, allow researchers to learn about the main grinding mechanisms (impact, abrasion, or attrition) and their dependence on the operating conditions of the mill [30, 49]. DEM models can also be used to study the influence of design parameters, such as the mill diameter, aspect ratio, and liner profile, on the charge dynamics and grinding performance [11, 140].

However, DEM simulations of ball mills are computationally intensive, particularly in the case of models which represent fine particles and long grinding times [181]. This problem has been addressed by employing various strategies, such as coarse-graining (representing a group of particles with the use of a single larger particle), periodic boundary conditions (simulating a slice of the mill), and parallel computing [181]. The fact that the accuracy of DEM models depends on the proper calibration of the contact parameters and on the validation against experimental data represents and additional constraint [172].

2.2.3 Coupling DEM with Population Balance Models (PBMs)

Although DEM simulations provide detailed information on the charge motion and energy distribution in a ball mill, they do not directly predict the evolution of the particle size distribution or the product throughput. Solving this problem requires DEM models to be coupled with population balance models (PBMs) that describe the breakage and transport of ore particles in the mill [45, 172].

In a coupled DEM-PBM approach, the DEM simulation is used to calculate the collision energies and frequencies between the grinding media and ore particles, which are then fed into the PBM as input parameters [45]. The PBM consists of a set of size-discretized mass balance equations that account for the rates of particle breakage, the distribution of children fragments, and the flow of particles into and out of the mill [45]. The breakage rates and distribution functions in the PBM are typically calibrated using laboratory-scale batch grinding tests or data collected on-site [45, 46].

By iteratively solving the DEM and PBM equations, the coupled model can predict the evolution of the particle size distribution over time, as well as the product throughput and energy consumption of the mill [172]. The DEM-PBM approach has been successfully applied in simulations of industrial ball mills and in efforts at optimizing their operating conditions, such as the ball size distribution, mill speed, and filling degree [45, 152].

However, the accuracy of DEM-PBM models depends on the quality of the breakage data used for calibrating the PBM and on the ability of the DEM model to simulate the relevant contact forces and energy spectra [172]. Additionally, the computational cost of the coupled model can be very high, particularly in the case when simulations involve fine particles and complex mill geometries [181].

2.2.4 SPH for Modeling Slurry Flow

In wet grinding, the presence of a slurry phase in the ball mill can significantly influence the charge dynamics and grinding performance. The slurry influences the viscous damping of the particle motions, the formation of a pool in the toe region of the mill, and the transport of fine particles out of the mill [29]. Cleary et al. also propose a method for accurately modeling these effects by coupling DEM models with Smoothed Particle Hydrodynamics (SPH) methods in order to simulate the slurry flow [29, 32].

SPH is a meshless Lagrangian method that represents the slurry as a set of discrete particles, each carrying local properties such as density, viscosity, and pressure [29]. The motion of the SPH particles is accounted for by the Navier-Stokes equations, which are solved using a kernel interpolation technique which smooths the properties over a local region around each particle [29]. The coupling between the DEM and SPH models is possible owing to exchange of momentum and forces at the particle-fluid interfaces [29].

DEM-SPH models have been used to study the influence of slurry properties, such as the solids concentration and rheology, on the charge motion and grinding efficiency of ball mills [29, 32]. The simulations discussed in these publications have revealed that a slurry pool may form in the toe region of the mill, and that this pool can significantly dampen the impact forces and reduce the breakage rates [29]. The models have also shown how the slurry viscosity affects the transport of fine particles out of the mill, and how higher viscosities may lead to reduced classification efficiency and increased overgrinding [32].

Despite their potential, DEM-SPH models of ball mills still face several challenges and require further development [32]. The problems to be solved include the high computational cost of simulating large numbers of SPH particles, the difficulty in accurately

modeling the complex rheology of the slurry, and the need for experimental validation of the coupled model predictions [32]. As research in this area continues, DEM-SPH models are expected to gain importance as tools for optimizing the design and operation of wet grinding systems.

2.2.5 Applications of Models for Process Understanding, Scale-up, and Optimization

New advanced modeling and simulation techniques, e.g. DEM, PBMs, and SPH, provide detailed data on the complex interactions between the grinding media, ore particles, and slurry. As such they enable new perspectives for research into ball mills, their scale-up and optimization and allow designs of more efficient and sustainable grinding systems [45, 172].

One of the primary purposes of ball mill models is to facilitate the transition from laboratory or pilot-scale tests to full-scale industrial mills [71]. DEM simulations allow analyses not only of the charge motion and energy distribution in mills of different sizes, but also of scaling relationships based on such dimensionless parameters as the Froude number and the charge-to-ball mass ratio [85, 100]. PBMs, on the other hand, can be calibrated in laboratory breakage tests and then used in predictions of the product size distribution and energy consumption for industry-scale mills [45]. Combined DEM and PBM models may provide complex scale-up methodologies that allow for the influence of mill design, operating conditions, and ore properties on the grinding performance [45, 71].

Another important application of ball mill models is in the optimization of mill operating conditions for specific ore types and product requirements [45]. DEM simulations can be used to study the influence of such parameters as the ball size distribution, mill speed, and filling level on the charge dynamics and grinding efficiency [11, 140]. On the other hand, PBMs can be used to predict the effect of these parameters on the product size distribution and energy consumption, and to identify optimal operating parameters that balance throughput, energy efficiency, and product quality [45, 59]. PBM, when coupled with DEM-SPH models can be thus used to optimize the slurry properties, such as the solids concentration and viscosity, for improved grinding performance and reduced overgrinding [29, 32].

In addition to aiding research efforts at scale-up and optimization, ball mill models can be used to provide important information on the grinding mechanisms and their impact on the mill design and operating conditions [172]. DEM simulations can also provide details on the collision forces, energy spectra, and particle breakage events inside the mill. Such details can be used to identify the main grinding mechanisms (impact, abrasion, or attrition) and their relative contributions to the overall size reduction [30, 49]. PBMs may be employed as tools in studies of the influence of particle size, shape, and mechanical properties on the breakage rates and distribution functions, as well as in the development of more accurate and predictive breakage models [45, 172]. DEM-SPH models can serve as a source of data on the complex interactions between the grinding media, ore particles, and slurry, as well as on their effect on the charge dynamics and grinding efficiency [29, 32].

2.2.6 Scaling Strategies and Problems

The scale of ball mill designs can be currently increased from laboratory or pilot scale to full industrial scale by following several approaches. One of them is to employ population

balance models (PBMs) for predicting the performance of full-scale mills on the basis of correlations describing the breakage rate and breakage distribution parameters as a function of such variables as mill diameter, ball size, ball load, particle load, and mill speed [71]. However, although most existing PBM scale-up correlations were defined on the basis of mono-size ball charges and narrow feed size distributions, the size distributions of both the grinding media and feed material used industrial mills are typically much broader [71].

Industrial mills are also sized with the use of the empirical energy-size reduction relationships, e.g. the Bond work index method. In such methods, power requirements are estimated from a single-size marker (e.g. 80% passing size) and from specific energy consumption [46]. However, they do not allow for such important factors as circulating load, classifier efficiency, ball size distribution, and slurry rheology [46].

Mechanistic DEM-based models of charge motion are the principle behind a new approach to mill scale-up. They allow for the main design and operating variables like mill speed, ball size, mill filling, and liner design [181]. The data produced by the DEM-based models are then fed into Population Balance Models in order to allow predictions of product size distributions in full-scale mills [181, 45].

The geometric, kinematic, and dynamic similarity in mill scale-up processes can also be maintained by employing dimensional analysis and similarity principles. For example, although mill diameter, length, and ball size are typically scaled proportionally to each other, mill speed is reduced in proportion to the inverse square root of the diameter, so that the percentage proportion of critical speed can be maintained [107]. Such approaches are typically based on an assumption that the power draw is scaled together with the mill volume.

However, the above approaches do not offer a complete solution to the mill scale-up problems. One reason for such a situation may be that some assumptions used in many ball mill models, such as perfect mixing of grinding media and particles, may not always be valid, especially at high mill frequencies and large ball-to-particle size ratios [152]. As a result, the model predictions may show inaccuracies.

Another significant problem results from linear wear, which is in particular due to impacts from non-spherical ore particles. The predicting and mitigating of liner wear requires complex modeling of particle motions and collisions with the use of such methods as DEM [186]. However, accurate predictions of the liner wear profile in large industrial mills are computationally intensive and require a number of DEM simulations. Machine learning models trained on DEM data may reduce this computational cost, but still need to be validated with the use of full-scale simulations [83].

The characterizing of breakage behavior is also more complicated in the case of irregularly shaped particles than in the case of spherical particles. Its analysis requires multi-layer particle breakage experiments and models [188]. The optimization of the grinding media (ball size distribution, material, etc.) depends on a balance between energy efficiency, product size, and mill capacity, and therefore detailed experiments and models are required in order to identify an optimal configuration for a particular application [190, 129].

Complex scaling constants may solve some of these problems and result in improvements to the accuracy of mill scale-up predictions. Well-formulated scaling constants and detailed experimental models allowing for such main factors as charge motion, liner design, and feed properties may be offered as an aid in integrating contradictory scaling laws. They may also account for scale-dependent mechanisms and improve the accuracy

and confidence of performance predictions for industrial mills [68, 130]. As a result, mill design and mill operating parameters can be optimized with limited dependence on empirical factors. However, detailed sampling surveys and model calibration on industrial mills are still often required for fine-tuning the scale-up factors and improving the accuracy of model predictions [157].

In summary, ball mill scale-up remains a complex problem and requires a combination of empirical, semi-empirical and mechanistic modeling approaches based on industrial data. Such emerging techniques as DEM are not yet commonly adopted due to some of their limitations. The development of complex scaling constants based on careful experiments and detailed modeling may lead to improvements in the accuracy and applicability of scale-up predictions. However, the computational cost, complex particle-slurry interactions, and variability in ore properties and operating conditions still remain as problems for further research.

2.2.7 Current Limitations and Research Gaps in Modeling

Despite intensive research into ball mill modeling and simulations, some limitations and research gaps still remain in the area of improving the accuracy, reliability, and applicability of these models. They include:

1. Computational efficiency: DEM simulations of ball mills are computationally intensive, particularly in the case when fine particles and long grinding times are modeled [181]. The development of more efficient algorithms, coarse-graining methods, and parallel computing techniques is necessary to enable the simulation of industrial-scale mills with realistic particle sizes and grinding times [181].

2. Breakage modeling: The accuracy of PBMs and DEM-PBMs depends on the quality of the breakage data used to calibrate the breakage rates and distribution functions [172]. More advanced breakage models could account for the influence that particle size, shape, and mechanical properties have on the breakage behavior. As a result, the predictive capabilities of such models would be improved [45].

3. Slurry modeling: The presence of a slurry phase in wet grinding mills can significantly influence the charge dynamics and the grinding performance. However, accurate models representing the complex rheology and the interactions of the slurry with the grinding media and with ore particles are difficult to develop [32]. A need remains for more complex and efficient DEM-SPH models, as well as for the integration of advanced rheological models and experimental validation techniques [32].

4. Model validation: Ball mill models need to be verified against experimental data from industrial mills in order to ensure their accuracy and reliability [45]. However, detailed measurements of the charge motion, energy distribution, and particle size evolution in industrial mills are not easily available due to the harsh operating conditions and limited access to the mill interior [181]. This problem may be solved by applying advanced sensor technologies, such as acoustic emission sensors, strain gauges, and particle size analyzers, as well as by integrating these sensors with DEM and PBM models in order to enable real-time monitoring and validation of mill performance [45].

5. Multi-component modeling: Although the majority of ball mill models are based on a binary mixture of grinding media and ore particles, industrial mills often process multi-component ores having different hardness, density, and breakage characteristics [45]. Further research shoudl involve the development of multi-component PBMs and DEM-PBMs capable of accounting for the interactions and breakage behavior of different ore types [45].

6. Optimization and control: Ball mill models should be integrated with algorithms and control systems, so as to enable the real-time optimization and control of mill performance in response to changing ore properties, product requirements, and operating conditions [45]. Complex and efficient optimization and control strategies should be also integrated with DEM, PBM, and DEM-SPH models [45].

The above limitations and research gaps can be addressed in a collaborative effort of the industry, academia, and technology providers, which can result in the development of new experimental techniques, computational methods, and modeling frameworks. Further research into ball mill modeling and simulation may contribute to the development of more efficient, sustainable, and cost-effective grinding operations in the mineral-processing industry.

2.3 Measurement and Monitoring Techniques

Accurate measurements and the monitoring of ball mill performance are an important aspect in optimizing grinding efficiency, product quality, and energy consumption. The monitoring of mill operating parameters, such as power draw, charge motion, and particle size distribution, can be performed with the use of various techniques ranging from conventional methods to advanced sensor-based and data-driven approaches. The following section reviews the state-of-the-art techniques in ball mill measurement and monitoring and discusses their applications for improved process control and optimization.

2.3.1 Conventional Methods

Ball mill performance is typically monitored in both direct and indirect measurements of such operating parameters as power draw, feed and product size distributions, as well as mill sound and vibration levels [70].

Power draw is one of the most commonly used such indicators, as it reflects the energy consumed by the grinding process and is sensitive to changes in operating conditions, e.g. to mill speed, filling characteristics, and ore hardness [70]. Power draw can be measured with a wattmeter or calculated from the torque and rotational speed of the mill motor [158]. Specific energy consumption, defined as the energy consumed per unit mass of the processed ore, is often used as a benchmark for comparing the efficiency of different mills or operating conditions [70].

Feed and product size distributions are typically measured using sieve analysis or laser diffraction techniques, which provide information on the particle size reduction level obtained in the mill and on the efficiency of the classification system [158]. The relationship between the energy consumption and the particle size reduction is represented as the Bond work index, and it can be calculated from the feed and product size distributions and used to predict the performance of the mill for different ore types and operating conditions [70].

Mill sound and vibration levels provide qualitative information on the charge motion and liner wear inside the mill [158]. Experienced operators can often detect changes in the mill performance by listening to the sound of the mill or by feeling the vibrations on the mill shell [158]. However, these methods are subjective and do not provide quantitative data for process control and optimization.

2.3.2 Sensor-based Methods

More detailed and quantitative information on the mill operating conditions and on the charge motion may be provided by sensor-based methods, which employ acoustic emission sensors, strain gauges, accelerometers, and embedded sensors in the mill liners or grinding balls [45].

The charge motion and breakage rates inside the mill are monitored with acoustic emission (AE) sensors, which detect high-frequency stress waves generated by particle impacts and fracture events [167, 170]. AE sensors are mounted on the mill shell or liners and provide real-time data on the impact energy and frequency of the grinding media and ore particles [167]. The relevant information is extracted from the AE data with the use of such signal processing techniques as wavelet analysis and pattern recognition, and can be subsequently related to the mill operating conditions and performance [170].

On the other hand, the charge motion and the impact forces inside the mill are monitored with strain gauges and accelerometers which measure the deformation and acceleration of the mill shell, respectively [89, 11]. These sensors provide data on the toe and shoulder angles of the charge, the impact force distribution along the mill length, and the mill vibration characteristics [89, 11]. The data from multiple sensors are then combined with the use of data fusion techniques so as to provide a more comprehensive view of the mill dynamics [166].

Measurements of the impact forces and energy distributions inside the mill are performed directly with embedded sensors, such as instrumented grinding balls or liners with built-in accelerometers or pressure sensors [112, 180]. These sensors provide data required to validate DEM simulations and optimize the mill operating conditions [180]. The limitations of such sensors include their durability and data transmission capability in the harsh mill environment [112].

2.3.3 Soft-Sensors and Data-Driven Models

Soft-sensors (virtual sensors), are based on data-driven models and used to estimate the main process variables from available measurements. They provide real-time monitoring and control of ball mill performance [168]. These models employ advanced statistical and machine learning techniques, e.g. principal component analysis, artificial neural networks, and support vector machines, to establish a relationship between such measured variables as power draw, feed rate, and product size distribution and the desired process outcomes, for example grinding efficiency and product quality [168].

One example of an application of soft-sensors for ball mills is the use of neural networks to predict the product particle size distribution from the mill operating conditions and feed characteristics [170]. The neural network model is trained on historical data from the mill and can be updated online with real-time measurements of the feed and product size distributions [170]. The predicted particle size distribution is then used to adjust the mill operating conditions, such as the feed rate and ball filling degree [170].

Another example is the use of support vector regression in predictions of the mill power draw from the feed rate, ball filling degree, and ore hardness [133]. The model is trained on data from DEM simulations and validated against experimental data from a pilot-scale mill and can be used to predict e.g. the power draw [133].

Soft-sensors and data-driven models may provide real-time monitoring and control of ball mill performance, without the need for expensive and invasive sensors [168]. However, the accuracy and reliability of these models result from the quality and quantity of the available data, as well as from the ability to adapt to changes in the mill operating conditions and ore characteristics [168]. The integration of soft-sensors with mechanistic models, such as DEM and PBM, may provide a more complex and flexible framework for mill optimization and control [45].

2.3.4 Control and Optimization Strategies

The measurement results and monitoring techniques are used in grinding process control and optimization strategies to increase the energy efficiency, product quality, and throughput of ball mills [45].

One common approach is the application of Model Predictive Control (MPC), in which a model of the mill is developed for predicting the future behavior of the system and optimizing the control actions over a specified time horizon [74]. The model can be based on mechanistic principles, such as DEM and PBM, or on data-driven techniques, such as neural networks and support vector machines [74]. The control parameters, such as the feed rate, ball filling degree, and mill speed, are optimized to minimize the cost function which represents the desired performance criteria [74].

Another approach consists in adjusting the mill operating conditions with the use of expert systems and rule-based control which employ a set of predefined rules and heuristics, as well as the available measurements and process knowledge [158]. Such rules can be based on empirical correlations, operator experience, or process simulations, and can be updated online using machine learning techniques [158].

Optimization strategies, e.g. genetic algorithms and particle swarm optimization are based on a specific objective function and constraints [45]. Such an objective function can be based on a single criterion, e.g. on energy consumption or product size, or on a weighted combination of multiple criteria, e.g. on throughput, product quality, and wear rate [45]. The optimization can be performed offline, using historical data and process models, or online, using real-time measurements and adaptive models [45].

The effectiveness of control and optimization strategies for ball mills depends on the accuracy and reliability of the available measurement techniques and models, as well as on the ability of the latter to represent complex and time-varying grinding processes [45]. Advanced control and optimization algorithms, such as reinforcement learning and multi-objective optimization, thus represent an area for further research [45].

2.4 Emerging Tools and Future Directions

The above-discussed literature presents the current solutions in ball mill modeling, simulation, and optimization. It also indicates some of the remaining research problems and issues. This section reviews the tools and future research directions with a particular focus on the aspects addressed in this dissertation, i.e. on the development of digital twins, the evaluation of scaling constants, and the application of multivariate analysis techniques

which allow more information on the complex interactions which occur within ball mills. Successful solutions in this research area may translate into more efficient, sustainable, and cost-effective grinding operations.

The proposed research builds on the existing knowledge and techniques, as discussed in this literature review, and in particular on DEM-PBM models [45], sensor-based monitoring [167, 170], and the integration of modeling and measurement techniques [139].

A digital twin of a laboratory ball mill has a potential to offer accurate virtual representations of grinding processes. Its calibration is believed to be possible with the use of a systematic methodology based on advanced modeling techniques, e.g. DEM-SPH simulations, integrated with experimental methods, e.g. video recordings and sensor measurements. Owing to this approach, the twin is expected to provide accurate and detailed information on the complex interactions between the grinding media, ore particles, and slurry within the mill [32, 148].

A scaling constant may be viewed as a potential parameter for maintaining similar milling performance regardless of different mill scales and thus requires proper evaluation. Investigations of the impact of the scaling constant on size reduction degree, specific energy, and specific energy per rotation in both dry and wet milling conditions are here expected to provide a quantitative measure which can be used to perform ball mill scale-up without affecting its optimal performance [71, 130].

The calibrated digital twin can be subsequently used to perform a multivariate analysis of copper ore milling, which is believed to provide new information on load dynamics and the dominant types of forces within the mill. The proposed methodology, combining digital twin development, scaling constant evaluation, and multivariate analysis, addresses several research gaps and challenges identified in the literature review.

2.4.1 Development and Implementation of a Calibrated Digital Twin

A properly calibrated digital twin is expected to provide a virtual environment that accurately represents the physical system together with the load dynamics and the dominant types of forces inside the mill. In this work, the calibration methodology integrates advanced modeling techniques, such as DEM-SPH simulations, with experimental methods, including video recordings and sensor measurements.

DEM-SPH simulations provide detailed models of charge motion, energy dissipation, and particle breakage mechanisms. However, their accuracy depends on the proper calibration of model parameters and validation against experimental data [32]. High-speed video imaging allows the identification of the charge motion and the slurry flow patterns within the mill and can be thus used to validate the DEM-SPH simulations [76, 88]. On the other hand, sensor measurements of e.g. power draw, rotational speed and torque, provide real-time data on the operating conditions and performance of the mill [167, 170].

The data collected in the simulations are then used in the multivariate analysis of the impact of various operational parameters on the main performance indicators, such as size reduction, energy consumption, and force distribution inside the mill in a range of operating scenarios.

2.4.2 Evaluation of the Scaling Constant

The scaling constant is expected to provide a quantitative measure that can be used to increase the scale of the ball mill without affecting its optimal performance. In this research, the evaluation of the scaling constant is based on the analysis of the consistency of its impact on three aspects of milling performance: size reduction degree, specific energy, and specific energy per rotation. These indicators are used as a measure of the effectiveness of the scaling constant in both dry and wet milling conditions.

Another issue addressed in this work is the impact of operational parameters, e.g. mill diameter, filling degree, rotational speed, lifter size, lifter numbers, and slurry properties, on the main performance indicators and milling efficiency. This impact is here analyzed with the use of both experimental studies and simulations in the digital twin. The experimental studies involve applying various values of operational parameters and measuring the corresponding performance indicators.

The simulations in the digital twin are expected to complement the experimental studies by enabling the manipulation of the operational parameters in a wider range of scenarios and the identification of their impact on such performance indicators as load dynamics and force distribution.

2.4.3 Future Research Directions and Recommendations

Several further research directions can be identified in the field being the object of this study, as discussed below.

One important direction for future research includes further tests and validation of the scaling constant on a wider range of mill sizes and ore types, with additional experimental studies and simulations [71, 130].

Another direction involves tests on industrial-scale copper ore mills with an aim to validate the findings of this study and assess the applicability of the scaling constant approach in real conditions. Collaborations with industry partners could facilitate access to industrial-scale mills and enable the collection of relevant data for validation and optimization purposes [157].

Future research should also focus on other remaining research gaps identified in the literature review. One such area is the modeling of multi-component and multi-phase systems, which are common in industrial ball mills but often not accurately represented in current models [45]. More advanced models capable of describing the interactions between different ore types, particle sizes, and slurry properties may offer an even more realistic representation of the milling process and help optimize mill performance in a greater number of application scenarios.

Another issue is to integrate wear and breakage models into a unified computational framework that can predict the evolution of particle size and shape distributions, as well as the liner and media profiles, over time [146]. This task requires the development of advanced computational methods and experimental techniques capable of accurately characterizing the wear and breakage behavior of different materials under various operating conditions.

The optimization of mill design and operation is another area for future research. Such a task should be performed with consideration to a large number of variables and constraints that have a complex and nonlinear impact on mill performance and energy efficiency [45]. Advanced optimization algorithms, such as machine learning and artificial intelligence-based solutions, as well as computational frameworks, optimize the time

required to solve the high-dimensional and multi-objective problems. Such data-driven approaches can be integrated, with mechanistic models to create hybrid optimization methodologies.

Finally, future research should also focus on the integration of ball mill models with models of upstream and downstream processes, such as crushing, classification, flotation, and dewatering models. Such an approach may enable the optimization of the entire mineral processing circuit [70]. It would require integrated frameworks for the modeling of the interactions and dependencies between different unit operations and as a result enable the identification of optimal operating strategies for the entire plant.

In conclusion, this research provides a basis for more detailed investigations and optimization of ball milling processes through the development of a digital twin, the evaluation of a scaling constant, and the multivariate analysis of copper ore milling. The remaining areas for research in this field include the refinement of the scaling constant approach, the validation of the findings on industrial-scale mills, the modeling of multi-component and multi-phase systems, the integration of wear and breakage models, the optimization of mill design and operation, and the integration with upstream and downstream processes. Addressing these challenges and opportunities will require a collaborative effort between industry, academia, and technology providers, as well as the development of new experimental techniques, computational methods, and modeling frameworks.

Chapter 3

Theoretical Background of Numerical Environment

This chapter discusses the theory behind the simulation of the behavior of charge during dry milling and wet milling with slurry. The elements typically modeled in such simulations include balls, ore, water and steel parts of the mill. Some multiphase approaches may also allow for the interaction with gas phase (air), as a slurry consisting of solid fraction, gas, and water has unique properties due to the interactions between the three components.

The solid fraction of the slurry contains primarily particles of ground ore. Their size decreases with the grinding time and significantly affects both the viscosity of the slurry and its flow behavior [154]. These properties are important for physical simulations. Solid particles present in the slurry affect its turbidity and transparency. However, these characteristics are less relevant and are not the object of this analysis. The slurry also contains grinding media in the form of steel balls. Both the balls and ore particles can be modeled as discrete elements with known density, hardness, and size distribution, i.e. the parameters that have the greatest impact on grinding efficiency and energy consumption.

The particle size determines the settling velocity, the conditions of friction between particles, and interactions with other components of the slurry [151]. The density of the ground ore also has an influence on the suspendability, resistance to motion, and spatial distribution of particles [96]. The shape of particles determines their velocity distribution, intermolecular interactions, and the dynamics of sedimentation processes under quiescent conditions [193]. The hardness of solid particles translates into their resistance to deformation [19], and as such it affects particle-particle interactions, interactions with the mill surface, as well as grinding and comminution processes. Finally, particle size distribution has an impact on the grinding uniformity, sedimentation and mixing processes, as well as on interactions with other components of the slurry [134].

Mill elements, on the other hand, can be simulated as one solid body having all properties except size distribution identical to those of the discrete elements. Both the mill lining and the grinding media are typically steel elements and their wear and corrosion may thus have a significant impact on mill performance.

In wet grinding, the main component of the slurry is water, which serves as a carrier for solid particles and dissolved gases, determining their dynamics in the mill. The influence of water on the viscosity of the slurry, in this case mainly due to its quantity rather than any particular physicochemical properties, is also considerable, albeit smaller than that of solid particles [192]. The solubility of gases and the dynamics of certain chemical processes depend on the temperature of the water [155], which increases with time, as the grinding

process entails the release of significant amounts of heat. The main parameters of the fluid that need to be considered in a numerical model are density and viscosity, which depend on its temperature. The density affects the balance of forces within the slurry, as well as the behavior of the interactions between solid particles and gas [64]. Viscosity, on the other hand, translates into the flow resistance of the slurry [3] and is important in models of the slurry flow, as it affects the resistance of solid particles, the friction between slurry components, and the velocity distribution within the system.

3.1 Simulation Environment

DualSPHysics [52] is open-source software for simulations of physical phenomena based on the Smoothed Particle Hydrodynamics (SPH) meshless method. Over the past two decades, it has been intensively developed and applied in such areas as violent hydrodynamics of coastal and offshore structures, galaxy and planetary formation, multiphase flows and mixing in process industries, large deformations of solids and structures, damage and failure modeling, fluid-structure interaction, as well as computer graphics and games [156, 67, 118, 111]. DualSPHysics is capable of accelerating SPH simulations by employing both Central Processing Unit (CPU) via the OpenMP shared memory and Graphical Processing Unit (GPU), via the Compute Unified Device Architecture (CUDA) programming framework. It is available under the GNU Lesser General Public License (LGPL) and examples and is hosted on GitHub for public access and collaboration.

Being optimized for GPU acceleration, DualSPHysics provides increased flexibility and processing speed by using CUDA kernels for single GPU use, hierarchical templates, and cell-linked neighbor lists [51, 53]. The software package also includes tools for generating inputs and new test case workflows, along with various pre- and post-processing tools for data analysis and visualization.

Since version 5.0, DualSPHysics is also coupled with the Discrete Element Method [52]. This research was performed with the newest stable version 5.2.0.

3.2 SPH formulation

3.2.1 Interpolants and Kernel Functions

In the domain Ω, the continuous integral formulation of Smoothed Particle Hydrodynamics (SPH) for a differentiable function $f(\mathbf{r}), \mathbf{r} \in \mathbb{R}^d$, is expressed through the convolution of a kernel function W with f, as shown in:

$$\langle f(\mathbf{r}) \rangle := \int_{\Omega} f(\mathbf{r}')W(\mathbf{r} - \mathbf{r}', h)d\mathbf{r}'. \tag{3.1}$$

Here, the angle brackets $\langle \cdot \rangle$ signify an approximation, $\mathbf{r}' \in \Omega$ serves as an intermediary positional variable, and $W(\mathbf{r}, h)$ represents a positive kernel function characterized by the following equation:

$$W(\mathbf{r}, h) = \frac{1}{h^d}\omega(q), \tag{3.2}$$

where $h > 0$ denotes the smoothing length and $q = |\mathbf{r}|/h$ is the normalized distance. The function $\omega : \mathbb{R} \to \mathbb{R}$ is defined as a smooth, non-negative function whose properties are

described by:

$$\int_{\Omega} \omega(q) d\mathbf{r} = \frac{1}{h^d}, \tag{3.3}$$

This function has a compact support, as illustrated in: (Figure 3.1),

$$\omega(q) = 0 \text{ for } |\mathbf{r}| \geq kh, k \in \mathbb{R}^+. \tag{3.4}$$

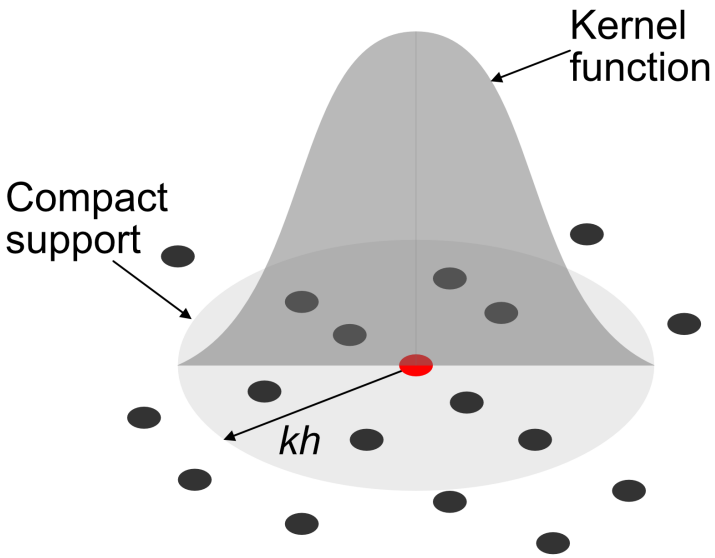

Figure 3.1: Configuration and compact support of the kernel function (based on [52])

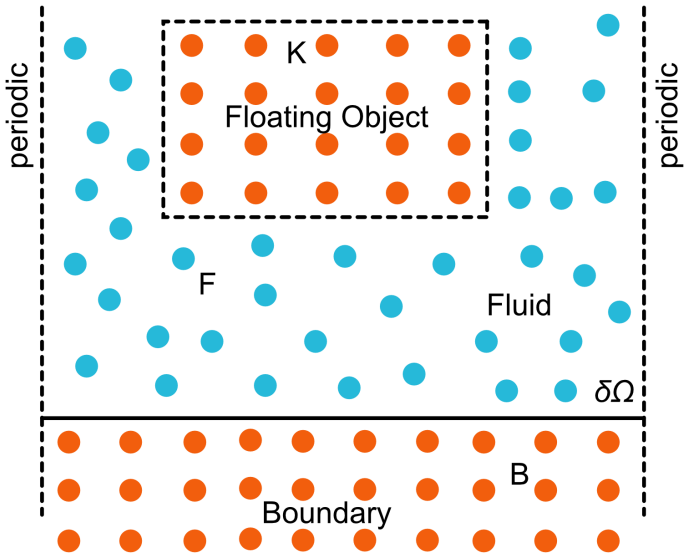

Figure 3.2: Illustration of various particle sets a ∈ P, with P encompassing all particles within the domain (based on [52])

The literature knows numerous smoothing kernels [47]. The one used in the software is represented by Eq. (3.2) and conforms to the criteria which are described with the function $W : \mathbb{R}^d \to \mathbb{R}$ in Eqs. (3.3) and (3.4). The kernel is characterized by its positive

definition over the support domain $\forall \mathbf{r}' \in \Omega; W(\mathbf{r}-\mathbf{r}', h) > 0$, exhibiting a monotonically decreasing and sufficiently smooth behavior over the interval kh, and

$$\lim_{h\to 0} W(\mathbf{r}, h) = \delta(\mathbf{r}), \tag{3.5}$$

where δ is the Dirac delta function, as described in [102, 122]. The DualSPHysics software employs various kernel functions, and notably the third-order B-splines kernel (cubic spline) [122]

$$\omega(q) = a_D \begin{cases} 1 - \frac{3}{2}q^2 + \frac{3}{4}q^3 & 0 \le q \le 1 \\ \frac{1}{4}(2-q)^3 & 1 < q \le 2 \\ 0 & \text{otherwise} \end{cases}, \tag{3.6}$$

where a_D^d is $10/7\pi$ and $1/\pi$ in 2-D and 3-D, respectively.

The commonly used fifth-order Wendland function is characterized by reduced pairing instability [182]. This C^2 kernel function has a positive kernel Fourier transform [47, 150], and is as follows:

$$\omega(q) = a_d \left(1 - \frac{q}{2}\right)^4 (2q+1) \quad 0 \le q \le 2, \tag{3.7}$$

with a_D^d specified as $10/7\pi$ in 2-dimensional spaces and $1/\pi$ in 3-dimensional spaces.

The SPH discrete approximation of the convolution between W and f can be described as follows:

$$\langle f(\mathbf{r}_a)\rangle = \sum_{b\in P} f(\mathbf{r}_b) W(\mathbf{r}_a - \mathbf{r}_b, h)\Delta r_b^d, \quad a = 1, \ldots, N, \tag{3.8}$$

where the subscripts a, b represent the interacting neighboring discrete particles within the set P, which consists of all particles in the domain and includes particles in the fluid F, boundary B, and any floating objects K, as depicted in Figure 3.2. The set P is the union of F and B, where K is a subset of B. The term ΔV_b denotes the volume V associated with the b-th particle in P. For simplicity, the notation $\langle\cdot\rangle$ is further omitted.

Detailed in formation on SPH is available in [124, 177], and [178]. Additionally, analogous integral and discrete formulations can be developed for the gradient operator of a specific function f, as follows:

$$\frac{\partial f(\mathbf{r})}{\partial \mathbf{r}} = \int_\Omega f(\mathbf{r}') \frac{\partial W}{\partial \mathbf{r}}(\mathbf{r} - \mathbf{r}', h)\, d\mathbf{r}', \tag{3.9}$$

using the convolution theorem,

$$\frac{\partial f(\mathbf{r})}{\partial \mathbf{r}} * W = f * \frac{\partial W}{\partial \mathbf{r}}. \tag{3.10}$$

The discrete gradient is thus:

$$\frac{\partial}{\partial \mathbf{r}_a} f(\mathbf{r}_a) := \sum_{b\in P} f(\mathbf{r}_b) \frac{\partial}{\partial \mathbf{r}_a} W(\mathbf{r}_a - \mathbf{r}_b, h) V_b, \quad a = 1, \ldots, N. \tag{3.11}$$

3.2.2 Governing Equations

The behavior of a compressible fluid is represented by the fundamental governing Navier-Strokes equations, which can be expressed as the continuity and momentum equations based on a Lagrangian framework as follows:

$$\frac{d\rho}{dt} = -\rho \nabla \cdot \mathbf{v}, \tag{3.12}$$

and

$$\frac{d\mathbf{v}}{dt} = -\frac{1}{\rho}\nabla P + \mathbf{\Gamma} + \mathbf{f}, \tag{3.13}$$

here, d is the total or material derivative, $\mathbf{v}$ is the velocity vector, ρ is density, P is pressure, $\mathbf{\Gamma}$ represents the dissipation terms, and $\mathbf{f}$ denotes accelerations due to external forces like gravity.

3.2.3 SPH Discretization of the Governing Equations

The mass conservation property of SPH,

$$\frac{dm}{dt} = 0, \tag{3.14}$$

where the mass is conserved exactly within a Lagrangian particle, causes a density change due to the volumetric change of the term at the right-hand side of Eq. (3.12). In the SPH formalism, the discrete form of the continuity equation at a point a with position $\mathbf{r}_a$ is as follows [124]:

$$\left.\frac{d\rho}{dt}\right|_{a\in P} = \sum_{b\in P} \frac{m_b}{\rho_b}\mathbf{v}_{ab}\cdot\nabla_a W_{ab} + D_a, \tag{3.15}$$

where $W_{ab} = W(\mathbf{r}_a - \mathbf{r}_b, h)$ and $(\cdot)_{ab} = (\cdot)_a - (\cdot)_b$. The second term on the right-hand side is the numerical diffusion term for density [4]. The discrete form of Eq. (3.13) in an SPH formalism is

$$\left.\frac{d\mathbf{v}}{dt}\right|_{a\in F} = -\sum_{b\in P} m_b\left(\frac{P_a + P_b}{\rho_a\rho_b}\right)\nabla W_{ab} + \langle\Gamma\rangle_a + \mathbf{f}, \tag{3.16}$$

where a symmetric SPH operator is employed, ensuring conservation of momentum [14] for the pressure term, and the discrete representation of the dissipation terms is discussed in more detail in the Dissipation Terms subsection.

Density diffusion terms

DualSPHysics incorporates two formulations of density diffusion terms (DDT), which serve as a high-frequency numerical noise filter that enhances the stability of the algorithm by smoothing the density and, as a result, the pressure. This improvement is crucial due to the inherent spuriousness in pressure calculations within the weakly compressible SPH framework. This spuriousness arises from the collocated arrangement (in velocity and density) and from the explicit approach (in time integration). These terms are described as:,

$$D_a = \delta h_c \sum_{b\in P} \psi_{ab}\cdot\nabla W_{ab} V_b, \tag{3.17}$$

where δ describes the strength of the diffusion term. The term ψ_{ab} is derived from the Neumann–Richtmeyer artificial dissipation, as introduced by Molteni and Colagrossi [120]:

$$\psi_{ab} = 2(\rho_b - \rho_a)\frac{\mathbf{r}_{ab}}{\|\mathbf{r}_{ab}\|^2}, \tag{3.18}$$

Modified by Fourtakas et al. [60] Eq. (3.18) includes the dynamic component of the density, as follows:

$$\psi_{ab} = 2\left(\rho_{ba}^{(\mathrm{T})} - \rho_{ab}^{(\mathrm{H})}\right)\frac{\mathbf{r}_{ab}}{\|\mathbf{r}_{ab}\|^2}, \tag{3.19}$$

where superscripts (T) and (H) represent, respectively, the total and hydrostatic components of the density for a weakly compressible and barotropic fluid. The hydrostatic pressure is locally constructed as follows:

$$P_{ab}^{(\mathrm{H})} = \rho_0 g z_{ab}. \tag{3.20}$$

Although both terms exhibit inconsistencies near the truncated kernel support [4] (such as at a free-surface or a wall boundary), resulting in a net outwards vector contribution, the latter term enhances the behavior of pressure near wall boundaries by acting on the dynamic pressure.

Dissipation terms: Artificial viscosity

The momentum equation can be expanded with an artificial diffusive term based on the Neumann-Richtmyer artificial viscosity [121] in order to reduce oscillations and stabilize the SPH framework. The artificial viscosity term is included as part of the SPH gradient operator on the right-hand side of Eq. (3.16):

$$\Pi_{ab} = \begin{cases} \left(-\alpha \frac{\overline{c_{ab}}}{\overline{\rho_{ab}}}\right) \frac{h \mathbf{v}_{ab} \cdot \mathbf{r}_{ab}}{r_{ab}^2 + \eta^2}, & \mathbf{v}_{ab} \cdot \mathbf{r}_{ab} < 0, \\ 0, & \mathbf{v}_{ab} \cdot \mathbf{r}_{ab} \geq 0 \end{cases}, \tag{3.21}$$

where $\overline{(\cdot)_{ab}} = \frac{(\cdot)_a + (\cdot)_b}{2}$. Here, c is the numerical speed of sound, and α is the coefficient of artificial viscosity. The parameter $\eta = 0.001h^2$, with $\{\eta \in \mathbb{R}; r_{ab} > \eta\}$, is used to ensure that the operator is non-singular. It can be demonstrated that $\Pi_{ab} \propto \nu_0 \nabla^2 \mathbf{v}$, where ν_0 is the kinematic viscosity [124, 58]. The momentum equation, augmented by artificial viscosity, is formulated as follows:

$$\left.\frac{d\mathbf{v}_a}{dt}\right|_{a \in F} = -\sum_{b \in P} m_b \left(\frac{P_a + P_b}{\rho_a \rho_b} + \Pi_{ab}\right) \nabla W_{ab} + \mathbf{f}, \tag{3.22}$$

Its simplicity causes the artificial viscosity formulation to be commonly used in SPH as a viscous dissipation term.

Dissipation terms: Laminar viscosity

Lo and Shao [104] offer an approximation of the viscous dissipation of momentum in the laminar flow regime in DualSPHysics:

$$\nu_0 \nabla^2 \mathbf{v}_a = \sum_{b \in P} m_b \left(\frac{4\nu_0 \mathbf{r}_{ab} \cdot \nabla W_{ab}}{(\rho_a + \rho_b)(\mathbf{r}_{ab}^2 + \eta^2)}\right) \mathbf{v}_{ab}, \tag{3.23}$$

where ν_0 is the kinematic viscosity of the fluid. The laminar viscous term diverges near the free-surface [37].

Dissipation terms: Sub-particle scale model

DualSPHysics incorporates the large eddy simulation Sub-Particle Scale (SPS) model [66], as described by Dalrymple and Rogers [41] who use Favre averaging within a weakly compressible framework. The SPS stress tensor τ is described in Einstein notation in the superscripts i, j as:

$$\tau^{ij} = \overline{v^i v^j} - \overline{v}^i \overline{v}^j, \tag{3.24}$$

and modeled by an eddy viscosity closure as:

$$\frac{\tau^{ij}}{\rho} = 2\nu_{\text{SPS}}\left(S^{ij} - \frac{1}{3}S^{ii}\delta^{ij}\right) - \frac{2}{3}C_l\Delta^2\delta_{ij}|S^{ij}|^2. \tag{3.25}$$

Here, $\nu_{\text{SPS}} = [C_s^2\Delta]^2|S^{ij}|$, where $C_s = 0.12$ is the Smagorinsky constant, $C_\Delta = 0.0066$, Δ is the initial particle spacing, and $|S^{ij}| = \frac{1}{2}(S^{ij}S^{ij})^{1/2}$, S^{ij} being an element of the SPS strain tensor. This relationship is used together with the variationally consistent strain tensor.

In the case of the pressure gradient (Eq. 3.16), the discrete form of the term is as follows [41]:

$$\frac{1}{\rho}\nabla\cdot\tau_a^{ij} = \sum_{b\in P} m_b\left(\frac{\tau_a^{ij}+\tau_b^{ij}}{\rho_a\rho_b}\right)\nabla^i W_{ab}. \tag{3.26}$$

In its final form, the momentum dissipation term is expressed in DualSPHysics as:

$$\mathbf{\Gamma}_a = \sum_{b\in P} m_b\left(\frac{4\nu_0\mathbf{r}_{ab}\cdot\nabla W_{ab}}{(\rho_a+\rho_b)(r_{ab}^2+\eta^2)}\right)\mathbf{v}_{ab} + \sum_{b\in P} m_b\left(\frac{\tau_a^{ij}+\tau_b^{ij}}{\rho_a\rho_b}\right)\nabla^i W_{ab}. \tag{3.27}$$

3.2.4 Equation of State and Compressibility

In the SPH formulation employed in DualSPHysics, the relationship between density and pressure is expressed as an Equation of State (EOS), which describes the weak compressibility of the fluid, calculated from the numerical speed of sound [123],

$$P = \frac{c_s^2\rho_0}{\gamma}\left[\left(\frac{\rho}{\rho_0}\right)^\gamma - 1\right], \tag{3.28}$$

where γ is the polytropic index (typically 7 for water), ρ_0 is the reference density, and $c_s = \sqrt{\frac{dP}{d\rho}}$ represents the numerical speed of sound [7].

The numerical speed of sound c_s, selected on the basis of a typical length scale and timescale of the domain, allows time steps to be significantly increased during explicit time integration in comparison to the case based on the physical speed of sound [7]. Given $c_s = 10\|\mathbf{v}\|_{\max}$ where $\|\mathbf{v}\|_{\max} = \sqrt{gh_0}$, h_0 being the initial fluid height in the domain, the variation in density does not typically exceed approximately 1%. However, this condition should be continuously monitored as the 1% threshold may be occasionally exceeded, and the compressibility may thus be no longer considered 'weak'. In such cases, the speed of sound should be increased in order to reduce the time step, resulting in longer computational times.

3.2.5 Time Integrators and Time Step

DualSPHysics employs two explicit time integration schemes. For brevity, the governing equations are written as

$$\frac{d\mathbf{v}_a}{dt} = F_a; \quad \frac{d\rho_a}{dt} = R_a; \quad \frac{d\mathbf{r}_a}{dt} = \mathbf{v}_a. \tag{3.29}$$

The time integrators are briefly introduced below.

Verlet time integration scheme

The Verlet schemes [175] are commonly used in molecular dynamics as efficient tools providing a second-order accurate integration in space. This approach utilizes a velocity Verlet variant that eliminates the need for multiple computational steps within a single iteration. Accordingly, the Weakly Compressible Smoothed Particle Hydrodynamic (WCSPH) variables are calculated according to the following equations:

$$\begin{aligned}\mathbf{v}_a^{n+1} &= \mathbf{v}_a^{n-1} + 2\Delta t \mathbf{F}_{a'}^n,\\ \mathbf{r}_a^{n+1} &= \mathbf{r}_a^n + \Delta t \mathbf{v}_a^n + \frac{1}{2}\Delta t^2 \mathbf{F}_{a'}^n,\\ \rho_a^{n+1} &= \rho_a^{n-1} + 2\Delta t R_a^n.\end{aligned}$$

Integration across a staggered time interval causes the density and velocity equations to become decoupled, resulting in the potential divergence of the integrated values. Therefore, an intermediate correction step is required every N_s steps (with the recommended $N_s \approx 40$), as in the following equations:

$$\begin{aligned}\mathbf{v}_a^{n+1} &= \mathbf{v}_a^n + \Delta t \mathbf{F}_{a'}^n,\\ \mathbf{r}_a^{n+1} &= \mathbf{r}_a^n + \Delta t \mathbf{v}_a^n + \frac{1}{2}\Delta t^2 \mathbf{F}_{a'}^n,\\ \rho_a^{n+1} &= \rho_a^n + \Delta t R_a^n,\end{aligned}$$

where the superscript $n \in \mathbb{N}$ is the time step and $t = n\Delta t$.

Symplectic time integration scheme

The symplectic position Verlet time integration scheme [98] offers second-order temporal accuracy. Its time-reversibility and symmetry in the absence of diffusive terms renders it particularly useful for Lagrangian methods and allows it to preserve geometric properties. In the absence of dissipative forces, the position Verlet scheme is given by:

$$\mathbf{r}_a^{n+1/2} = \mathbf{r}_a^n + \frac{\Delta t}{2}\mathbf{v}_a^n, \tag{3.30}$$

$$\mathbf{v}_a^{n+1} = \mathbf{v}_a^n + \Delta t \mathbf{F}_a^{n+1/2}, \tag{3.31}$$

$$\mathbf{r}_a^{n+1} = \mathbf{r}_a^n + \frac{\Delta t}{2}\mathbf{v}_a^{n+1}. \tag{3.32}$$

However, as the viscous forces are and the density increase in DualSPHysics, an $(n+\frac{1}{2})$ increment step becomes necessary, and thus a half-step velocity Verlet method is employed for calculations of the velocity for both the acceleration evolution and the density evolution at $\mathbf{F}(\mathbf{r}_{n+\frac{1}{2}})$ and $\mathbf{R}(\mathbf{r}_{n+\frac{1}{2}})$, respectively. The approach adopted in DualSPHysics is formulated as,

$$\mathbf{r}_a^{n+1/2} = \mathbf{r}_a^n + \frac{\Delta t}{2}\mathbf{v}_a^n, \tag{3.33}$$

$$\mathbf{v}_a^{n+1/2} = \mathbf{v}_a^n + \frac{\Delta t}{2}\mathbf{F}_a^n, \tag{3.34}$$

$$\mathbf{v}_a^{n+1} = \mathbf{v}_a^n + \Delta t \mathbf{F}_a^{n+1/2}, \tag{3.35}$$

$$\mathbf{r}_a^{n+1} = \mathbf{r}_a^n + \Delta t \frac{\mathbf{v_a}^{n+1} + \mathbf{v_a}^n}{2}, \tag{3.36}$$

where $\mathbf{r}^{n+\frac{1}{2}}$ replaces $\mathbf{r}^{n+1}$ in Eq. (3.30) in order to remove dependency on $\mathbf{u}^{n+\frac{1}{2}}$. Subsequently, the evolution of density follows the half time steps in accordance with the symplectic position Verlet scheme below [138]:

$$\rho_a^{n+\frac{1}{2}} = \rho_a^n + \frac{\Delta t}{2} R_a^n \tag{3.37}$$

$$\rho_a^{n+1} = \rho_a^n \frac{2 - \epsilon_a^{n+\frac{1}{2}}}{2 + \epsilon_a^{n+\frac{1}{2}}}, \tag{3.38}$$

$$\text{where } \epsilon_a^{n+\frac{1}{2}} = -\left(\frac{R_a^{n+\frac{1}{2}}}{\rho_a^{n+\frac{1}{2}}}\right) \Delta t. \tag{3.39}$$

Variable time step

The time integration is constrained by the Courant–Friedrichs–Lewy (CFL) condition, which is important in explicit time integration schemes, as it helps confine the numerical domain within the physical domain of dependence [125]:

$$\Delta t_f = \min_a \left(\frac{h}{\left|\frac{d\mathbf{v}_a}{dt}\right|}\right), \quad \Delta t_c = \min_a \left(\frac{h}{c_s + \max_b \left(\frac{|h\mathbf{v}_{ab}\cdot\mathbf{r}_a|}{r_{ab}^2+\eta^2}\right)}\right), \tag{3.40}$$

$$\Delta t = C_{CFL} \min(\Delta t_f, \Delta t_c), \tag{3.41}$$

where $\left|\frac{d\mathbf{v}_a}{dt}\right|$ is the magnitude of particle acceleration. The variable time step is defined as a minimum between Δt_f and Δt_{cv}, and it is constrained by the Courant number C_{CFL}, which is typically from 0.1 to 0.2.

3.2.6 Boundary Conditions

DualSPHysics is provided with several boundary conditions. The boundary conditions for solids are discretized by a set of boundary particles $a \in \mathbf{B}$ that differ from the fluid particles $\mathbf{F}$. Due to the Lagrangian nature of SPH, the motion of solid boundaries can also be defined directly by the user.

Dynamic Boundary Conditions (DBC) are simply represented as fixed particles, and their density is computed with the use of the continuity equation and pressure values obtained from the equation of state. As the definition of such boundaries is not complicated and their computations are relatively stable and efficient, they are an effective solution for complex geometries. They were validated with dam-break flows as well as with wave flumes, and they were successfully simulated in real engineering applications [2, 191]. However, an unphysical gap is formed between the fluid and these solid boundaries when the fluid approaches the boundary, and as a result the accuracy of pressure measurements on the boundary decreases. Therefore, DualSPHysics is also provided with another solution, in which the density of solid particles is calculated by linear extrapolation from ghost positions within the fluid domain [57]. In this second approach, the gap is avoided and pressures of the boundary particles in still water converge to hydrostatic pressure.

Dynamic boundary conditions

DBC represents a solid wall using a collection of boundary particles **B**, with the following continuity equation [39]:

$$\left.\frac{d\rho}{dt}\right|_{a\in B} = \rho_b \sum_{b\in F} \frac{m_b}{\rho_b} \mathbf{v}_{ab} \cdot \nabla W, \tag{3.42}$$

while the position of these particles is updated from:

$$\left.\frac{d\mathbf{v}}{dt}\right|_{\forall a\in B} = \mathbf{F}^{(\text{imposed})} \tag{3.43}$$

where $\mathbf{F}^{(\text{imposed})}$ is the force exerted on moving boundary particles by the fluid. Such motion can be calculated from the user-predefined function or from accelerations accumulated over time. Due to the increase in density calculated from Eq. (3.42), the pressure in the momentum equation for particle $a \in F$ increases, producing a repulsive force between the fluid and boundary particles. This simplified boundary approach is particularly useful in GPU implementation, as it allows code optimization through the use of vector lists [39].

3.2.7 Particle Shifting Algorithm

The anisotropic distribution of particles results in an additional discretization error due to the zeroth- and higher-order kernel moments (i.e. the discrete version of Eq. (3.3)). This problem is of particular importance in the case of negligible or large dynamics [123] and violent flows where particles may not have an isotropic distribution. In DualSPHysics, the near-isotropic particle distribution is maintained with the use of the Fickian-based particle shifting algorithm, as described in Lind et al. [101]:

$$\delta\mathbf{r}_a\big|_{a\in F} = -D_s \nabla C_a, \tag{3.44}$$

where $\delta\mathbf{r}_a$ is the shifting distance, ∇C_a is the kernel gradient and D_s is expressed as

$$D_s = A_s h \|\mathbf{v}_a\| \Delta t, \tag{3.45}$$

where A_s is a control parameter and $\|\mathbf{v}_a\|$ is the magnitude of velocity for particle a [161]. A constraint based on the magnitude of particle velocity mitigates the risk of excessive displacement and prevents the subsequent loss of data due to the transition of particles across the domain cells. The recommended range for A_s is between 1 and 6, with the value of 2 being specified by Skillen et al. [161]. Details for calculating ∇C_a are discussed in [52].

3.3 DEM and DCDEM

The solid-fluid and solid-solid interactions are addressed in DualSPHysics by incorporating the Distributed Contact Discrete Element Method (DCDEM) into its Smoothed Particle Hydrodynamics (SPH) models. This method, in which forces between a fluid and solid particle pair are calculated using SPH, and solid-solid interactions are modeled using DEM, employs an explicit integration method and is part of the DualSPHysics meshless framework. This innovative approach, initially introduced in [40], enables an accurate representation of complex solid shapes based on a particle-based method, in which the

particles are subjected to a rigid body constraint. With the use of specific non-linear contact models, the system is capable of simulating various material behaviors using three primary parameters: Poisson ratio, Young's modulus, and dynamic friction coefficient [22, 16, 40]. Although the model has significant advantages, it also shows limitations typical of general DEM approaches, e.g. potential stability issues due to its explicit nature, high demand for computational power or inaccurate simulations of extended frictional contacts, as well as the risk of artificial geometry effects in low-resolution simulations caused by the spherical particle shapes.

3.3.1 Method Formulation

In the framework of Smoothed Particle Hydrodynamics (SPH), the domain of the fluid is represented as a constellation of nodal points. These points correspond to such physical parameters as position, velocity, density, and pressure, approximated on the basis of their spatial coordinates. Their movement being synchronized with the movement of the fluid, from the Lagrangian perspective the nodes change their properties over time, under the influence of interactions with adjacent nodes. As indicated by the term itself, "Smoothed Particle Hydrodynamics", these nodes reflect the mass of a fluid segment. They are thus referred to as "particles", and their movement is smoothed, ignoring individual rotational dynamics. This methodology is based on the principles of integral interpolation theory [124]. An effective transition from a continuous integral representation to a discrete set of Lagrangian points is the result of discretization:

$$A_i \approx \sum_j A_j W(\mathbf{r}_{ij}, h) V_j. \tag{3.46}$$

Known as the summation approximation, it is applied to all particles j, for which the distance $|\mathbf{r}_{ij}| = |\mathbf{r}_i - \mathbf{r}_j|$ does not exceed the smoothing length h. Here, V_j represents the volume associated with particle j, A_i is the variable being estimated at particle i, and W is the kernel, or weight function. This approach does not ensure first order consistency, i.e. such in which the estimation of the kernel precisely replicates a linear polynomial function. This limitation is due to the intrinsic errors linked to the discretized representation:

$$\sum_j V_j W(\mathbf{r}_{ij}, h) \approx 1. \tag{3.47}$$

They can become significant, especially near open boundaries or areas of discontinuity where the kernel W fails to maintain compact support. This problem is solved by applying e.g. Shepard's and Moving Least Squares (MLS) methods. In a procedure suggested by Colagrossi and Landrini [38], spatial derivatives are determined based on the gradient of the kernel. This study employs a Quintic kernel, as proposed by Wendland [182]:

$$W(\mathbf{r}_{ij}, h) = \alpha_D \left(1 - \frac{q}{2}\right)^4 (2q + 1), \quad 0 \leq q \leq 2, \tag{3.48}$$

where $q = |\mathbf{r}_{ij}/h|$ and $\alpha_D = 21/16\pi h^3$, for a 3D case.

3.3.2 Discretization of Rigid Body Equations and Contact Forces with DCDEM

As proposed by Koshizuka et al. [92], a rigid body I is modeled with the use of a group of particles. The relative positions of the particles do not change, in effect allowing the volume of I to be represented by this particle ensemble. For reference purposes, this assembly is also labeled as I. The behavior of these particles is described by a unique set of equations distinct from those applied to conventional SPH particles. The dynamics of the rigid body are characterized by Newton's laws, and the discretization process is achieved by summing the individual contributions from each particle, expressed as:

$$M_I \frac{d\mathbf{V}_I}{dt} = \sum_{k \in I} m_k \frac{d\mathbf{v}_k}{dt}, \tag{3.49}$$

$$I_I \frac{d\mathbf{\Omega}_I}{dt} = \sum_{k \in I} m_k (\mathbf{r}_k - \mathbf{R}) \times \frac{d\mathbf{v}_k}{dt}, \tag{3.50}$$

where the rigid body I is characterized by its mass M_I, velocity $\mathbf{V}_I$, inertia tensor $\mathbf{I}_I$, angular velocity $\mathbf{\Omega}_I$, and center of mass $\mathbf{R}$. These vector properties are recalculated at each time step. The force per unit mass acting on a particle k within the particle ensemble that constitutes I is represented by $m_k \frac{d\mathbf{v}_k}{dt}$, where m_k signifies the mass of particle k. This force is the resultant of various other forces acting on the body, e.g. gravity, fluid resistance, and the normal or frictional forces resulting from interactions with other solids. As such, the term $m_k \frac{d\mathbf{v}_k}{dt}$ can encompass a range of force types: interactions with fluid particles are described by the fluid momentum equation, while interactions with solid particles are determined by additional derived forces. Such an approach to force calculation allows an improved integration of solid and fluid dynamics.

Equation (3.16) used for the direct evaluation of local interactions between fluid and solid phases facilitates the incorporation of a viscous framework and thus provides a mechanism allowing for viscous drag closure [23]. This model is based on the concept of Dynamic Boundary Conditions [39] and on the specifications described in Equations (3.49) and (3.50), and thus it does not require any arbitrary, *ad-hoc* adjustments. The dynamics are fully derived from the fundamental, particle-specific solutions of Equations (3.49) and (3.50). However, it shows a tendency to overestimate density [143, 153], possibly due to an entropy increase at the interface. This phenomenon causes the spacing between fluid and solid particles to expand as a result of the force exerted by the pressure gradient, affecting the accuracy of viscous force calculations at that interface [38]. The addition of the δ-SPH diffusive term to Equation (3.15) is suggested as a solution to this problem [23].

If two particles, being part of either a boundary or a rigid body, interact, their dynamics are represented by the Discrete Element Method (DEM). The resultant contact force $\mathbf{F}_i^{\mathrm{T}}$ acting on particle i due to a collision with particle j, is analyzed as $\mathbf{F}_n$ and $\mathbf{F}_t$, which correspond to the normal and tangential force components, respectively. These components are further subdivided into a repulsion force $\mathbf{F}^r$, generated by the deformation of the material, and a damping force $\mathbf{F}^d$, implemented to account for energy dissipation throughout the deformation process. The mechanics of the DEM interactions between two particles are shown in Figure 3.3.

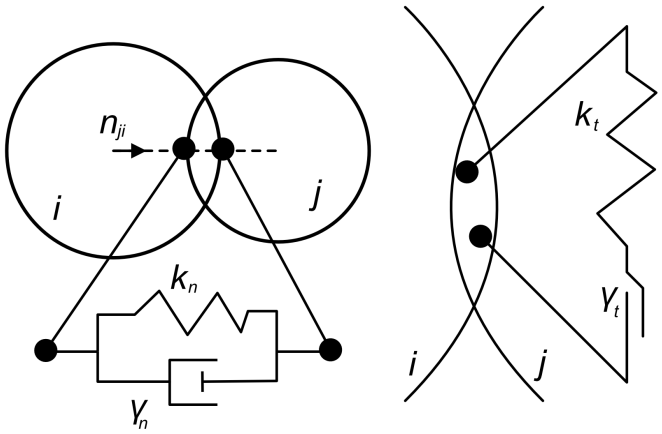

Figure 3.3: Schematic view of DEM mechanism. Left – normal interaction; Right – tangential interaction. (based on [22])

The normal forces are given by a modified, non-linear, Hertzian model [95, 16]:

$$\mathbf{F}_{n,ij} = \mathbf{F}_n^r + \mathbf{F}_n^d = k_{n,ij}\delta_{ij}^{3/2}\mathbf{e}_{ij} - \gamma_{n,ij}\delta_{ij}^{1/4}\dot{\delta}_{ij}\mathbf{e}_{ij}, \tag{3.51}$$

where the stiffness constant for the interacting pair ij is $k_{n,ij}$, and the particle overlap $\delta_{ij} = \max(0, (d_i + d_j)/2 - |\mathbf{r}_{ij}|)$ approximates material deformation. The unit vector between the centers of mass for the particles is denoted as $\mathbf{e}_{ij}$, with the rate of normal deformation being $\dot{\delta}_{ij} = \mathbf{v}_{ij} \cdot \mathbf{e}_{ij}$, and the damping constant being $\gamma_{n,ij}$. This nonlinear formulation helps mitigate some of the limitations inherent in using constant restitution coefficients and fixed contact durations for particle pairs. It thus represents a greater number of behaviors for a broad spectrum of contacts [94]. The stiffness and damping constants are given by:

$$k_{n,ij} = -\frac{4}{3}E^*\sqrt{R^*}; \quad \gamma_{n,ij} = C_n\sqrt{6M^*E^*\sqrt{R^*}}, \tag{3.52}$$

with C_n of the order of 10^{-5} [99]. The other parameters are given by:

$$\frac{1}{E^*} = \frac{1-\nu_I^2}{E_I} + \frac{1-\nu_J^2}{E_J}; \quad R^* = \frac{r_i r_j}{r_i + r_j}; \tag{3.53}$$

$$M^* = \frac{m_I m_J}{m_I + m_J}, \tag{3.54}$$

where E is the Young modulus, ν is the Poisson ratio and m is the mass of the body.

For tangential interactions between particles, friction is depicted with a linear dashpot model, limited by maximum force resulting from the Coulomb friction law, as defined by the kinetic friction coefficient μ_f. This linear methodology offers an optimal balance between the fidelity of the model at the demand for computational power. Although more elaborate models offer better performance in specific tasks, such as representing the rolling friction, their effectiveness is often limited in general applications. A sigmoidal function modifies the Coulomb law and thus ensures a smooth transition of the friction forces from zero to maximum values as the tangential velocity increases. As a result, the model becomes more realistic [176].

$$\mathbf{F}_{t,ij} = \min(\mu_{f,IJ}\mathbf{F}_{n,ij}\tanh(8\dot{\delta}_{ij}^{t})\mathbf{e}_{ij}^{t} \cdot (\mathbf{F}_{t}^{r} + \mathbf{F}_{t}^{d}), \tag{3.55}$$

where

$$\mathbf{F}_{t}^{r} + \mathbf{F}_{t}^{d} = k_{t,ij}\delta_{ij}^{t}\mathbf{e}_{ij}^{t} - \gamma_{t,ij}\dot{\delta}_{ij}^{t}\mathbf{e}_{ij}^{t}. \tag{3.56}$$

The model replicates the mechanisms of static and dynamic friction with the use of a penalty method. Rather than allowing a static adhesion of the body at the point of contact, it employs a spring-damper mechanism. Assuming that the time scales for normal and tangential contacts are identical, [79] proposes the tangential stiffness to be calculated as $k_t = \frac{2}{7}k_n$. An adequate description of the time scale of rigid contacts and the preservation of the system within its stability region require an additional component in the dynamic equation, as indicated by [99]:

$$\Delta t_{\mathrm{DEM}} = \min_{i}\left(\frac{\pi}{50}\sqrt{\frac{k_{n,ij}}{m_{IJ}}}\right). \tag{3.57}$$

This class of DEM models is referred to as a 'soft sphere' approach, since it employs the particle overlap to deform the spring-damper system. This formulation provides a particle-wise force estimate which, coupled with the rigid body idea, allows the generalization of the geometry, as it does not require information on normal directions or other forms of topology and instead it solves arbitrarily complex geometries by resolving the local interactions.

Chapter 4

Research Goal and Objectives

The optimization of ball mill operations has encountered problems resulting inter alia from the difficulties in scaling up from laboratory models to actual industrial applications.

The current approach to ball mill design and operation relies on empirical knowledge and trial-and-error methods, and often results in suboptimal performance, excessive energy consumption, and increased operational costs. A solution to this problem requires a more systematic and scientific approach to collecting data which describe the principles behind ball mill scale up processes.

Such new research approaches have been enabled by recent advancements in computational modeling and simulation techniques, e.g. the Discrete Element Method (DEM) and Smoothed Particle Hydrodynamics (SPH). These tools provide information on the interactions between the grinding media, ore particles, and slurry, thus reducing the need for complicated experiments. The purpose of this research is to use these advanced modeling techniques and experimental methods for acquiring detailed information on the process of ball mill scale up.

4.1 Research Goal

The primary goal of this research is to gain insights into the laboratory ball mill scale-up by investigating the influence of operational parameters on milling performance and energy efficiency for selected mill diameters.

Detailed analyses of the complex dynamics within ball mills, as well as of the interactions between the grinding media, mill interior, and slurry, are here performed by combining advanced modeling techniques, such as the Discrete Element Method (DEM) and Smoothed Particle Hydrodynamics (SPH) with experimental methods. The following points represent the particular objectives of this research.

4.2 Research Objectives

To achieve the primary goal of this research, the following objectives have been established:

Develop a Systematic Methodology for Calibrating a Digital Twin

Develop a systematic methodology for calibrating a digital twin of a laboratory ball mill by integrating advanced modeling techniques (DEM-SPH simulations) with experimental

methods (video recordings and sensor measurements). This objective aims to create a reliable and accurate virtual representation of the ball mill, which will serve as a basis for further investigations and analyses.

Develop and Evaluate a Scaling Constant

Develop and evaluate a scaling constant as a potential parameter for maintaining similar milling performance for different mill scales. Perform tests in order to verify whether maintaining the scaling constant at the same level results in:

1. consistent size reduction degree
2. similar specific energy
3. comparable specific energy per rotation

Investigate these relationships in both dry and wet milling conditions. This objective aims to establish a quantitative measure that allows ball mill scale up without affecting its optimal performance.

Perform Multivariate Analysis with the Use of Calibrated Digital Twin

Apply the calibrated digital twin in a multivariate analysis of copper ore milling and use the simulations to acquire information on load dynamics and the dominant types of forces within the mill.

Investigate the Impact of Operational Parameters in Each Experimental Series

Investigate the impact of such operational parameters as mill diameter, filling degree, rotational speed, lifter size, lifter number, and slurry properties on the main performance indicators, including size reduction, energy consumption, and force distribution within the mill. Identify the most influential factors affecting ball mill performance and efficiency.

Identify and Quantify Correlations Between Parameters and Metrics for Different Scales

Identify and quantify correlations between mill diameter, operational parameters, and performance metrics in dry and wet milling environments and use them in the development of scale-up strategies. Establish relationships between mill size and performance applicable in the design and operation of ball mills in different scales.

Identify Future Research Directions

Provide recommendations for future research directions, with particular focus on refining the scaling constant approach and on tests that can be performed on industrial-scale copper ore mills to improve efficiency.

Chapter 5

Materials and Methods

This chapter presents the materials, methods, and experimental setup used in the analyses of the ball mill scale up process and in the development of a scaling constant. The experiments were conducted in a custom-designed laboratory-scale ball mill with exchangeable drums of various diameters. The mill was provided with sensors measuring power draw, torque, and rotational speed. The motion of the grinding media and ore particles inside the mill was recorded with a high-speed video camera.

The copper ore used in the experiments was prepared by mixing rocks from different exploration regions. It had known properties and size distribution. The grinding media were in the form of steel balls of various sizes, and their size distribution was calculated from the Bond equilibrium state equation. The rheology of the copper ore slurry used in the wet milling experiments was measured with a viscometer.

The experimental methodology involved assessing the size distribution and milling time, as well as identifying such data as the dynamic angle of repose and slurry surface profile from the video recordings. The milling process was studied on the basis of DEM-SPH simulations, and the model parameters were calibrated to match the experimental results.

The relationships between operational parameters and performance metrics for different mill scales was identified in a correlation analysis. A scaling constant was subsequently developed with an aim of replicating the energy transfer to ore during the milling process performed on different scales, and the proposed scaling strategy involved adjusting the rotational velocity and size distribution of the grinding media.

The scaling constant was tested both in controlled experiments and with the ANOVA-based statistical analysis. The Design of Experiments (DoE) approach served as a tool for further analyses into the influence of various operational parameters on mill performance. The results of the DoE analysis were interpreted using standardized effect sizes, regression equations, and model summary R^2 fits.

5.1 Test Stand and Materials

This section describes the laboratory-scale ball mill setup, including the exchangeable drums, sensors, and video recording equipment. It also presents the preparation process and the properties of the copper ore and steel balls, as well as the copper ore slurry used in both the dry and wet milling experiments.

5.1.1 Laboratory Ball Mill Specifications

The experiments were conducted using a custom-designed laboratory-scale ball mill with exchangeable drums 300, 400, and 500 mm in diameter. The internal diameter of each drum is 8 mm smaller than the external diameter. The mill has a transparent wall that allows real-time observations and recordings of the material distribution within the mill, as required for computer vision analysis (Figure 5.1).

Figure 5.1: Ball mills with various drum sizes

The mill is driven by a 1.5 kW electric motor with a rotational speed of 1415 RPM (revolutions per minute), and the drive is transferred from the motor to the drive shaft through a worm gear with a ratio of 25. The rotational speed of the drum can be controlled from 0 to the nominal 56.6 RPM by adjusting the supply voltage frequency with an inverter. This procedure also allowed RPM values above the critical speed for all mill drums. The mill shaft is supported by two ball bearings, and a quick coupler (conical and screw connection) allows the use of various drum diameters. The material is loaded through an opening in the drum. The mill can also accommodate up to 8 lifters arranged at uniform distances. Two sets of lifters were used in this research: one being 5 mm and another 15 mm in height. A schematic technical drawing of the mill is provided in Figure 5.2.

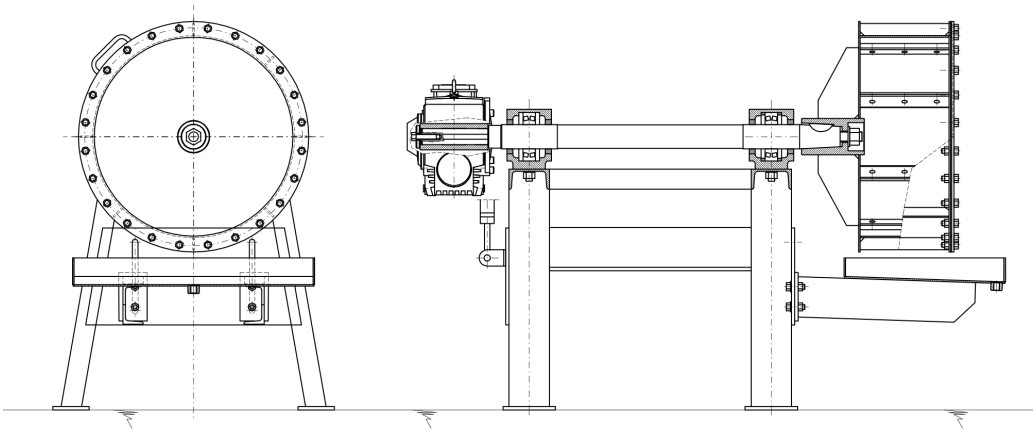

Figure 5.2: Schematic of laboratory-scale ball mill

The critical speed (N_c), given in RPM, is derived from the balance of gravitational and centrifugal forces and is calculated for the average mass-wise ball using the formula [70]:

$$N_c = \frac{1}{2\pi}\sqrt{\frac{g}{R-r}} \times 60, \tag{5.1}$$

where g is the acceleration due to gravity ($9.81\,\mathrm{m/s^2}$), R is the radius of the mill (in meters), and r is the radius of the balls (in meters).

5.1.2 Sensors

The experimental setup was provided with various sensors and devices measuring and recording the main parameters of the motor and drum shaft. The active power of the motor was determined on the basis of a signal from the inverter, while the torque of the drum shaft was measured with an HBM S2M/500N strain gauge mounted on the reaction arm of the gearbox. The rotational speed of the drum was recorded with the Hohner 36-131-2000 incremental encoder. The signals were acquired with the use of a BMCM measurement system operating at a sampling frequency of 50 Hz. The system comprised an analog signal amplifier BP16, a strain gauge data acquisition device AD16f, and a digital signal acquisition device IO16. The data was analyzed and interpreted in the NextView 4.6 software provided with an interface for real-time data visualization and recording into editable formats.

5.1.3 Video Recordings

The milling process was recorded through the transparent wall of the mill with the use of a Phantom VEO410L high-speed camera with a Carl Zeiss 100mm F2 lens and a polarizing filter. The camera was set to record images at 300 fps (frames per second), providing details on the motion of the grinding media and ore particles inside the mill. The position of the camera allowed the mills of all diameters to fit within the frame. The recordings of the charge motion inside the mill, saved with a resolution of 512x512 pixels in mp4 format, included the cascading and cataracting behavior of the grinding media and ore particles. Each recording comprised 18,000 frames, equivalent to one minute of mill operation, and was performed after a one-minute startup phase. This short recording time was dictated by the limitations of the transparent wall, which developed scratches already after several minutes, compromising the quality of the recordings. Therefore, the recordings had to be made at the beginning of the milling process.

5.1.4 Materials Properties

This subsection details the properties, preparation, and size distribution of the copper ore and steel balls used in the experiments. It also describes the preparation and rheological measurements of the copper ore slurry for wet milling experiments.

Copper Ore Properties and Sample Preparation

The copper ore used in the experiments was prepared by mixing rocks from all exploration regions of KGHM Polkowice, Lubin, and Rudna. The ore was crushed in a jaw crusher and sieved in 2 mm sieves in order to obtain feed with a dominant grain size (d_{80}) of

0.876 mm. A similar feed size is used in the industrial process of the 1st/2nd stages of copper ore milling. The ratio of the ore sample mass to its volume measured in water was $2194.93 \pm 98.51\,\mathrm{kg/m^3}$, and is referred hereinafter as ore density.

The approximately 800 kg of ore samples were reduced and averaged into 32 smaller parts in 5 iterations of the splitting operations performed in the Jones splitter (Figure 5.3). Each of the ore parts was stored in one of 32 containers and before it was used in an experiment, it was further reduced in size either in a Jones splitter or by conning and quartering, depending on the mass required in a particular experiment.

Figure 5.3: Jones splitter for sample preparation

The purpose of the preparation process was to produce not a general sample representative of all Polish copper ore deposits, but rather a uniform sample having a consistent behavior, and thus allowing comparable effects, in each experiment. The prepared ore feed was subjected to impact breakage, abrasion, and attrition grinding mechanisms inside the mill, depending on the operating conditions.

The ore consists of dolomite, sandstone, and shale in unknown proportions, which vary depending on the region. The literature indicates that sandstone content is between 13.5-72%, dolomite—22-72.6%, and shale—6-13.9% [174]. After mixing rocks from all of the regions, the composition of the ore is expected to be more balanced, with about 45% of sandstone and dolomite, and about 10% of shale. The grindability work index for copper ore stones and mixes of them ranges from 8.3 to 16.9 kWh/t [174].

Grinding Media Properties

The grinding media used in this study were steel balls with a nominal diameter of 35 mm. They were selected on the basis of industry guidelines [55] and commercial availability. The steel balls contribute to impact breakage and abrasion of the ore particles. The measured density of the steel balls was $7800.92 \pm 55.41\,\mathrm{kg/m^3}$. The range of ball sizes was from 15 to

35 mm, with 5 mm increments. The size distribution of the steel balls was determined using the Bond equilibrium state equation [13, 55]:

$$y = \left(\frac{x}{B}\right)^{3.8}, \tag{5.2}$$

where y is the percentage of the total equilibrium charge that passes a given size x (mm), and B is the makeup/recharge size of the balls (mm). The steel balls and the prepared load can be seen in Figures 5.4 and 5.5, respectively.

Figure 5.4: Assortment of grinding ball sizes

Figure 5.5: Representative grinding media and ore charge

Slurry Preparation and Rheology Measurements

Copper ore slurry for wet milling experiments was prepared by mixing the ore with water. For the purpose of simulations, the viscosity of the slurry was characterized using an

AMETEK Brookfield viscometer (Figure 5.6). Initially, five slurry viscosity measurements were performed for the same standardized material subjected to different milling times of 0-60 minutes and with densities from 1500 to 1700 kg/m^3. The measured viscosity ranged between 0.008 and 0.042 Pa·s, with lower values corresponding to lower densities and shorter milling times, indicating that viscosity increases with both density and milling time.

Figure 5.6: Viscometer for copper ore slurry analysis

The wet milling experiments were performed for slurry densities outside the previously measured ranges. The density was approximated by mixing ore and water based on their known densities. The purpose was to develop a reproducible method suitable for an industrial scale, and therefore the target density is closely approximated through direct mixing in specific proportions. Of several models tested for the ability to fit the data and extrapolate viscosity values, some yielded unrealistic or even negative values. A Random Forest Regressor model was eventually developed as a tool capable of predicting and extrapolating the absolute viscosity, ν_a, in Pascal-seconds (Pa·s), with allowance for the milling time and density as variables.

The slurry density used for calibrating the numerical model was 1400 kg/m^3. The model predicted an absolute viscosity of approximately 0.01134 Pa·s for a specific test scenario with a slurry density of 1400 kg/m^3 and with a milling time of 15 minutes. This time duration represents half of the time intended for the entire experiment. The model demonstrated an R^2 value of 0.8402, indicating a good fit to the data and reliable prediction capabilities. The kinematic viscosity, ν, for the copper ore slurry was calculated by dividing the absolute viscosity by the density of the slurry:

$\nu = \frac{0.01134}{1400} \approx 8.10 \times 10^{-6}$ m^2/s.

The positive value of kinematic viscosity indicates that the material has a good resistance to flow and shows real physical behavior under given conditions.

5.2 Size Distribution and Milling Time Assessment

The sample was prepared for size distribution measurements following a consistent procedure, in which the sample size varied depending on the adopted measuring technique. In

the case of feed grain size distribution, the sample was initially reduced in Jones splitters (Figure 5.3) and then assessed in a dry sieving procedure (Figure 5.7). In all dry milling experiments, the product was subjected to initial size reduction in a smaller Jones splitter. However, in the case of the pilot exploratory milling, the size reduction of the product was measured by wet sieving, as dry sieving is unsuitable for assessing the d_{80} grain size produced in wet milling.

Figure 5.7: Stack of sieves for particle size distribution

The samples were further reduced to laboratory size using the coning and quartering method, as shown in Figures5.8 and 5.9). In the wet milling experiments, the slurry was removed from the mill and transferred to a container. The mill was subsequently washed with a water hose in order to remove the residual material and also transfer it to the container. Due to the excess water in the container, the material was allowed to settle at its bottom, and then the water above the settled material was removed from the container. The remaining water was mixed with the ore using a stirrer until a uniform slurry was obtained. Samples were then taken from different parts of the container using a needle-free syringe. Such a procedure allowed a more representative sample, which was then transferred to a silicone mold.

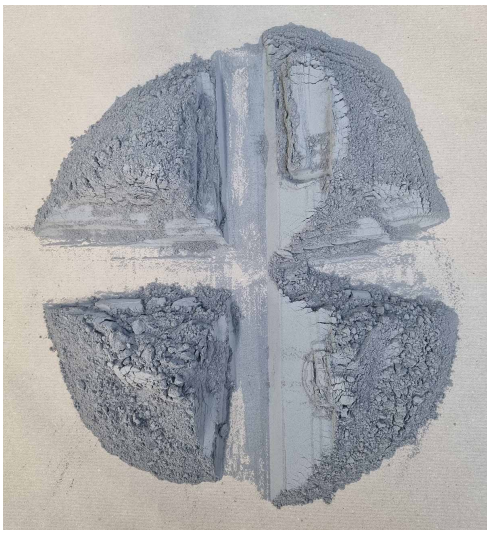

Figure 5.8: Sample preparation with a quartering method

Figure 5.9: Prepared sample batches ready for analytical testing

The prepared wet samples (Figure 5.11) were transferred to an oven and dried for a several hours. The dried samples were consolidated and carefully processed with low force in a ceramic mortar and pestle in order to remove potential lumps and allow grain size analysis. The standard procedure of coning and quartering was then applied, as described above.

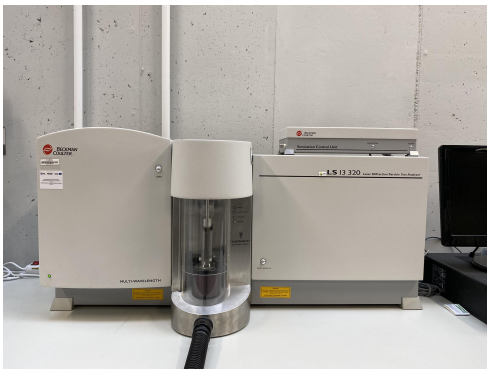

Figure 5.10: LS 13 320 Particle size analyzer for milling product granulometry

For the larger number of product samples obtained in the final experimental series (48 samples in total), the Laser Diffraction method was chosen due to its high accuracy and repeatability of measurements for a broad range of particle sizes (0.017 μm to 2000 μm). The particle size distribution of the product after grinding in the laboratory mill was identified with the use of an LS 13 320 particle size analyzer (Figure 5.10). The particle size distribution is measured by analyzing laser diffraction patterns formed when a laser beam passes through a sample of particles. The employed powder head is designed for analyzing bulk materials and ensures even distribution of the sample and optimal conditions for precise measurements. In laser diffraction, the bulk material is dispersed in air or another gas and passed through a laser beam in order to avoid agglomeration.

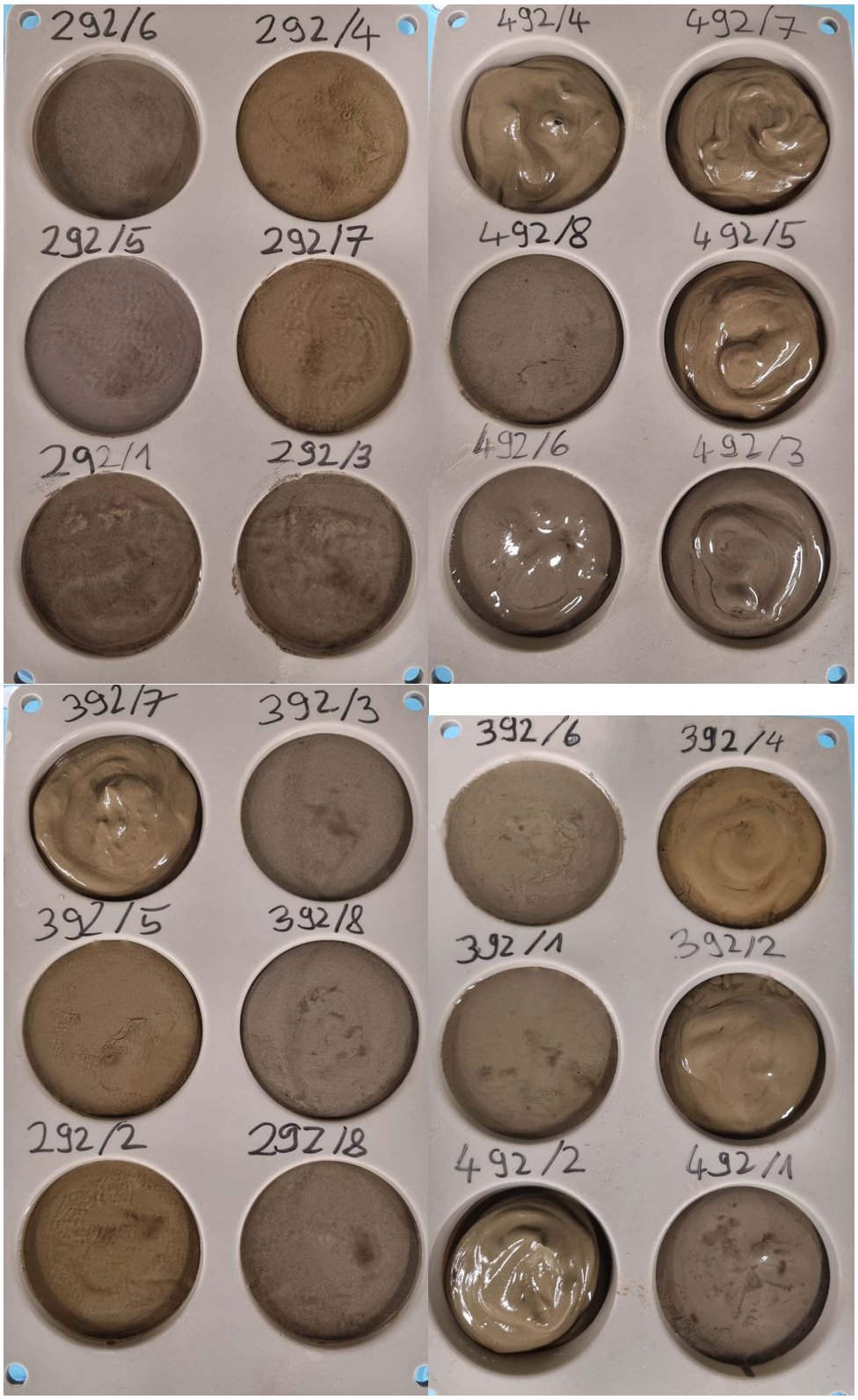

Figure 5.11: Set of wet milling samples labeled for drying process

5.2.1 Size Distribution Analysis

The size distribution analysis for each product and feed followed industry standards, and the cumulative size distribution curves were fitted to the sieve analysis data. The horizontal axis represented the sieve size opening, and the vertical axis represented the cumulative percentage passing. The size for 80% passing (D_{80} for feed or d_{80} for product) was interpolated on the basis of the two closest measurements. The study focused on the size reduction parameter, defined as D_{80}/d_{80}, which indicates the ratio of the feed grain size (D_{80}) to the product grain size (d_{80}) and thus demonstrates the effectiveness of the process.

In the case of sieve analysis, the percentage passing for each sieve was calculated by mass. In contrast, laser size measurements were performed by volume, providing direct diameters of particles and more detailed results. However, it is important to note that if the copper ore consists of materials with different densities and grindabilities, such as dolomite, sandstone, and shale, the results may be to some extent biased. For example, the measurements can be biased if a material with lower density is much finer than other materials. In order to simplify the assessment of d_{80}, an assumption was made that differences in the mass of minerals in individual fractions would not significantly affect the results. Based on another assumption, calculations of the cumulative percentage by volume have an identical effect as calculations by mass, because the volume is multiplied by the average density of the ore. This assumption was necessary in the absence of a simple method for determining the prominence of different mineral types in each fraction for such a large sample size.

5.2.2 Milling Time

The effect of milling time on particle size distribution translates into the optimal duration for the experimental series. A shorter milling time was preferred, as it allows the identification of the most dynamic changes in ore size distribution. The experiments were conducted on an averaged standardized copper ore sample, in a mill provided with the medium diameter (400 mm) drum, a filling degree of 0.4, and a critical speed of 0.75. Three grinding times were selected for the initial dry milling experiments: 40, 60, and 80 minutes.

The cumulative percentage passing curves for different milling times are presented in Figure 5.12. It demonstrates that longer milling times result in finer particle size distributions. For the 40, 60, and 80-minute milling times, the d_{80} values were 0.103 mm, 0.08 mm, and 0.068 mm, respectively, with the corresponding size reduction degrees of 8.5, 10.95, and 12.88. These results indicate that the size reduction degree increases with longer milling times.

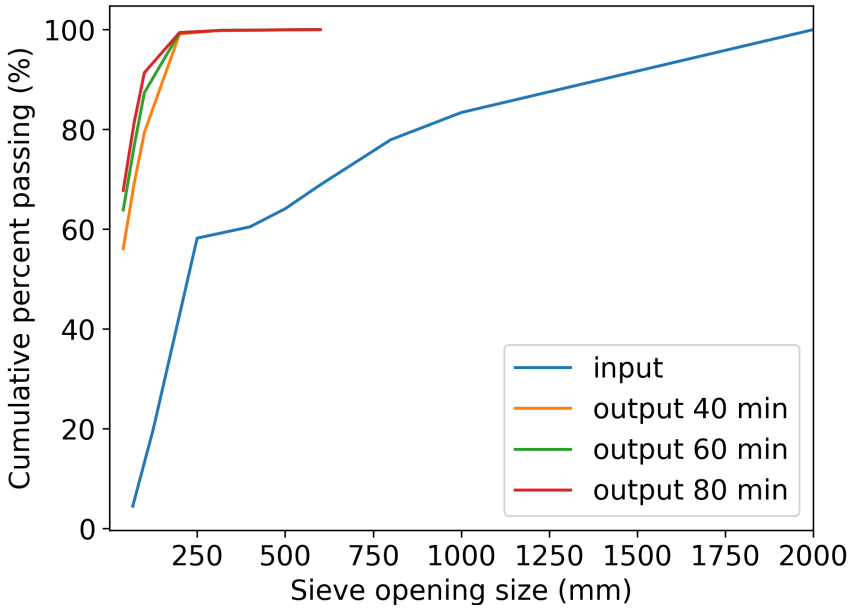

Figure 5.12: Cumulative percent passing for various milling durations

The relationship between milling time and d_{80} was analyzed with the use of various fitting functions, including linear, polynomial, exponential, logarithmic, and power-law models (Figure 5.13). The goodness of fit was evaluated using the Sum of Squared Residuals (SSR), and the logarithmic fit provided the best description of the data (SSR=4.214e-06). This logarithmic relationship suggests that the most significant size reduction occurs early in the milling process, and the size reduction rate decreases as the milling time increases.

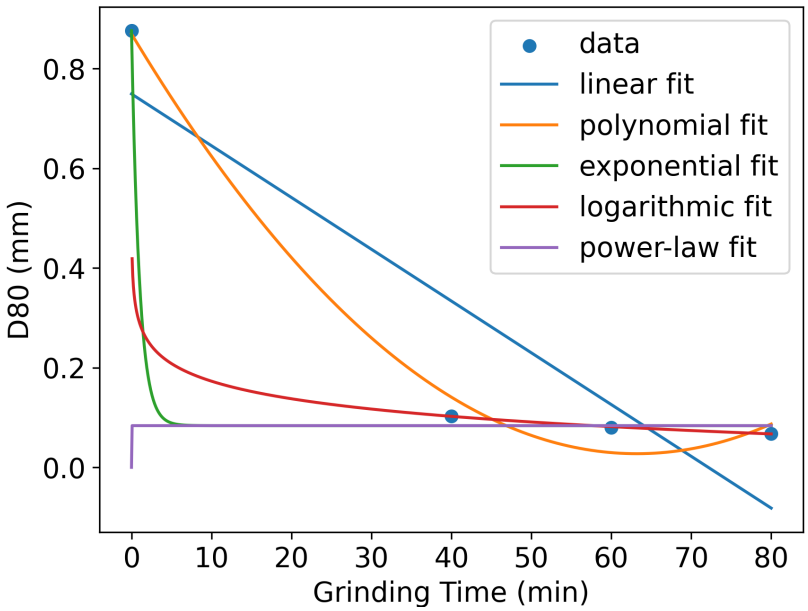

Figure 5.13: Fitting functions for milling time vs. d_{80} relationship

Based on the above findings, a 30-minute milling time was selected for further experiments, as it offers a balance between the desired size reduction and a reasonable experiment duration, and as it ensures that the most dynamic changes in feed size distribution are recorded.

5.3 Video Analysis

This section presents methods used for analyses of the high-speed video recordings of the milling process, including image pre-processing, ball segmentation, and the extraction of relevant data, such as the dynamic angle of repose and slurry surface profile. The above are used for calibration and experimental series recordings.

5.3.1 Calibration Recordings

This subsection describes the image pre-processing steps as well as methods used for the analyses of calibration recordings. These methods include ball segmentation performed with the use of the Segment Anything Model (SAM), dry milling analysis with thresholding, and wet milling analysis with the use of the semi-automated approach with an interactive GUI.

Image Pre-processing

The video analysis procedure begins by loading the video and sampling frames at regular intervals. The mill outline is then detected using the Hough Circle Transform (Figure 5.14), which allows the frames to be centered and resized to match the actual mill dimensions. An additional mask is applied in order to ensure that the focus is solely on the internal part of the drum (Figure 5.15). A set of 100 frames separated by equal time steps is extracted from each recording for further analysis.

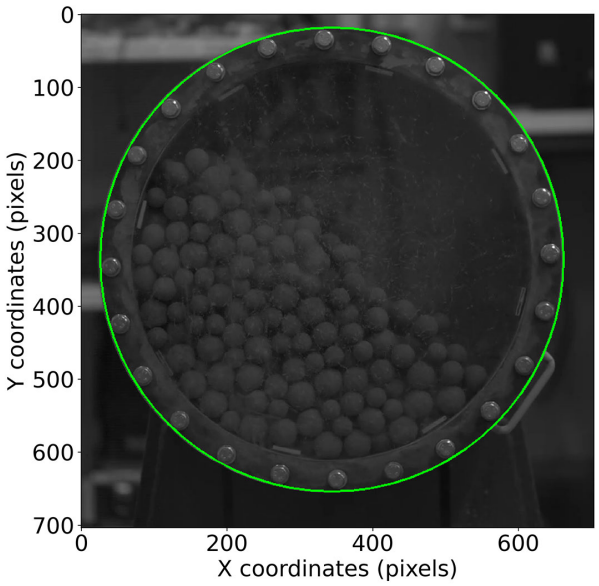

Figure 5.14: Edge detection in mill visualization

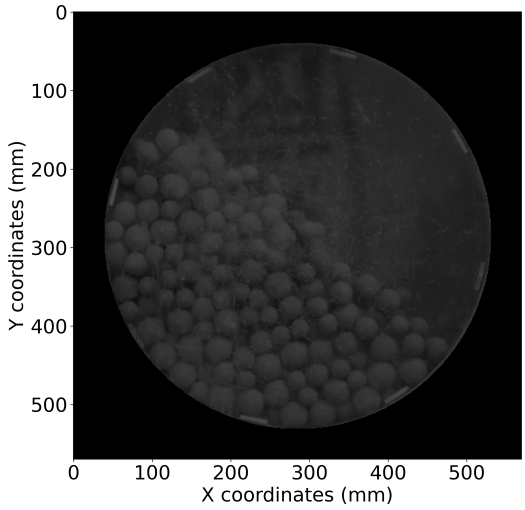

Figure 5.15: Processed image with masking, centering, and scaling

Balls Only Analysis

The image segmentation and the generation of masks for the balls in the load in the rotating drum were performed with the Segment Anything Model (SAM) by Meta [91]. The SamAutomaticMaskGenerator detected the balls and generated their masks (Figure 5.16). The binary masks were then accumulated in the form of a heatmap in order to identify regions with frequent ball presence. The heatmap was subjected to thresholding and smoothing techniques (Figure 5.17) so as to extract the top edge coordinates of the ball load (shoulder). The dynamic angle of repose was calculated for the cascading balls by performing linear regression on these coordinates (Figure 5.18). The points located 60 mm to the right of the highest detected point were excluded in order to ensure that the line is fitted to the most linear part of the slope. For debugging purposes and threshold adjustment, the fitted line was visualized over the original frames (Figure 5.19).

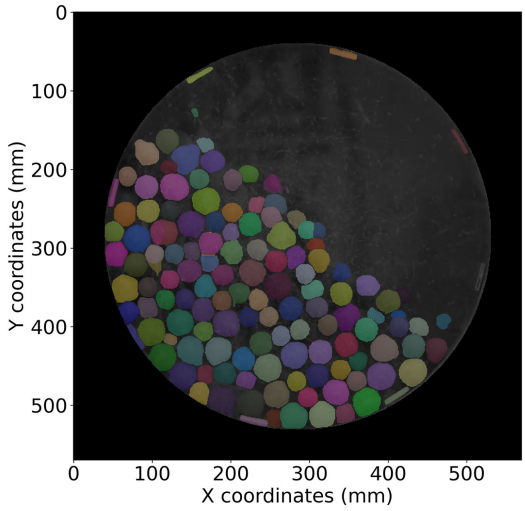

Figure 5.16: Ball segmentation using Segment Anything Model (SAM)

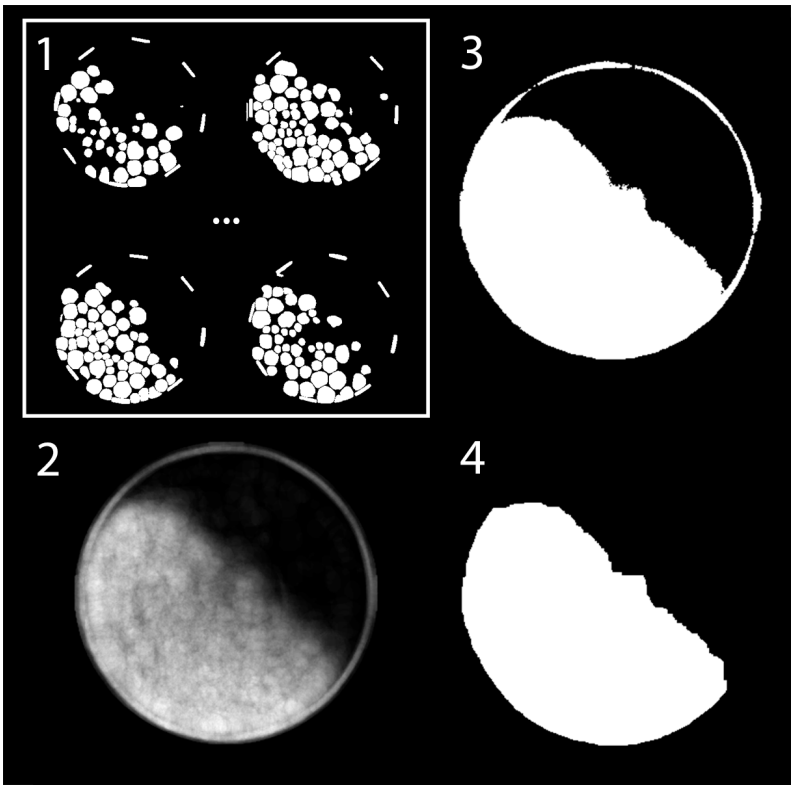

Figure 5.17: Stages of image analysis for mill interior—1: binary images from masks, 2: heatmap generation, 3: thresholding, 4: post-smoothing

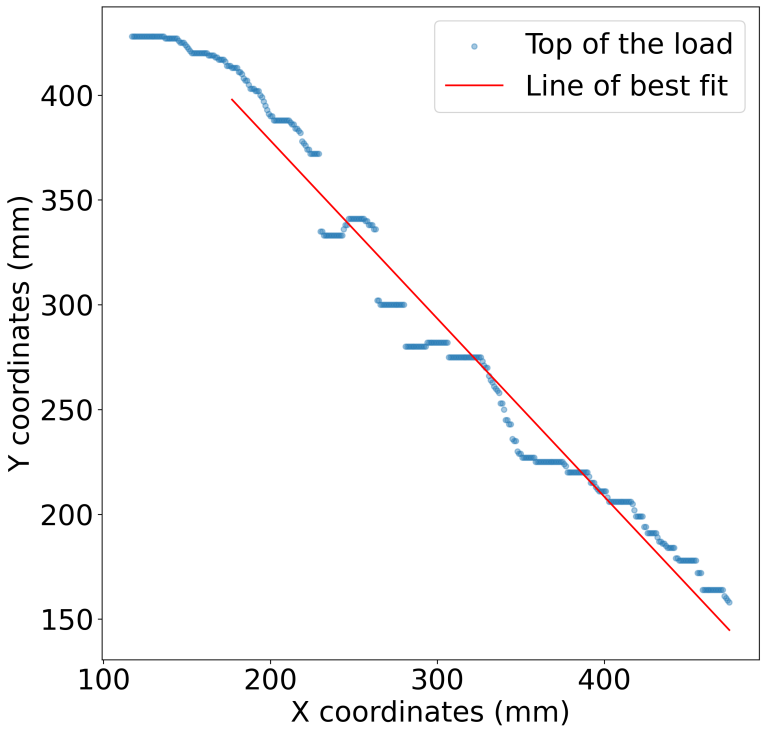

Figure 5.18: Top load position detection and linear fit analysis

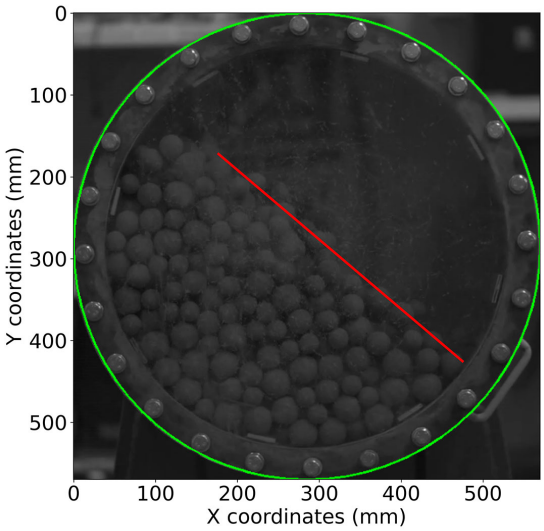

Figure 5.19: Overlay of detected charge angle in mill recording

Dry Milling Analysis

The difference between dry milling analysis and the balls-only scenario lies in the initial detection and isolation of the mill load area. The main steps in the dry milling analysis include applying thresholding directly to pre-processed images so as to generate binary images (Figure 5.20), to create a heatmap from the binary images, and to apply again thresholding and smoothing. The top edge of the load is then detected, and its coordinates are extracted. Finally, the dynamic angle of repose is calculated using linear regression on the extracted coordinates, as was the case in the previous method.

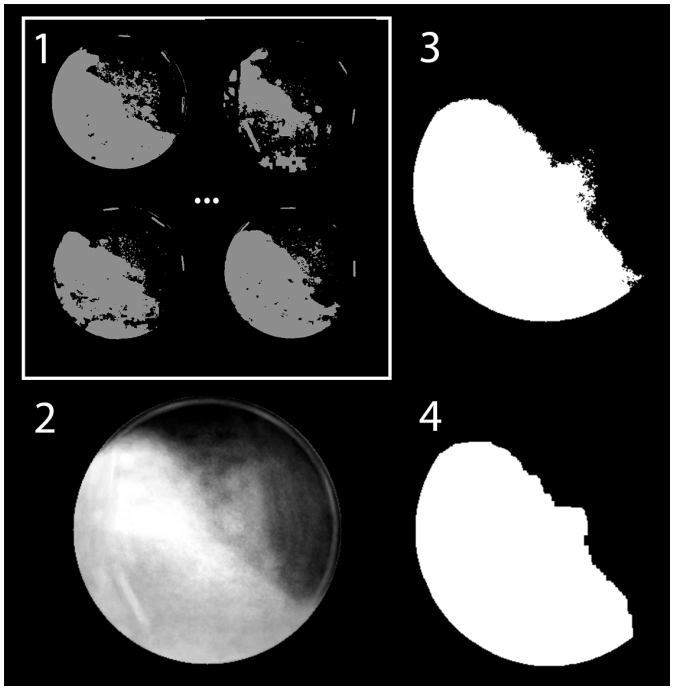

Figure 5.20: Image processing sequence for dry milling analysis—1: binary images, 2: initial heatmap, 3: post-threshold heatmap, 4: smoothed final image

Wet Milling Analysis

Wet milling entails complications which prevent the application of fully automated computer vision techniques. Therefore, a semi-automated approach utilizing an interactive GUI was developed.

This method is based on the phenomenon of slurry pooling. As a slurry pool forms in the toe region of the mill, the slurry surface profile can be detected owing to the balls scraping slurry from the transparent wall when they pass over the slurry surface.

The main steps in the analysis include: (1) manually selecting points in order to delineate the slurry surface with the use of the custom GUI (Figure 5.21) over 100 time steps; (2) preparing and correcting the selected points for the coordinate system used in the analyses; (3) fitting a quadratic curve to the selected points in order to model the slurry surface; (4) calculating the fit parameters and evaluating the fit uncertainty; and (5) visualizing the fitted curve with the original data points and confidence interval bounds.

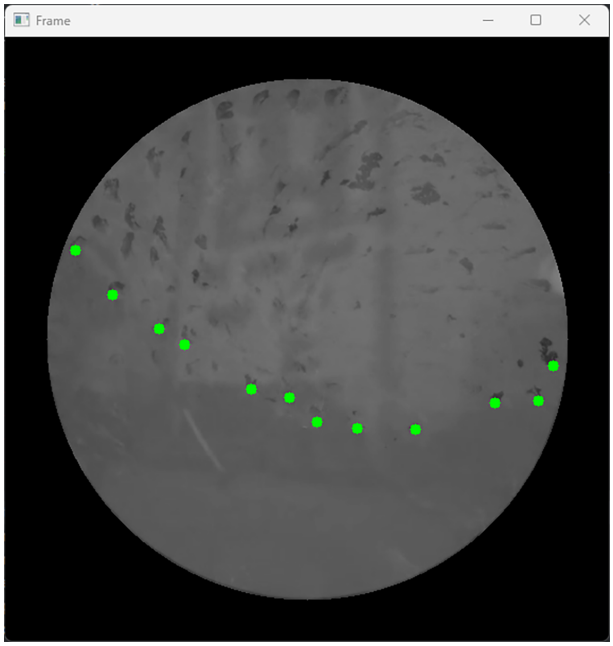

Figure 5.21: Custom GUI for delineating the slurry surface

5.3.2 Normalization of Experiment Recordings and Data Extraction

The video-analysis code is designed to process multiple recording files sequentially, as well as to employ additional pre-processing steps not used in the case of the calibration recordings. The purpose of the entire process, implemented with the use of the Python OpenCV library, is to normalize the recordings and ensure consistent thresholding across all files.

The visibility and contrast of the mill region is enhanced by applying histogram equalization to the cropped frames. This technique normalizes the brightness distribution and improves the overall image quality. The equalized frames are then converted to binary images using a thresholding operation, similar to the thresholding used in the calibration process. The result is a binary mask, in which white pixels represent the charge in the mill and black pixels represent the background.

In the final experimental series, the extracted charge area is not used to calculate the dynamic angle of repose, but rather to determine the center of gravity of the binary mask, which represents the effective mass of the entire charge reduced to a single point with coordinates (c_x, c_y).

The behavior of the mill over time is analyzed by selecting a subset of 100 frames from the video recording at regular intervals. The centroid coordinates are calculated for each selected frame and used as a basis for the calculation of the average centroid position, serving as a representative measure of the overall location of the charge in the mill.

The centroid coordinates are then transformed into a coordinate system, consistent with the system used later in the simulation environment, with the point (0, 0) located at the center of the rotational axis. The final calculations include the length of the moment arm and the angle between the vertical axis and the arm from the mill center to the midpoint of the centroid.

5.4 DEM-SPH Simulation Methodology

The milling process was studied with the use of Discrete Element Method-Smoothed Particle Hydrodynamics (DEM-SPH) simulations in the DualSPHysics open-source framework. The simulations were arranged so as to precisely replicate the experimental conditions and enable a direct comparison between the simulated and experimental results. The DEM-SPH simulations provide valuable information on the milling process, and in particular on the particle-level dynamics and interactions within the mill, which are difficult to observe experimentally.

5.4.1 Geometry and Material Property Definitions

The mill geometry and material properties for the DualSPHysics simulator were defined in an XML script. The main components of the geometry definition include the mill drum, modeled as a cylinder with dimensions matching the experimental setup, and the lifters, modeled as boxes with specified dimensions and spacing. The grinding media were modeled as spherical particles with a size distribution based on the experimental data. For wet milling simulations, the slurry was modeled as SPH particles whose properties were based on the experimental rheology measurements and set density. All materials, including the drum and balls, were modeled as steel elements with identical parameters.

The material properties, such as density, Young's modulus, Poisson's ratio, and coefficients of restitution and friction, were assigned to the corresponding elements in the XML script. These properties are listed in Tables A.1 and A.2 in Appendix A.

5.4.2 Simulation Parameters and Solver Settings

The DualSPHysics solver settings and parameters were carefully adjusted so as to ensure numerical stability, accuracy, and computational efficiency. A fixed time step (DtFixed) of 1e-5 s was used for time stepping, while the interpolation was performed with the Wendland kernel function. The artificial viscosity was used with a viscosity value based on experimental measurements. The interactions between the particles and the mill boundaries were analyzed with the use of the Dynamic Boundary Conditions (DBC). The particle positions were corrected using full shifting mode in order to maintain a uniform particle distribution and prevent particle clustering.

The simulation parameters and their corresponding values are listed in Table A.2. These settings were selected on the basis of a combination of numerical stability, accuracy, and computational efficiency requirements so as to ensure that the simulations closely mimicked the experiment conditions while maintaining a reasonable computation time.

5.4.3 Boundary and Initial Conditions

The mill walls and lifters were assigned boundary conditions reflecting their functions in the simulation as moving objects. The initial conditions for the positions and velocities of the balls were based on the experimental setup and allowed for such factors as the filling degree and the distribution of grinding media. These examples of initial conditions are shown in Figure 5.22.

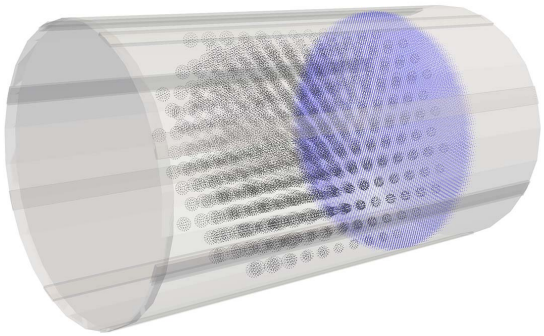

Figure 5.22: Simulation setup showing fixed and moving boundaries with grinding media

In the simulation environment, each floating object, referred to as a free moving object, requires a set of initial position coordinates. One of the related problems is how to densely pack the spheres while leaving space for the slurry, which is initially created inside a defined cube. The cube volume was defined in each simulation run on the basis of the slurry volume used in the experiment. The problem of possible overlapping required a workaround approach.

In order to ensure proper sphere packing and to avoid overlaps, the mill is initially modeled as an extended cylinder, and a moving wall is used to compress the particles into the desired volume during the first few seconds of the simulation, as shown in Figure 5.23. A hexagonal grid was developed for each mill diameter in such a manner that the distances between the grid nodes are sufficient to accommodate the balls with the largest diameters without causing them to overlap with each other or with the lifters inside the mill. The thus developed matrix was placed multiple times in the 3D space inside the cylinder, with equal distances from each other, so as to avoid overlapping.

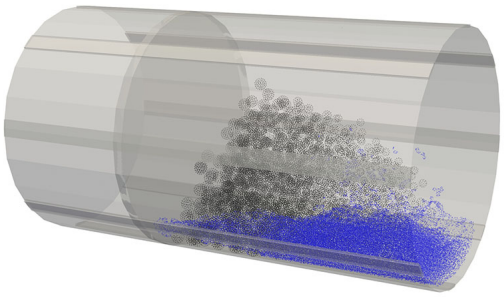

Figure 5.23: Initial particle compression with moving mill wall simulation

The geometry and the XML file for the simulations were produced with a dedicated custom algorithm. It iterates over the data in the experimental design table and over the corresponding parameters, such as the number of balls of each diameter, and populates the geometry with the proper ball sizes, lifter configuration, and slurry volume for each run of the simulation. This automated approach ensures consistent and accurate geometry generation for each simulation case.

5.4.4 Simulation Data Output and Post-processing

The simulation served to collect such relevant data as the positions of grinding media and slurry particles, as well as the forces acting on the grinding media. The data was recorded at specified intervals, as illustrated in Figure 5.24. The data was then post-processed in order to extract information comparable to that obtained in experimental measurements.

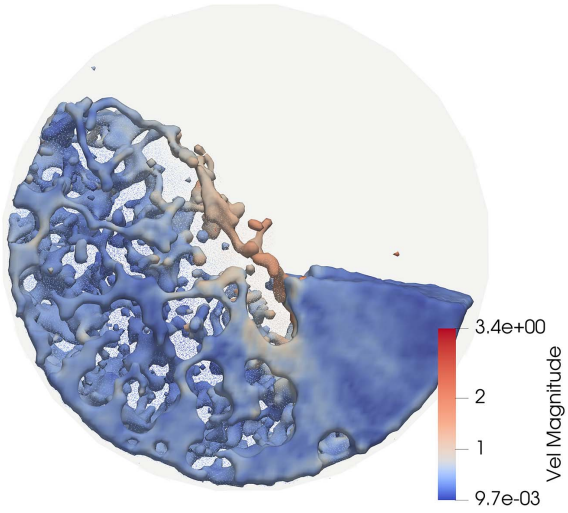

Figure 5.24: Final charge distribution and velocity profile in ball mill simulation

After each simulation, data about ball positions was extracted (Figure 5.25, on the left) for each of the sampled time steps. Due to the use of the same lifter heights for all mill diameters, in the mill having the smallest diameter some single balls were lifted higher than the others and fell down freely; this phenomenon produced the balls that can be seen in the air on the left-hand side in Figure 5.25. For that reason, a heatmap (Figure 5.25, on the right) showing the most frequent positions of the balls in the charge was created with

an aim to decrease the impact of the lifted balls on the overall angle measurements. This phenomenon occurred in the recordings and simulation, so the same further analysis flow was used for comparable results. The dynamic angle of repose was calculated from the positions of the steel balls, as in the case of the data from the experimental recordings. The center of gravity and center of circulation of the grinding media were also determined from the position data.

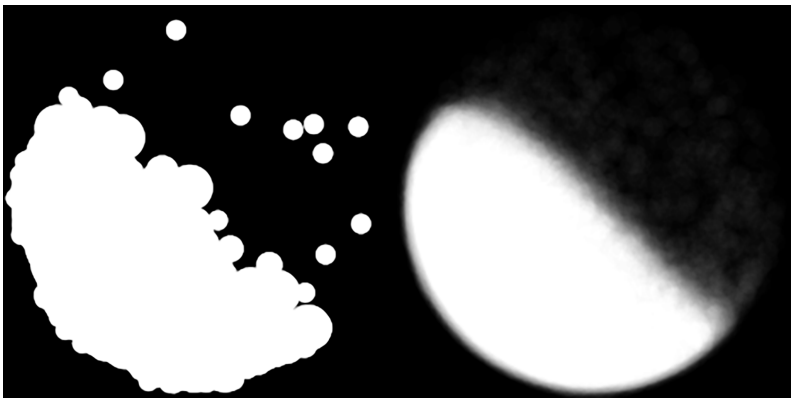

Figure 5.25: Binary image of sphere positions and corresponding heatmap from simulation data

For wet milling simulations, the slurry surface profile was extracted from the positions of the SPH particles representing the slurry. This information is of significant value for analyzing the behavior of the slurry within the mill during the milling process.

The data from the simulations was used for the calibration and validation of the DEM-SPH model. Owing to the comparison of the simulation results with the experimental data, the model can be assessed for accuracy and reliability. This comparison allows the identification of any discrepancies between the simulated and experimental results. As a result, the model may be further refined if necessary. The calibrated and validated DEM-SPH model can be then used to predict the performance of the mill under various operating conditions, and thus to aid the optimization of both mill design and operational parameters.

Forces

In the DualSPHysics simulation, the forces acting on the steel balls can be extracted from the output CSV files, which contain tangential and normal force components (F_x, F_y, F_z) for each steel ball (mk) at each time step. The high-level approach for extracting and analyzing the forces involves two main steps: (1) extracting forces by reading force components from CSV files and calculating the resulting force magnitude (F) for both tangential and normal forces; (2) computing the ratio of tangential force to normal force (F_t/F_n) for each steel ball and the average force ratio for all steel balls and time steps.

As incorporating real material properties requires significant computational power and extended simulation time, the simulations were not calibrated to provide realistic force magnitudes. However, analyses of the proportions of forces still provide valuable information on the dynamics of the ball milling process, such as the degree of abrasion and impact-driven mechanisms.

The force proportion analysis can be extended so as to allow investigations of spatial and temporal variations of forces within the mill drum, the identification of local hotspots,

and the design of milling equipment with uniform force distribution and minimized wear and tear. A heatmap with hexagonal binning was generated on the basis of a Python function to represent the distribution and intensity of the average tangential to normal force ratio over the two-dimensional space of the mill drum. This visualization technique enables the identification of areas where shearing or impact forces dominate and provides further information on the milling process and potential optimization opportunities.

Center of Gravity and Center of Circulation

The simulation data consists of two main components: an XML definition file, which contains the initial setup and parameters, and a CSV file, which stores time-dependent data, including the positions and velocities of floating objects. The center of gravity and the center of circulation is determined from this data in the following steps: (1) extract the number of floating objects and their radii from the XML file; (2) process the CSV file in order to extract the position coordinates (x and z) for each object at each time step; (3) calculate the center of gravity using the weighted average of the position coordinates, with weights determined by the masses of the objects. With a spherical shape assumed, the mass of each object is proportional to the cube of its radius; (4) calculate the center of circulation by taking the geometric centroid of the floating objects, which is the average of their position coordinates.

Additional calculations may provide further data on the orientation and tilt of the system, e.g. on the angles between the vertical axis and the lines connecting the origin with the center of gravity and center of circulation (moment arms). These angles are the source of information about the distribution of mass and the overall tilt of the system.

5.5 Simulation Calibration Methodology

The DEM-SPH model parameters were calibrated so as to match the experimental results. The calibration process was performed in three stages: (1) balls only, (2) dry milling, and (3) wet milling. The main calibration parameters were the Coefficient of Restitution (COR) and the coefficient of kinetic friction (μ_k). The COR affects the degree of impact breakage and energy dissipation during particle collisions.

The COR is the ratio of final to initial relative velocities between two particles after a collision. It determines the elasticity of collisions and affects energy dissipation. The μ_k is the ratio of maximum to normal friction force between two surfaces and determines the frictional behavior of the system.

The calibration ranges for these parameters were based on values provided in the literature and obtained in preliminary simulations. The COR varied from 0.3 to 0.55, while the μ_k varied from 0.3 to 0.7. Higher values of these parameters caused the simulations to become unstable.

It is important to note that copper ore particles are not simulated directly, as their majority is under 1 mm in size, and simulating them directly would cause the experiments to require unreasonably long computation times. Instead, this research employs an approach consisting in adjusting contact parameters between grinding media so as to simulate the behavior of balls as if in the presence of ore particles.

In the ball-only scenario, only the ball-to-ball contact parameters were taken into account. In the dry milling case, the ball-to-ball contact parameters were adjusted to compensate for the lack of ore and to model the impact of ore on the behavior of the

grinding media. In the wet milling scenario, the parameters from the ball-only case were used, and the ore with the water were modeled as slurry SPH particles.

This calibration approach enables an accurate representation of the milling process in the DEM-SPH model. It allows for the effects of ore particles without directly simulating them, thus reducing computational complexity and simulation time.

5.5.1 Iterative Calibration Algorithm

The calibration process for the DEM-SPH model involves several steps: (1) define initial parameter values and ranges based on the literature and preliminary simulations; (2) run DEM-SPH simulations for the three mill diameters using the current parameter values; (3) extract relevant data from the simulations, e.g. the dynamic angle of repose or slurry surface profile; (4) update parameter value and return to step 2.

Three simulations with three different mill diameters were performed for each iteration, and the obtained angles of repose were compared to those extracted from the processed images. The Sum of Square Errors (SSE) was recorded for each iteration. The ball calibration data from the first six iterations, along with the coefficient and SSE combinations, served to interpolate values between the points. The calibration algorithm was designed in such a manner that the successive combinations of the tested coefficients resulted in the lowest SSE in the interpolated space. The algorithm is stopped when the three successive combinations do not provide a result optimized with respect to the previous best combination.

The entire sets of data, including the measured angles from the simulations performed as part of the ball calibration, were still useful for calibrating the balls in the presence of ore, as the ore was not simulated separately. All of the measured angles were compared to those measured from dry milling recordings so as to obtain an initial interpolated response surface. The subsequently employed algorithm was not changed, and it explored combinations that could reduce SSE until three successive tests did not provide the best result.

Calibration of the liquid required adjusting either kernel parameters or viscosity or both. The behavior of the liquid was considered satisfying when the slurry surface curves for both the recordings and the simulations fitted within the 95% confidence intervals of each other.

This iterative calibration process ensures that the DEM-SPH model accurately represents the real-world milling process by allowing the model parameters to be tuned in such a manner that the difference between the simulated and the experimental results is minimized. The calibration is performed systematically, starting with ball-only simulations and progressively incorporating ore and slurry effects, so that each component of the model is properly calibrated before moving on to the next stage.

5.5.2 Calibration Experiments

The first run in each series of designed experiments was a calibration run and was thus performed with 30% of the critical speed instead of the nominal speed for the run.

Balls Only: The ball-only experiments were performed in order to calibrate such DEM model parameters as the coefficient of restitution and the coefficient of friction. These

experiments were conducted for different ball size distributions and mill operating conditions. The results from the experiments were compared with the simulations so as to adjust the model parameters. Figure 5.26 shows the mill prepared for the calibration experiment with the cascading charge comprising balls only.

Figure 5.26: Ball mill filled with grinding media

Dry Milling: Dry milling experiments were conducted with copper ore and grinding media in order to calibrate the DEM steel ball parameters with adjustment for ore particles. Figure 5.27 shows the mill prepared for the calibration experiment with the charge comprising balls and ore. The experiments were performed with varying parameters and for three mill diameters. The experimental results were compared with the simulations so as to adjust the model parameters.

Figure 5.27: Ball mill with dry feed

Wet Milling: Wet milling experiments were conducted in order to calibrate the SPH model parameters with adjustment for the slurry phase, including viscosity and kernel parameters. Figure 5.28 shows the mill prepared for the calibration experiment with the

charge comprising slurry and balls. The slurry used in the experiments consisted of the grinding media with water and copper ore. The calibration was performed only for a slurry density of 1400 kg/m^3 because higher-density slurries adhered extensively to the transparent wall, complicating the observation of the process.

Figure 5.28: Ball mill with wet charge

The calibration process was performed systematically, starting with ball-only experiments aimed at calibrating the DEM model parameters, followed by dry milling experiments aimed at adjusting the parameters of steel balls so that they behave as if in the presence of ore particles, and finishing with wet milling experiments aimed at calibrating the SPH model parameters for the slurry phase. A comparison of the experimental results with the simulations at each stage allowed the model parameters to be iteratively adjusted so as to ensure that the DEM-SPH model accurately represents the real-world milling process under various operating conditions and material compositions.

5.6 Sensor Data Analysis

The analyses also involved data form the mill sensors, including the power draw, torque, and rotational speed of the mill. The data was used in calculations of the energy consumption under different operating conditions and served to provide information on the influence of various parameters on the efficiency of the mill. Furthermore, the relationships between the operating parameters and the performance metrics was used to identify the optimal settings for the mill. The analysis of the operation of the mill also focused on detecting anomalies or instabilities which could potentially lead to equipment failure or reduced product quality.

5.6.1 Signal Pre-processing

The first step in the signal pre-processing pipeline was to detect and remove outliers from the raw data using the Z-score method. The Z-score was calculated for each data point, and points exceeding a specified threshold (default: 3 standard deviations) were considered outliers (Figure 5.29). These outliers were then replaced with the mean value of the non-outlier data points. This process is applied to each signal in the original data, including RPM, power, and torque, so as to ensure data integrity and reduce the influence of extreme values on subsequent analyses.

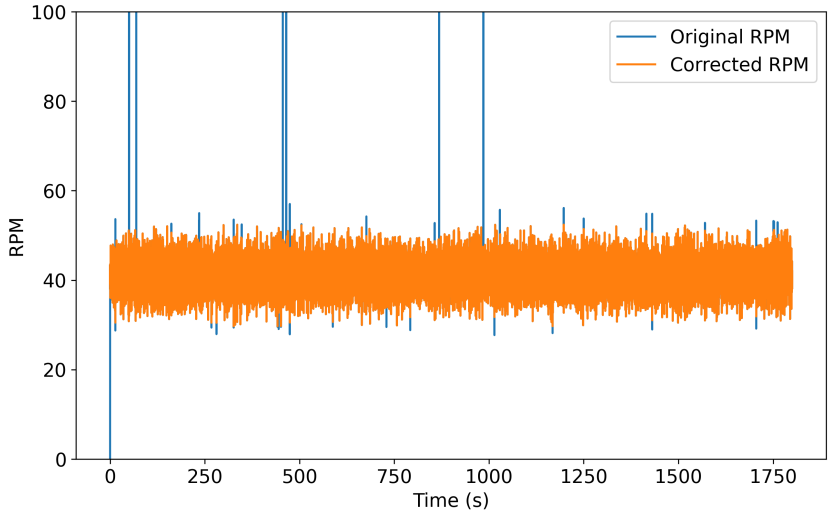

Figure 5.29: RPM signal correction

After the outliers were removed, the Savitzky-Golay filter was applied in order to smooth the signal and reduce high-frequency noise while preserving the underlying trends (Figure 5.30). The Savitzky-Golay filter is a digital smoothing filter that fits a polynomial of a specified order to a sliding window of data points. For the purpose of this analysis, a window size of 3001 was selected, as it corresponds to a duration of 1 minute at the sampling rate of 50 Hz (1 sample every 0.02 seconds). Owing to this larger window size, the overall trends can be observed in a minute- rather than second-scale, as short-term variations are smoothed and the longer-term behavior of the signal is emphasized. The polynomial order is set to 3, which is a value typically sufficient for observations of general trends without overfitting to noise.

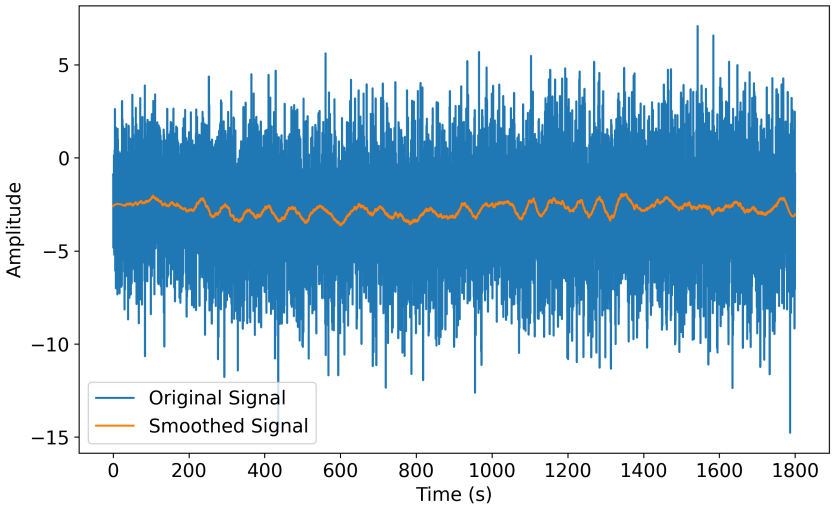

Figure 5.30: Signal smoothing analysis with Savitzky-Golay filtering technique

The choice of the window size and of the polynomial order depended on the specific characteristics of the signal and the desired level of smoothing. The application of the

Z-score outlier removal and the Savitzky-Golay filter allows a better adjustment of the pre-processed for further analysis and feature extraction.

5.6.2 Signal Statistics

The relevant metrics and characteristics are extracted from the preprocessed signals with the use of various statistical measures. These include the mean, which represents the average value of the signal over the entire measurement period, and the standard deviation, which quantifies the variability by measuring the dispersion of signal values around the mean. The minimum and maximum values are also identified in order to find the range of values recorded during the measurement. The coefficient of variation (CV), calculated as the ratio of the standard deviation to the mean, expresses the relative variability of the signal. Skewness and kurtosis are used in the assessment of the asymmetry and peakedness or flatness of the signal distribution, respectively. They provide information on the shape of the distribution as compared to the normal distribution.

In addition to these statistical measures, steady-state analysis is performed for both torque and power signals. The analysis is aimed at evaluating the stability of the operation of the mill and the consistency of the signal trend during the grinding process. The steady-state mean is calculated as the average value of the signal during the second half of the measurement duration. This calculation is based on an assumption that the mill reaches a stable operating condition after the initial transient phase. The steady-state standard deviation quantifies the variability around the steady-state mean during this stable period.

Furthermore, transient state analysis of torque and power signals allows information on the dynamic behavior of the system and its response to operational changes or disturbances. The main metrics computed in this analysis include rise time, settling time, and overshoot. Rise time is defined as the time during which the signal rises from a lower level to 90% of the steady-state mean value. It is determined by identifying the initial peak that exceeds this 90% threshold. Settling time is a time stamp representing the time when the signal leaves the specific tolerance range around its steady-state mean value. It is calculated by locating the last peak that meets the 90% steady-state mean criterion. Overshoot represents the maximum value that the signal reaches when exceeding its steady-state mean value during the transient phase. It is identified by finding the maximum peak deviation above the steady-state mean among the identified peaks. If no peaks meet the defined criteria, these metrics are considered to remain undefined and to indicate the absence of significant transient behavior within the observed range.

The calculating of these statistical measures, performing steady-state analysis, and conducting transient state analysis enable a comprehensive characterization of the signals, as well as comparisons between different operating conditions and mill configurations, thus facilitating the identification of optimal settings and the detection of anomalies or instabilities in the operation of the mill.

5.6.3 Measured Signals

The performance of a ball mill is monitored and analyzed with the use of sensors that record the following signals during each measurement:

RPM Signal: The rotational speed signal, expressed in revolutions per minute (further referred to as RPM signal), represents the angular velocity of the ball mill. It provides

information about the operating speed of the mill and its stability over time. A comparison of the RPM signal to the set rotational speed value, which is selected on the basis of the mill diameter and grinding conditions, allows the evaluation of both the performance of the mill and the effectiveness of the control system. The analysis of the RPM signal includes calculating both the mean deviation, which is the average difference between the actual and the set rotational speed values, and the standard deviation of deviation, which quantifies the variability or dispersion of the RPM deviations from the set RPM. The operating stability of the mill is additionally assessed by calculating the percentage of time during which the RPM signal remains within an acceptable range (±5% of the set RPM).

Torque Signal: The torque signal represents the moment acting on the ball mill. It provides information on the mechanical stress and energy transfer within the mill. The relationship between the torque signal and the power draw of the mill is identified in correlation analyses. The correlation coefficient calculated between the absolute values of torque and power signals serves to quantify the strength and direction of their linear relationship. A high positive correlation indicates that an increase in absolute torque is associated with an increase in power draw, while a low or negative correlation suggests a weaker or inverse relationship. This analysis aids the understanding of the mill dynamics and performance.

Power Signal: The power signal represents the electrical power draw by the motor of the ball mill. It provides information about the energy consumption of the mill during the grinding process. The total energy consumed by the mill during the measurement period is calculated by integrating the power signal over time, and is thus an overall measure of the energy requirements in the grinding process. This analysis identifies the energy efficiency of the mill and potential areas for optimization.

Signal Analysis: The measured signals (RPM, torque, and power) are analyzed with the use of various techniques in order to assess the performance of the mill, identify relationships between operating parameters, and detect anomalies or instabilities. Statistical measures are calculated for all signals, while steady-state analyses and transient state analyses are performed specifically for torque and power signals. The statistical measures include the mean, standard deviation, minimum, maximum, coefficient of variation, skewness, and kurtosis, which comprehensively characterize the signals. The steady-state analysis evaluates the stability and consistency of mill operation during the grinding process, while the transient state analysis investigates the dynamic behavior and response of the system to operational changes or disturbances.

5.7 Correlation Analysis

The correlation analysis served to investigate the relationships between operational parameters and performance metrics for different mill diameters, in both dry and wet milling conditions. It was aimed at identifying the main correlations and trends that describe the scaling behavior of ball mills, as well as the factors influencing their performance.

Pearson's Correlation Coefficient (Pearson's r) was used to quantify the strength and direction of linear relationships between variables. Pearson's r ranges from -1 (perfect

negative linear relationship) to 1 (perfect positive linear relationship), with 0 indicating no linear relationship. The 'pearsonr' function from the 'scipy.stats' module in Python was employed in the computations of the correlation coefficients and p-values.

The statistical significance of correlations was assessed using p-values, which represent the probability of observing a given correlation coefficient by chance, assuming no true relationship between variables. A commonly used threshold for statistical significance is $p < 0.05$, which indicates that the observed correlation is unlikely to have occurred by chance.

The experiments performed for all scales included 24 dry milling experiments and 24 wet milling experiments. Together with the Python scipy library, the results of these experiments served to calculate correlation matrices for both dry and wet milling conditions. The correlation coefficients between each pair of parameters were calculated so as to quantify the strength and direction of their linear relationship.

The correlation matrices were filtered with respect to their statistical significance and correlation strength. Correlations with p-values above 0.05 were considered statistically insignificant and were excluded. Correlations with coefficients between -0.4 and 0.4 were considered weak and were also excluded. As a result, the focus remained only on moderate to strong correlations. The filtered correlation matrices were visualized on heatmaps in order to highlight the main relationships between the parameters.

The filtered correlation matrices were also analyzed for notable correlations and trends. Each parameter was examined individually, considering its correlations with other parameters and performance metrics. The interpretation of the correlations allowed for the experimental design and the related potential biases introduced by this design. The analysis focused on identifying relevant relationships, such as the impact of operational parameters on performance metrics and the mutual influence of different parameters.

5.8 Scaling Constant and Scaling Strategy

The scaling constant is expected to aid the replication of the parameters of the energy transfer to ore for different scales of the milling process. This approach has a potential to allow consistent milling effectiveness and energy utilization metrics, such as size reduction, specific energy, and specific energy per rotation. These metrics, based on the available measurement results, represent the complicated milling process. In order to be comparable across scales, these metrics, as well as the scaling constant, must be scale-agnostic. Total energy consumption and torque acting on the mill drum are thus unsuitable for this purpose.

Linear scaling of mill geometry and grinding media size is not feasible due to the complex dynamics involved. Instead, this study focuses on the necessary adjustments in rotational velocity and size distribution of the grinding media which ensure consistent energy utilization in larger diameter mills. The aim is to calculate the scaling constant value for a small mill with reference operational parameters and then set the rotational speed and size distribution in such a manner that a mill with a larger diameter would have the same scaling constant value as the reference mill without modifications to other operational parameters (filling degree, number of lifters, lifter height).

This aim is achieved by systematically varying the rotational speed of the mill and the size distribution of the grinding media in order to explore a parameter space for optimal conditions.Such variations have a direct influence on both the kinetic energy of the grinding media (i.e. the impact breakage potential of the grinding media) and the

scaling constant. The exploration is performed by minimizing the difference between the calculated scaling constant and the reference scaling constant value of the base mill.

Different combinations of ball diameters and rotational speeds were explored with the use of a numerical solver. The solver compares the scaling constant calculated for the larger diameter mill to the reference scaling constant calculated for the base mill. The scaling constant represents detailed parameters that may affect energy transfer through the grinding media, such as the number of balls per total working area, which can be compared across scales to calculate the number of contacts per one square meter of the total working area, as these translate directly into the number of contacts. Rotational speed also directly affects the impact rate and is therefore employed in the scaling constant, as are the maximum potential and kinetic energies of the ball inside the mill.

The scaling constant is thus a measure of the maximum energy transfer rate through contact points between balls per active working area, which can be compared and maintained across scales. This approach enables the replication of energy transfer to ore during milling processes performed on different scales, potentially leading to consistent milling effectiveness and energy utilization.

5.8.1 Calculation of Total Working Area

The total working area A_{total} is the sum of the surface areas of all balls in the load (A_{balls}) and the effective working area of the mill (A_{mill}). The A_{balls} is calculated by summing the surface areas of all balls from $i = 1$ to N, where each ball can have a different diameter (d_i):

$$A_{\text{balls}} = \sum_{i=1}^{N} \pi d_i^2. \tag{5.3}$$

The A_{mill} is considered to be half of the full internal surface area of the mill. This simplification is based on an assumption that only half of the internal surface is in contact with the load at any given time. The internal surface area of the mill is approximated as the surface area of a cylinder, and is calculated using the internal radius (R_{int}) and the length of the cylindrical section (l):

$$A_{\text{mill}} = \frac{1}{2} \cdot (2\pi R_{int} l + 2 \cdot \pi R_{int}^2) = \pi R_{int}(l + R_{int}). \tag{5.4}$$

The combination of the surface areas of the balls with the effective working area of the mill allows the total working area A_{total}. This value is an important factor in the scaling constant, as it enables the comparison of the number of contact points per one square meter of the combined ball-and-mill surface across different scales, and thus it directly impacts the number of contact points and the energy transfer rate.

5.8.2 Energy Considerations

The maximum possible total energy transferred to the average-size grinding medium in a mill is the sum of its maximum potential energy ($PE^{\max}_{\text{ball(avg)}}$) and its maximum kinetic energy ($KE^{\max}_{\text{ball(avg)}}$). For an average ball, this can be expressed as:

$$E^{\max}_{\text{ball(avg)}} = PE^{\max}_{\text{ball(avg)}} + KE^{\max}_{\text{ball(avg)}}, \tag{5.5}$$

where, $PE^{\max}_{\text{ball(avg)}}$ is the maximum energy due to the height h to which the average ball in the load can be lifted, while $KE^{\max}_{\text{ball(avg)}}$ represents the maximum kinetic energy that the average ball can obtain inside the mill due to the rotation of the mill, considering only linear velocity.

The maximum potential energy is calculated as:

$$PE^{\max}_{\text{ball(avg)}} = m_{\text{ball(avg)}} g h_{\max} = \frac{4}{3}\pi r^3_{\text{ball(avg)}} \rho g (D_{int} - r_{\text{ball(avg)}}), \tag{5.6}$$

where $m_{\text{ball(avg)}}$ is the mass of the average ball, g is the acceleration due to gravity, $h_{\max}$ is the maximum height that the ball can reach, $r_{\text{ball(avg)}}$ is the average ball radius, ρ is the density of the ball material, and D_{int} is the internal diameter of the mill.

The maximum kinetic energy is calculated as:

$$KE^{\max}_{\text{ball(avg)}} = \frac{1}{2} m_{\text{ball(avg)}} v^2_{\max} = \frac{2}{3}\pi r^3_{\text{ball(avg)}} \rho \cdot (\omega_{rad} \cdot (R_{int} - r_{\text{ball(avg)}}))^2, \tag{5.7}$$

where $v_{\max}$ is the maximum linear velocity of the ball, ω_{rad} is the angular velocity of the mill in radians per second, and R_{int} is the internal radius of the mill.

The average ball radius ($r_{\text{ball(avg)}}$) is calculated as:

$$r_{\text{ball(avg)}} = \frac{1}{2} \sum_{i=1}^{n} p_i \times d_i, \tag{5.8}$$

where n is the total number of size fractions, p_i is the percentage of mass per the i^{th} size fraction (normalized as a fraction of 1), and d_i is the diameter of the i^{th} fraction.

With both the maximum potential energy and the kinetic energy of an average ball within the mill, allowed for in the scaling constant, it can more effectivelly represent the complicated factors which affect the energy transfer and enable more accurate comparisons between different mill scales.

5.8.3 Operational Definition of the Scaling Constant

The scaling constant, denoted as κ, is defined by the following equation:

$$\kappa = E^{\max}_{\text{ball(avg)}} \cdot \frac{N}{A_{\text{total}}} \cdot \omega_{RPM}, \tag{5.9}$$

where $E^{\max}_{\text{ball(avg)}}$ represents the maximum possible energy (both kinetic and potential) of an average ball within the load, measured in Joules (J), N is the total number of balls in the load, A_{total} is the total effective working area available for the balls and the interior surfaces of the mill to perform work, provided in square meters (m^2), and ω is the rotational speed of the mill, expressed in revolutions per minute (RPM).

The scaling constant κ can be redefined so that it represents the maximum power draw per square meter of working area by dividing it by 60 seconds per minute. The result is in the form of the following equation:

$$\kappa_{SI} = \frac{\kappa}{60} [\text{W/m}^2]. \tag{5.10}$$

This redefinition is a more intuitive approach to the scaling constant in terms of power per unit area, which is particularly useful when comparing mills of different sizes and at different operating conditions.

By incorporating the maximum possible energy of an average ball, the total number of balls, the total effective working area, and the rotational speed of the mill, the scaling constant κ represents the essential factors that influence energy transfer and milling efficiency. Maintaining a consistent value of κ for different mill scales is expected to result in similar milling performance and energy utilization, enabling more accurate scale-up predictions and optimizations.

5.9 Methodology of Scaling Constant Testing

The response metrics are measured in controlled experiments for each experimental run. The metrics include size reduction, specific energy, and specific energy per rotation. Whether the resulting metrics remain invariant for different mill scales is verified with the use of statistical analysis, specifically Analysis of Variance (ANOVA). Additionally, a Design of Experiments (DoE) is incorporated for each experimental series in each scale to gain further insight into the experiments and other operational parameters that may impact mill efficiency, size reduction, and power draw.

5.9.1 Methodology and Implications of Testing

The experimental design ensured that the independence of observations assumption was met. The Shapiro-Wilk test was used to assess normality within each group (300, 400, and 500 mm mills), and the p-value > 0.05 indicated that the normality assumption was met. The homogeneity of variances across groups was ensured with the help of Levene's test, and if the p-value was greater than 0.05, the equal variances assumption was considered met. In cases where the p-value was less than or equal to 0.05, one-way ANOVA was replaced with Welch's ANOVA.

The choice of the hypothesis test depended on the normality and homogeneity of variances assumptions. If both were met, one-way ANOVA was used. When normality was met but equal variances were violated, Welch's ANOVA was employed. If normality was violated, the Kruskal-Wallis H test was utilized. Post-hoc pairwise comparisons were conducted when the hypothesis test indicated significant differences among groups. Tukey's HSD test was found unnecessary for both one-way ANOVA and Welch's ANOVA, and Dunn's test with Bonferroni correction was performed for the Kruskal-Wallis H test.

The magnitude of differences between groups was assessed by calculating the effect size measures. For Welch's and one-way ANOVA, partial eta-squared (η_p^2) was used, with interpretations as follows: small effect ($0.01 \leq \eta_p^2 < 0.06$), medium effect ($0.06 \leq \eta_p^2 < 0.14$), and large effect ($\eta_p^2 \geq 0.14$).

The results were interpreted so as to determine if the the scaling constant allowed the metrics to be maintained at the same level across different ball mill scales.

5.10 Design of Experiments (DoE)

Design of Experiments (DoE) is a systematic approach used to plan, conduct, analyze, and interpret controlled tests to evaluate the effects of multiple input variables on the output variable, with the goal of improving or optimizing the process or product being tested. In this study, the effects of the main operating variables on mill performance for both dry and wet milling were investigated by employing a 2-level fractional factorial

design. It allows analyses of the most important factors in an experiment based only on a fraction of the total number of experiments that would be required for a full factorial design. In effect, the test is more efficient and cost-effective.

The fractional factorial designs were developed using Minitab Statistical Software, and they resulted in a resolution of IV for dry milling and III for wet milling. Each experimental design was run three times for each mill diameter. The lifter reference (0) mean values, i.e. 6 lifters having a height of 10 mm, later served to select the high and low values for experiments. The average reference filling degree was set to 0.4, and the reference rotational speed was calculated as 75% of the critical speed for the smallest mill diameter.

The ball sizes selected for the experiment ranged from 15 to 35 mm. The size distribution was calculated on the basis of the Bond Equilibrium state equation, with the balls accounting for 60% of the filled volume (total mill volume x filling degree) and the remaining 40% filled by ore or slurry. For example, a filling degree of 0.5 indicates that 50% of the internal volume of the mill is effectively utilized for the balls and the milled material. It is assumed that approximately 60% of this volume is filled with steel balls, translating to 30% of the total volume of the mill.

In the case of larger scales, the rotational speed and ball sizes were recalculated so that the scaling constant was maintained at the same level as for the smallest diameter. For both the 400 and 500 mm mills the scaling constant was calculated with the use of the reference average values of the parameters. The values for lifter configuration were selected on the basis of the test stand capabilities, while the reference filling degree and rotational speed were adjusted to the industry standards [55].

The DoE approach was based on a fractional factorial design with the following factors and levels:

- Lifter height: 5 mm (-1), 15 mm (+1)
- Filling degree: 30% (-1), 50% (+1)
- Number of lifters: 4 (-1), 8 (+1)
- Mill rotational speed: 90% (-1) and 110% (+1) of the reference speed for given scale

For the 400 mm mill, the reference rotational speed was 0.733 of the critical speed, and the ball size distribution was in the range of 20-35 mm. For the 500 mm mill, the reference rotational speed was 0.712 of the critical speed, and the ball size distribution range was 25-35 mm.

For wet milling, the slurry density values were selected so as to cover a broad spectrum of possible densities relevant to mineral processing operations. The reference density was set to 1600 kg/m^3, with a 200 kg/m^3 difference on each side to cover a wide spectrum of densities, resulting in 1400 kg/m^3 (-1) and 1800 kg/m^3 (+1).

The experimental matrices with coded values are presented in Figure 5.1 for dry milling and in Figure 5.2 for wet milling.

Table 5.1: Design of Experiments (DoE) table for dry milling experimental series

Run ID	Rotational Speed	Filling Degree	Number of Lifters	Height of Lifters
d1	-1	1	1	-1
d2	1	1	-1	-1
d3	1	-1	1	-1
d4	-1	-1	-1	-1
d5	1	1	1	1
d6	1	-1	-1	1
d7	-1	-1	1	1
d8	-1	1	-1	1

Table 5.2: Design of Experiments (DoE) table for wet milling experimental series

Run ID	Rotational Speed	Filling Degree	Number of Lifters	Height of Lifters	Slurry Density
w1	-1	-1	-1	1	1
w2	1	-1	-1	-1	-1
w3	-1	1	-1	-1	1
w4	1	1	-1	1	-1
w5	-1	-1	1	1	-1
w6	1	-1	1	-1	1
w7	-1	1	1	-1	-1
w8	1	1	1	1	1

5.10.1 Analysis of Results

The analysis was performed in Minitab statistical software for each experimental series and for all response metrics, resulting in a total of 36 analyses (6 series and 6 metrics). The analysis employed stepwise selection of terms with an alpha value of 0.15 for both removing and entering terms.

In the context of the Minitab-based factorial Design of Experiments (DOE) analysis, "stepwise selection of terms" refers to a methodical approach for selecting the most significant factors and interactions that influence the outcome variable. This process is particularly valuable in factorial DOE, in which many factors and their interactions need to be potentially considered, and it is important to identify which of them have a considerable impact on the response.

The stepwise selection of terms involves the following steps:

1. Identification of all possible terms: initially, the analysis is performed for all possible factors and their interactions, including the main effects, two-way interactions, and higher-order interactions, depending on the factorial design.

2. Selection criteria: the stepwise procedure uses statistical criteria, such as p-values from hypothesis tests (e.g., F-tests), to decide which terms to add or remove from the model. Terms with p-values below a certain threshold indicate significant effects.

3. Stepwise procedure: the procedure can be a forward selection (starting with a minimal model and adding terms), a backward elimination (starting with a full model and removing terms), or a bidirectional elimination (combining both the forward selection and the backward elimination).

4. Model refinement: the iterative process continues until adding or removing terms does not significantly improve the model based on the selection criteria; the result is a refined model that includes only statistically significant factors and interactions.

The main focus in the results is placed on the standardized effects, regression equations, and the model summary R^2 fits. Standardized effects are the estimated impacts of factors on the response variable. They are scaled to have a uniform measurement scale and they facilitate the comparison of effects across different units of measurement.

R^2represents the proportion of variance in the dependent variable explained by the independent variable(s) in a regression model. R^2(adj), or adjusted R^2, adjusts the R^2 value based on the number of predictors relative to the number of data points, accounting for the potential increase in R^2simply due to adding more predictors. R^2(pred), or predicted R^2, indicates how well the model is expected to predict responses for new observations not included in the model estimation.

Other results, including ANOVA and Pareto charts, are also present in the analysis results and can be found in the appendix.

5.11 Summary

This chapter presents the materials, methods, and experimental setup used to investigate the scaling behavior of ball mills and the development of a scaling constant. The experiments were performed in a specially designed laboratory-scale ball mill with exchangeable drums of different diameters, equipped with sensors measuring power draw, torque, and rotational speed. A high-speed video camera recorded the motion of the grinding media and ore particles inside the mill.

The copper ore and steel balls used in the experiments were characterized in terms of their properties, preparation process, and size distribution. The rheology of the copper ore slurry used in wet milling experiments was measured with a viscometer. The experimental methodology involved analyzing the product size distribution and the milling time, as well as the video recordings, which served as a source of such data as the dynamic angle of repose and slurry surface profile.

The milling process was studied by conducting the DEM-SPH simulations, and the model parameters were calibrated to match the experimental results. The relationships between operational parameters and performance metrics across different mill scales were identified in correlation analyses. A scaling constant was developed with an aim to replicate the energy transfer to ore during the milling process for different scales, and the proposed scaling strategy was based on adjusting the rotational velocity and size distribution of the grinding media.

The methodology for testing the scaling constant involved controlled experiments and statistical analysis using ANOVA. Further information on the effects of various operational parameters on mill performance was acquired with the use of the Design of Experiments (DoE) approach. The results of the DoE analysis were interpreted using standardized effects, regression equations, and model summary R^2fits.

Chapter 6

Results

This chapter presents the main results and findings from the experimental study on ball mill scale-up. It begins with the calibration results, including experimental measurements and simulation convergence for ball-only, dry milling, and wet milling cases. The chapter then provides detailed results for the dry and wet milling experimental series, covering sensor measurements (rotational speed, torque, power draw), product size distribution, simulations (force ratio, charge position), and correlations between torque and simulated data. Design of Experiments (DoE) analysis provides the most influential operational parameters for various response variables such as mean torque, force ratio, size reduction, and energy consumption metrics. Statistical tests verify the validity of scaling assumptions based on the scaling constant. Finally, correlations across mill scales, analyzed for both dry and wet milling processes, reveal the most important relationships and trends in the milling process. The discussed results can be used in ball mill scale-up, process optimization, and in the analysis of the impact of various operational parameters on milling performance.

6.1 Calibration

The calibration section presents the results of the experimental measurements and simulation convergence for the ball-only, dry milling, and wet milling cases. It includes the measured dynamic angles of repose, the calibration of ball parameters through iterative simulations, and a comparison of experimental and simulated data for the wet milling case. The section serves as a basis for the subsequent analysis of the dry and wet milling experimental series.

6.1.1 Experimental Measurements

The Experimental Measurements subsection presents the results of the physical experiments conducted for the ball-only, dry milling, and wet milling cases. It includes the dynamic angles of repose measured in the ball-only case for various drum diameters, as well as the dynamic angles recorded during the dry milling process, and the slurry surface profile analyzed for the wet milling case. These experimental measurements provide the basis for calibrating the simulation models and validating them as accurate representations of the real-world milling conditions.

Balls Only Case: The dynamic angles of repose measured for recordings of the balls inside the drum were found to be 43.25°, 42.15°, and 40.35° for the 300, 400, and 500 mm mills, respectively.

Dry Milling Case: The dynamic angles recorded during the dry milling processes were 54.24°, 41.97°, and 47.67° for the 300 mm, 400 mm, and 500 mm mills, respectively. These values are less accurate, as the extraction of the load area from the recording was more challenging and as the method was not resistant to the reflections on the wall.

Wet Milling Case: The curve fitted to the data from the wet milling recording is presented in Figure 6.1.

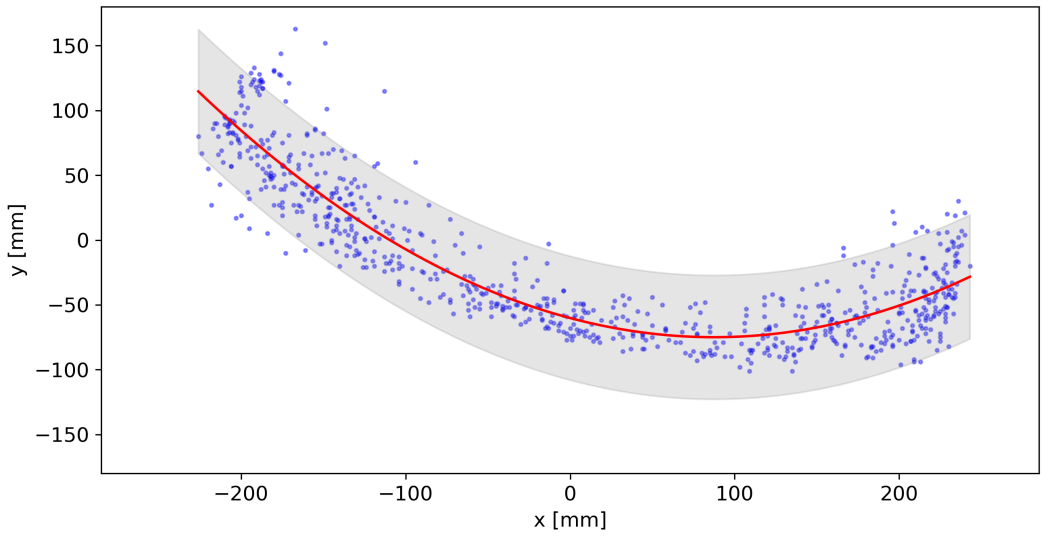

Figure 6.1: Points of surry surface detected with GUI, the fitted curve, and the confidence interval

6.1.2 Simulation Convergence

The Simulation Convergence subsection describes the process of calibrating the simulation models so that they match the experimental measurements for the ball-only, dry milling, and wet milling cases. It presents the iterative approach employed in determining the optimal coefficients of restitution and kinetic friction for the balls, the selection of the best iteration based on the lowest sum of squared errors (SSE) between the experimental and the simulated angles for the dry milling case, and the comparison of the simulated and experimental slurry surface profiles for the wet milling case. The subsection discusses the convergence of the simulation models which accurately represent the real-world milling conditions, providing a reliable foundation for further analysis and optimization of the milling process.

Balls Only Case: The calibration of the ball behavior started with 18 initial simulations (6 measurements for each of the 3 diameters). New local minima were discovered until the 10^{th} iteration, after which no better combination was found. The final parameters for the simulation balls, i.e. the coefficient of restitution and the coefficient of kinetic

friction, were 0.390 and 0.496, respectively. In total, 13 iterations resulting in 39 simulations were performed. The results of the ball behavior calibration are shown as heatmaps in Figure 6.2. These maps demonstrate the relationship between two critical parameters: the coefficient of restitution and the coefficient of kinetic friction, using a color gradient that represents the sum of squared errors (SSE). Specifically, the x-axis corresponds to the coefficient of restitution, which quantifies the elasticity of collisions, and the y-axis corresponds to the coefficient of kinetic friction, which is a measure of the resistance to motion. Contour lines represent constant SSE values, and the color gradient from green to red indicates ascending SSE values, thus reflecting the fidelity of the simulation parameters to the experimental observations. The optimal parameters are marked in red and exhibit the lowest SSE. They represent the most accurate simulation values determined in the iterative calibration process.

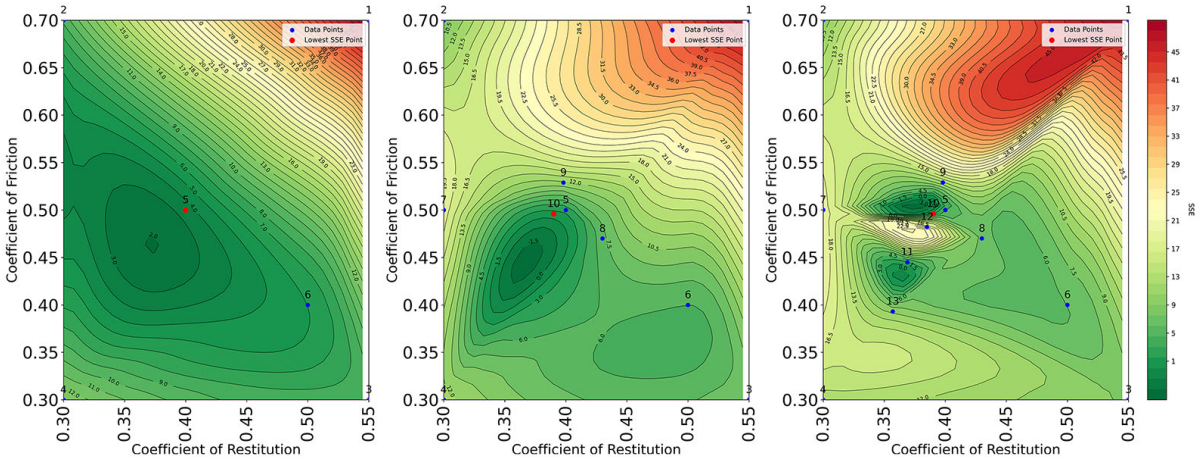

Figure 6.2: Calibration results for ball coefficient of restitution and friction

Dry Milling Case: For the dry milling calibration, all of the angles resulting from the previous calibration were considered in the calculations of the initial response surface with the new SSE value. The comparison of the angles simulated in the 12^{th} iteration of the previous calibration with the experimental angles provided the best result and the new lowest SSE. Three possible local minima were explored, but none gave lower SSE than the previous best combination from the 12^{th} iteration. Therefore, the selected values of the parameters are 0.385 for the coefficient of restitution and 0.482 for the coefficient of kinetic friction. These parameters are less accurate because the angle of repose for the load measured from the recording is less precise. The dry milling calibration results are shown in Figure 6.3 as a heatmap.

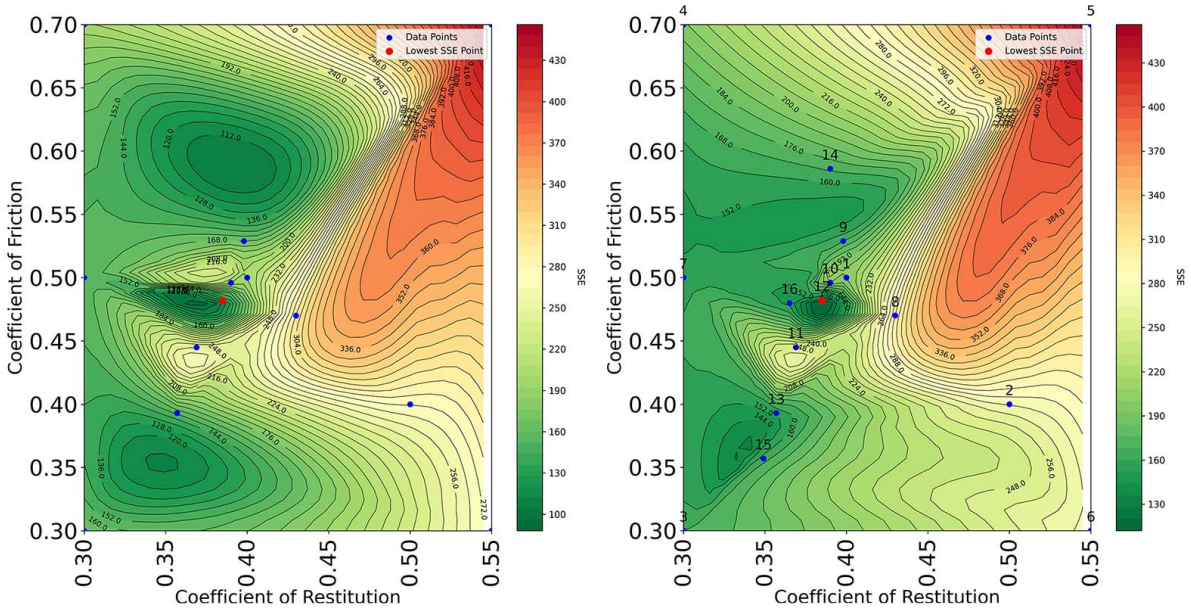

Figure 6.3: Dry milling calibration results for ball coefficient of restitution and friction

Wet Milling Case: Extracted water elevation points for all time steps, cleaned as described in the previous chapter, are presented in Figure 6.4.

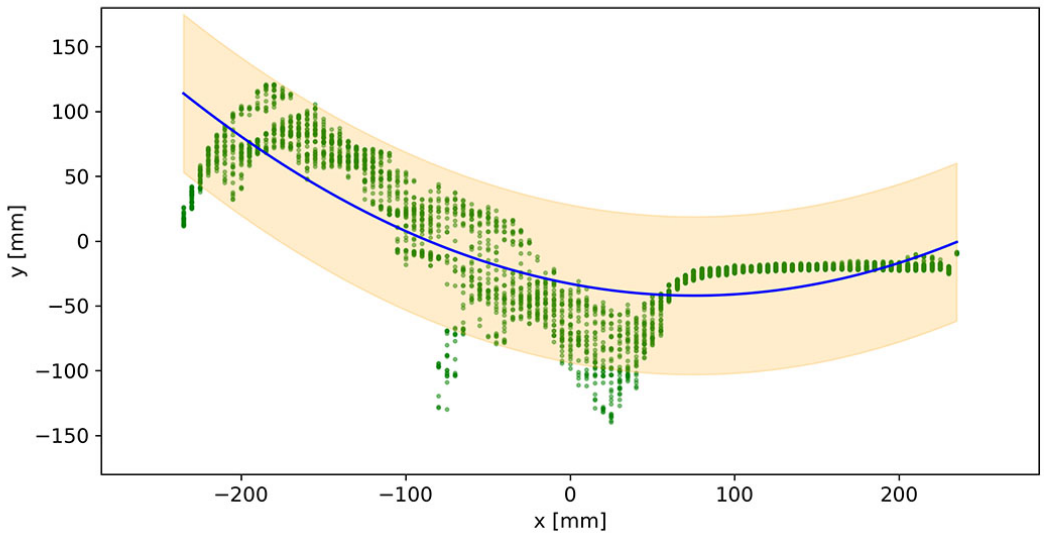

Figure 6.4: Points of the slurry surface extracted from the simulation, with fitted curve and 95% confidence interval

A comparison of this data to the data extracted from the recording (Figure 6.5) indicates that the fitted curves fit inside each other's confidence intervals. This fact indicates that adjusting the density and viscosity of the fluid to realistic values provides a satisfying match in the behavior of the simulated slurry, including the slurry pooling in the toe region.

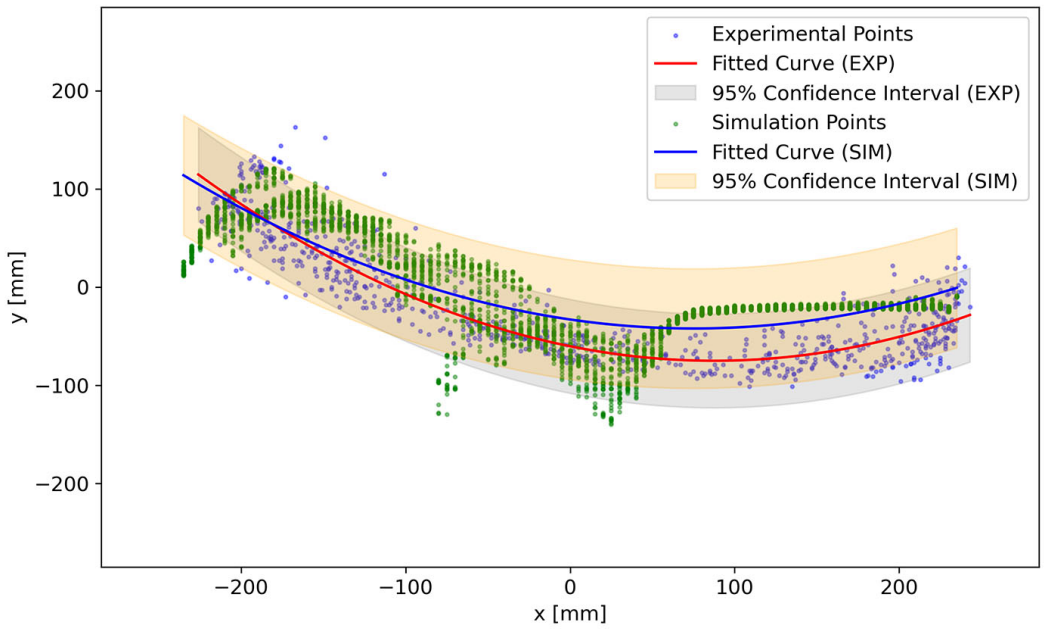

Figure 6.5: Comparison of experimental data and simulation results for wet milling calibration

Key Points – Calibration – Dry/Wet Milling:

- Experimental dynamic angles of repose were measured for ball-only and dry milling cases at various drum diameters.
- Ball parameters were calibrated in iterative simulations, converging on optimal coefficients of restitution and kinetic friction.
- Dry milling calibration was built upon the ball calibration results, by selecting the best iteration based on lowest SSE between experimental and simulated angles.
- In wet milling calibration, slurry surface profiles from experiments and simulations were compared and showed good agreement when the fluid density and viscosity were adjusted to realistic values.

6.2 Dry Milling Experimental Series Results

This section presents the findings from the comprehensive analysis of the dry milling experiments conducted at various mill diameters. It covers the sensor measurements, including rotational speed, torque, and power draw, providing insights into the stability, variability, and efficiency of the milling process. The section also examines the product size distribution and offers a comparison of the effectiveness in achieving finer particle sizes and higher size reduction ratios for mills with different diameters. Additionally, it presents the results of the dry milling simulations, focusing on the force ratio and charge position, and explores the correlations between torque and simulated data. The section concludes with an analysis of the recordings. It discusses computer vision techniques used

to identify the centroid coordinates of the charge and offers a novel approach to monitoring mill operation. It also provides a comprehensive description of the dry milling process and the factors influencing its performance.

6.2.1 Sensor Measurements

This subsection presents the results obtained from the various sensors employed in the dry milling experiments, including rotational speed, torque, and power draw. It analyzes the stability and control of the rotational speed of the mill, the variability and transient behavior of the torque signal, and the power consumption trends across different mill diameters. The subsection also investigates the correlations between torque and power draw, providing insights into the energy dynamics of the milling process. It also offers detailed operational characteristics of the mill and describes the factors influencing its performance, providing grounds for process optimization and control.

Rotational Speed

This study investigates the rotational speed control and stability of the mill during dry grinding experiments conducted with three different mill diameters: 300 mm, 400 mm, and 500 mm. The experimental data, including the RPM signals for each diameter, is presented in Appendix B and Figure B.1, with statistical measures of each signal summarized in Table B.1.

The analysis reveals that the mean RPM values closely align with the set RPM values across all mill diameters, indicating well-controlled mill rotational speeds. This finding is reinforced by the low standard deviations (ranging from 0.07 to 0.16) and a consistent coefficient of variation of 0.00, which indicate minimal fluctuations and stable operation. Furthermore, the skewness and kurtosis values of the data are close to zero and three, respectively, suggesting that the RPM distributions are symmetric and similar to a normal distribution. This characteristic implies that deviations from the set RPM values are symmetrically distributed without significant outliers, which fact is in agreement with the expected operational behavior.

Although the measured RPM values are slightly albeit consistently higher than the set values, the deviation remains within a small range (1.11 to 3.15 RPM). This observation demonstrates the accuracy and precision of the rotational speed control system. The consistency of the system is further evidenced by the fact that the RPM signal remains within $\pm 5\%$ of the set RPM for nearly the entire time (100% for most measurements). Interestingly, the deviation between the set and the measured RPM values appears to scale with mill diameter, with the smallest diameter showing the most significant differences. This observation suggests that the effectiveness of the rotational speed control system may be inversely related to mill size and indicates an area for potential system optimization and future research.

In summary, the results indicate that the mill maintains a stable, controlled, and consistent rotational speed close to the desired set points during the dry grinding process. While the performance of the control system is effective, the consistent pattern of actual RPM being higher than the set points across all mill diameters suggests a potential area for system improvement. Future research should focus on improving the rotational speed control system, with a specific emphasis on compensating for mill diameter effects and on finding the source of the systematic bias in RPM measurements.

Key Points – Rotational Speed Sensor Measurements – Dry Milling:

- Mean RPM values closely align with set RPM values, indicating well-controlled rotational speeds across all mill diameters.
- Low standard deviations and consistent coefficient of variation signify minimal fluctuations and stable operation.
- Rotational speed distributions are symmetric and similar to a normal distribution, suggesting symmetrically distributed deviations without significant outliers.
- All measured RPM values are insignificantly albeit consistently higher than the set values; however, they remain within a small (5%) deviation range.
- The deviation between the set and the measured RPM values scales with mill diameter, with the smallest diameter showing the most significant differences.

Torque

The torque measurements for dry milling experiments were conducted across three mill diameters: 300 mm, 400 mm, and 500 mm (Figure 6.6). The analysis of the results allows several main observations on the behavior of torque signals and their relationship with operating conditions and mill scale.

Across all scales, the consistent negative mean torque values indicate a resistance force exerted by the mill charge on the moving ball mill due to gravity. The coefficient of variation (CV) analysis reveals that the smallest diameter mill (300 mm) exhibits moderate to high variability in torque signals, suggesting a more significant impact of operating conditions on torque generation at this scale. In contrast, the larger diameter mills (400 mm and 500 mm) generally show low CV values, with a few moderate values, indicating more stable torque responses despite the inherent process variability (Tables C.1, C.2 C.3 in Appendix C).

The variations in skewness and kurtosis values suggest non-uniform distributions of torque values, potentially influenced by factors such as filling degree, rotational speed, and lifter configurations. Runs 2 and 3, with higher rotational speed and lower lifter height, show positive skewness and kurtosis above 3 for all mill sizes, while run 4, with lower settings for all parameters, shows negative skewness and a kurtosis closer to the higher range, indicating a more dispersed spread of torque across its range.

Direct comparisons of runs with varying operating conditions confirm the expected trends in torque values. Runs 6 and 3, both with higher rotational speed and low filling degree, result in lower torque across all scales, while runs 1 and 8, with high filling degree and low rotational speed, yield higher torque values.

The detailed steady-state and transient analysis provides important information on the dynamics of the milling process. Rise times for most measured values are under one minute, with a tendency towards 30 seconds. Settling times are close to 1800 seconds (the experiment duration) for most cases, indicating stable fluctuations near the steady-state mean. However, missing values for certain experiments, particularly for the 500 mm diameter mill, suggest an absence of transient behavior.

The observation that torque values and their variability increase with mill diameter is of particular importance for understanding scale-up effects. Additionally, the varying correlation between torque and power draw across scales and conditions points to a complex interaction which involves multiple factors beyond those measured. The absence of

a consistent strong correlation between torque and power across different mill diameters suggests that other factors play significant roles in the energy dynamics of the milling process. Therefore, future experimental setups should include these factors for a more comprehensive analysis.

Key Points – Torque Sensor Measurements – Dry Milling:

- Smaller diameter mills exhibit higher torque variability, while larger mills show more stable responses.
- Skewness and kurtosis variations suggest non-uniform torque distributions influenced by operating conditions.
- Runs 2 and 3, with higher rotational speed and lower lifter height, exhibit positive skewness and kurtosis above 3 for all mill sizes.
- Run 4, with lower settings for all parameters, shows negative skewness and a kurtosis closer to the higher range.
- Runs 6 and 3, both with higher rotational speed and low filling degree, result in lower torque across all scales.
- Runs 1 and 8, with high filling degree and low rotational speed, yield higher torque values.
- Rise times tend to 30 seconds while the settling time is close to the time of the experiment; however some missing values, especially for the largest diameter, suggest the absence of transient behaviour.
- Torque values and variability increase with mill diameter, crucial for understanding scale-up effects.
- Varying correlation between torque and power draw suggests complex interactions involving multiple factors.

Power Draw

Power draw signals were recorded for all dry milling experiments across the mill diameters of 300, 400, and 500 mm, with 8 experiments conducted for each diameter (see Figure 6.7 and Appendix D, Tables D.1, D.2, and D.3). While the signal charts alone did not allow clear observations, the data suggests that more than one operational parameter directly influences the power draw. This fact seems important for further detailed analysis aimed at identifying the main parameters involved.

As expected, low rotational speed and low filling degree result in lower power draw, while high filling degree and high rotational speed lead to higher power draw. Runs 2 and 5 (high filling degree and high rotational speed) tend to be in the higher spectrum of power draw across scales, while runs 4 and 7 (low rotational speed and low filling degree) tend to be in the lower spectrum.

The power signals exhibit low variance, with all measurements below 10%. Transient behavior, specifically the rise times under 1 minute in duration across all mill diameters, suggests efficient responsiveness to starting conditions. Settling times being close to the

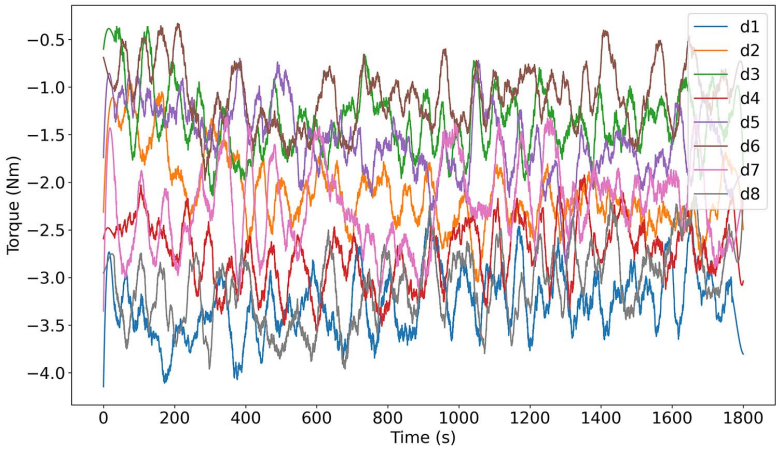

(a) D=300 mm

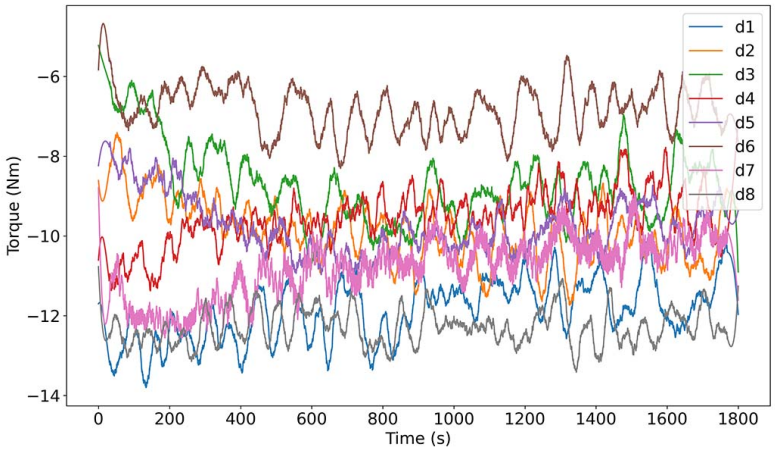

(b) D=400 mm

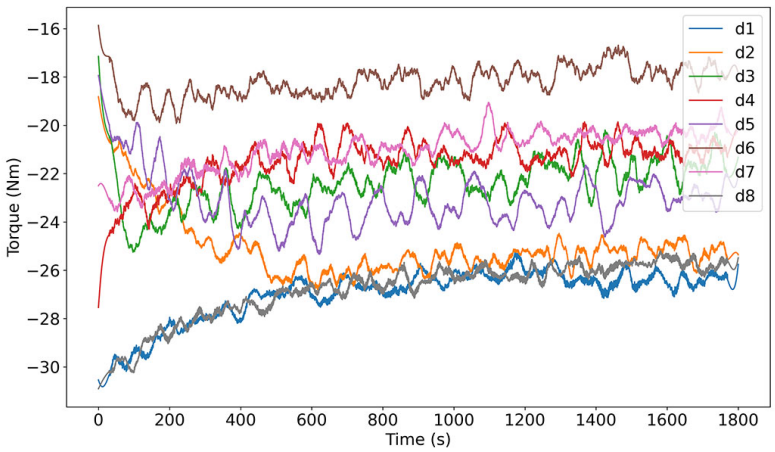

(c) D=500 mm

Figure 6.6: Pre-processed torque signals for dry milling experiments at different mill diameters

end times of the experiments for all runs across scales indicate that mills may maintain steady-state operation throughout the experiment.

As expected, an increase in mean power consumption along with mill diameter, from 71.407 W in the 300 mm mill to 202.167 W in the 500 mm mill, serves as evidence of the scaling effect on power draw. The standard deviation of power consumption also increases with mill diameter, from 2.447 in the 300 mm mill to 12.783 in the 500 mm mill, indicating greater variability in absolute values of power demand in larger mills, but similar variability in relative values, such as the coefficient of variation (CV), is similar across all experiments.

Notably, the documented effect of rotational speed and filling degree, particularly on skewness and kurtosis, provides detailed information on their impact on power draw variability. Runs 2 and 5 (high filling degree and high rotational speed), which tend to be in the higher spectrum of power draw across scales, also show negative skewness across all scales and higher values on the spectrum of kurtosis in each experimental series (except for the 300 mm mill). This relationship between the operational parameters and the statistical descriptors of the power signal offers a broader perspective on process control and optimization.

Key Points – Power Draw Sensor Measurements – Dry Milling:

- Multiple operational parameters directly influence power draw, with rotational speed and filling degree as the main factors.
- Runs 2 and 5 (high filling degree and high rotational speed) tend to be in the higher spectrum of power draw across scales.
- Runs 4 and 7 (low rotational speed and low filling degree) tend to be in the lower spectrum of power draw.
- Power draw signals show low variance and quick adaptation to changes, indicating efficient responsiveness and steady-state operation.
- Power consumption increases with mill diameter, demonstrating the scaling effect on power draw.
- Runs 2 and 5 (high filling degree and high rotational speed), which tend to be in the higher spectrum of power draw across scales, also show negative skewness across all scales and higher values on the spectrum of kurtosis in each experimental series (except for the 300 mm mill).

6.2.2 Product Size Distribution

The product size distribution analysis for dry milling experiments across the 300, 400, and 500 mm mill diameters provides information on the effectiveness of the milling process in terms of reducing particle size (Table 6.1, Figures E.1, E.2, and E.3 in Appendix E). The d_{80} values, which represent the particle size at which 80% of the material is finer, show a decreasing trend with increasing mill diameter. The average d_{80} values for the 300, 400, and 500 mm mills are 225.5, 177.8, and 154.9 μm, respectively. These numbers suggest that larger mill diameters are more effective in achieving finer particle sizes under dry milling conditions.

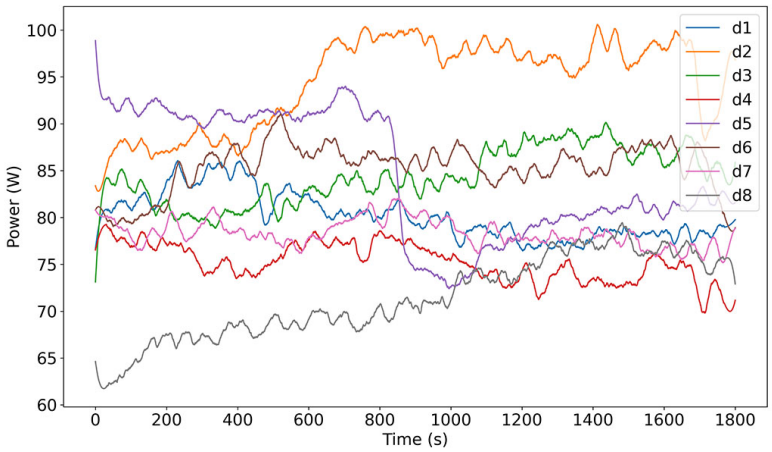

(a) D=300 mm

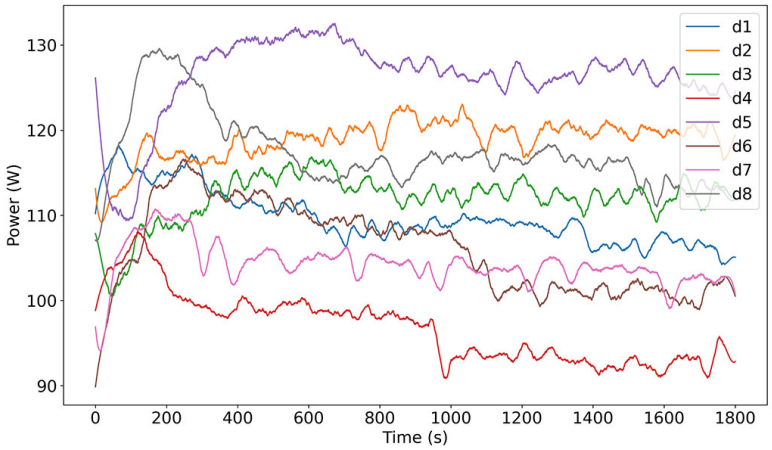

(b) D=400 mm

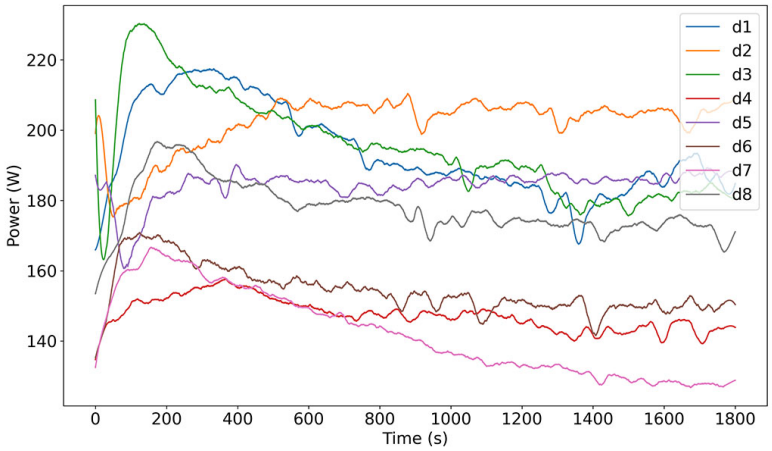

(c) D=500 mm

Figure 6.7: Pre-processed power signals for dry milling at different mill diameters

Table 6.1: Particle size reduction results for dry milling at various mill diameters

Run No.	300 mm: d_{80} (μm)	size reduction	400 mm: d_{80} (μm)	size reduction	500 mm: d_{80} (μm)	size reduction
1	194.7	4.499	178.4	4.910	158.8	5.517
2	227.0	3.859	242.3	3.616	171.8	5.100
3	271.6	3.226	157.1	5.576	119.3	7.344
4	218.0	4.018	147.4	5.942	126.9	6.904
5	299.6	2.923	195.0	4.492	179.4	4.884
6	209.7	4.178	172.7	5.073	156.7	5.591
7	181.0	4.841	170.2	5.148	162.1	5.404
8	202.5	4.327	159.7	5.486	164.7	5.320
Average	225.5	3.984	177.8	5.030	154.9	5.758

Size reduction ratios, calculated as the ratio of feed D_{80} to product d_{80}, provide a measure of milling efficiency. The average size reduction ratios for the 300, 400, and 500 mm mills are 3.984, 5.030, and 5.758, respectively, indicating that milling efficiency improves with increasing mill diameter. The 500 mm mill achieves the highest average size reduction. It is important to note that this metric alone might not represent all aspects of milling efficiency, such as energy consumption or time efficiency.

The cumulative size distribution curves for each mill diameter (Figures E.1, E.2, and E.3) show a progressive shift towards finer particle sizes as mill diameter increases, confirming the trend observed in the case of the d_{80} values and the size reduction ratios. These findings support the hypothesis that larger mill diameters are more effective in achieving finer particle sizes and higher size reduction ratios under dry milling conditions, possibly due to enhanced charge motion, as well as to an optimal combination of cascading and cataracting.

Key Points – Product Size Distribution – Dry Milling:

- Mills with larger diameters achieve finer particle sizes, as indicated by lower d_{80} values.
- The average size reduction ratios for the 300, 400, and 500 mm mills are 3.984, 5.030, and 5.758, respectively.
- The 500 mm mill demonstrates the highest effectiveness and efficiency in dry milling.

6.2.3 Simulations

This subsection presents the results of the dry milling simulations conducted using the calibrated models. Figure 6.8 shows examples of simulation runs with the same operational parameters across all mill scales, providing a visual comparison of the charge motion and distribution. The subsection analyzes the force ratio, which represents the ratio of tangential to normal forces acting on the balls, and the charge position, characterized by the center of circulation (CoC) and the center of gravity (CoG), as well as by the specific type of motion. It examines the spatial distribution of force ratios within the mill and the influence of operational parameters on the charge position. It also provides information on the dynamics of the dry milling process and the factors affecting the efficiency and performance of the mill.

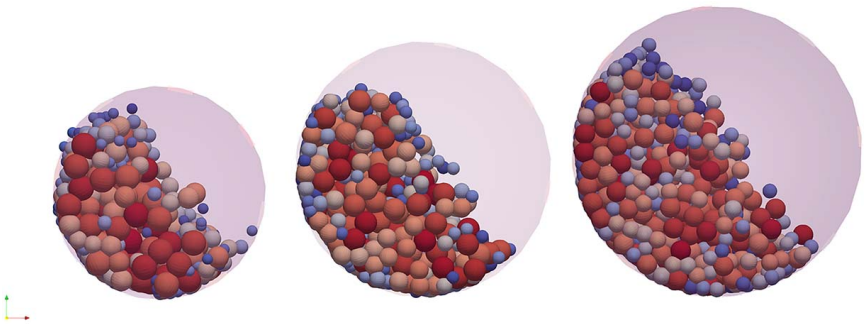

Figure 6.8: Comparison of the simulations with identical parameters across scales for dry milling

Force Ratio

The force ratio analysis for dry milling experiments across the 300, 400, and 500 mm mill diameters provides important details on the dynamics of the milling process. Table 6.2 presents the average ratios of tangential to normal forces acting on the balls for each run, while Figures F.1, F.2, and F.3 illustrate the spatial distribution of force ratios within the mill. It is important to note that the white space in the figures indicates that no ball was present at that spot in any of the analyzed time steps. However, the figures do not represent how often the balls occupied a specific place, but only whether they were present at that point, and what type of force was dominant at that particular point.

Table 6.2: Tangential to normal force ratios in dry milling at different mill diameters

Run No.	Force Ratio (300 mm)	Force Ratio (400 mm)	Force Ratio (500 mm)
1	0.927	1.302	1.192
2	0.829	1.276	1.158
3	0.864	1.223	1.110
4	0.856	1.251	1.135
5	0.873	1.249	1.143
6	0.812	1.173	1.076
7	0.845	1.207	1.114
8	0.915	1.298	1.184

The predominance of tangential forces in most runs suggests that the most typical grinding mechanisms are abrasion and attrition, which are beneficial for achieving finer particle sizes. Impact breakage, associated with higher normal forces, seems to be less prevalent in these simulations. The differences in force ratios can be attributed to variations in operational parameters, as evidenced by the range of force ratios demonstrated across the runs for each mill diameter. The 300 mm mill shows ratios ranging from 0.812 to 0.927, the 400 mm mill—from 1.173 to 1.302, and the 500 mm mill—from 1.076 to 1.192.

The optimal force ratio depends on the desired outcome of the milling process, whether it is to maximize energy efficiency, reduce particle size, or achieve a specific particle shape. This fact suggests the need for a more detailed approach to controlling milling parameters beyond simply pursuing a 'high' or 'low' force ratio. The absence of a clear

pattern in the force ratio distribution across diameters and runs indicates a complex interaction between the mill design and its operational parameters that might not be intuitive. The specific conditions that produce optimal force dynamics for desired milling outcomes require further investigation.

Runs 1, 2, 5, and 8 in both the 400 mm and 500 mm mills show patterns in force distribution (broader area of the dominating tangential force) positively correlated with the filling degree, indicating a direct relationship between this operational parameter and the force distribution across the mill. This observation suggests that adjustments to the filling degree could be a controllable means for optimizing the milling performance. Additionally, runs 3 and 4 in the 500 mm mill show the greatest size reduction alongside higher energy consumption per ore mass, suggesting a problem of balancing the energy use and the milling efficiency. Further analysis could explore whether these operational settings offer a net benefit when considering both energy costs and the value of the increased size reduction.

A more detailed analysis of how tangential and normal forces interact within the milling process could lead to more sophisticated control strategies, such as adjusting the number and height of lifters or modifying the speed coefficient so as to adjust the milling process to specific material characteristics or desired outcomes.

Key Points – Force Ratio – Dry Milling:

- The predominance of tangential forces in most runs suggests that the typical grinding mechanisms are abrasion and attrition, which are beneficial for achieving finer particle sizes.
- Optimal force ratio depends on desired outcome of milling process (energy efficiency, particle size reduction, or specific particle shape).
- Complex interaction between mill design and operational parameters suggests that further investigation is needed into specific conditions producing optimal force dynamics.
- Runs 1, 2, 5, and 8 in both the 400 mm and 500 mm mills show patterns in force distribution (broader area of dominating tangential force) positively correlated with filling degree.
- Balancing energy use and milling efficiency requires consideration to both energy costs and the value of increased size reduction.

Charge Position

The charge (simulated grinding media) position in dry ball milling is an important aspect that influences the grinding efficiency and overall mill performance. The center of circulation (CoC) and the center of gravity (CoG) are two main parameters used to characterize the charge position. Table F.1 in Appendix F presents the CoC and CoG data for various dry ball milling simulations.

The CoC angle ranges from 52.47° to 65.08°, while the CoG angle ranges from 51.05° to 63.84°. The CoC moment arm varies from 0.0387 m to 0.1447 m, and the CoG moment arm varies from 0.0436 m to 0.1451 m. These ranges provide a quantitative information on the position of the charge in the simulations.

Further analysis of the data revealed potential correlations between the mill diameter and both the CoC and the CoG positions. As expected, larger mill diameters seem to have larger moment arms. This fact suggests that the mill diameter plays a significant role in determining the charge position.

The variability in the CoC and CoG angles and arms across different runs with identical diameter but different conditions indicates the sensitivity of charge positioning to operational parameters. Optimizing mill operations may involve fine-tuning these parameters with an aim of achieving the desired charge position and grinding efficiency.

Interestingly, the CoC and CoG angles remain within a narrow range (less than 1 degree of variance) for certain runs, particularly those with higher lifter heights (runs 5, 6, and 7) and a higher number of lifters (runs 1, 5, and 7). This observation suggests that lifter size and quantity may contribute to maintaining similar load dynamics while scaling the mill. However, it is important to note that the stability of the charge position is not solely dependent on lifters but also on the combination of the lifter setup with other operational parameters such as filling degree and rotational speed.

Key Points – Simulated Charge Position – Dry Milling:

- Mill diameter correlates with the CoC and CoG positions and moment arms.
- Charge position is sensitive to such operational parameters as speed and lifter configurations.
- The CoC and CoG angles remain within a narrow range (less than 1 degree of variance) for certain runs, particularly those with higher lifter heights (runs 5, 6, and 7) and a higher number of lifters (runs 1, 5, and 7).
- Higher lifter size and quantity may contribute to stable load dynamics during scaling.
- Charge position stability depends on a combination of the lifter setup and other operational parameters.

Qualitative Analysis of Movement in Dry Milling Simulations

Figure 6.9 shows the dominant type of charge motion observed in the simulations. It varies from cascading (rolling or tumbling) through cataracting to centrifuging, depending on the operational parameters. Cascading motion is characterized by a continuous circulation of the charge, with particles rolling down the free surface. The result is a combination of abrasion, attrition, and some impact breakage. Cataracting occurs when particles are thrown clear of the charge into the free space above, falling on parabolic trajectories, and impacting the toe of the charge or mill shell. This type of movement leads to higher energy impact breakage.

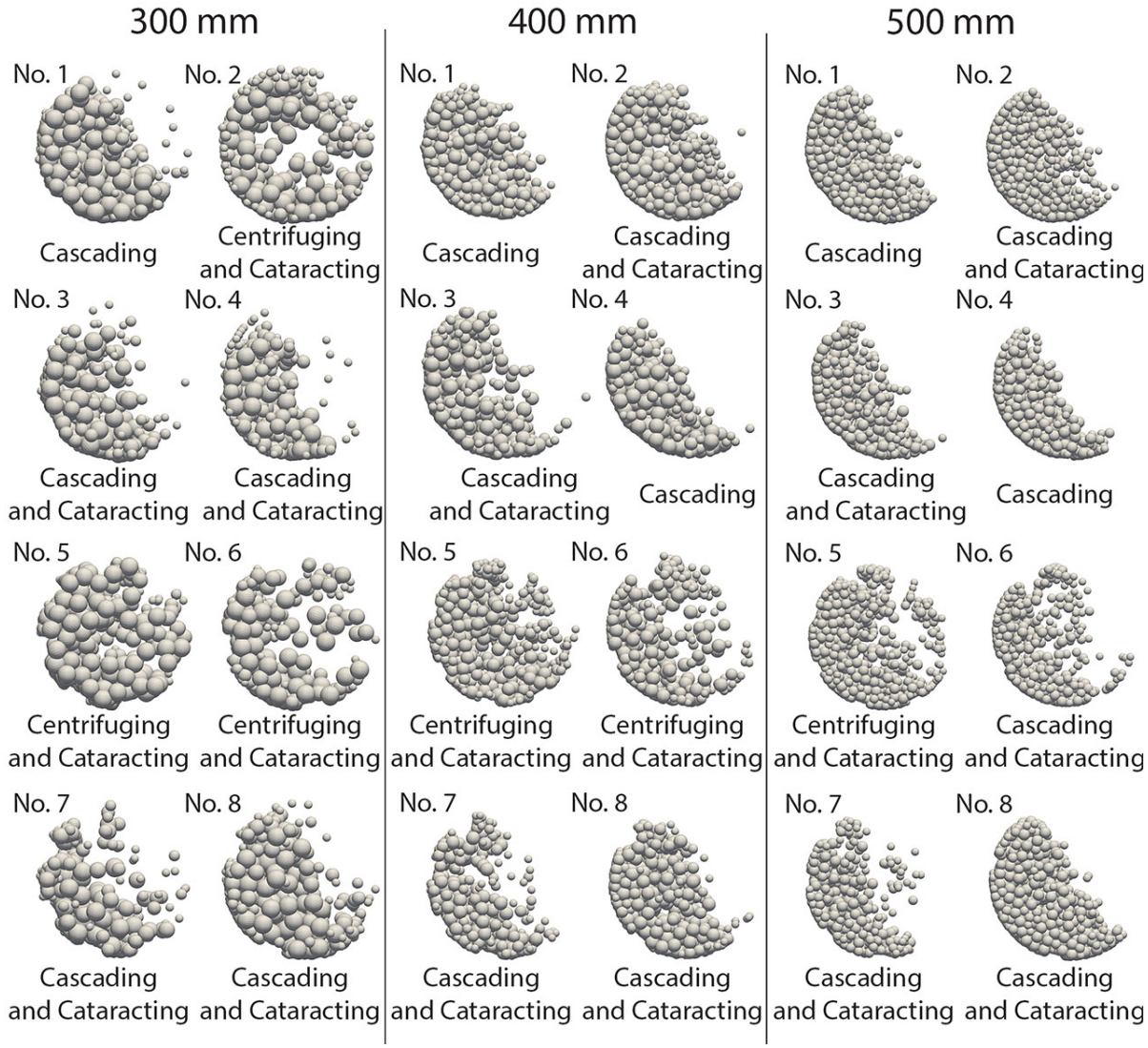

Figure 6.9: Dominant type of charge motion

The dominant type of motion is a combination of cascading and cataracting, but for specific cases, there is an observable shift from centrifuging to cataracting and from cataracting to cascading as the diameter increases. The most stable runs across scales, exhibiting the same type of dominant motion, are runs 1, 3, 5, 7, and 8. The most common denominator of operational parameters for these runs is the number of lifters; 4 out of 5 runs with the same type of movement across scales have a higher number of lifters, except for run 8.

Run 2 shifts from centrifuging and cataracting at the diameter of 300 mm to cascading and cataracting at higher diameters. Run 4 moves from cascading and cataracting to just cascading at higher diameters. Run 6 is centrifuging and cataracting at the diameters of 300 and 400 mm but shifts toward cascading and cataracting at the 500 mm diameter. For the runs that shift the type of movement across scales (runs 2, 4, and 6), the common values are a lower number of lifters, lower lifter height, lower filling degree, and higher speed. This fact may mean that more lifters can stabilize the type of charge movement across scales, while fewer lifters with lower height, as well as lower filling degree, and higher speed can increase the effect of scale on charge behavior.

At the lowest diameter, 3 runs (2, 5, 6) approximate the centrifuging motion, which may impact experimental results, in particular the measured torque and size reduction. All these runs have higher rotational speed, suggesting that the selected upper limit of rotational speed could be too high. However, run 3, with lower lifters and lower filling degree, represents the desired cascading and cataracting type of movement even with higher rotational speed.

The optimal movement, a mixture of cascading and cataracting, is present in runs 3, 4, 7, and 8 in the 300 mm mill. The operational parameters do not have any patterns. It could be hypothesized that optimal movement is produced by a combination of lower lifters with lower filling degree and higher lifters with lower rotational speed, or fewer lifters with lower rotational speed and more lifters with lower filling degree.

For the 400 mm ball mill, optimal charge type movement is achieved in runs 2, 3, 7, and 8. Here, higher lifters are combined with lower rotational speed, while lower lifters are combined with higher rotational speed. The number of lifters is combined with the filling degree; in the mentioned runs higher filling degree is combined with fewer lifters and vice versa.

For the 500 mm ball mill, optimal runs 2, 3, 6, 7, and 8 show a slight dominance in higher rotational speed, lower filling degree, fewer lifters, and higher lifters across all parameters.

Key Points – Charge Movement in Simulations – Dry Milling:

- The dominant type of charge motion for most cases is cascading and cataracting.
- There is an observable shift from centrifuging to cataracting and from cataracting to cascading as the diameter increases.
- More lifters can stabilize the type of charge movement across scales—runs 1, 3, 5, 7, 8 have the same type of movement across scales and 4 out of 5 (except for run 8) have more lifters.
- For runs 2, 4, 6 fewer lifters with lower height, lower filling degree, and higher speed can increase the effect of scale on charge behavior.
- Lower diameter mills are more prone to centrifuging, and this fact may impact experimental results.
- Optimal movement, a mixture of cascading and cataracting, is achieved through specific combinations of lifter height, filling degree, and rotational speed.
- The influence of operational parameters on optimal charge motion varies with mill diameter.

6.2.4 Recordings

The analysis of the recorded dry ball milling performance, as presented in Table F.2 in Appendix F, provides information on the behavior of the mill charge under various operational parameters. The centroid, which represents the center of gravity of the masked area representing the mill charge (grinding media and ore particles), is calculated for each frame at each time step and then averaged for the entire simulation.

As expected, the variation in the centroid coordinates and the corresponding angle suggest differences in the charge position and orientation within the drum across different runs. Notably, only run 4, whose angle from the vertical axis to the centroid of the charge area is lower than 90° for all scales, provides a clear indication of how operational parameters influence charge positioning. This observation is consistent with the expectation that lowering all of the modified parameters results in a lower shoulder position and, consequently, in a lower center of gravity.

In most of the other runs with lower rotational speeds, such as runs 1, 7, and 8, the angles also tend towards or below 90 degrees. Interestingly, even runs 7 and 8, which have higher mill lifter heights, have angles below 90 degrees for the drum diameters of 400 and 500 mm. This counter intuitive finding suggests that rotational speed, expressed as a fraction or percentage of critical speed, may have a more significant impact on the charge shoulder position than the mill lifter height.

The innovative data collection method, which utilizes computer vision to record the centroid coordinates of the charge, offers a novel approach to monitoring mill operation. Analyses of its accuracy, limitations, and potential for real-time optimization could inform its applicability and effectiveness in industrial settings.

Key Points – Recordings – Dry Milling:

- The CoG coordinates and angles vary across runs, indicating differences in charge position and orientation.
- Run 4, with all parameters lowered, consistently shows angles below 90°, confirming the influence of operational parameters on charge positioning.
- In most of the runs with lower rotational speeds, such as runs 1, 7, and 8, the angles also tend towards or below 90 degrees.
- Interestingly, even runs 7 and 8, which have higher mill lifter heights, show angles below 90 degrees for the 400 and 500 mm drum diameters.
- Rotational speed may have a more significant impact on charge lifting height than lifter height does.

Qualitative Analysis of Movement in Recordings

Figure 6.10 shows the dominant type of charge motion observed in the recorded experiments. It varies in a manner analogical to that described in the Qualitative Analysis of Movement in Dry Milling Simulations part.

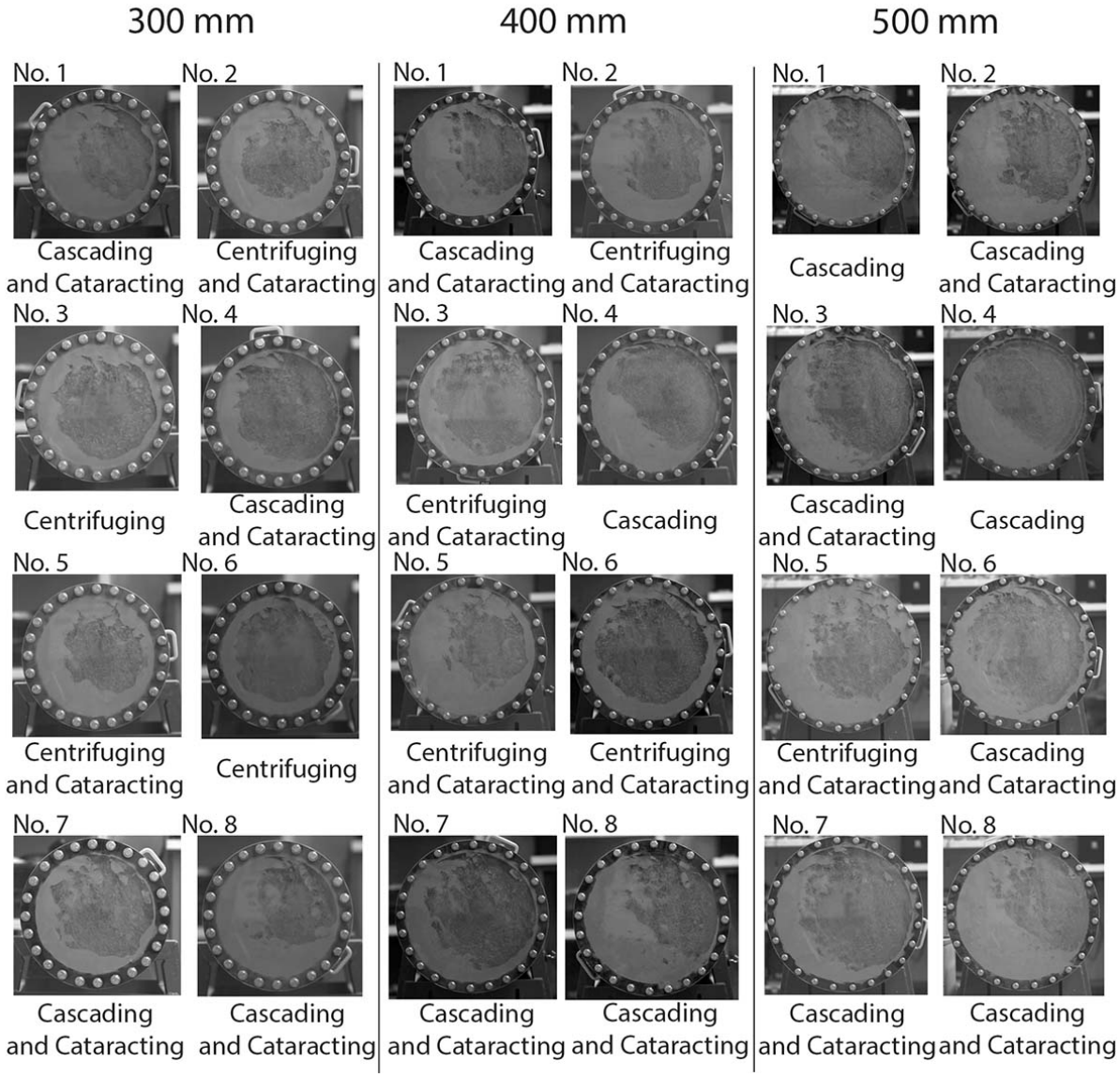

Figure 6.10: Dominant type of charge motion in recorded experiments of dry milling

The dominant types of movement observed in the recordings were cascading and cataracting. Runs 5, 7, and 8 showed the same type of motion across all mill diameters. For the remaining runs, the movement type was observed to change with the increasing diameter, from centrifuging to cataracting and from cataracting to cascading.

For the 300 mm diameter mill, the optimal type of movement—a combination of cascading and cataracting - was observed in runs 1, 4, 7, and 8, which were all performed with lower rotational speeds. Similarly, for the 400 mm diameter mill, runs 1, 7, and 8 showed the same optimal motion, with the exception of run 4, which had all operational parameters set to low values. In this case, the combination of cascading and cataracting changed to cascading only.

In the case of the 500 mm ball mill, optimal motion was observed in runs 2, 3, 6, 7, and 8, which demonstrated a slight dominance of higher rotational speed, lower filling degree, fewer lifters, and higher lifters across all parameters. Conversely, Run 5, with all operational parameters at high levels, showed centrifuging across all scales.

Key Points – Charge Movement in Recordings – Dry Milling:

- Dominant types of movement: cascading and cataracting.
- Stable motion across scales in Runs 5, 7, and 8.
- Movement type has a trend from centrifuging to cataracting and from cataracting to cascading as diameter increases.
- Optimal motion (cascading and cataracting) observed at lower rotational speeds for the 300 mm and 400 mm mills.
- For the 500 mm mill, optimal motion was obtained with higher rotational speed, lower filling degree, fewer lifters, and higher lifters.
- Run 5 (all parameters at high levels) showed centrifuging across all scales.

6.2.5 Torque Correlation Analysis Results

The Torque Correlation Analysis Results subsection explores the relationships between the measured torque and various simulated and recorded parameters in the dry milling experiments. It is divided into three sub-subsections: Simulated CoG and CoC, Recorded CoG and Torque, and Comparison of Recordings and Simulations. The first sub-subsection investigates the correlations between the torque, the simulated center of gravity (CoG), and center of circulation (CoC) of the grinding media. It identifies the main factors influencing torque and the potential for optimization. The second sub-subsection analyzes the correlations between the torque, the recorded CoG, and other metrics. It provides insights into factors which influence torque in a real-world ball mill setting. The third sub-subsection compares the simulated and the recorded CoG parameters and serves to validate the accuracy of the simulation models and to identify areas for further research.

Simulated CoG and CoC

The correlations between torque and the simulated center of gravity (CoG) and the center of circulation (CoC) of the grinding media, were calculated based on the data in Table F.1 in Appendix F. The scatter plots of torque versus the angles and moment arms of the center of circulation (CoC) and the center of gravity (CoG), presented in Figure L.1 in Appendix L, reveal a weak negative trend between torque and CoC/CoG angles compared to the strong positive correlation with moment arm length. The CoC and CoG are important in descriptions of the circulation of the charge within the ball mill, as the CoC located along the equilibrium surface differentiates the ascending charge from the descending charge. Although the correlation with the moment arm was expected, this finding shifts the focus towards optimizing the moment arm length for torque management.

Pearson's correlation analysis further supports these observations. The correlation coefficients (Pearson's r) between the torque and the CoC/CoG angles are -0.292 and -0.209, respectively, indicating a weak negative correlation. In contrast, the correlation coefficients between the torque and the CoC/CoG arm lengths are 0.826 and 0.825, respectively, suggesting a strong positive correlation. The p-values for the arm length correlations are 0.000, indicating high statistical significance, while the p-values for the angle correlations are 0.166 and 0.328, and suggest that the negative correlations are not statistically significant.

Among the most important insights from this analysis are the high correlations between the arm lengths (CoC and CoG) and the torque and the suggestion that the CoC seems a minimally more effective predictor of torque. These findings highlight the relevance of charge position, as measured by the CoC and the CoM, in the optimization of mill design and operational efficiency.

Key Points – Simulated CoG and CoC – Dry Milling:

- Weak negative trend is observed between torque and CoC/CoG angles.
- Strong positive correlation is observed between torque and moment arm length.
- High correlation is observed between arm lengths (CoC and CoG) with torque.
- CoC is potentially a minimally more effective predictor of torque than CoM.
- Charge position (CoC and CoG) is relevant for mill design optimization and operational efficiency improvement.

Recorded CoG and Torque

The correlation analysis conducted on the recorded center of gravity (CoG) and torque metrics, based on the data in Table F.2 in Appendix F, offers detailed information on the factors influencing torque in ball mill experiments. The scatter plots in Appendix L serve as a descriptive tool and are used to visualize the correlation between the torque and each variable, confirming the described trends and offering a more intuitive understanding of the relationships between the data.

The correlation analysis revealed significant relationships between the measured torque and the investigated variables. The strong positive linear relationship between the charge mass and the torque (Pearson's r=0.898, p-value=0.000) directly attributes higher torque values to increased load mass. This correlation is both statistically significant and operationally important, confirming the behavior as expected and offering a straightforward strategy for influencing torque via charge mass adjustments.

Similarly, the significant and strong positive correlation between the arm length and the torque (Pearson's r=0.823, p-value=0.000) demonstrates the influence of geometric factors on the torque. It is important that moment arm length has almost as strong impact on the torque as the charge mass does. The adjusting of the arm length, implicitly through other operational settings, may translate into optimizing mill performance.

The moderate negative relationship between the angle and the torque (Pearson's r= -0.512, p-value=0.011) is an indicator of more complex dynamics, as increasing angles correlate with the decreasing torque. This observation suggests that angle adjustments, through operational or design modifications, may also have an influence on torque management, although the more scattered plot for the torque vs. the angle implies more complicated interactions that go beyond the linear correlation and that could be further explored in the context of the complexities of the effect of the angle on the torque.

Key Points – Recorded CoG and Torque Correlation – Dry Milling:

- Significant relationships exist between the measured torque and the load mass, angle, and arm length.

- Strong positive linear relationship is observed between the load mass and the torque, as well as between the arm length and the torque.
- The moment arm length has almost as strong impact on the torque as the charge mass does.
- Moderate negative relationship between the angle and the torque suggests a potential for torque management through angle adjustments.

Comparison of Recordings and Simulations

This section discusses the comparison between the center of gravity (CoG) of the grinding media obtained from the simulations and the CoG of the full charge obtained from the recordings. The aim is to assess how well the behavior of a real mill can be predicted in simulations. Figure L.3 in Appendix F illustrates the simulated versus the measured CoG angles and arms.

The validation of the simulated CoG angles and moment arms against measured values translates into the precision and applicability of simulation models in predicting real-world ball mill behavior. Correlation analyses comparing the simulated and the actual CoG measurements are important for validating the simulation accuracy. The scatter plots comparing the simulated and the measured CoG angles and arms serve to support the quantitative correlation analysis.

The moderate to strong positive correlations between the simulated and the measured CoG parameters, with Pearson's r values of 0.549 (p=0.005) for the CoG angles and 0.677 (p=0.000) for the CoG arms, prove the effectiveness of the simulation model in representing the most important aspects of mill charge dynamics. The substantial correlation between the simulated and the measured CoG arms, with the higher Pearson's r value, indicates that arm length predictions from simulations are particularly reliable.

However, room for further research exists. Identifying new factors and investigating those not yet fully analyzed could improve the accuracy and predictive potential of the model. Discrepancies between simulations and measurements could be also explored, along with their potential reasons.

The difference identified between the simulation and the recorded values may be attributed to the fact that the simulations covered only the grinding media, while the recordings reflected the full charge. This observation confirms the complexity of real-world milling environments. Investigating the impact of integrating ore characteristics into simulations could enhance the realism of the model. The discrepancies and additional influencing factors not yet identified in the here analyzed models require further investigation.

Key Points – Comparison of Recordings and Simulations – Dry Milling:

- The simulated CoG angles and arms were validated against the measured values in order to assess the accuracy of simulation models and their applicability in predicting real-world ball mill behavior.
- The identified moderate to strong positive correlations between the simulated and the measured CoG parameters confirm the effectiveness of the simulation model in representing the main aspects of mill charge dynamics.

- The substantial correlation between the simulated and the measured CoG arms indicates that the arm length predictions from the simulations are particularly reliable.
- The observed discrepancies between the simulations and the measurements suggest room for further research, such as investigations of additional factors and integrating ore characteristics into simulations.

6.3 Wet Milling Experimental Series Results

This section presents the findings from the comprehensive analysis of the wet milling experiments conducted for various mill diameters. It discusses the sensor measurements, including the rotational speed, torque, and power draw, providing insights into the stability, variability, and efficiency of the wet milling process. The section also examines the product size distribution, comparing the effectiveness of different mill diameters in achieving finer particle sizes and higher size reduction ratios under wet conditions. Additionally, it presents the results of the wet milling simulations, focusing on the force ratio and charge position, and it explores the correlations between the torque and the simulated data.

6.3.1 Sensor Measurements

This subsection presents the results obtained from the sensors used during the wet milling experiments, including rotational speed, torque, and power draw. It analyzes the stability and control of the mill rotational speed in the presence of slurry, the variability and transient behavior of the torque measurements under wet conditions, and the power consumption trends across the three mill diameters. The subsection also investigates the correlations between the torque and the power draw. Additionally, it explores the impact of slurry density on the accuracy of the rotational speed control system and on the variability of the torque and power signals.

Rotational Speed

During wet milling experiments, the rotational speed measurements were performed for three mill diameters. Each experimental series consisted of 8 experiments, resulting in a total of 24 measurements (Figure G.1 and Table G.1 in Appendix G).

The mean RPM values for each wet measurement are close to the set RPM values. This fact indicates that the rotational speed of the mill was well-controlled and maintained at desired levels, even in the presence of slurry. This information is important, as it confirms that the operational parameters were well-controlled despite the complexity introduced by the wet conditions.

The standard deviation of the RPM signal is relatively low (0.05 to 0.22), suggesting minimal fluctuations and stable operation of the mill during wet grinding. This observation demonstrates the reliability of the test equipment under varying wet conditions.

The coefficient of variation (CV) is consistently very low for all wet measurements, confirming the stability and consistency of the rotational speed during the wet grinding process. Low CV confirms the precision of the control system, although the non-zero standard deviations indicate some variation.

Skewness values are generally close to zero, indicating a relatively symmetric RPM distribution, albeit some measurements show minimally negative or positive skewness.

Kurtosis values range from 2.29 to 6.09, with most values close to 3, indicating the RPM distribution is similar to a normal distribution. Only few measurements show higher kurtosis values. These statistics are interesting for understanding the data distribution but not critical from the operational perspective.

The mean deviation from the set RPM is relatively small (0.77 to 3.16), indicating that actual RPM values are close to desired set points. Slightly lower deviation values for larger diameters suggest better control with larger diameters. This fact emphasizes the precision of the milling process control.

The standard deviation of deviation is low (0.05 to 0.22), further confirming the consistency and accuracy of RPM control and proving the reliability of the control mechanism.

The percentage of time the RPM signal remains within acceptable limits ($\pm 5\%$ of set RPM) is very high for most wet measurements, albeit with several exceptions, demonstrating well-maintained rotational speed within specified limits throughout the entire process.

Overall, the results indicate that the rotational speed of the mill is stable, well-controlled, and consistently maintained at desired set points, with low variability, small deviations, and a high percentage of time within the acceptable limits. The presence of slurry does not seem to significantly affect the stability and control of the rotational speed.

It is interesting to note that all of the measured RPM values are higher than the set RPM values, albeit still within acceptable limits. In each experimental series, there were 4 experiments with high rotational speed and 4 experiments with low rotational speed. The measurements are grouped together as expected, but the range of the RPM values inside the low and high groups becomes wider together with the mill diameter.

In the mill with the greatest diameter, run 2 and run 4 tend toward lower values within the high-speed group, while run 5 and run 7 in the lower group also tend towards lower RPM values. Interestingly, all of these runs have lower slurry density, and they also have the lowest deviation of the mean from the set RPM value. It could be hypothesized that the accuracy of the rotational speed control system is influenced by both the slurry density and the formation of a slurry pool in the toe region.

Key Points – Rotational Speed Sensor Measurements – Wet Milling:

- The rotational speed of the mill was well-controlled and maintained at desired levels during wet milling, despite the presence of slurry.
- Low standard deviation and coefficient of variation indicate minimal fluctuations and stable operation.
- Mean deviation from set RPM is small (up to 5%), confirming the precision of the control system.
- The percentage of time within acceptable RPM limits is high, demonstrating consistent control.
- Slurry density may impact the accuracy of the rotational speed control system. Runs with lower slurry density have the lowest deviation from the set RPM.
- The presence of slurry pooling in the toe region of the mill may influence the stability and control of the rotational speed.

Torque

The torque measurements were conducted for three mill diameters: 300 mm, 400 mm, and 500 mm, with 8 experiments for each diameter, totaling 24 experiments (Tables H.1, H.2, and H.3 in Appendix H). All experiments were performed under wet milling conditions with the presence of slurry. The mean torque values across all scales were consistently negative, indicating the resistance force exerted by the mill charge on the moving ball mill due to gravity.

The standard deviation and coefficient of variation (CV) values indicate moderate to high measurement variability and dispersion. Notably, two CV values exceeded 100%, indicating that the standard deviation for those measurements was larger than the absolute mean value. This high variability could be attributed to the complexities of the motion of the charge and to the grinding mechanisms within the mill, e.g. during cascading and cataracting, as well as to the combination of impact breakage and abrasion.

Transient analysis did not reveal the transient state for most runs with lower slurry density at the 400 mm and 500 mm diameters. However, for other runs, the mills required a considerable amount of time to stabilize, with rise times ranging from 40.2 s to 1330.72 s (Figure 6.11). The shortest rise times were observed for the smallest mill diameter. For most runs, the settle time approached the end time of the experiment (1800 s), indicating that the signal was out of the range close to the steady-state mean at the end of the experiment.

The correlation between the measured torque and the power depended on slurry density. Measurements with higher slurry density (1, 3, 6, 8) tended to have a very high correlation between torque and power. In contrast, for lower slurry densities, the correlation was significantly different, with very low and sometimes even negative correlations observed across all scales.

Key Points – Torque Sensor Measurements – Wet Milling:

- Moderate to high variability and dispersion was observed in measurements, with some CV values exceeding 100%.
- Transient state was not observed for most runs with lower slurry density at larger diameters.
- Rise times ranged from 40.2 s to 1330.72 s, with shortest times for the smallest mill diameter.
- High correlation between the torque and the power was observed for higher slurry densities, while low or negative correlation was observed for lower densities

Power Draw

The power draw measurements were performed for three different mill diameters (300 mm, 400 mm, and 500 mm) under wet milling conditions, with eight experiments conducted for each diameter. The measurement data are presented in Tables I.1, I.2, I.3 in Appendix I, and the signal plots in Figure 6.12.

Mean power consumption shows a clear increasing trend correlated with the increase in mill diameter. This fact indicates higher energy requirements for larger mills under wet milling conditions. As the mill size increases, so does the power required to achieve effective

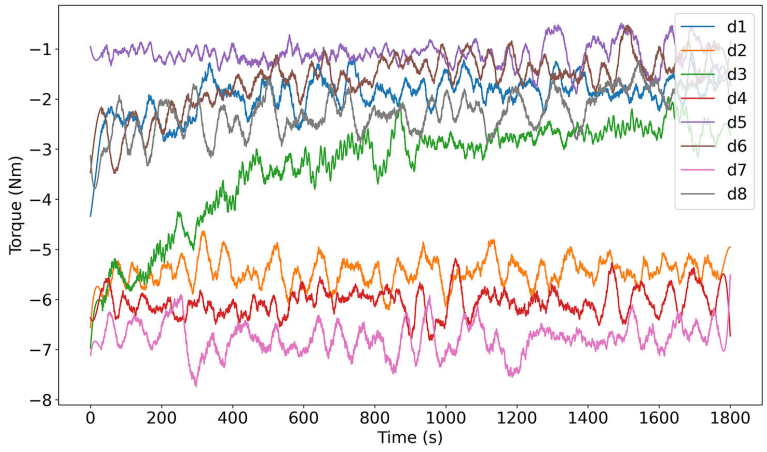

(a) D=300 mm

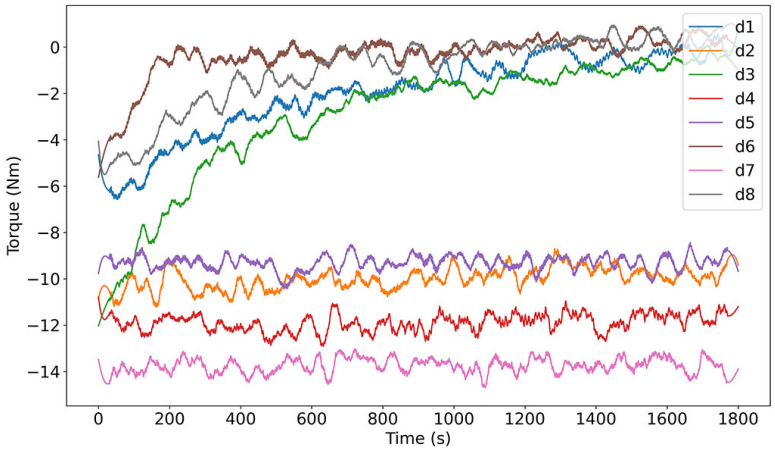

(b) D=400 mm

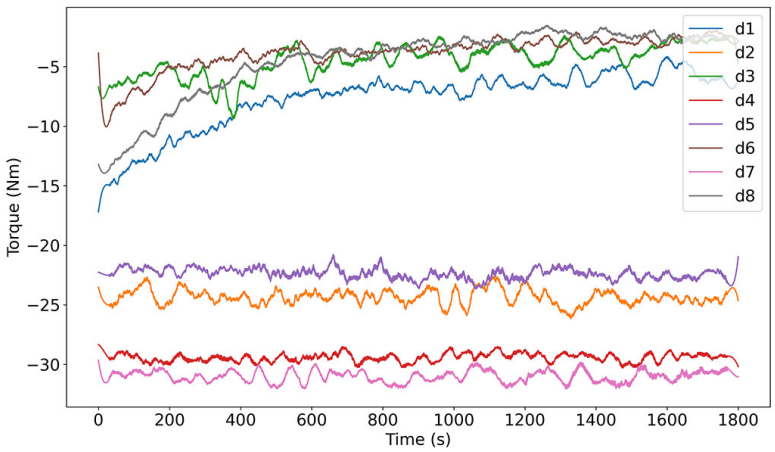

(c) D=500 mm

Figure 6.11: Pre-processed torque signals for wet milling experiments at different mill diameters

grinding. Additionally, the variability in power consumption, as shown by the standard deviation, generally increases with the size of the mill. This observation suggests that larger mills are more susceptible to fluctuations in power use. However, the coefficient of variation (CV) for all experiments shows mostly low to moderate variance without any strong trend, with only a slight increase in values as the scale increases. This fact implies that although absolute variations in power consumption increase with scale, probably due to the larger charge volume and more intensive charge motion, the relative variations remain relatively stable.

The steady-state mean power indicates consistent power requirements during the reported stable operational phase. The power requirements increase with mill diameter. This is an important factor in designing and implementing operational control measures which ensure sustained grinding effectiveness and energy efficiency. Furthermore, the fact that overshoot values increase with mill diameter may indicate a higher initial energy expenditure required to bring larger mills to operational stability. This initial energy expenditure may be related to the need to overcome the inertia of the larger charge mass and to establish the desired charge motion, such as cascading or cataracting, depending on the operating conditions. This observation is crucial for the process startup phase, suggesting that larger systems may require more careful control in order to minimize energy waste due to overshoot.

The transient analysis, including the rise and settling times, shows consistently low rise times, mostly under one minute, indicating that the mill quickly reaches stable power draw after the initial startup phase. The settle time for all measurements is over 1760 s, which is very close to the end of the experiment, meaning that the operating conditions were stable throughout the entire experiment duration, and the values were not out of the range around the steady-state mean.

Lastly, although negative skewness was recorded for most of the experiments with lower slurry density, there is no recognizable pattern in the kurtosis values.

Key Points – Power Draw Sensor Measurements – Wet Milling:

- Mean power consumption increases with mill diameter, indicating higher energy requirements for larger mills.
- Variability in power consumption increases with mill size, but relative variations (CV) remain stable.
- Steady-state mean power indicates consistent power requirements during stable operation, critical for design and control.
- Overshoot values increase with mill diameter, suggesting the need for careful control during startup to minimize energy waste.
- Low rise times ($<$ 1 min) indicate quick stabilization of power draw after startup, while long settle times ($>$ 1760s) show stable operation throughout experiments.
- Experiments with lower slurry density tend to result in negative skewness.

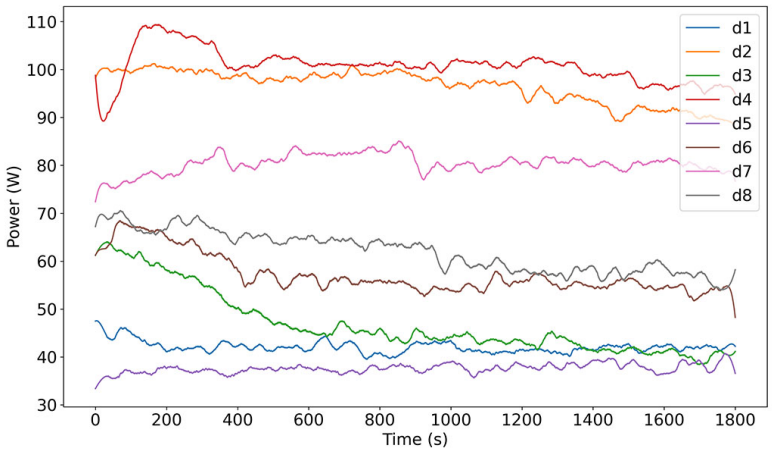

(a) D=300 mm

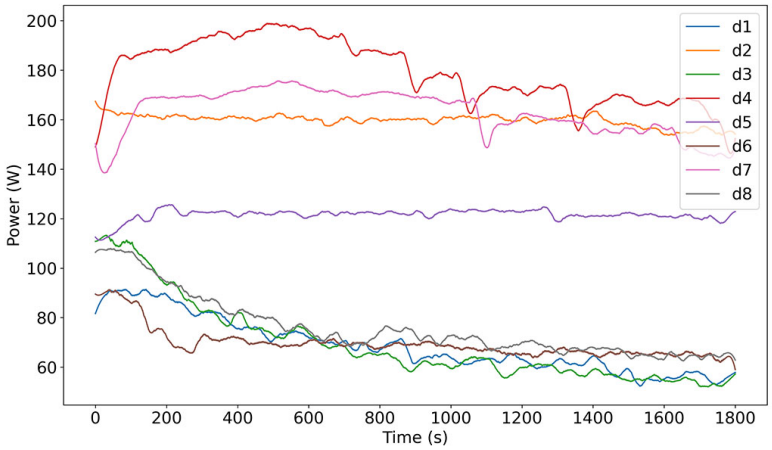

(b) D=400 mm

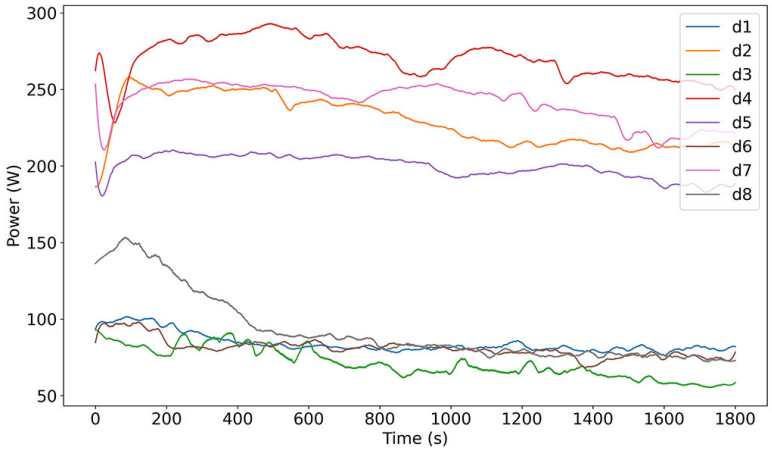

(c) D=500 mm

Figure 6.12: Pre-processed power signals for dry milling at different mill diameters

6.3.2 Product Size Distribution

The product size distribution analysis for wet milling experiments provides valuable insights into the complex relationships between mill diameter, slurry properties, and operational parameters. Table 6.3 presents the d_{80} values and size reduction ratios for each run, while Figures J.1, J.2, and J.3 in Appendix J illustrate the cumulative size distribution curves for milled products.

Table 6.3: Particle size reduction results for wet milling at various mill diameters

Run No.	300 mm: d_{80} (μm)	size reduction	400 mm: d_{80} (μm)	size reduction	500 mm: d_{80} (μm)	size reduction
1	357.3	2.452	118.0	7.424	188.6	4.644
2	66.7	13.143	45.6	19.211	54.3	16.141
3	218.9	4.002	224.2	3.908	217.5	4.028
4	79.1	11.079	77.2	11.354	81.8	10.704
5	125.8	6.965	85.4	10.253	101.6	8.626
6	268.6	3.262	255.6	3.428	226.9	3.861
7	75.4	11.613	68.7	12.750	70.1	12.492
8	347.7	2.520	221.2	3.961	278.4	3.147
Average	192.4	6.879	137.0	9.036	152.4	7.955

The average d_{80} values for the 300, 400, and 500 mm mills are 192.4, 137.0, and 152.4 µm, respectively, with the 400 mm mill achieving the finest average d_{80} value. Interestingly, the 500 mm mill shows minimally coarser products compared to the 400 mm mill. This fact suggests that the relationship between mill diameter and product size distribution in wet milling is complex and may be influenced e.g. by slurry properties and rheology. The factors behind this non-linear relationship require further analysis.

In terms of milling efficiency, the average size reduction ratios for the 300, 400, and 500 mm mills are 6.879, 9.036, and 7.955, respectively. The 400 mm mill achieves the highest average size reduction ratio. It indicates the best milling efficiency among the three mill diameters under wet milling conditions. This fact is important for understanding the efficiency trends and performing a more detailed analysis of the reasons behind the higher efficiency of the 400 mm mill.

The cumulative size distribution curves for each mill diameter in wet milling reveal a wide range of particle size distributions, probably influenced by the different grinding mechanisms, such as impact breakage, abrasion, and attrition, that dominate under various operating conditions. The curves for the 400 mm and 500 mm mills show a more considerable shift towards finer particle sizes, consistent with the lower d_{80} values and higher size reduction ratios observed for these mill diameters.

Runs with lower slurry density are observed to result in significantly higher size reduction rates compared to runs with high slurry density. This clear pattern suggests that slurry pooling in the toe region or its dumping properties may change and impact the efficiency of impact breakage. Slurry density may thus seem to be an important factor in optimizing in wet milling.

Key Points – Product Size Distribution – Wet Milling:

- The 400 mm mill achieves the finest average d_{80} value and highest size reduction ratio, suggesting an optimal scale for wet milling efficiency.
- In terms of milling efficiency, the average size reduction ratios for the 300, 400, and 500 mm mills are 6.879, 9.036, and 7.955, respectively.

- The relationship between mill diameter and product size distribution in wet milling is complex and influenced by such factors as slurry properties and rheology.
- Slurry density appears to be an important factor in wet milling, with lower densities resulting in higher size reduction ratios.
- Further investigation into slurry characteristics is necessary so that the multifactorial nature of milling efficiency in wet conditions can be fully understood.

6.3.3 Simulations

This subsection presents the results of the wet milling simulations conducted on the calibrated models. Figure 6.13 shows examples of simulation runs with identical operational parameters across all mill scales under wet conditions, providing a visual comparison of the charge motion and distribution in the presence of the slurry. The subsection analyzes the force ratio, which is the ratio of tangential to normal forces acting on the balls, and the charge position, characterized by the center of circulation (CoC) and the center of gravity (CoG). It examines the spatial distribution of force ratios within the mill and the influence of operational parameters, including slurry density, on the charge position. It also provides information on the dynamics of the wet milling process, the factors affecting the efficiency and performance of the mill under wet conditions, and the differences between wet and dry milling simulations. The findings allow a better understanding of the complex interactions between the grinding media and the slurry in the wet milling process, as well as of the dominant types of charge motion, such as cascading, cataracting, and slurry pooling.

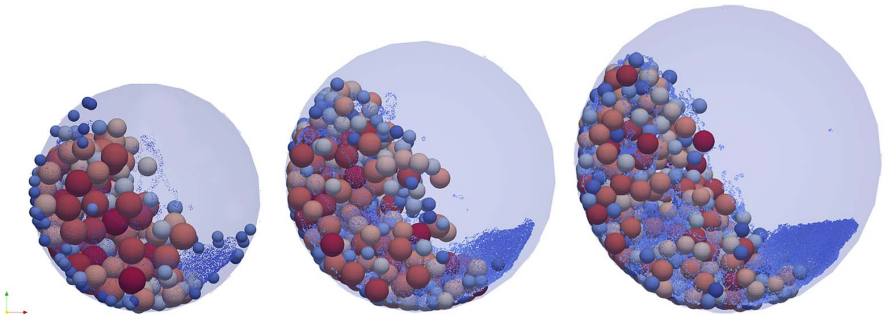

Figure 6.13: Comparison of the simulations with identical parameters across scales for wet milling

Force ratio

The force ratio, defined as the ratio of tangential to normal forces acting on the balls, is important in the analyses of the dynamics of wet milling. Table 6.4 presents the average force ratios for each run, while Figures K.1, K.2, and K.3 in Appendix K show the spatial distribution of force ratios within the mill.

Table 6.4: Tangential to normal force ratios in wet milling at different mill diameters

Run No.	Force Ratio (300 mm)	Force Ratio (400 mm)	Force Ratio (500 mm)
1	0.810	1.203	1.164
2	0.836	1.201	1.152
3	0.918	1.291	1.206
4	0.840	1.204	1.129
5	0.848	1.210	1.164
6	0.785	1.152	1.116
7	0.970	1.351	1.240
8	0.800	1.124	1.045

Wet milling shows a range of force ratios: from 0.785 to 0.970 for the 300 mm mill, from 1.124 to 1.351 for the 400 mm mill, and from 1.045 to 1.240 for the 500 mm mill. The highest force ratio is observed for the 400 mm mill diameter at run 7 (1.351). This fact suggests that certain combinations of operational parameters can lead to significantly increased tangential forces. The variation in force ratios can be attributed to the different grinding mechanisms, such as impact breakage, abrasion, and attrition, which are influenced by the charge motion and operating conditions. Interestingly, run 7 has the highest ratio for each diameter, while run 8 has the smallest or second smallest ratio for all diameters. The two runs differ in slurry density, lifter height, and rotational speed, with run 8 having all operational parameters at a high level and run 7 having those three parameters at a lower level. This observation indicates that the above parameters or their interactions may have the most significant impact on the force ratio.

The lowest mill diameter (300 mm) consistently shows the lowest force ratios, while the difference between the 400 mm and 500 mm mills is much smaller. However, for the same runs, the force ratio values are always slightly lower for the 500 mm mill compared to the values for the 400 mm mill.

A consistent trend can be observed in the spatial distribution of force ratios (Figures K.1, K.2, and K.3), with the largest area of tangential force domination occurring in runs 3, 4, and 7. The only parameter shared between these runs is the higher filling degree.

Key Points – Force Ratio – Wet Milling:

- Force ratio varies with mill diameter, with the lowest ratios observed in the 300 mm mill and the highest in the 400 mm mill.
- Run 7 has the highest force ratio for each diameter, while run 8 has the smallest or second smallest ratio for all diameters. Run 8 has all operational parameters at a high level and run 7 has slurry density, lifter height, and rotational speed at a lower level.
- Higher filling degree (runs 3, 4, 7) is associated with larger areas of tangential force domination within the mill.
- For the same runs, the force ratio values are always slightly lower in the 500 mm mill compared to the values in the 400 mm mill.

Charge Position

Table K.1 in Appendix K presents the calculated center of circulation (CoC) and center of gravity (CoG) angles and arms for various ball mill diameters and cases under wet milling conditions. The data is based on the results of simulations for the grinding media (steel balls) and their respective center of gravity and center of circulation positions.

The CoC angle ranges from 50.34° to 61.07°, while the CoG angle varies between 50.45° and 59.28°. The CoC arm values are from 0.0334 m to 0.1308 m, and the CoG arm values are from 0.0408 m to 0.1315 m. As expected, the moment arms differ across mill diameters. However, some runs maintain lower ranges of variation within the angles:

- Run 2: CoC range of 1.24°, CoG range of 0.66°
- Run 7: CoC range of 1.77°, CoG range of 0.81°
- Run 4: CoC range of 2.07°, CoG range of 1.61°
- Run 5: CoC range of 2.22°, CoG range of 1.29°

Interestingly, the four runs with lower slurry density (2, 7, 4, 5) have more stable ranges of angles across scales compared to the other four runs with higher density. This observation suggests that lower slurry density may promote a more consistent charge motion, possibly due to different slurry pooling and dampening effects in the toe region of the mill. Furthermore, runs 2 and 7, which have the lowest difference in angles across scales, also share a lower lifter height. This fact implies that the lifter height parameter may influence the stability of the charge behavior in the ball mill.

Key Points – Charge Position – Wet Milling:

- CoC and CoG angles and arms vary across ball mill diameters and individual cases under wet milling conditions.
- Runs (2, 7, 4, 5) with lower slurry density show more stable ranges of angles across scales.
- Runs 2 and 7, which have the lowest difference in angles across scales, also share a lower lifter height.

Qualitative Analysis of Movement

The grinding media and approximate slurry surface based on the SPH slurry particles were analyzed for all DEM-SPH simulations across all scales, as shown in Figure 6.14. In the simulations, runs 5-8 showed stable behavior across all scales, possibly due to the higher number of lifters. The lifter number may thus seem an important parameter in the reproducibility of charge behavior across scales. Slurry pooling in the toe area was the most considerable in runs with the dominant cascading motion.

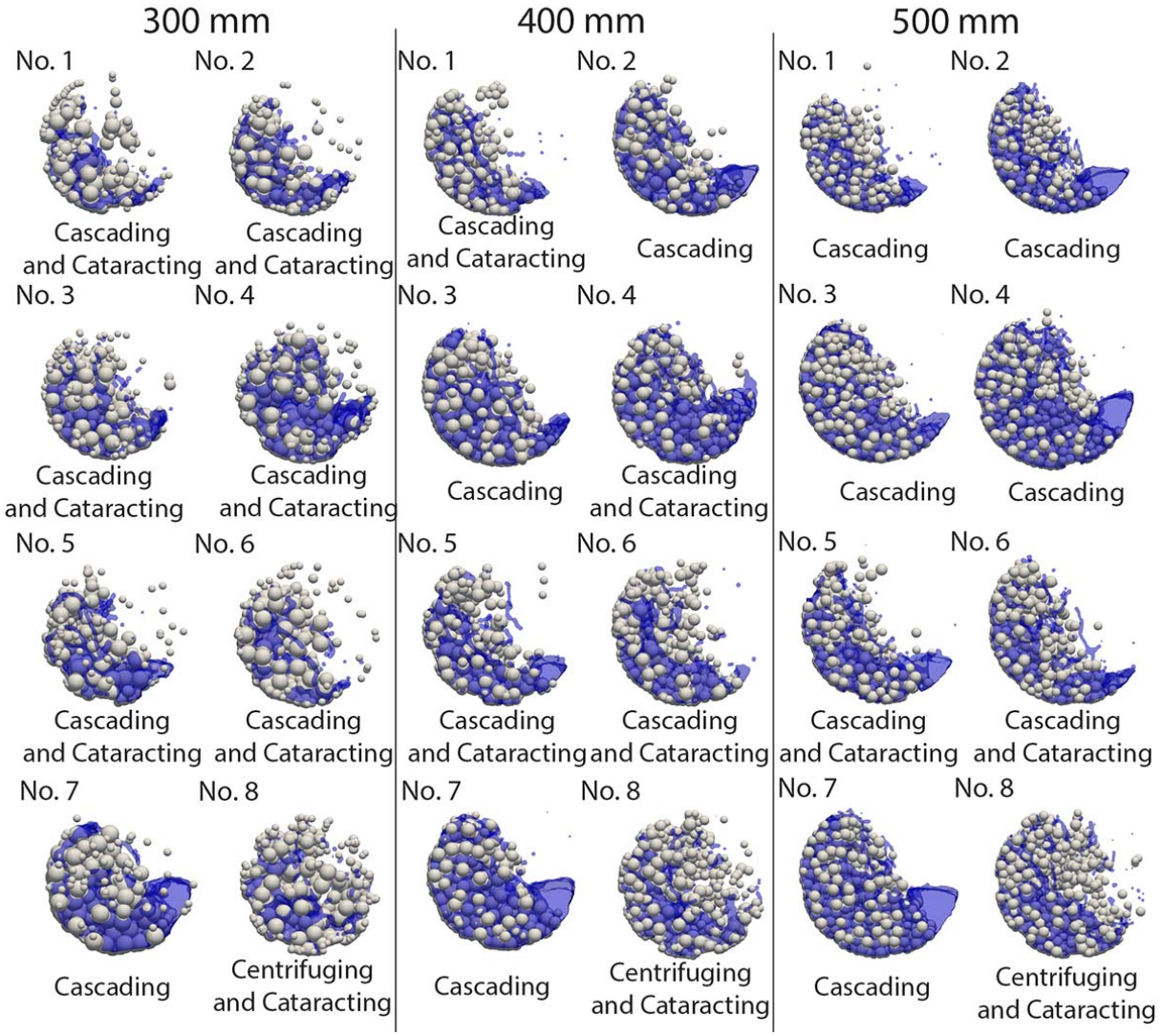

Figure 6.14: Dominant type of charge motion

Run 8 demonstrated centrifuging motion across all scales, with all operational parameters at higher values. Runs with optimal movement across all scales had both lower filling degree and more lifters. In runs 1-4, a considerable shift from cataracting to cascading motion occurred as the diameter increased. These runs had fewer lifters, and this modification may account for the amplified effect of other parameters and scale on charge behavior. Slurry pooling in the toe area was most significant in runs with the dominant cascading motion.

Key Points – Charge Movement in Simulations – Wet Milling:

- Runs 5-8 showed stable behavior across all scales, possibly due to a higher number of lifters, indicating the importance of lifter number in reproducibility of charge behavior.
- Slurry pooling in the toe area was most prominent in runs with cascading as the dominant motion.

- Run 8 exhibited centrifuging across all scales, with all operational parameters at higher values.
- Runs with optimal movement had lower filling degree and more lifters.
- Runs 1-4 showed a shift from cataracting to cascading as diameter increased, possibly due to fewer lifters amplifying the effect of other parameters and scale on charge behavior.

6.3.4 Torque Correlation with Simulated Data

The analysis of the correlation between torque and the center of circulation (CoC) and center of gravity (CoG) parameters reveals significant relationships (refer to Figure M.1 in Appendix M). The results show strong negative correlations between torque and both the CoC angle (Pearson's r=-0.628, p-value=0.001) and the CoG angle (Pearson's r=-0.555, p-value=0.005). This finding is important as it suggests that an increase in the CoC or CoG angle, probably due to changes in charge motion such as increased cataracting or a higher shoulder position, causes the torque required for the milling process to decrease. This observation may have significant implications for the optimization of energy consumption in the milling process.

Furthermore, the analysis reveals moderately positive and statistically significant correlations between torque and the CoC arm (Pearson's r=0.436, p-value=0.033) and between torque and the CoG arm (Pearson's r=0.419, p-value=0.041). This fact indicates that torque increases together with the arm lengths, suggesting a direct relationship between the size of the circulation/mass center arms and the energy required for milling. This insight could be used to adjust milling parameters, such as mill speed or lifter design, so that the charge motion and grinding mechanisms could be optimized for improved energy efficiency.

It is noteworthy that both angles have a higher impact on the torque than the arms do, with the CoC angle and arm having slightly higher torque predictive power compared to their CoG counterparts. The significant relationship between the values measured in the simulations and the torque measured in the experiments confirms the validity of the simulation data, which can be used to predict the behavior of the multiphase charge modeled with SPH for slurry (ore and water) and with DEM for steel balls serving as the grinding media.

Although the correlations are moderate and statistically significant, they are not perfect and indicate that the models and tools used for DEM-SPH simulations require further improvement. The scatter plots (Figure M.1) illustrate the relationships between the torque and the CoC/CoG angles and arms for wet milling, with clear negative trends for the angles and moderate positive trends for the arms. This relationship is consistent with the correlation analysis results.

Key Points – Torque Correlation with Simulated Data – Wet Milling:

- Strong negative correlations between torque and both the CoC and CoG angles suggest that increased angles lead to decreased torque and potential energy savings.
- Moderate positive correlations between torque and the CoC/CoG arms indicate that larger arm lengths result in higher torque and energy requirements.

- Angles have a higher impact on torque than arms do, and the CoC parameters show slightly higher predictive power.
- Significant relationships between the simulated and the experimental data validate the use of DEM-SPH simulations for predicting multiphase charge behavior.
- Room for improvement exists in the models and tools used for DEM-SPH simulations.

6.4 DoE Results

This section compares the experiments for both dry and wet milling conditions using Fractional Design of Experiments. The detailed results of the analysis, performed with Minitab statistical software, are presented in Appendix N. The appendix contains the standardized effects, regression equations and other detailed statistics for each design, and for different diameters and milling conditions (dry/wet). A comparison of these results across the six designs allows the identification of the operational parameters with the most significant impact on the analyzed response parameters. The appendix also contains tables with raw data used for the Fractional DoE analysis. Data from the dry milling experiments and simulations is presented in Table N.1, and for the wet milling experiments—in Table N.2.

The response parameters examined for both dry and wet milling include mean torque, tangential to normal force ratio, size reduction, energy consumed, energy consumed per mass unit, and energy consumed per mass per rotation. The analysis of these parameters provides insights into the differences between dry and wet milling processes and the key factors influencing their performance.

6.4.1 Mean Torque

The analysis of absolute torque values across various mill setups indicates several relationships between operational parameters and torque. Filling degree seems to be an important factor in most setups, with the exception of the 500 mm mill under wet milling conditions. As expected, a higher filling degree positively correlates with torque owing to the increased gravitational force which the mill must overcome due to a heavier charge.

In dry milling, rotational speed also significantly impacts torque values within the analyzed range. The negative correlation between the speed and the torque suggests that increased speed leads to decreased torque. Additionally, lifter configuration affects torque, particularly in the 300 mm dry mill, which exhibits the highest adjusted R^2 value and strong predictive power. In this case, more lifters and higher lifters result in lower torque, possibly by promoting the cataracting motion and reducing the overall gravitational force on the mill shell. For larger diameters, the 500 mm mill includes lifter height, but both 400 and 500 mm mills have lower R^2 values. This observation may indicate that the model can only partially describe the torque behavior based on the input parameters. The remaining variance can be explained by lifter configuration. However, the data was not sufficiently clear for this effect to be identified as statistically significant for these diameters.

In wet milling, the effect of slurry density dominates other parameters, with higher density leading to lower torque. Models for the 400 and 500 mm mills demonstrate high predictive power, with nearly 90% of torque behavior accounted for by slurry density

and filling degree, or slurry density alone. This fact indicates the crucial role of setting appropriate slurry density for optimal mill performance in wet milling.

The response of the 500 mm wet mill to filling degree adjustments suggests possible non-linear or threshold effects at larger scales, which requires additional investigation. The varying predictive power of regression models, particularly in wet conditions indicates the complexity of wet milling and the need for more sophisticated models or additional variables to fully represent the torque behavior.

Its consistent significance in wet milling across all mill sizes emphasizes the impact of slurry density on energy efficiency and operational costs and renders it an important object of further optimization efforts. Table 6.5 presents the standardized effects, regression equations, and adjusted R^2 values for the various mill setups. In dry milling, rotational speed also significantly affects torque values within the analyzed range. The negative correlation between speed and torque suggests that increasing speed leads to decreased torque, probably due to the transition from the cascading to the cataracting motion.

Table 6.5: DoE analysis summary with Standardized Effects for mean torque with regression equations and R^2 values for dry and wet milling conditions

Parameter	**300 Dry**	**300 Wet**	**400 Dry**	**400 Wet**	**500 Dry**	**500 Wet**
filling degree (f_d)	25.69	1.86	3.84	2.2	5.1	x
number of lifters (n_l)	-5.49	x	x	x	x	x
lifter height (l_h)	-14.71	x	x	x	-1.86	x
rotational speed (ω)	-51.38	x	-4.63	x	-2.12	x
slurry density (ρ)	N/A	-2.29	N/A	-10.71	N/A	-9.75
Regression Equation for: Torque=	8.003 +3.275f_d -0.03500n_l -37.50l_h -0.10565ω	9.64 +10.42f_d -0.00640ρ	17.87 +9.84f_d -0.2301ω	41.14 +9.95f_d -0.02420ρ	25.19 +23.44f_d -170.8l_h -0.220ω	102.58 -0.05414ρ
R^2	99.92%	63.47%	87.85%	95.98%	89.46%	94.06%
R^2(adj)	99.80%	48.86%	82.99%	94.38%	81.56%	93.07%
R^2(pred)	99.40%	6.48%	68.90%	89.72%	57.85%	89.44%

Key Points – Torque – DoE:

- Filling degree is an important factor in most setups; it is positively correlated with torque.
- In dry milling, rotational speed impacts torque values within the analyzed range. The negative correlation between speed and torque suggests that increasing speed leads to decreased torque, probably due to the transition from the cascading to the cataracting motion.
- Lifter configuration (lifter height and number) can impact torque, particularly in the 300 mm dry mill. The more and the higher the lifters, the lower the torque.
- Slurry density dominates other parameters in wet milling, with higher density leading to lower torque.
- The response of the 500 mm wet mill suggests possible non-linear or threshold effects at larger scales.

- The predictive power of the regression models varies, accounted for by the complexity of wet milling.
- The consistent significance of slurry density in wet milling emphasizes its importance for energy efficiency and operational costs.

6.4.2 Force Ratio

The force ratio, defined as the average tangential to normal force acting on the grinding media, is an indicator of the dominant forces during the milling process. A Design of Experiments (DoE) analysis was conducted in order to investigate the effects of various parameters on the force ratio under both dry and wet milling conditions across different mill scales (300, 400, and 500 mm). The standardized effects, regression equations, and adjusted R^2 values for each condition are summarized in Table 6.6.

The filling degree was observed to most significantly influence the force ratio in most conditions. It was positively correlated with the dominance of tangential forces. The only exception was the 500 mm wet mill, whose model did not include filling degree. However, this model also had lower predictive power. This fact suggested that the remaining variance might be explained by filling degree, which was not statistically significant in the experimental data. These findings emphasize the importance of filling degree in optimizing milling efficiency, particularly in dry conditions or smaller mills.

Rotational speed was the second most influential parameter across all setups, displaying a negative correlation with the dominance of tangential forces. As rotational speed increases, the dominance of normal forces acting on the grinding media also increases, which is an expected behavior. Higher speeds result in higher shoulder—the grinding media are lifted higher, and as a result impact breakage is greater than abrasion and attrition.

The effect of lifters on the force ratio is more complicated. While the number of lifters seems to have no impact on the dominance of tangential forces across all setups, their height has a significant negative impact. This is expected, as higher lifters, in an effect comparable to that of higher rotational speeds, lift the grinding media higher and generate greater impact forces. This effect was not observed in the 300 mm dry milling model, which had the lowest R^2 values, suggesting that the remaining variance could be explained by lifter height. Interestingly, the interaction between filling degree and lifter height is significant in the 400 and 500 mm dry mills, indicating complex interdependencies that cannot be explained by simple additive effects. Although higher lifters, when considered in isolation, lead to decreasing dominance of tangential forces (abrasion and attrition), the combination of higher lifters and higher filling degree intensifies these grinding mechanisms. This important observation demonstrates the need to consider parameter interrelations when optimizing mill operation.

In wet milling, the increasing of slurry density causes a consistent decrease in the force ratio across all scales, suggesting a dampening effect of heavier and more viscous slurries on tangential forces. This negative correlation indicates the complex role of slurry properties in milling efficiency and the need for careful control of slurry density to achieve optimal force ratios. Adjusting slurry density seems a valuable tool for optimizing the grinding process and controlling the dominance of tangential and normal forces, as it allows operators to control the process and change the balance between impact breakage and the grinding mechanisms of abrasion and attrition.

Table 6.6: DoE analysis summary with standardized effects for force ratio with regression equations and R^2 values for dry and wet milling conditions

Parameter	**300 Dry**	**300 Wet**	**400 Dry**	**400 Wet**	**500 Dry**	**500 Wet**
filling degree (f_d)	2.06	17.11	13.02	3.31	17.4	x
number of lifters (n_l)	x	x	x	x	x	x
lifter height (l_h)	x	-14.5	-6.01	-4.12	-5.61	-3.47
rotational speed (ω)	-2.04	-19.59	-6.58	-6.07	-9.92	-5.44
slurry density (ρ)	N/A	-12.44	N/A	-3.18	N/A	-2.52
$f_d * l_h$	x	x	3.03	x	2.3	x
Regression Equation for: Force Ratio=	0.988 $+0.209 f_d$ -0.00333ω	1.3163 $+0.3113 f_d$ $-5.275 l_h$ -0.005746ω -0.000113ρ	1.3774 $+0.1813 f_d$ $-9.42 l_h$ -0.003322ω $+15.75 f_d * l_h$	1.842 $+0.2550 f_d$ $-6.35 l_h$ -0.00907ω -0.000123ρ	1.2420 $+0.2225 f_d$ $-5.15 l_h$ -0.003890ω $+8.00 f_d * l_h$	1.7740 $-5.30 l_h$ -0.00936ω -0.000096ρ
R^2	62.66%	99.71%	98.85%	96.15%	99.32%	92.31%
R^2(adj)	47.72%	99.33%	97.32%	91.02%	98.41%	86.55%
R^2(pred)	4.41%	97.96%	91.83%	72.63%	95.16%	69.26%

Key Points – Force Ratio – DoE:

- Filling degree is the most significant factor influencing force ratio, with a positive correlation to tangential force dominance in most conditions.
- Rotational speed is negatively correlated with tangential force dominance, as higher speeds lead to greater normal (impact) forces.
- Lifter height has a significant negative impact on tangential force dominance, while the number of lifters has no effect.
- Interactions between filling degree and lifter height are significant in larger dry mills, highlighting the importance of considering parameter interrelations.
- In wet milling, increasing slurry density decreases the force ratio across all scales, suggesting a dampening effect on tangential forces.

6.4.3 Size Reduction

Size reduction, defined as the ratio of feed D_{80} grain size to product d_{80} grain size, was modeled using multiple linear regression for various mill scales and operating conditions. The adjusted R^2 (R^2(adj)) values, which account for the number of predictors relative to the number of data points, were used to assess the predictive power of each model (Table 6.7).

For dry milling, the results were inconsistent across scales. The 300 mm and 400 mm models exhibited low predictive power, and the 300 mm dry mill showed a negative correlation between rotational speed and size reduction, which accounted for only 45% of the variation. The 400 mm model included both rotational speed and filling degree, with filling degree having a larger negative impact on size reduction. The 500 mm model, which had higher confidence, included filling degree and lifter height as factors which both negatively influenced size reduction. However, this model also demonstrated a complicated relationship between these two parameters, suggesting that their combined effect increases size reduction.

In wet milling, slurry density had the most significant impact on size reduction, with higher densities leading to decreased size reduction. The 300 mm wet milling model also included lifter height, which negatively affected size reduction.

The fact that all models demonstrated low to medium predictive power indicates that the parameters considered (slurry density, filling degree, lifter height, and the interaction between filling degree and lifter height) are important factors influencing size reduction. The relationship between the filling degree and the lifter height in the 500 mm dry mill suggests a complex, non-linear relationship affecting size reduction.

Table 6.7: DoE analysis summary with standardized effects for size reduction with regression equations and R^2 values for dry and wet milling conditions

Parameter	**300 Dry**	**300 Wet**	**400 Dry**	**400 Wet**	**500 Dry**	**500 Wet**
filling degree (f_d)	x	x	-2.15	x	-5.74	x
number of lifters (n_l)	x	x	x	x	x	x
lifter height (l_h)	x	-2.03	x	x	-4.76	x
rotational speed (ω)	-2.62	x	-1.18	x	x	x
slurry density (ρ)	N/A	-6.88	N/A	-3.95	N/A	-4.97
$f_d * l_h$	x	x	x	x	3.69	x
Regression Equation for: Size Reduction=	8.36 -0.0705ω	39.69 -225l_h -0.01910ρ	10.06 -4.04f_d -0.0662ω	43.88 -0.02178ρ	11.726 -12.63f_d -375.6l_h +710$f_d * l_h$	40.24 -0.02018ρ
R^2	53.29%	91.13%	61.23%	72.18%	94.54%	80.48%
R^2(adj)	45.50%	87.58%	45.72%	67.55%	90.45%	77.23%
R^2(pred)	16.95%	77.29%	0.75%	50.55%	78.17%	65.30%

Key Points – Size Reduction – DoE:

- Dry milling results were inconsistent across scales, with low to medium predictive power.
- For lower diameters and under dry milling conditions, rotational speed has a negative effect on size reduction.

- In wet milling, slurry density was the most significant factor, negatively impacting size reduction.
- Filling degree, lifter height (negative impact), and their relationship (positive impact) were identified as important factors influencing size reduction.
- The relationship between the filling degree and the lifter height in the 500 mm dry mill is complex and non-linear.

6.4.4 Energy Consumed

The energy consumed during the milling process is an important factor used in assessing the efficiency and optimization potential of both dry and wet milling setups. In this analysis, the energy consumption is measured in joules (J), and the adjusted R^2 values are used to evaluate the predictive power of the regression models.

As shown in Table 6.8, rotational speed consistently influences energy consumption across all dry milling setups, indicating a direct correlation between the two variables. This finding was expected, as milling with higher rotational speeds typically requires more energy to be maintained. In contrast, the wet milling setups show a different trend, with the rotational speed being included in the model only for the 300 mm mill. For the 400 mm and 500 mm wet mills, the negative correlation with slurry density is the dominant parameter and accounts for the majority of the variability in energy consumption (over 85% based on the R^2(adj)).

In the case of dry milling, particularly for larger diameters (400 mm and 500 mm), the filling degree appears to have the most significant positive effect on energy consumption. This observation was also expected, as an effective grinding of a higher mass of the material requires more energy. It is important to note that all models, except for the 400 mm and 500 mm wet milling setups, have low to moderate predictive power, suggesting that not all important variables were taken into account in those models.

Interestingly, slurry density inversely affects energy consumption under wet milling conditions across all diameters. This finding indicates that denser slurries may reduce the cascading and cataracting motion of the charge and translate into lower energy consumption during the milling process. It also demonstrates the potential for using slurry density as a tool for obtaining energy savings in wet milling processes. By optimizing the slurry density, it may be possible to minimize energy consumption.

In larger dry mills (400 mm and 500 mm), the filling degree positively correlates with energy consumption, revealing the impact of charge volume on energy dynamics. Additionally, the tests in the 500 mm dry mill setup suggest that higher lifters can intensify the cataracting motion of the charge and translate into more efficient energy use by increasing the impact breakage. This observation demonstrates the importance of lifter height optimization as a method for energy savings through mechanical improvements.

Table 6.8: DoE analysis summary with standardized effects for energy consumed with regression equations and R^2 values for dry and wet milling conditions

Parameter	**300 Dry**	**300 Wet**	**400 Dry**	**400 Wet**	**500 Dry**	**500 Wet**
filling degree (f_d)	x	x	4.16	x	3.5	x
number of lifters (n_l)	x	x	x	x	x	x
lifter height (l_h)	x	x	x	x	-2.35	x
rotational speed (ω)	3.53	2.45	2.73	x	2.2	x
slurry density (ρ)	x	-2.4	x	-6.91	x	-10.04
Regression Equation for: Energy Consumed=	48809 +1587ω	64142 +3976ω -120.5ρ	74201 +119748f_d +1521ω	815643 -382.3ρ	74934 +267544f_d -3590975l_h +3795ω	1386309 -688.0ρ
R^2	67.54%	70.20%	83.19%	88.84%	84.97%	94.38%
R^2(adj)	62.12%	58.28%	76.47%	86.99%	73.69%	93.44%
R^2(pred)	42.29%	23.71%	56.97%	80.17%	39.87%	90.01%

Key Points – Energy Consumed – DoE:

- Rotational speed directly correlates with energy consumption in dry milling.
- Slurry density is the dominant factor in wet milling.
- Filling degree has a significant positive effect on energy consumption in larger dry mills.
- Slurry density inversely affects energy consumption in wet milling, offering potential for energy savings.
- Higher lifters in the 500 mm dry mill can reduce energy consumption through more dynamic charge lift and drop mechanics.
- Regression models provide a quantitative basis for predicting energy consumption, but varying predictive accuracy suggests room for model refinement.

6.4.5 Specific Energy

Specific energy, measured in joules per kilogram of ground ore, is a crucial metric for assessing the efficiency of the milling process. Analyses across most of the experimental setups identify the filling degree as an important parameter negatively correlated with the energy required to grind one kilogram of ore. This observation suggests that within the specified range (0.3-0.5), a higher filling degree leads to lower energy consumption per unit mass of ore. Consequently, the filling degree should be considered when designing and optimizing the operation of a mill, as it could lead to more efficient energy utilization.

For mills with smaller diameters, the rotational speed also exhibits a positive correlation with the specific energy. This fact indicates that the impact of rotational speed on energy consumption may decrease with increasing mill scale. In the case of wet milling, the slurry density seems the most significant parameter across all measured variables, displaying an inverse correlation with specific energy. This phenomenon can be attributed to the formation of a slurry pool in the toe region of the mill, which exerts buoyancy forces on the charge and dampens impacts. This effect becomes more noticeable for larger

mill diameters, and a relationship between filling degree and slurry density is observed for the 500 mm mill. The high predictive power of the model for this measurement suggests that the interplay between filling degree and slurry density is important for understanding energy consumption in wet milling.

It is noteworthy that the dry milling setup for the 500 mm diameter does not take into account rotational speed, which may contribute to the lower predictive power of the model. This fact suggests that a portion of the variability in energy consumption could still be accounted for by the rotational speed, even in larger diameter mills. Furthermore, while rotational speed positively correlates with energy intake in smaller diameter dry mills (300 and 400 mm), the absence of this correlation in larger diameters and wet conditions suggests different underlying mechanics.

Lastly, the discrepancy between the adjusted and the predicted R^2 values in certain experimental setups (refer to Table 6.9) indicates that more complex models may be required to fully represent the underlying phenomena governing energy consumption in the milling process.

Table 6.9: DoE analysis summary with standardized effects for specific energy with regression equations and R^2 values for dry and wet milling conditions

Parameter	**300 Dry**	**300 Wet**	**400 Dry**	**400 Wet**	**500 Dry**	**500 Wet**
filling degree (f_d)	-16.38	x	-12.77	-2.42	-3.71	-4.48
number of lifters (n_l)	x	x	x	x	x	x
lifter height (l_h)	x	x	x	x	x	x
rotational speed (ω)	4.29	1.88	2.6	x	x	x
slurry density (ρ)	N/A	-3.63	N/A	-8.88	N/A	-17.36
$f_d * \rho$	N/A	x	N/A	x	N/A	2.55
Regression Equation for: Specific Energy=	40277 -72439f_d +305.7ω	134138 +2323ω -138.7ρ	31188 -43744f_d +172.8ω	382404 -97586f_d -178.7ρ	37372 -37590f_d	556454 -525220f_d -291.1ρ + 269$f_d * \rho$
R^2	98.29%	76.98%	97.14%	94.43%	69.59%	98.79%
R^2(adj)	97.60%	67.78%	96.00%	92.20%	64.52%	97.89%
R^2(pred)	95.61%	41.08%	92.68%	85.74%	45.93%	95.18%

Key Points – Specific Energy – DoE:

- Filling degree is negatively correlated with specific energy, suggesting its importance in optimizing energy utilization.
- Rotational speed positively impacts specific energy in smaller diameter dry mills, but its effect is reduced in larger diameter mills and in wet conditions.
- Slurry density is the most significant parameter in wet milling, showing an inverse correlation with specific energy
- The relationship between filling degree and slurry density is crucial for understanding energy consumption in wet milling, especially for larger mill diameters.
- Discrepancies between the adjusted and the predicted R^2 values suggest more complex models are needed to fully represent the underlying phenomena.

6.4.6 Specific Energy per Rotation

Specific energy per rotation is a measure of the amount of energy in joules required to grind one kilogram of ore intake per mill rotation. Across most of the experimental setups (Table 6.10), filling degree is observed as an important parameter negatively correlated with the energy needed per kilogram of ore. This observation suggests that a higher filling degree within the specified range (0.3-0.5) translates into lower energy consumption per kilogram of ore per rotation. The filling degree is thus an important parameter to consider when designing and optimizing the operation of a mill for energy efficiency.

Rotational speed is another significant factor, included in half of the models (300 dry, 400 dry, and 500 wet). In these models, rotational speed is always inversely correlated with specific energy per rotation, indicating that lower rotational speeds require less specific energy per rotation during grinding. The two models that did not allow for rotational speed (400 wet and 500 dry) have much lower predictive power. This fact suggests that this parameter is important for explaining the remaining variability in specific energy per rotation, as indicated by the very definition of this metric.

In wet milling, the impact of slurry density is the most significant among all of the measured parameters, exhibiting an inverse correlation. This effect is more evident for larger mill diameters (400 and 500 mm), where a relationship between filling degree and slurry density is observed as an important factor determining the charge motion and grinding mechanisms within the mill. The high predictive power of these models demonstrates the importance of this relationship. However, the 300 mm wet mill model, which includes only slurry density, has the lowest R^2values, accounting for only about 67% of the variability based on the adjusted R^2.

The significant negative standardized effects of filling degree, slurry density, and rotational speed on specific energy across various setups suggest that these parameters have a considerable influence on the charge motion, grinding mechanisms, and energy utilization within the mill. Further investigation into the relationship between these factors and their impact on such phenomena as the position of the center of circulation and the relative importance of impact breakage, abrasion, and attrition could help identify some of the principles behind milling efficiency.

Table 6.10: DoE analysis summary with standardized effects for specific energy per rotation with regression equations and R^2 values for dry and wet milling conditions

Parameter	**300 Dry**	**300 Wet**	**400 Dry**	**400 Wet**	**500 Dry**	**500 Wet**
filling degree (f_d)	-12.82	x	-11.98	-6.67	-5.26	-9.32
number of lifters (n_l)	x	x	x	x	x	x
lifter height (l_h)	x	x	x	x	-1.93	x
rotational speed (ω)	-2.19	x	-3.93	x	x	-2.48
slurry density (ρ)	N/A	-3.89	N/A	-24.87	N/A	-38.88
$f_d * \rho$	N/A	x	N/A	3.23	N/A	5.17
Regression Equation for: Specific Energy per rotation=	37.24 -37.76f_d -0.1042ω	140.5 -0.0699ρ	34.25 -27.49f_d -0.1748ω	332.5 -292.9f_d -0.1703ρ +0.1455$f_d * \rho$	29.03 -26.56f_d -195l_h	427.4 -376.7f_d -0.416ω -0.2138ρ +0.1922$f_d * \rho$
R^2	97.12%	71.57%	96.93%	99.41%	86.28%	99.80%
R^2(adj)	95.97%	66.84%	95.71%	98.97%	80.80%	99.53%
R^2(pred)	92.63%	49.46%	92.15%	97.64%	64.88%	98.56%

Key Points – Specific Energy per Rotation – DoE:

- As filling degree is negatively correlated with specific energy per rotation, higher filling degrees may lead to lower energy consumption per kilogram of ore per rotation.
- Rotational speed is inversely correlated with specific energy per rotation in half of the models; this fact indicates that lower speeds require lower specific energy per rotation.
- In wet milling, slurry density has the most significant impact on specific energy per rotation, with an inverse correlation being more evident for larger mill diameters.
- Slurry density and filling degree correlate positively with specific energy per rotation.

6.5 Scaling Constant Testing of Assumptions

This section focuses on statistical tests aimed to determine whether maintaining the value of the scaling constant at a certain level would allow specific metrics to remain at a similarly constant level. The tests were performed on datasets from 6 experiments, 3 for dry milling and 3 for wet milling. The mean values of the resulting measured parameters across ball mill scales were compared with drum diameters of 300, 400, and 500 mm.

6.5.1 Results of Testing for Dry Milling

Testing Differences in Mean Size Reduction: The Shapiro-Wilk test was used to assess the normality of data distribution within each scale. The results showed that the data were normally distributed for the 300 mm (statistic=0.953, p-value=0.739) and 400 mm (statistic=0.941, p-value=0.624) scales, but not for the 500 mm scale (statistic=0.822, p-value=0.049).

The Kruskal-Wallis H test was then employed to test the null hypothesis that the medians of size reduction are equal across the scales. The result (statistic=13.205, p=0.001) indicated significant differences in medians.

In order to identify which mill scales differ with respect to mean size reduction, Dunn's post-hoc test with Bonferroni correction was used for pairwise comparisons of size reduction medians between scales. The results showed significant differences between the 300 mm and 500 mm scales (p-value=0.001), while the differences between the 300 mm and 400 mm scales (p-value=0.054) and the 400 mm and 500 mm scales (p-value=0.688) were not statistically significant.

Testing Differences in Mean Specific Energy: The Shapiro-Wilk test indicated that the data were normally distributed within each scale (300 mm: statistic=0.875, p-value=0.170; 400 mm: statistic=0.861, p-value=0.124; 500 mm: statistic=0.898, p-value=0.274).

Levene's test was used to test the null hypothesis of equal variances across scales. The result (statistic=5.561, p-value=0.012) indicated unequal variances.

Due to the unequal variances, Welch's ANOVA was employed to test the null hypothesis of equal means across scales. The results (F(2, 13.499)=3.010, p-value=0.083, η_p^2=0.292) showed no significant differences in means, but a large effect size (η_p^2=0.292) was observed.

Testing Differences in Mean Specific Energy per Rotation: The Shapiro-Wilk test indicated that the data were normally distributed within each scale (300 mm: statistic=0.847, p-value=0.089; 400 mm: statistic=0.921, p-value=0.442; 500 mm: statistic= 0.963, p-value=0.838).

Levene's test (statistic=1.902, p-value=0.174) indicated equal variances across scales.

A one-way ANOVA was conducted to test the null hypothesis of equal means across scales. The results showed no significant differences in means (F(2, 21)=0.801, p-value= 0.462, η_p^2=0.071) and medium effect size.

6.5.2 Results of Testing for Wet Milling

Testing Differences in Mean Size Reduction: The Shapiro-Wilk test indicated that the data were normally distributed within each scale (300 mm: statistic=0.850, p-value=0.096; 400 mm: statistic=0.906, p-value=0.325; 500 mm: statistic=0.888, p-value= 0.222).

Levene's test (statistic=0.086, p-value=0.918) indicated equal variances across scales.

As both the normality and the homogeneity of variances assumptions were met, a traditional one-way ANOVA was performed to test the null hypothesis of equal means across scales. The results showed no significant differences in means (F(2, 21)=0.382, p-value=0.687, η_p^2=0.035) and small effect size.

Testing Differences in Mean Specific Energy: The Shapiro-Wilk test indicated that the data were normally distributed within each scale (300 mm: statistic=0.882, p-value=0.196; 400 mm: statistic=0.873, p-value=0.162; 500 mm: statistic=0.855, p-value= 0.108).

Levene's test (statistic=0.500, p-value=0.614) indicated equal variances across scales.

As both normality and homogeneity of variances assumptions were met, a traditional one-way ANOVA was conducted to test the null hypothesis of equal means across scales. The results showed no significant differences in means (F(2, 21)=0.029, p-value=0.972, η_p^2=0.003) and very small effect size.

Testing Differences in Mean Specific Energy per Rotation: The Shapiro-Wilk test indicated that the data were normally distributed within each scale (300 mm: statistic=0.8906, p-value=0.237; 400 mm: statistic=0.850, p-value=0.095; 500 mm: statistics= 0.841, p-value=0.078).

Levene's test (statistic=4.000, p-value=0.034) indicated unequal variances across scales.

Due to the unequal variances, Welch's ANOVA was used to test the null hypothesis of equal means across scales. The results (F-statistic=0.436, p-value=0.655) indicated no significant differences in means, with a small effect size (η_p^2=0.034) of scale on specific energy per rotation.

Key Points – Scaling Constant Testing of Assumptions:

- Dry milling showed significant differences in size reduction medians across scales, particularly between 300 mm and 500 mm scales.
- Dry milling showed no significant differences in mean specific energy and mean specific energy per rotation across scales.

- Wet milling showed no significant differences in mean size reduction, mean specific energy, and mean specific energy per rotation across scales.
- The effect sizes of the mill scale on the measured parameters were large for dry milling specific energy and medium for dry milling specific energy per rotation.
- The effect size of the mill scale on the measured parameters were very small to small for all parameters in wet milling.

6.6 Correlations Across Mill Scales

This section investigates the relationships between various operational parameters and performance metrics across different mill diameters for both dry and wet milling conditions (as discussed in separate subsections). It aims to identify the main correlations and trends that can provide insights into ball mill scale-up and the factors influencing ball mill performance.

6.6.1 Dry Milling

All experimental results from all scales, i.e. altogether 24 dry milling experimental results, were analyzed for correlations. The correlations are presented in the correlation matrix in Figure L.4 in Appendix L. The correlations were filtered by p-value; statistically not significant values were removed, they were also filtered by correlation coefficient; observations between -0.4 and 0.4 were also removed, so that only moderate to strong correlations are presented. The resultant statistically significant correlations are presented in the matrix in Figure 6.15. All detailed correlation values and their p-values are presented in the tables in Appendix L.

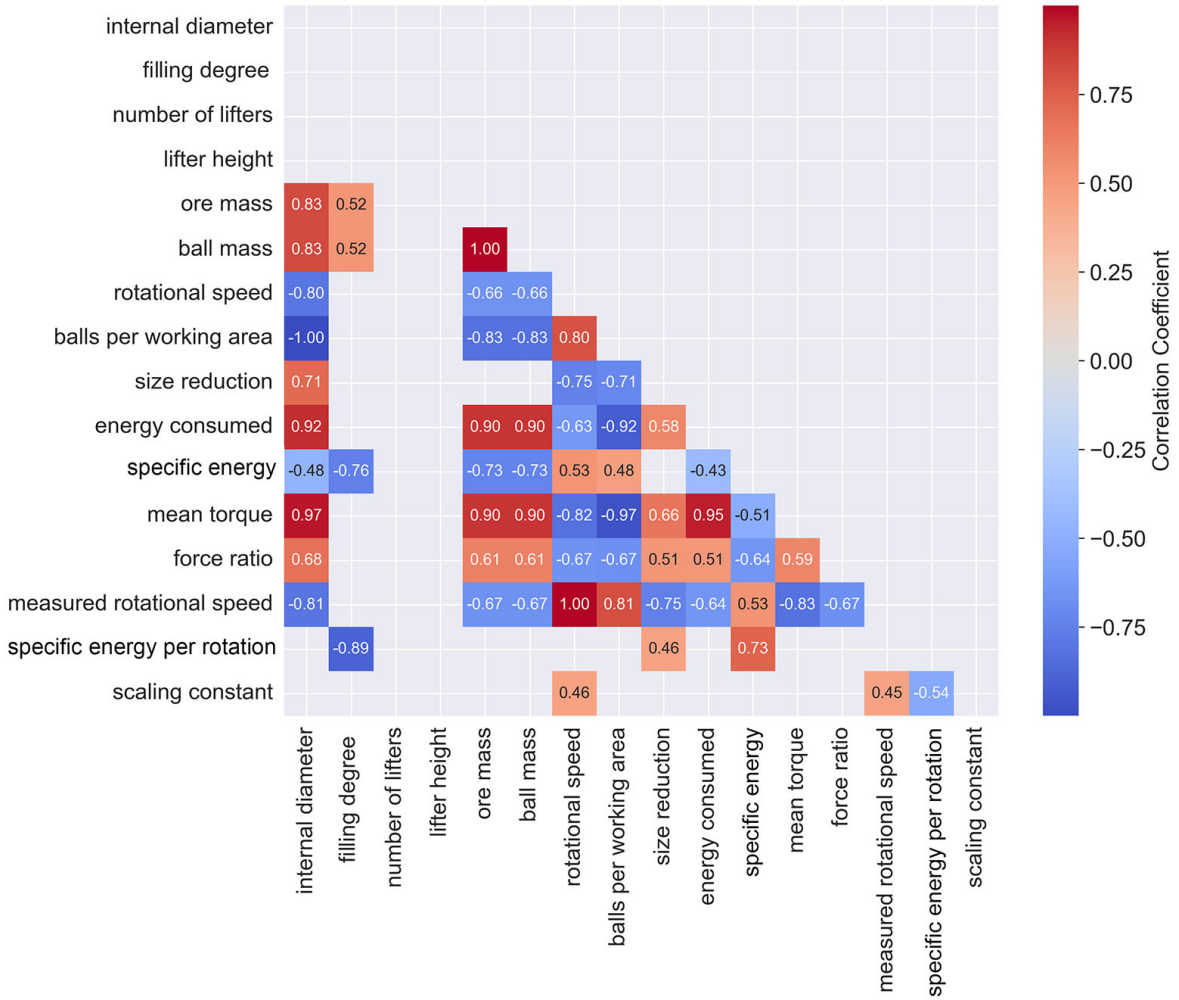

Figure 6.15: Filtered correlation matrix highlighting main relationships in dry milling parameters

Internal Diameter: Internal diameter has, as expected, a very strong positive correlation with absolute mean torque, and energy consumed, as well as with ball and ore masses. Internal diameter is observed to have a strong inverse correlation with rotational speed and the number of balls per working area (which is only the result of the bias due to the experimental design). Interestingly, a high positive correlation coefficient is observed with both size reduction level and force ratio. Mill diameter is also inversely correlated with specific energy.

Filling Degree: Filling degree has the strongest positive correlation with ore mass and ball mass, which is expected. Filling degree also has a very strong negative correlation with energy utilization metrics, specific energy, and specific energy per rotation, suggesting that higher filling degree reduces the values of both metrics.

Ball/Ore Mass: Ball and ore mass have the same correlation coefficient, plus coefficient 1 for the relationship with each other because they had the same proportions across all experiments. It is interesting to note that the mass of charge balls/ore has a strong positive correlation with the force ratio; the higher mass of ore/balls, the higher dom-

inance of tangential forces. This phenomenon is here well observed because mass is an absolute measure that changes across scales, while filling degree is a relative value, so it did not have statistical significance when compared to the force ratio values. Also, higher mass is inversely correlated with rotational speed, which may present a bias in fractional experimental design because both values were preset. Ball mass is also inversely correlated with specific energy (this fact suggests that larger diameters with higher masses are a more efficient solution which requires lower specific energy). The balls per working area parameter is also observed to have the strongest negative correlation coefficient with ore/ball masses. This finding again shows bias due to experimental design and adjustment for the scaling constant.

Rotational Speed and Measured Rotational Speed: The set rotational speed and the measured rotational speed have almost the same correlation coefficient with the measured values, plus a coefficient of 1 with each other. Some of the correlations are biased by the experimental design and do not provide any insight. These include the balls per working area, ore and ball masses, and internal diameter parameters. Although not evident, the energy consumed and mean torque parameters are also biased by experimental design because the rotational speed ranges vary between diameters, and larger diameters also need more energy and higher torque to overcome larger gravitational forces acting on the charge. Rotational speed also has a moderate correlation with scaling constant. This observation may indicate that a large portion of changes in values of the scaling constant can be attributed to rotational speed. Also, a strong negative correlation was observed between rotational speed and both force ratio and size reduction, indicating that higher speed results in bigger dominance of normal forces and lower size reduction.

Balls per Working Area: The balls per working area parameter has a lot of biased correlations that are the result of experimental design, and this fact should be taken into account during the analysis of the results. The analysis of other correlations not biased by the design indicates that this parameter has a strong negative correlation with force ratio and size reduction. Consequently, more balls per their active working area (smaller balls, more densely packed) result in increased dominance of normal forces acting between them and thus in limited size reduction.

Size Reduction: Internal diameter positively affects size reduction, and negatively correlates with the number of balls per working area and with rotational speed. Also, size reduction can be better predicted by torque than by energy consumed, probably due to its relationship with the grinding mechanisms occurring within the mill. It is also worth noting that size reduction is only moderately correlated with specific energy per rotation.

Energy Consumed: The energy consumed parameter has a very strong correlation with torque, which was expected, and obvious correlations with mill diameter, as well as with ball, and ore masses. It also shows a strong positive correlation with force ratio and size reduction. This fact may indicate that maintaining the dominance of tangential forces while producing finer products requires more energy. A negative correlation with specific energy implies that when more power is supplied to the system, the grinding of one kilogram of ore requires less power. However this observation may be biased by the operational design and larger mills may be more energy efficient. A similar observation

may apply to a very strong negative correlation with the balls per working area parameter, which is also biased by the experimental design.

Specific Energy: A strong positive correlation with specific energy per rotation was in fact expected, as these metrics vary only upon the incorporation of rotational speed. This parameter is also strongly influenced by rotational speed. This metric is not as biased by the experimental design as total energy intake because here the values are adjusted to one kilogram of ore and can be compared directly across scales. Therefore, an interesting moderate positive correlation with the balls per working area parameter is observed, which suggests that the presence of more balls per working area requires more specific energy. Specific energy is inversely correlated with the energy consumed, internal diameter, ball and ore masses, and mean torque parameters, suggesting that the process is more efficient with larger mills (that consume more energy and have larger torques). A very strong inverse correlation with filling degree is worth noting; it shows that higher filling degrees are more energetically optimal/efficient.

Mean Torque: These are obvious correlations. Positive: with diameter, energy consumed, ball mass, and ore mass. Biased: with rotational speed and the balls per working area. Interesting: moderately strong positive with force ratio and size reduction, moderate negative with specific energy.

Force Ratio: Several parameters have a moderate impact on force ratio. Positive correlation: with diameter, ball mass, and ore mass. Negative correlations: with rotational speed and the balls per working area (parameters that can be controlled). Dominance of tangential force correlates also with an increase in the measured absolute values of torque, greater size reduction, greater total energy consumption, and lower specific energy.

Specific Energy per Rotation: Specific energy per rotation has very few correlations. Of the operational parameters, it is affected with a very strong negative correlation by filling degree. It is also moderately correlated with other metrics such as size reduction and specific energy. This fact implies that optimization could help improve one metric (e.g., size reduction) without sacrifice to another (e.g., specific energy per rotation), as they are not fully aligned, and some variation is not explained by their relationship. Specific energy per rotation is also inversely correlated with the scaling constant.

Scaling Constant: It is correlated only with rotational speed and specific energy per rotation. The correlation with rotational speed is expected because it was taken into consideration when calculating the value of the scaling constant, and the correlation with specific energy per rotation suggests that this metric is most easily maintained at the same level during the scale-up process with the use of the scaling constant.

Key Points – Correlations Across Scales – Dry Milling:

- Internal diameter has a high positive correlation with size reduction and force ratio, and is inversely correlated with specific energy.
- Higher filling degree reduces specific energy and specific energy per rotation.
- Higher mass of ore/balls results in a greater dominance of tangential forces.

- Higher rotational speed results in a greater dominance of normal forces and in limited size reduction.
- Rotational speed has moderate correlation with the scaling constant.
- More balls per working area result in an increased dominance of normal forces and in limited size reduction.
- Torque can be a better predictor of size reduction than energy consumed.
- Size reduction is moderately correlated with specific energy per rotation.
- Maintaining dominance of tangential forces while producing finer product requires more energy.
- Higher filling degrees are more energetically optimal/efficient.
- Dominance of tangential force correlates with an increase in torque, size reduction, and total energy consumption, and with a decrease in specific energy.
- Rotational speed and the balls per working area (the parameters that can be controlled) have negative correlations with force ratio.
- Torque has moderately strong positive correlations with force ratio and size reduction, and a moderate negative correlation with specific energy.
- There is moderate positive correlation between specific energy and the balls per working area.
- There is a strong positive correlation between specific energy and specific energy per rotation.
- Specific energy per rotation is the most responsive metric to the scaling constant (inversely correlated).

6.6.2 Wet Milling

All experimental results from all scales, i.e. altogether 24 dry milling experiments, were analyzed for correlations. All correlations are presented in the correlation matrix in Figure M.2 in Appendix M. The correlations were filtered by p-value; statistically not significant values were removed, and by correlation coefficient filtered out between -0.4 and 0.4, so that only moderate to strong correlations are presented. The resultant statistically significant correlations are presented in the matrix in Figure 6.16. All detailed correlation values and their p-values are presented in the tables in Appendix L. Only non-obvious correlations and those unbiased by experimental design are discussed.

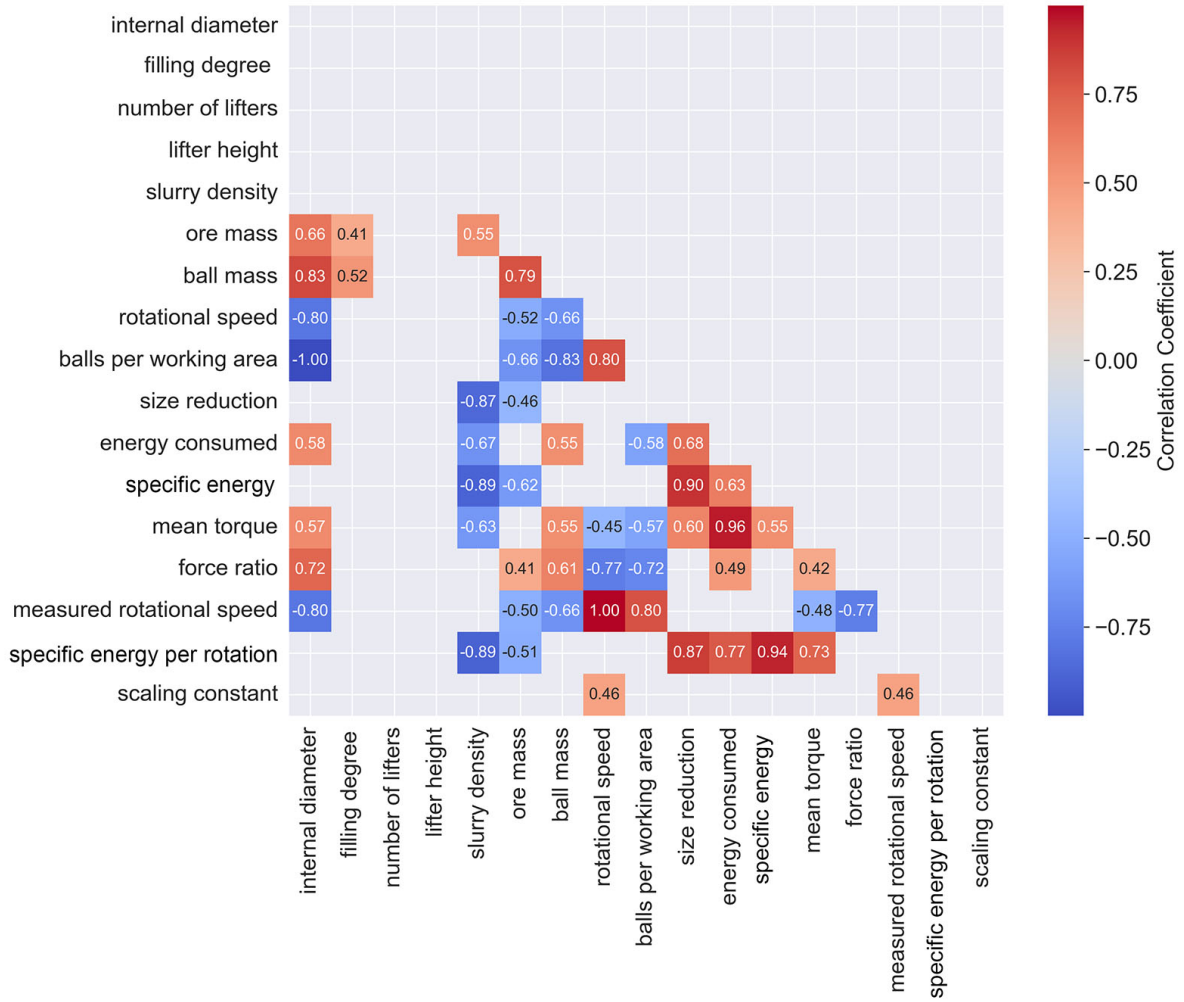

Figure 6.16: Filtered correlation matrix with main relationships between wet milling parameters

Internal Diameter: The correlation analysis of wet milling parameters shows several important findings regarding the relationships between various factors and their impact on the milling process. A high correlation between mill diameter and force ratio indicates that as the diameter increases, the dominance of tangential forces also increases. This observation suggests that larger mill diameters favor tangential force dominance in the milling process.

Slurry Density: Slurry density seems to be an important parameter in the optimization of wet milling. It exhibits a moderate negative correlation with energy consumption and a high negative correlation with size reduction, energy intake per mass, and specific energy per rotation. This inverse relationship indicates a trade-off between energy utilization and size reduction when slurry density is adjusted. Higher slurry densities lead to improved energy utilization but at the cost of reduced size reduction, probably due to different slurry pooling in the toe region of the mill, which exerts buoyancy forces on the charge and dampens the impacts.

Ore Mass: A moderately positive correlation between ore mass and force ratio suggests that an increase in ore mass results in greater tangential force dominance. Interestingly, size reduction is inversely correlated with ore mass, probably as an indirect result of higher ore mass leading to higher slurry density, which has a stronger correlation with size reduction. Additionally, ore mass has a moderate negative correlation with such energy utilization metrics as specific energy per rotation and specific energy. This fact indicates that experiments with larger ore masses (i.e., larger mills) are more energy efficient.

Ball Mass: Ball mass exhibits a moderate positive correlation with force ratio. Higher ball mass thus seems to contribute to the dominance of tangential forces in the milling process.

Rotational Speed and Measured Rotational Speed: The set rotational speed and the measured rotational speed have a very high correlation (0.999), confirming that the process was well-controlled. The scaling constant has a moderate positive correlation with rotational speed. This fact is expected since rotational speed is allowed for in the calculation of the constant value. A strong negative correlation between force ratio and rotational speed suggests that higher speeds allow the grinding media to be lifted higher, leading to higher impact forces and a decrease in tangential force dominance.

Balls per Working Area: The number of balls per working area is strongly negatively correlated with force ratio. As the number of balls per working area increases, the dominance of normal force becomes greater, possibly due to a higher impact rate resulting from a larger number of balls.

Size Reduction: Size reduction has very strong positive correlations with other metrics, such as specific energy and specific energy per rotation. A moderate positive correlation with both total energy consumed and the resulting torque indicates that these factors can serve as predictors of the expected size reduction. The strong negative correlation between size reduction and slurry density is noteworthy, as it emphasizes the importance of this parameter.

Energy Consumed: The fact that energy consumed has a moderate positive correlation only with size reduction implies that the energy utilization is influenced by other unidentified factors. The inverse moderate correlation between energy consumed and slurry density further emphasizes the significance of slurry density in the milling process.

Specific Energy: A very strong correlation between specific energy and specific energy per rotation indicates that during wet milling, the energy utilized for the purpose of size reduction is stable and linearly correlated. Notably, it also has a very strong negative correlation with slurry density.

Mean Torque: Mean torque has a moderate correlation with size reduction. This fact suggests that torque can be a predictor of the resulting value. Mean torque also has a low to moderate positive correlation with force ratio and that relationship indicates that higher torque results in higher tangential force dominance. The moderate inverse correlation

between mean torque and slurry density once again emphasizes the significance of slurry density.

Force Ratio: Force ratio analysis shows that the dominance of tangential forces increases with mill diameter, ball mass, and ore mass, while it decreases with an increase in the number of balls per working area and in rotational speed. Higher dominance of tangential forces is associated with higher torque values and higher energy consumption. Force ratio influences the relative importance of the main grinding mechanisms: impact, abrasion, and attrition. Higher tangential force dominance may favor abrasion and attrition, while lower force ratios may promote impact breakage.

Specific Energy per Rotation The fact that specific energy per rotation has a very strong positive correlation with specific energy and with size reduction suggests that during wet milling, energy utilization for the purpose of size reduction is stable and linearly correlated. Specific energy per rotation also has a very strong negative correlation with slurry density, whose importance is thus again emphasized.

Scaling Constant Scaling constant has only one moderate and statistically significant correlation with rotational speed. This fact indicates that it is independent of other parameters.

Key Points – Correlations Across Scales – Wet Milling:

- Larger mill diameters favor tangential force dominance in the wet milling process.
- Slurry density has moderate negative correlation with energy consumed and high negative correlation with size reduction, specific energy and specific energy per rotation and moderate inverse correlation with torque.
- Ball mass and ore mass cause tangential force dominance to increase, while the number of balls per working area and rotational speed cause it to strongly decrease.
- Size reduction is strongly correlated with specific energy and specific energy per rotation, and moderately correlated with total energy consumed and the resulting torque.
- The scaling constant is independent of most parameters, with only a moderate correlation with rotational speed.
- Specific energy has very strong correlation with specific energy per rotation.

6.7 Summary

This chapter presented the main results and findings from the experimental study on ball mill scale-up, covering both dry and wet milling conditions across various mill diameters. The calibration results served as a basis for the subsequent analysis, as they helped determine the optimal coefficients of restitution and kinetic friction for the balls and validate the accuracy of the simulation models in representing real-world milling conditions.

The results of dry milling final experimental series provide insights into the stability, variability, and efficiency of the milling process owing to sensor measurements, product size distribution analysis, simulations, and correlations. The analysis indicated the relative importance of impact breakage, abrasion, and attrition mechanisms under different operating conditions. The rotational speed was found to be well-controlled and stable across all mill diameters, while the torque measurements showed moderate to high variability. Power draw increased with mill diameter, and different mill diameters were compared with respect to the effectiveness in achieving finer particle sizes and higher size reduction ratios. The simulations demonstrated the spatial distribution of force ratios within the mill and the influence of operational parameters on the charge motion, including cascading, cataracting, and the position of the toe and shoulder regions. Correlations between torque and the simulated data provided information on the energy dynamics of the milling process.

The results of wet milling experimental series indicate the unique challenges and opportunities due to the presence of slurry in the mill, e.g. slurry pooling in the toe region and its impact on the charge dynamics and grinding mechanisms. Sensor measurements demonstrated the impact of slurry density on the accuracy of the rotational speed control system and the variability of torque and power measurements. Product size distribution analysis showed the complex relationship between mill diameter, slurry properties, and milling efficiency. The simulations provided insights into the dynamics of the wet milling process and the differences between wet and dry milling conditions. The correlations between torque and the simulated data validated the accuracy of the DEM-SPH simulation models in representing multiphase charge behavior.

Design of Experiments (DoE) analysis identified the most influential operational parameters for various response variables, such as mean torque, force ratio, size reduction, and energy consumption metrics. The analysis revealed complex interactions and nonlinear relationships between the parameters and indicated the need for careful optimization and control of milling processes.

Statistical tests verified the validity of scaling assumptions based on the scaling constant. While some differences were observed across scales, particularly in dry milling, the effect sizes were generally small to moderate, suggesting that preserving the scaling constant at a certain level may not always allow specific metrics to remain at a similarly constant level.

Correlations across mill scales for both dry and wet milling provided insights into both the ball mill scale-up behavior and the factors influencing mill performance. Internal diameter, filling degree, ball mass and ore mass, rotational speed, and slurry density were found to have significant correlations with various performance metrics, such as size reduction, force ratio, and energy consumption. The analysis indicated the trade-offs between energy efficiency and size reduction, as well as the importance of optimizing operational parameters for desired milling outcomes.

In conclusion, this chapter provided a comprehensive overview of the experimental findings, offering insights into ball mill scale-up, process optimization, and the impact of various operational parameters on milling performance under both dry and wet conditions. The presented results and correlations may serve as a basis for further research and optimization of ball milling processes across different scales and milling environments.

Chapter 7

Conclusions and Implications

This chapter synthesizes the main findings of the research and discusses their implications for ball mill scale-up and optimization. The study investigated the influence of operational parameters on milling performance and energy efficiency across selected mill diameters. It aimed to develop a more systematic approach to the understanding of the basic principles behind ball milling across different scales.

The chapter assesses the validity of the simulation models. It also focuses on the influence of charge motion, torque, and the effects of scale on the milling process, and examines the main metrics describing its efficiency. The findings are contextualized within the broader literature and described from the perspective of their contributions to research on charge dynamics, energy efficiency, and the impact of operational parameters on milling performance. The findings emphasize the importance of lifter design and slurry density, as well as of the relationship between certain operational parameters. The findings also point to some limitations of this study, which are discussed in the final sections of this chapter along with proposed directions for future research.

7.1 Synthesis and Discussion of Key Findings

This section synthesizes the most important findings of the research and discusses the validity of the simulation models in the context of charge motion, torque, scale effects, and main process efficiency metrics in both dry and wet milling environments.

7.1.1 Validity of Simulation Models

The validity of the simulation results was ensured by carrying out a calibration process. Experimental dynamic angles of repose were measured for ball-only and dry milling cases across various drum diameters *(*see section: *Calibration – Dry/Wet Milling)*. Ball parameters were calibrated in iterative simulations, converging on optimal coefficients of restitution and kinetic friction *(Calibration – Dry/Wet Milling)*. The dry milling calibration was based on the ball calibration results, which served to select the best iteration with the lowest SSE between the experimental and the simulated angles *(Calibration – Dry/Wet Milling)*. For wet milling, the calibration compared slurry surface profiles from the experiments and simulations. It showed good agreement, as the fluid density and viscosity were adjusted to realistic values *(Calibration – Dry/Wet Milling)*. The simulation calibration gave promising results, allowing correct representation of the behavior of real mill charge.

After performing the experimental series and reproducing all experiments in the simulation environment, a comparison with recordings data was performed for dry milling. The simulated center of gravity (CoG) angles and arms were validated against the measured values in order to assess the accuracy and applicability of the simulation models in predicting real-world ball mill behavior *(*see section: *Comparison of Recordings and Simulations – Dry Milling)*. Moderate to strong positive correlations between the simulated and the measured CoG parameters were found to support the effectiveness of the simulation model in representing the main aspects of mill charge dynamics in dry milling *(Comparison of Recordings and Simulations – Dry Milling)*. The substantial correlation between the simulated and the measured CoG arms indicates that arm length predictions from simulations are particularly reliable *(Comparison of Recordings and Simulations – Dry Milling)*. However, some discrepancies between the simulations and the measurements suggest room for model improvement by investigating additional factors and integrating ore characteristics into simulations *(Comparison of Recordings and Simulations – Dry Milling)*.

Another significant qualitative factor which validates the simulations is the fact that the dominant type of movement in real experiments *(Charge Movement in Recordings – Dry Milling)* showed a limited shift in comparison to the simulated results *(Charge Movement in Simulations – Dry Milling)*. The shift was from cataracting towards centrifuging and from cascading towards cataracting for the same runs. This behavior was expected because the real rotational speed measured in experiments was only to a limited extent higher than the set values used in the simulations *(Rotational Speed Sensor Measurements – Dry Milling)*.

In the case of wet milling, the validity of simulations is further confirmed by the comparison of significant relationships between the simulated and the experimental data. Although they validate the use of DEM-SPH simulations for predicting multiphase charge behavior *(Torque Correlation with Simulated Data – Wet Milling)*, room for improvement is observed in the models and tools used for DEM-SPH simulations *(Torque Correlation with Simulated Data – Wet Milling)*. As in the case of dry milling, the charge behavior shifted between simulations and real experiments. This finding was expected, as the values of all rotational speeds measured in wet milling experiments exceeded the set values, particularly for the smallest diameter *(Rotational Speed Sensor Measurements – Wet Milling)*.

7.1.2 Charge Motion

This subsection compares the quantitative and qualitative data about charge movement extracted from the simulations (dry and wet milling) and from the recordings (only for dry milling).

The comparison of the simulations with the recordings in dry milling allows an observation that the dominant type of charge motion for most cases is cascading and cataracting *(Charge Movement in Simulations – Dry Milling, Charge Movement in Recordings – Dry Milling)*. A shift can be observed from centrifuging to cataracting and from cataracting to cascading as the diameter increases *(Charge Movement in Simulations – Dry Milling, Charge Movement in Recordings – Dry Milling)*. The dominant motion type and its trend shift similarly across all experiments, indicating a good match between the simulations and the recordings.

More lifters can stabilize the type of charge motion across scales. Runs 1, 3, 5, 7,

and 8 have the same type of movement across scales in the simulations, and 4 out of the 5 runs (except run 8) involve more lifters *(Charge Movement in Simulations – Dry Milling)*. Stable motion across scales is also observed in runs 5, 7, and 8 in the recordings *(Charge Movement in Recordings – Dry Milling)*. There is a partial match between stable runs from the simulated and from the recorded data. Run 1 and run 3 in the experiments match the type of motion for the largest scale, which may be expected behavior because the difference between the real and the set RPM values was the most significant for the smallest diameters, resulting in a 100% match in the charge type behavior for the 500 mm scale, but only a 7/8 match for the 400 mm and a 5/8 match for the 300 mm scale.

The influence of operational parameters on optimal charge motion varies with mill diameter *(Charge Movement in Simulations – Dry Milling)*. Optimal movement, a mixture of cascading and cataracting, is achieved through specific combinations of lifter height, filling degree, and rotational speed *(Charge Movement in Simulations – Dry Milling)*. Optimal motion (cascading and cataracting) is observed at lower rotational speeds for the 300 mm and 400 mm mills in the recordings *(Charge Movement in Recordings – Dry Milling)*. For the 500 mm mill, optimal motion typically results from higher rotational speed, lower filling degree, fewer lifters, and higher lifters *(Charge Movement in Recordings – Dry Milling)*. Run 5 (all parameters at high levels) showed centrifuging across all scales in both the simulations and the recordings *(Charge Movement in Recordings – Dry Milling)*. Lower diameter mills are more prone to centrifuging, which may impact experimental results *(Charge Movement in Simulations – Dry Milling)*.

The quantitative data from the recordings confirms the varying motion of the charge and its average position. The CoG coordinates and angles vary across runs, indicating differences in charge position and orientation *(Recordings – Dry Milling)*. Charge position is sensitive to operational parameters, such as rotational speed and lifter configurations *(Simulated Charge Position – Dry Milling)*. The CoC and CoG angles remain within a narrow range (less than 1 degree of variance) for certain runs, particularly for those with higher lifter heights (runs 5, 6, and 7) and with a higher number of lifters (runs 1, 5, and 7) *(Simulated Charge Position – Dry Milling)*. Higher lifter size and number may contribute to stable load dynamics during scale-up *(Simulated Charge Position – Dry Milling)*. Interestingly, even runs 7 and 8, which involve higher mill lifter heights, show angles below 90 degrees for drum diameters of 400 and 500 mm *(Recordings – Dry Milling)*. The stability of the charge position depends on a combination of the lifter setup and other operational parameters *(Simulated Charge Position – Dry Milling)*. The fact that in most of the runs with lower rotational speeds, such as runs 1, 7, and 8, the angles tend towards or below 90 degrees *(Recordings – Dry Milling)* suggests that rotational speed may have a more significant impact on charge lifting height than the lifter height does. Run 4, with all parameters lowered, consistently shows angles below 90 degrees. This fact demonstrates the influence of operational parameters on charge positioning *(Recordings – Dry Milling)*. Runs 1, 2, 5, and 8 in both the 400 mm and 500 mm mills show patterns (broader area of tangential force dominance) in the force distribution positively correlated with the filling degree *(Force Ratio – Dry Milling)*.

The comparison of the qualitative data with the quantitative data suggests that the angles and arm lengths of the CoC and CoG for different diameters are as presented in Tables 7.1 and 7.2. The tables present the angles and arms measured in the simulation for the center of circulation (CoC) of the grinding media, for the center of gravity (CoG) of the grinding media, and for the CoG measured from the recordings for the full charge.

Table 7.1: Comparison of measured center of circulation and gravity angles with dominant type of motion in dry milling

Type of Motion	**CoC 300 mm**	**CoC 400 mm**	**CoC 500 mm**	**Average CoC**
Centrifuging and Cataracting	60.89-65.08	61.19-61.44	61	61.75
Cataracting and Cascading	56.93-62.12	56.5-61.37	55.8-60.93	58.53
Cascading	55.72	52.47-55.6	52.51-55.02	54.26
Type of Motion	**CoG 300 mm (sim)**	**CoG 400 mm (sim)**	**CoG 500 mm (sim)**	**Average CoG (sim)**
Centrifuging and Cataracting	59.54-63.84	59.85-60.04	60.25	60.62
Cataracting and Cascading	55.49-58.92	55.14-59.93	55.14-60.38	57.36
Cascading	54.29	51.05-54.22	51.85-54.61	53.2
Type of Motion	**CoG 300 mm (rec)**	**CoG 400 mm (rec)**	**CoG 500 mm (rec)**	**Average CoG (rec)**
Centrifuging	112.15-134.29	N/A	N/A	123.22
Centrifuging and Cataracting	96.35-98.02	106.98-123.17	87.64-92.67	105.33
Cataracting and Cascading	80.61-126.15	80.61-92.22	73.94-100.8	90.43
Cascading	N/A	65.76	55.01-83.2	67.99

Table 7.2: Comparison of arm relative to internal ball radius for measured center of circulation and gravity with dominant type of motion in dry milling

Type of Motion	**CoC 300 mm**	**CoC 400 mm**	**CoC 500 mm**	**Average CoC**
Centrifuging and Cataracting	0.26-0.31	0.32-0.4	0.35	0.32
Cataracting and Cascading	0.38-0.46	0.4-0.51	0.41-0.54	0.45
Cascading	0.4	0.45-0.58	0.47-0.59	0.5
Type of Motion	**CoG 300 mm (sim)**	**CoG 400 mm (sim)**	**CoG 500 mm (sim)**	**Average CoG (sim)**
Centrifuging and Cataracting	0.3-0.35	0.35-0.43	0.38	0.35
Cataracting and Cascading	0.4-0.49	0.41-0.52	0.42-0.55	0.47
Cascading	0.42	0.46-0.58	0.47-0.59	0.5
Type of Motion	**CoG 300 mm (rec)**	**CoG 400 mm (rec)**	**CoG 500 mm (rec)**	**Average CoG (rec)**
Centrifuging	0.1	N/A	N/A	0.1
Centrifuging and Cataracting	0.15-0.17	0.11-0.17	0.16	0.15
Cataracting and Cascading	0.1-0.26	0.19-0.25	0.17-0.24	0.2
Cascading	N/A	0.19	0.19-0.22	0.2

Both angles measured from the simulations for each type of motion overlap to a great extent between the diameters, showing a clear trend. The average angles for the cascading motion are the lowest around 53-54 degrees; for cascading and cataracting they are around 57-58 degrees, and for the motion that starts to centrifuge they are about 60-61 degrees. A small, approximately 3-4 degrees difference is observed between each type of motion.

The arms measured from the simulations demonstrate that the closer the motion approaches centrifuging, the lower the relative arm is. For the motion type in which the charge is further from the axis of rotation (cascading), the relative arm is on average 0.5. This fact means that the center is at half of the internal radius of the mill.

It is worth noting that the measurements from the recordings are completely different than the measurements from the simulations. However, they also show a trend of lowering the relative arm as the motion type shifts towards centrifuging. In the case of the simulations, the measurements involved only balls, while in the case of the recordings, they involved all of the charge, comprising balls and ore. Some differences are thus possible.

In wet milling, the CoC and CoG angles and arms varied across ball mill diameters and cases *(Charge Position – Wet Milling)*. Runs (2, 7, 4, 5) with lower slurry density showed more stable angle ranges across scales *(Charge Position – Wet Milling)* and more prominent pool formation at the toe region. Slurry pooling in the toe area was most prominent in runs with the dominant cascading motion *(Charge Movement in Simulations – Wet Milling)*. Runs 2 and 7, which had the lowest difference in the angles across scales, also shared a lower lifter height *(Charge Position – Wet Milling)* and tended to show cascading motion in most experiments, except the runs for the smallest diameter. Runs

5-8 showed stable behavior across all scales, possibly due to a higher number of lifters. This observation indicates the importance of lifter number in the reproducibility of charge behavior *(Charge Movement in Simulations – Wet Milling)*. Run 8 showed centrifuging across all scales, with all operational parameters set to higher values *(Charge Movement in Simulations – Wet Milling)*. The runs with optimal movement had lower filling degrees and more lifters *(Charge Movement in Simulations – Wet Milling)*. Runs 1-4 showed a shift from cataracting to cascading as the mill diameter increased, possibly due to the fact that a reduction in the number of lifters may amplify the effect of other parameters and scale on the charge behavior *(Charge Movement in Simulations – Wet Milling)*.

Wet milling is described only by the simulation data. The angles are approximately 52.5 degrees for cascading, 55-56 degrees for cataracting and cascading, and 58-59 degrees for centrifuging and cataracting (see Table 7.3). In the case of wet milling, the relative arms for the cascading motion are not significantly different from the relative arms for the cascading and centrifuging motion. Therefore, this metric cannot serve alone to distinguish the motion type. The average relative arm is much smaller only in the case of centrifuging (Table 7.4).

Table 7.3: Comparison of measured center of circulation and gravity angles with dominant type of motion in wet milling

Type of Motion	**CoC 300 mm**	**CoC 400 mm**	**CoC 500 mm**	**Average CoC**
Centrifuging and Cataracting	60.95	58.37	57.97	59.1
Cataracting and Cascading	53.98-61.07	53.04-59.17	51.76-57.13	56.08
Cascading	52.11	51.23-54.26	50.34-53.84	52.78
Type of Motion	**CoG 300 mm**	**CoG 400 mm**	**CoG 500 mm**	**Average CoG**
Centrifuging and Cataracting	59.28	57.22	57.55	58.02
Cataracting and Cascading	52.93-59.26	52.73-58.02	51.64-56.9	55.17
Cascading	51.26	50.93-53.75	50.45-54.03	52.52

Table 7.4: Comparison of arm relative to internal ball radius for measured center of circulation and gravity with dominant type of motion in wet milling

Type of Motion	**CoC 300 mm**	**CoC 400 mm**	**CoC 500 mm**	**Average CoC**
Centrifuging and Cataracting	0.23	0.31	0.35	0.3
Cataracting and Cascading	0.25-0.41	0.33-.05	0.5-0.51	0.41
Cascading	0.33	0.39-0.48	0.36-0.53	0.42
Type of Motion	**CoG 300 mm (sim)**	**CoG 400 mm (sim)**	**CoG 500 mm (sim)**	**Average CoG (sim)**
Centrifuging and Cataracting	0.28	0.33	0.36	0.32
Cataracting and Cascading	0.29-0.45	0.34-0.51	0.5-0.52	0.44
Cascading	0.35	0.39-0.49	0.36-0.53	0.43

In summary, the comparison of charge motion between dry and wet milling simulations and recordings reveals the following most important findings.

Key Findings:

1. Cascading and cataracting are the dominant types of charge motion in most cases for both dry and wet milling.

2. A shift from centrifuging to cataracting and from cataracting to cascading is observed as the mill diameter increases in both dry and wet milling.

3. More lifters can stabilize the type of charge movement across scales in both dry and wet milling.

4. The influence of operational parameters on optimal charge motion varies with mill diameter in both dry and wet milling. Optimal motion is achieved through specific combinations of lifter height, filling degree, and rotational speed.

5. Quantitative data from the recordings and the simulations confirms the varying motion of the charge and its average position, with the CoG coordinates and angles varying across runs.

6. Charge position stability depends on a combination of lifter setup and other operational parameters in both dry and wet milling.

7. Rotational speed may have a more significant impact on shoulder height than lifter height in dry milling.

8. In wet milling, runs with lower slurry density show more stable ranges of angles across scales and more significant pool formation at the toe region.

9. The average angles for the cascading, cataracting and cascading, and centrifuging and cataracting motions are similar in both dry and wet milling simulations.

10. The relative arms for wet milling are not as distinguishable between different motion types as in dry milling, with only the average relative arm for centrifuging being significantly smaller.

These findings emphasize the importance of operational parameters, mill diameter, and the presence of slurry in assessments of charge motion in ball mills. The similarities and differences between dry and wet milling, as well as the relationships between qualitative and quantitative data, provide valuable insights for optimizing ball mill performance and understanding the effects of scaling on charge behavior.

7.1.3 Torque

The torque was measured directly on the mill during each experimental series. The analysis of torque statistics and comparisons with other measurements lead to several findings described below.

Smaller diameter mills exhibited higher torque variability, while larger mills showed more stable responses *(Torque Sensor Measurements – Dry Milling)*. This phenomenon could be attributed to the fact that lower diameter mills were more prone to centrifuging, which may impact experimental results *(Charge Movement in Simulations – Dry Milling)*. Additionally, the fact that the rise times were shortest for the smallest mill diameter *(Torque Sensor Measurements – Wet Milling)* indicates that the operation of smaller mills becomes stable after a shorter time.

On the other hand, larger diameter mills showed some missing values for rise times, especially for the largest diameter. This observation suggests the absence of transient behaviour *(Torque Sensor Measurements – Dry Milling)*. As expected, torque values increased with mill diameter *(Torque Sensor Measurements – Dry Milling)* due to the higher mass of the load and greater gravitational forces.

The presence of slurry had a significant impact on mill behavior. For most runs with lower slurry density at larger diameters, the absence of the transient state was observed *(Torque Sensor Measurements – Wet Milling)*, indicating that the presence of slurry with lower density stabilizes the behavior of the load. The correlation between torque and power was high for higher slurry densities but low or negative for lower densities *(Torque Sensor Measurements – Wet Milling)*. This phenomenon can be explained by the increased resistance within the mill at higher slurry densities. As a result, more energy is required to maintain motion and in effect the positive correlation between torque and power signals is observed for higher slurry densities. In contrast, lower slurry densities lead to less resistance, and fluctuations in torque might not be associated with power if the system can compensate for the lower resistance without the need to significantly increase the energy input.

The verification of the correlations of mean torque values across scales indicated that slurry density has a moderate inverse correlation with torque *(Correlations Across Scales – Wet Milling)*. In fact, slurry density was the most important parameter in wet milling, with higher density leading to lower mean torque *(Torque – DoE)*. This consistent significance of slurry density in wet milling demonstrates its role in energy efficiency and operational costs *(Torque – DoE)*.

The relationship between torque and charge position was also investigated. In the case of dry milling, a weak negative trend was observed between the torque and the simulated CoC/CoG angles (only for the grinding media) *(Simulated CoG and CoC – Dry Milling)*. Also, a moderate negative relationship between angle and torque suggested a potential for torque management through angle adjustments *(Recorded CoG and Torque Correlation – Dry Milling)*. The correlation was stronger in the case of the angle measured from the recordings than from the simulated data, possibly due to the small shift in the rotational speed between the real and the simulated experiments. High correlations were observed between the arm lengths (CoC and CoG) and the torque *(Simulated CoG and CoC – Dry Milling)*, with a strong positive linear relationship between load mass, arm length, and torque *(Recorded CoG and Torque Correlation – Dry Milling)*. Torque was influenced by the moment arm length to a practically identical extent as it was by the charge mass *(Recorded CoG and Torque Correlation – Dry Milling)*. The CoC arm was potentially a marginally better predictor of torque than CoG *(Simulated CoG and CoC – Dry Milling)*.

In wet milling, the situation is different. Strong negative correlations between torque and both the CoC and CoG angles suggest that increasing the angles leads to decreased torque and potential energy savings *(Torque Correlation with Simulated Data – Wet Milling)*. The addition of slurry to the simulations caused the angles to be a better predictor of torque. Moderate positive correlations between torque and the CoC/CoG arms indicate that larger arm lengths result in higher torque and energy requirements *(Torque Correlation with Simulated Data – Wet Milling)*. The angles had a higher impact on torque than the arms did, and the CoC parameters showed marginally higher predictive power *(Torque Correlation with Simulated Data – Wet Milling)*.

General observations included on the one hand skewness and kurtosis variations, which suggest that non-uniform torque distributions are influenced by operating conditions *(Torque Sensor Measurements – Dry Milling)*, and on the other hand—moderate to high variability and dispersion in measurements, with some CV values exceeding 100% *(Torque Sensor Measurements – Wet Milling)*.

The correlations in dry milling showed varying relationships between torque and power

draw, suggesting complex interactions involving multiple factors *(Torque Sensor Measurements – Dry Milling)*. The dominance of tangential force correlated with an increase in torque *(Correlations Across Scales – Dry Milling)*. This phenomenon was expected, as the dominance of tangential forces is related not as much to cataracting (causing higher impact forces) as to cascading. As a result, the charge is more concentrated in one place, the moment arm is longer, and the angle to the center of gravity has a lower value. Both of these changes are correlated with an increase in torque. In dry milling, rotational speed impacted torque values within the analyzed range, and a negative correlation suggests that increasing speed leads to decreased torque, probably due to the transition from the cascading to cataracting motion *(Torque – DoE)*. Torque had a moderately strong positive correlation with size reduction and a moderate negative correlation with specific energy *(Correlations Across Scales – Dry Milling)*.

Filling degree was a highly influential factor in most setups, and was positively correlated with torque *(Torque – DoE)*, as a higher filling degree results in more mass and higher gravitational forces in both dry and wet milling. Lifter configuration (height and number) can impact torque, particularly in the 300 mm dry mill, with more and higher lifters leading to lower torque *(Torque – DoE)*.

In wet milling, the predictive power of the regression models varied, demonstrating the complexity of the process *(Torque – DoE)*. The consistent significance of slurry density in wet milling emphasizes its importance in energy efficiency and operational costs *(Torque – DoE)*.

Some specific runs in dry milling showed interesting torque signal characteristics. Runs 2 and 3, with higher rotational speed and lower lifter height, had positive skewness and kurtosis above 3 for all mill sizes *(Torque Sensor Measurements – Dry Milling)*. The positive skewness implies that the torque data is skewed to the right, with more frequent small to moderate torque values and a longer tail of higher torque values. This fact indicates moments of high stress or load on the mill. The kurtosis above 3 suggests that extreme values (both high and low) are more likely than in a normal distribution, indicating potential for more frequent and extreme operational stress. These runs showed the cascading and cataracting load behavior for most cases across all scales. The positive skewness suggests that the mill often operates in a regime with normal cascading action but occasionally enters a state with a more aggressive grinding or cataracting action that could cause higher torque peaks. The heavy tails in the torque distribution could imply that extreme torque values, possibly associated with cataracting or erratic charge dynamics, occur more frequently than can be predicted from the normal distribution.

Run 4, with lower settings for all parameters, demonstrated negative skewness and a kurtosis closer to the higher range *(Torque Sensor Measurements – Dry Milling)*. This run showed only the cascading motion (for the 400 and 500 mm mills). The negative skewness implies more higher values and fewer lower values in the signal as compared to a normal distribution. This fact was expected because the behavior is steady and less turbulent, with the center of gravity in a similar place throughout the process, resulting in constant torque values with occasional dynamic events accounting for other lower values on the measured spectrum. The high kurtosis suggests that extreme values occur in the torque signal more frequently than would be expected in a normal distribution, with these extremes possibly indicating occasional but significant deviations from the optimal cascading motion.

Runs 6 and 3, both with higher rotational speed and low filling degree, resulted in lower torque across all scales *(Torque Sensor Measurements – Dry Milling)*. These runs

showed centrifuging for the 300 and 400 mm diameters, and cascading and cataracting for the 500 mm mills. The lower torque can be explained by the centrifuging motion, as the center of gravity is closer to the axis of mill rotation, resulting in a shorter moment arm and lower torque.

Runs 1 and 8, with high filling degree and low rotational speed, provided higher torque values *(Torque Sensor Measurements – Dry Milling)*. This observation seems logical, as a higher filling degree translates into more mass and higher gravitational forces and leads to higher torque values. The lower rotational speed prevents material from centrifuging, so the center of gravity is further away from the axis of rotation. The result is a longer moment arm and higher torque.

Interestingly, the kurtosis and skewness of the torque signal could be used as indicators of the charge dynamics in dry milling. It would be recommended to test this assumption on an industrial scale in real-time monitoring.

Key Findings:

1. Slurry density dominates other parameters in wet milling, with higher density leading to lower mean torque, it thus has an important role in energy efficiency and operational costs.

2. In dry milling, the correlation between torque and charge position was stronger with the angle measured from the recordings than from the simulated data, possibly due to the small shift in rotational speed between the real and the simulated experiments.

3. The addition of slurry to the simulations caused the simulated CoG angles to become a better predictor of torque in wet milling than in dry milling.

4. The dominance of tangential force correlated with an increase in torque in dry milling; this milling type involves less cataracting and more cascading, and as a result the charge is more concentrated and the moment arm is longer.

5. The kurtosis and skewness of the torque signal could be used as indicators of the charge dynamics in dry milling, as positive skewness and high kurtosis suggest occasional aggressive grinding or cataracting actions and more frequent extreme torque values.

6. Runs with higher rotational speed and low filling degree resulted in lower torque across all scales due to centrifuging, while runs with high filling degree and low rotational speed yielded higher torque values.

These findings indicate the complex relationships between operating parameters, charge dynamics, and torque in both dry and wet milling, and thus they provide insights for optimizing mill performance and energy efficiency.

7.1.4 Scale Effect and Scaling Constant

This subsection discusses the scale effects observed in the study and the performance of the developed scaling constant. It examines the process stability across different mill diameters, and the effectiveness of the scaling constant in maintaining consistent performance metrics. The analysis of the findings is intended to provide insights into the scaling behavior of ball mills and the potential for improving scale-up strategies.

Process Stability

In dry milling, the rotational speed was more effectively controlled at higher scales, with the deviation between the set and the measured RPM values decreasing as the mill diameter increased. The smallest diameter showed the most significant differences *(Rotational Speed Sensor Measurements – Dry Milling)*. Torque was more stable in the case of larger diameters, and smaller diameter mills showed higher torque variability *(Torque Sensor Measurements – Dry Milling)*. In the case of some runs at higher diameters, transient behavior was absent altogether *(Torque Sensor Measurements – Dry Milling)*. As expected, the power draw and the absolute values of torque increased together with increasing diameter *(Torque Sensor Measurements – Dry Milling, Power Draw Sensor Measurements – Dry Milling)*.

Interestingly, with a greater number and height of the lifters across scales, the identical charge motion type can be maintained across scales. Higher lifter size and quantity may contribute to stable load dynamics during scale-up *(Simulated Charge Position – Dry Milling)*. More lifters can stabilize the type of charge movement across scales, as seen in runs 1, 3, 5, 7, and 8, which have the same type of movement across scales, and 4 out of the 5 runs (except for run 8) have more lifters *(Charge Movement in Simulations – Dry Milling)*. In contrast, lower lifters, fewer lifters, lower filling degree, and higher speed can increase the scale effect *(Charge Movement in Simulations – Dry Milling)* and lead to the most significant shift in the type of charge movement. There is an observable shift from centrifuging to cataracting and from cataracting to cascading as the diameter increases *(Charge Movement in Simulations – Dry Milling, Charge Movement in Recordings – Dry Milling)*. The greatest deviation from the set RPM values was observed for the smallest diameters and caused the charge to centrifuge more often. This phenomenon may have an impact on the results *(Charge Movement in Simulations – Dry Milling)*. The DoE results did not allow the size reduction to be clearly explained by the operational parameters and by how their impact changes with scale increase. This fact may be a result of the deviation in the set and the real RPMs for the smallest diameter or due to other unidentified factors *(Size Reduction – DoE)*.

In wet milling, the rise times were smallest for the smallest diameters, but in the case of larger diameters, the rise time was either long or absent. This contrast may be due to the presence of slurry, which results in either the stability of mill operation or lack thereof *(Torque Sensor Measurements – Wet Milling)*. The transient state was absent for most runs with lower slurry density at larger diameters *(Torque Sensor Measurements – Wet Milling)*. Power draw increased with diameter as expected *(Power Draw Sensor Measurements – Wet Milling)*, and the process was relatively stable across scales. Absolute power draw variation increased together with power draw, but relative variations remained stable *(Power Draw Sensor Measurements – Wet Milling)*. Only the startup phase was more aggressive for larger diameters. This observation suggests that initial phase dynamics could be adjusted, and that in the case of greater diameters slower acceleration might translate into better energy utilization *(Power Draw Sensor Measurements – Wet Milling)*. Interestingly, the optimal charge motion type for achieving dominance of tangential forces was achieved in the medium scale and was not directly correlated with diameter *(Force Ratio – Wet Milling)*.

Key Findings:

1. In dry milling, rotational speed control and torque stability improved with increasing

mill diameter, while absolute torque and power draw values increased with diameter.

2. A greater number and height of the lifters across scales can help maintain consistent charge motion type during scale-up in dry milling.

3. Lower lifters, fewer lifters, lower filling degree, and higher speed can increase the scale effect and cause shifts in charge movement type from centrifuging to cataracting and from cataracting to cascading as diameter increases in dry milling.

4. In wet milling, the rise times were shortest for the smallest diameters, and the transient state was absent for most runs with lower slurry density at larger diameters.

5. In wet milling, power draw increased with diameter, and the process was stable across scales, with only the startup phase being more aggressive for larger diameters.

6. The optimal charge motion type at which dominance of tangential forces occurred in wet milling was achieved in the medium scale and was not directly correlated with diameter.

Scaling Constant

The developed scaling constant, which was the primary goal of this research, proved to be effective in maintaining a consistent level of specific energy and specific energy per rotation across different mill scales. The level of particle size reduction was also maintained, albeit only for wet milling. The analysis indicated that the scaling constant has a direct moderate correlation only with rotational speed for both dry and wet milling *(Correlations Across Scales – Dry Milling, Correlations Across Scales – Wet Milling)*. The scaling constant was found to be independent of most other parameters.

However, in the case of dry milling, size reduction was not completely maintained at a consistent level between scales, with significant differences observed in size reduction medians across scales, particularly between the 300 mm and 500 mm mill diameters *(Scaling Constant Testing of Assumptions)*. This discrepancy may be attributed to the fact that lower diameter mills are more prone to centrifuging, which can impact experimental results *(Charge Movement in Simulations – Dry Milling)*.

Further improvement of the scaling constant approach would require the incorporation of the findings of this study and inclusion of other parameters not accounted for in the scaling constant. These parameters should be accounted for in such a manner that the type of charge motion is consistently maintained while scaling. This condition can be verified in a numerical environment and then validated through laboratory tests so as to determine if size reduction remains consistent across scales.

Although the differences in size reduction were observed for dry milling, specific energy and specific energy per rotation were maintained at the same levels across scales for both dry and wet milling *(Scaling Constant Testing of Assumptions)*. The measured statistical effect size of scale on the measured parameters was greater for dry milling, and the specific energy per rotation metric was the most responsive to the scaling constant (showing inverse correlation) *(Correlations Across Scales – Dry Milling)*. In the case of wet milling, all parameters showed small effect sizes, indicating that the scaling constant performs better in wet milling conditions and maintains all metrics at the same level *(Scaling Constant Testing of Assumptions)*.

Key Findings:

1. The scaling constant is directly correlated only with rotational speed for both dry and wet milling.

2. Size reduction in dry milling was not maintained at the same level across scales, particularly between 300 mm and 500 mm mill diameters.

3. Specific energy and specific energy per rotation were maintained at the same levels across scales for both dry and wet milling.

4. The scaling constant works better in wet milling conditions, maintaining all metrics at the same level.

7.1.5 Main Process Efficiency Metrics

The power draw and energy consumption in ball mills are directly influenced by several operational parameters, with rotational speed and filling degree being the main factors in dry milling, and slurry density being the dominant factor in wet milling *(Energy Consumed – DoE)*. As expected, increasing the mill scale, rotational speed, and filling degree leads to higher power draw and energy consumption *(Power Draw Sensor Measurements – Dry Milling)*. This observation is evident from the dry experiments, where runs with high filling degree and high rotational speed (Runs 2 and 5) tend to be in the higher spectrum of power draw across scales, while runs with low rotational speed and low filling degree (Runs 4 and 7) are in the lower spectrum *(Power Draw Sensor Measurements – Dry Milling)*.

The energy consumption increasing with mill diameter demonstrates the scaling effect on power draw in both dry and wet milling *(Power Draw Sensor Measurements – Dry Milling, Power Draw Sensor Measurements – Wet Milling)*. In dry milling, rotational speed directly correlates with energy consumption *(Energy Consumed – DoE)*, and filling degree has a significant positive correlation with energy consumption in larger mills *(Energy Consumed – DoE)*. Higher lifters in the 500 mm dry mill can reduce energy consumption owing to enhanced charge lift and drop mechanics *(Energy Consumed – DoE)*. In wet milling, slurry density is the dominant factor affecting power draw, having an inverse relationship with energy consumption and offering a potential for energy savings *(Energy Consumed – DoE)*.

Regression models provide a quantitative basis for predicting energy consumption, but the varying predictive accuracy suggests some space for further model improvement *(Energy Consumed – DoE)*. Correlations across scales indicate that higher filling degrees are more energetically optimal/efficient in dry milling *(Correlations Across Scales – Dry Milling)*, while slurry density has a moderate negative correlation with energy consumed in wet milling *(Correlations Across Scales – Wet Milling)*.

Specific Energy

Specific energy is the energy consumed by 1 kg of ore during the milling process. Lower specific energy translates into energy savings. The filling degree is an important factor in optimizing energy utilization, with higher filling degrees leading to better energy utilization and lower specific energy *(Specific Energy – DoE; Correlations Across Scales – Dry Milling)*. However, specific energy can be reduced not only by higher filling degree

but also by increased charge volume, as specific energy decreases with an increase in scale *(Correlations Across Scales – Dry Milling)*.

The internal diameter of the mill is inversely correlated with specific energy *(Correlations Across Scales – Dry Milling)*, as confirmed by the observation that torque has a moderate negative correlation with specific energy due to greater diameter mills having higher absolute torque values and lower specific energy *(Correlations Across Scales – Dry Milling)*. In the case of smaller diameters, higher speeds lead to lower specific energy, but this fact may be due to centrifuging, which results in lower torque and power draw but also in smaller size reduction. Rotational speed positively impacts specific energy in smaller diameter dry mills, but its effect decreases in larger diameters and in wet conditions *(Specific Energy – DoE)*. In fact, specific energy is strongly correlated with specific energy per rotation. This relationship indicates that rotational speed does not have a significant impact on specific energy *(Correlations Across Scales – Wet Milling; Correlations Across Scales – Dry Milling)*.

Other interesting observations include the dominance of tangential force correlated with lower specific energy due to a greater share of the cataracting motion, which reduces torque and total energy consumption *(Correlations Across Scales – Dry Milling)*. Also, a moderate positive correlation is observed between specific energy and the number of balls per working area, as more contact points and faster energy transfer between balls lead to higher specific energy in dry milling *(Correlations Across Scales – Dry Milling)*.

In wet milling, slurry density appears to be the most significant parameter, showing an inverse correlation with specific energy *(Specific Energy – DoE; Correlations Across Scales – Wet Milling)*. The relationship between filling degree and slurry density seems crucial for understanding energy consumption in wet milling, especially for larger mill diameters, and may require further research *(Specific Energy – DoE)*. Additionally, size reduction is strongly correlated with specific energy in wet milling. This relationship demonstrates that higher energy input directly translates into greater size reduction *(Correlations Across Scales – Wet Milling)*.

Key Findings:

1. Higher filling degrees lead to better energy utilization and translate into lower specific energy.

2. Internal diameter is inversely correlated with specific energy.

3. Rotational speed has a limited impact on specific energy, particularly in larger diameters and wet conditions.

4. Slurry density is the most significant parameter in wet milling, showing an inverse correlation with specific energy.

5. The relationship between filling degree and slurry density seems crucial for understanding energy consumption in wet milling, especially in the case of larger mill diameters.

Specific Energy per Rotation

Filling degree is a variable that greatly affects energy consumption in milling operations. The analysis indicates that filling degree is negatively correlated with specific energy

per rotation and suggests that higher filling degrees lead to lower specific energy per rotation *(Specific Energy per Rotation – DoE)*. This finding is further supported by the observation that higher filling degree reduces specific energy per rotation across different scales *(Correlations Across Scales – Dry Milling)*. This effect is proven to be consistent in various experimental setups.

However, the relationship between filling degree and energy efficiency is not simple, as specific energy per rotation interacts with other factors such as slurry density. The interaction of slurry density with filling degree has a positive correlation with specific energy per rotation *(Specific Energy per Rotation – DoE)*, demonstrating a complex relationship of multiple variables that needs to be allowed for in determining milling efficiency.

Another important operational variable is rotational speed, which is inversely correlated with specific energy per rotation in half of the models. This fact indicates that lower speeds require less specific energy per rotation *(Specific Energy per Rotation – DoE)*. It also demonstrates the importance of considering rotational speed when optimizing milling processes for energy efficiency.

In wet milling, slurry density appears to be the most significant factor impacting specific energy per rotation. The inverse correlation between slurry density and specific energy per rotation becomes more evident for larger mill diameters *(Specific Energy per Rotation – DoE)*. This observation is further supported by the high negative correlation between slurry density and specific energy per rotation across different scales in wet milling *(Correlations Across Scales – Wet Milling)*.

Size reduction, the primary goal of milling, is related to energy efficiency. In dry milling, size reduction is moderately correlated with specific energy per rotation *(Correlations Across Scales – Dry Milling)*, while in wet milling, this correlation is strong *(Correlations Across Scales – Wet Milling)*. This difference in correlation strength is indicative of the varying effects of size reduction on energy consumption, depending on the milling environment.

The analysis also demonstrates that specific energy per rotation is the metric most responsive to scaling constant, demonstrating an inverse correlation *(Correlations Across Scales – Dry Milling)*. This finding connects the specific operational measures of milling to the theoretical principles of scale, demonstrating how changes in the scaling constant can significantly influence energy efficiency.

Key Findings:

1. Higher filling degrees lead to lower specific energy per rotation.
2. Slurry density interacts with filling degree, affecting specific energy per rotation.
3. Lower rotational speeds require lower specific energy per rotation.
4. In wet milling, slurry density has the most significant impact on specific energy per rotation.
5. Size reduction is correlated with specific energy per rotation; the strength of the correlation varies depending on the milling environment.
6. Specific Energy per rotation is highly responsive to changes in the scaling constant.

Size Reduction

The dry and wet milling experiments conducted across different mill diameters provide important insights into the factors influencing particle size reduction and milling efficiency. In dry milling, larger diameter mills generally produce finer particle sizes, as indicated by lower d_{80} values *(Product Size Distribution – Dry Milling)*. The average size reduction ratios for the 300, 400, and 500 mm mills are 3.984, 5.030, and 5.758, respectively, with the 500 mm mill demonstrating the highest effectiveness and efficiency *(Product Size Distribution – Dry Milling)*.

However, the results across scales in dry milling were inconsistent, with low to medium predictive power suggesting the influence of other factors, such as operational conditions or mill design *(Size Reduction – DoE)*. For lower mill diameters, high rotational speed was found to have a negative effect on size reduction *(Size Reduction – DoE)*. Furthermore, the relationship between filling degree and lifter height in the 500 mm dry mill is complex and non-linear, and indicates that advanced analyses of these factors are further needed to achieve optimal performance *(Size Reduction – DoE)*.

In contrast to the dry milling case, the 400 mm wet mill achieves the finest average d_{80} value and the highest size reduction ratio. This fact suggests an optimal scale for efficiency *(Product Size Distribution – Wet Milling)*. The average size reduction ratios for the 300, 400, and 500 mm mills are 6.879, 9.036, and 7.955, respectively *(Product Size Distribution – Wet Milling)*. However, the relationship between mill diameter and product size distribution in wet milling is complex and influenced by factors such as slurry properties and rheology *(Product Size Distribution – Wet Milling)*.

Slurry density again appears to be a critical factor in wet milling, with lower densities resulting in higher size reduction ratios *(Product Size Distribution – Wet Milling)*. This finding is supported by the high negative correlation between slurry density and size reduction *(Correlations Across Scales – Wet Milling)*. Further investigation into slurry characteristics is necessary so as to fully describe the multifactorial nature of milling efficiency in wet conditions *(Product Size Distribution – Wet Milling)*.

The design of experiments (DoE) analysis in wet milling identified slurry density as the most significant factor which negatively impacts size reduction *(Size Reduction – DoE)*. Additionally, filling degree, lifter height (negative impact), and their interaction (positive impact) were identified as important factors influencing size reduction *(Size Reduction – DoE)*.

From a cross-scale perspective, size reduction in dry milling is moderately correlated with specific energy per rotation *(Correlations Across Scales – Dry Milling)*. In wet milling, size reduction is strongly correlated with specific energy and specific energy per rotation, and moderately correlated with total energy consumed and with the resulting torque *(Correlations Across Scales – Wet Milling)*.

Key Findings:

1. Larger diameter mills produce finer particle sizes in dry milling.
2. The 500 mm mill demonstrates the highest effectiveness and efficiency in dry milling.
3. Dry milling results were inconsistent across scales, as they were influenced by operational conditions and mill design.
4. The 400 mm mill shows the finest average d_{80} value and the highest size reduction ratio in wet milling.

5. Slurry density is a critical factor in wet milling, with lower densities resulting in higher size reduction ratios.

6. Filling degree, lifter height, and their interaction influence size reduction in wet milling.

7. Size reduction is correlated with energy metrics in both dry and wet milling.

Size Reduction and Force Ratio

The relationship between force ratio and size reduction in dry milling is a complex phenomenon influenced by various operational parameters and charge dynamics. Experimental observations suggest that the predominance of tangential forces, associated with the abrasion and attrition grinding mechanisms, can be recommended for achieving finer particle sizes *(Force Ratio – Dry Milling)*. Mill internal diameter has a strong positive correlation with size reduction and force ratios, as larger mill sizes lead to an increase in tangential force dominance, which is correlated with higher size reduction *(Correlations Across Scales – Dry Milling)*. This phenomenon may be attributed to the higher charge volume and mass in larger mills and may result in increased gravitational forces acting on the cascading charge. In effect, the tangential forces become stronger than the friction resistance between the balls. The dominance of tangential forces thus seems to be influenced by the mass of ore and balls, with higher mass resulting in a greater dominance of tangential forces *(Correlations Across Scales – Dry Milling)*. Conversely, higher rotational speeds and a greater number of balls per working area lead to an increased dominance of normal forces and lower size reduction *(Correlations Across Scales – Dry Milling)*. Interestingly, the size distribution of the grinding media may also affect the force dominance, as smaller balls potentially increase the number of contacts between balls, leading to more direct impacts and an increase in normal force dominance.

Maintaining the dominance of tangential forces needed to produce finer products requires more energy *(Correlations Across Scales – Dry Milling)*. Experiments show that a higher ratio of tangential to normal forces is associated with increased torque, size reduction, and total energy consumption, but with lower specific energy *(Correlations Across Scales – Dry Milling)*. This observation suggests that maintaining tangential force dominance may translate into increased grinding efficiency understood as the energy consumed per kilogram of ore. Balance between energy consumption and milling efficiency requires considering both energy costs and size reduction *(Force Ratio – Dry Milling)*, and the optimal force ratio depends on the desired outcome of the milling process, such as energy efficiency, particle size reduction, or specific particle shape *(Force Ratio – Dry Milling)*.

Operational parameters and charge dynamics also have a significant impact on force ratio and size reduction. Higher filling degrees are associated with broader areas of tangential force dominance within the mill, as observed in both dry and wet milling experiments *(Force Ratio – Dry Milling, Force Ratio – Wet Milling)*. The filling degree has the most significant influence on force ratio. It has a positive correlation with tangential force dominance in most conditions *(Force Ratio – DoE)*. On the other hand, rotational speed and lifter height have a negative impact on tangential force dominance *(Force Ratio – DoE)*.

In wet milling, force ratio varies with mill diameter, with the lowest ratios observed in the 300 mm mill and the highest in the 400 mm mill *(Force Ratio – Wet Milling)*. The fact that increasing slurry density decreased the force ratio across all scales suggests a dampening effect on tangential forces *(Force Ratio – DoE)*. Tangential force dominance is

more common for larger mill diameters in the wet milling processes. It increases under the influence of ball mass and ore mass, and significantly decreases affected by the increasing number of balls per working area and rotational speed *(Correlations Across Scales – Wet Milling)*.

Key Findings:

1. Tangential force dominance is advantageous for achieving finer particle sizes in dry milling.
2. Mill diameter, mass of ore and balls, and filling degree positively correlate with tangential force dominance.
3. Greater rotational speed, number of balls per working area, and lifter height negatively impact tangential force dominance.
4. Maintaining tangential force dominance requires more energy but may lead to more energy-efficient grinding.
5. Optimal force ratio depends on the desired outcome of the milling process.
6. In wet milling, increasing slurry density decreases force ratio across all scales.

7.2 Contextualizing the Findings within the Literature

This section situates the main findings of the study within the broader context of the existing literature on ball mill optimization and scaling. The results are compared and contrasted with previous research in order to better illustrate their contributions to the understanding of charge motion, torque, energy efficiency, size reduction, and force dynamics in both dry and wet milling environments. The section also provides a comprehensive overview of how the findings align with and expand on the current state of knowledge in the field.

7.2.1 Charge Motion

The charge motion in tumbling mills is a factor significantly influencing grinding efficiency and energy consumption. This study investigated the effects of mill diameter, lifter configuration, and operational parameters on charge motion in both dry and wet milling using a combination of experimental measurements and numerical simulations.

It was found that an increase in the mill diameter entails a shift from centrifuging to cataracting and from cataracting to cascading charge motion in both dry and wet milling. This finding is consistent with previous studies showing that larger mill diameters promote higher energy impacts, but reduce the frequency of those impacts for a particular percent of critical speed [46, 82, 189, 107]. The type of charge motion regime changes from cascading to cataracting as the mill diameter increases [8]. However, very large diameter mills can become less efficient if not properly optimized, as the mill diameter, the mill speed, the charge volume, and the ball size distribution must be carefully balanced so that the desired charge motion and breakage rates can be maintained [107].

The results also showed that an increase in the number of lifters can stabilize the type of charge movement across scales under both dry and wet milling conditions. Lifters have

a significant impact on how the charge is lifted and projected. They influence the impact energy spectra, power draw, and overall grinding efficiency [132, 50, 25, 149, 142, 33]. An optimal lifter design depends not only on mill diameter but also on lifter width, height, angle and the overall lifter type [25].

The influence of operational parameters on optimal charge motion was found to vary with mill diameter in both dry and wet milling. Optimal motion is the result of specific combinations of lifter height, filling degree, and rotational speed. These parameters affect the stability and positions of the head, shoulder, impact toe and bulk toe of the charge in varying degrees [135, 33, 103, 11]. Charge motion is controlled primarily by rotational speed and also by lifter height, which is particularly important for the shoulder and toe positions, as they define impact energy [140, 33].

The quantitative data from the recordings and the simulations confirmed that the motion of the charge and its average position, as well as the center of gravity coordinates and angles vary across runs. Several methods are used in the recording and simulating of charge motion. They include the Discrete Element Method (DEM), Positron Emission Particle Tracking (PEPT), instrumented balls, high-speed video, and vibration sensors [116, 33, 141, 9, 8, 112, 187, 88, 76, 10, 80]. DEM is the most comprehensive simulation method, while experimental techniques provide data for calibration and validation of the numerical models [12, 141, 88].

The charge position stability was found to depend on a combination of the lifter setup and other operational parameters in both dry and wet milling. In dry milling, rotational speed seems to have a more significant impact on shoulder height than lifter height does. Rotational speed requires optimization in order to maximize grinding while avoiding excessive cataracting and liner wear. Lifter height should be adjusted so as to fine-tune the charge motion as lifters wear over time [33]. In wet milling, runs with lower slurry density showed more stable ranges of the CoC/CoG angles across scales and more prominent pool formation at the toe region. An increase in slurry density leads to a more damped and stable charge motion, decreases impact forces, causes the formation of a slurry pool, and influences power draw [162, 31, 29, 127, 159]. The slurry pool and viscous effects also need to be considered when modeling charge behavior in wet milling.

The average angles for the cascading, cataracting and cascading, and centrifuging and cataracting motions were found to be similar in both dry and wet milling simulations. However, the relative arms for wet milling are not as distinguishable between different motion types as in dry milling, and only the average relative moment arm for centrifuging is significantly smaller. Further detailed experimental or simulation studies may allow a better description of how the relative moment arms of each motion type change between dry and wet environments.

In summary, this study provides information on the complex relationship between mill design, operating conditions and environment, and on their influence on charge motion in tumbling mills. The results demonstrate the importance of lifter design, mill speed, and slurry properties in optimizing the charge motion for efficient grinding across different scales and milling types. Advanced modeling techniques, such as DEM, combined with experimental validation, provide tools which provide more information about these effects and allow designs of improved milling systems.

7.2.2 Torque

The torque required to rotate a tumbling mill is an important parameter that reflects the charge dynamics and energy efficiency of the milling process. This study investigated the effects of various operating conditions on torque in both dry and wet milling, and compared experimental measurements with simulated data.

In wet milling, the results showed that the importance of slurry density for energy efficiency and operational costs is greater than that of other parameters, with higher slurry density notably leading to lower mean torque. Previous studies have shown that an increase in slurry density generally decreases the impact forces and energy in the mill by dampening the collisions between grinding media [162, 187, 159]. Therefore, an optimal slurry density can maximize grinding efficiency, as excessively high densities can decrease both the mechanical intensity of grinding and the energetic efficiency [162, 187, 159]. Optimizing slurry density is thus crucial for achieving the desired balance between particle transport and impact dampening in wet milling processes.

In dry milling, the correlation between torque and charge position was stronger for the angle measured from the recordings than for the angle measured from the simulated data. This discrepancy may be due to the small shift in rotational speed between the real and the simulated experiments, as well as to other factors such as simplifications in the DEM model, accuracy of the input parameters, not modeled power losses, experimental vibrations, and insufficient simulation time [116, 18, 11, 109]. Careful model calibration and sufficiently detailed simulations, which require long computing time, are necessary for minimizing these differences and improving the predictive accuracy of torque based on charge angles in dry milling.

The addition of slurry to simulations caused the simulated center of gravity (CoG) angles to be a better predictor of torque in wet milling than in dry milling. The presence of a slurry pool at high filling degrees significantly affects the toe angle and charge dynamics, hindering predictions of torque based solely on the CoG angles [162, 132]. The currently developed advanced numerical models coupling DEM and CFD/SPH seem capable of better representing the complex multiphase interactions in wet mills, but industrial validation is still needed [114, 32].

The study also found that the dominance of tangential force is in correlation with an increase in torque in the case of dry milling, because it is related not as much to cataracting as to cascading. As a result, the charge is more concentrated and the moment arm is longer. The charge motion, influenced by operating parameters such as mill speed and lifter design, determines the tangential forces and torque acting on the mill shell [106, 145, 1]. Optimization of charge motion is thus important for maximized grinding efficiency without excessive power draw and liner wear.

Kurtosis and skewness of the torque signal were identified as potential indicators of the charge dynamics in dry milling, with positive skewness and high kurtosis suggesting occasional aggressive grinding or cataracting action and more frequent extreme torque values. However, the raw kurtosis and skewness values of the unfiltered torque signal may not be fully reliable. Advanced spectral analysis techniques applied to the torque signal, particularly those which filter and quantify noise levels, show promising results, as they provide characteristics of charge dynamics and other important parameters, e.g. mill filling degree [139, 169]. Thus a decision to pre-process torque signal prior to calculating kurtosis and skewness.

The study also confirmed that runs with higher rotational speed and low filling degree showed in lower torque across all scales due to centrifuging, while runs with high filling

degree and low rotational speed showed higher torque values. Rotational speed and filling degree are important operating variables that should be both optimized in order to achieve the desired torque and power draw for efficient grinding [139, 72, 48, 11, 194, 145, 131]. Speeds around 70-80% of critical and filling levels of 35-45% are typical for ball mills [70].

In conclusion, this study provides important insights into the complex relationships between operating conditions, charge dynamics, and torque under both dry and wet milling conditions. The findings indicate that parameters such as slurry density, rotational speed, and filling degree require optimization for maximizing grinding efficiency and minimizing energy consumption. The discrepancies between the experimental and the simulated data also point to the need for further improvement of numerical models so that they better represent the multiphase interactions and power losses in industrial mills.

7.2.3 Scaling

The scaling constant developed in this research is a novel parameter hypothesized to maintain performance metrics such as size reduction, specific energy, and specific energy per rotation at consistent levels across different scales of ball milling. The scaling constant aims to include the maximum average energy per ball in the charge, as well as rotational speed, number of balls, and the ball working area into a single parameter that can be used to compare mill performance across scales.

The findings from this study show that the scaling constant is directly correlated with rotational speed for both dry and wet milling. However, size reduction in dry milling was not maintained at the same level across scales, particularly between the 300 mm and 500 mm mill diameters. In contrast, specific energy and specific energy per rotation were maintained at consistent levels across scales for both dry and wet milling. The scaling constant was found to work better in wet milling conditions, as all of the metrics were maintained at the same level.

These findings can be contextualized within the broader literature on the scale-up and optimization of milling operations. Maintaining consistent performance across scales is a significant problem in the mining industry, and various approaches are employed to address this issue. Common methods include using dimensionless scale-up factors [130], establishing correlations between power-specific breakage rates and mill operating conditions [72], applying population balance models [113, 59], and utilizing the attainable region methodology [26]. The scaling constant developed in this study offers a new approach to this problem, as it offers a single parameter that represents the main mill variables.

The influence of rotational speed on milling performance, as presented in this study, is well-established in the literature. An increase in rotational speed up to 70-80% of critical speed generally improves grinding rates and power draw due to more intensive cataracting and ball impact energy [72, 194, 179, 61, 187, 162]. However, beyond this optimal range, grinding rates decrease as the charge starts to centrifuge [72, 194, 61]. The direct correlation between the scaling constant and rotational speed seems to support these findings.

The challenges in measuring and maintaining energy efficiency during scale-up, as encountered in this study, are also reflected in the literature. The low energy efficiency of ball mills, inaccurate measurements of energy dissipation, and complex influence of operating variables during scale-up it is difficult to optimize and maintain the efficiency of large-scale grinding processes [97, 173, 73, 30]. The ability of the scaling constant to maintain specific energy and specific energy per rotation across scales demonstrates its

potential in addressing the above challenges.

Mill diameter is significant in determining the results of milling operations, with larger diameters generally increasing breakage rates and impact energy [46, 131]. However, the effects are complex and depend on ore type and operating conditions [72]. The inconsistent size reduction observed in this study across mill diameters in dry milling suggests that scale-up processes be performed upon careful optimization.

Computational simulations, such as Discrete Element Method (DEM) and Population Balance Models (PBM), are increasingly used in predictions and optimization of milling operations at different scales [82, 100, 144, 45, 75]. The development of the scaling constant could potentially benefit from integration with these simulation techniques, so that its predictive capabilities, in terms of both the predictive power and accuracy, can be further improved.

Finally, the fact that the scaling constant performed better in wet milling than in dry milling seems to agree with the literature on the differences between these two conditions. Wet milling tends to produce finer, smoother, and more irregularly shaped particles, while dry milling has higher breakage rates and generates coarser, rounder particles [17, 136, 93]. The slurry present in wet milling absorbs impact energy and results in different wear patterns [43, 184], which may contribute to the better performance of the scaling constant in wet conditions.

In summary, the scaling constant developed in this research offers a novel approach to maintaining consistent performance across scales in ball milling. The findings, particularly the direct correlation with rotational speed and superior performance in wet milling, correspond to the established trends in the literature. However, the inconsistent size reduction in dry milling across mill diameters indicates the challenges that still remain in scaling up milling operations. Further research integrating the scaling constant with computational simulations and exploring its application in a wider range of operating conditions could help improve its predictive capabilities and potential for industrial application.

7.2.4 Energy

During this research, two main energetic factors were examined: specific energy and specific energy per rotation. Specific energy is the energy consumed per unit mass of milled ore, while specific energy per rotation is a measure established in this study to account for the energy consumed during one mill rotation at different rotational speeds.

The degree to which the mill drum is filled with the grinding media and the material has a significant impact on the energy efficiency of milling operations. An optimum filling degree maximizes energy utilization and grinding efficiency [26, 30, 131, 24]. At low filling degrees, insufficient load prevents the efficient utilization of the available energy, while at very high filling degrees, the grinding media and material can dampen the charge motion and reduce the intensity of grinding [48, 183, 137, 35]. The findings of this study are in agreement with the literature, showing that higher filling degrees lead to better energy utilization and lower specific energy.

Mill diameter is an other important factor affecting energy efficiency. Several studies have found that as mill diameter increases, the specific breakage rates for different particle sizes increase, and the maximum in each breakage rate curve shifts to coarser sizes [46]. However, the power draw increases more rapidly than the useful impact energy as diameter increases. As a result, the grinding performance is lower for identical operating conditions in larger mills [82]. The inverse correlation observed in this study between in-

ternal diameter and specific energy is not consistent with these findings, possibly because the scale increase was not sufficient, as in this research energy utilization was found to be more optimal for larger mills.

Rotational speed has a significant impact on the specific energy and grinding efficiency of ball mills, but this impact can be limited at higher speeds and in larger diameter mills. As mill speed increases, grinding rate and power draw initially increase substantially, reaching a maximum at an intermediate speed (typically around 70-80% of the critical speed) [100, 194, 179]. However, as speed increases further towards the critical speed, power continues to rise, but grinding rate decreases due to the centrifuging motion of the charge [100, 194, 107]. The findings of this study, showing a limited impact of rotational speed on specific energy, especially in larger diameters and wet conditions, correspond to these observations.

Slurry density also has an indirect effect on mill energy consumption, as its increase translates into increased mass and density of the charge, and thus into the damping and cushioning of impacts. An intermediate optimum slurry density balances these factors so that grinding efficiency and mill throughput can be maximized [162, 132, 56]. The strong inverse correlation between slurry density and specific energy found in this study indicates the importance of controlling slurry density as an operating parameter in wet milling.

The relationship between filling degree and slurry density is important for understanding energy consumption in wet milling, in particular for larger mill diameters. As the share of slurry filling increases in the total charge volume, the mill power draw initially increases linearly until a certain level U', beyond which the power decreases non linearly with further increases of the share of slurry in the mill filling [187, 132]. The optimal slurry filling U' for maximum power draw in large mills tends to be in the range of $1 < U' < 1.5$ for large mills [187]. The findings of this study emphasize the importance of considering the interaction between these parameters, particularly in mills of larger diameters.

Specific energy per rotation, a measure established in this study, provides additional insights into the energy consumption during milling. The findings show that higher filling degrees lead to lower specific energy per rotation, and that this measure is also affected by slurry density along with mill filling degree. Lower rotational speeds require lower specific energy per rotation, and in wet milling, slurry density has the most significant impact on specific energy per rotation. These observations are believed to contribute to a more comprehensive understanding of energy consumption in milling processes.

In summary, the findings of this study on specific energy and specific energy per rotation align with and extend the existing knowledge in the literature. The research emphasizes the importance of optimizing filling degree, mill diameter, rotational speed, and slurry density in such a manner that the energy efficiency in milling operations can be maximized. The introduction of specific energy per rotation as a new measure provides additional insights into the energy consumption during milling, particularly in relation to rotational speed and slurry density.

7.2.5 Size Reduction and Dominant Forces

The size reduction achieved in ball milling depends on various design and operational factors. In dry milling, larger mill diameters generally lead to finer particle sizes due to increased impact energy and breakage rates [27, 46]. In the present study, the 500 mm mill demonstrated the highest effectiveness and efficiency in dry milling. However, the results across different scales were inconsistent, probably due to variations in operational

conditions and mill design. Factors such as ball size distribution, scale-up correction factors, and feed size distribution can contribute to the variability of dry milling performance across scales [130, 20, 159, 32].

In wet milling, the 400 mm mill showed the finest average d_{80} value and the highest size reduction ratio. Although no definitive optimal scale is available for wet milling, various factors influence grinding efficiency and product size. Smaller grinding media, higher mill speeds, and lower slurry density generally favor finer grinding [93, 159, 77]. However, the optimal combination of parameters depends on the specific ore characteristics, mill design, and target product size. Pilot tests and models may provide data on suitable operating conditions for a given application [130, 45, 59].

Slurry density is an important factor to be considered in wet milling, as lower densities result in higher size reduction ratios. An increase in slurry density generally reduces the breakage rate and particle size reduction by cushioning impacts and increasing viscosity [162, 43, 159, 62]. The effect is most significant at high solids concentrations where the slurry becomes highly viscous. Optimized slurry density allows the desired product size and adequate material transport through the mill [132, 59].

Filling degree and lifter height also influence size reduction in wet milling. Higher lifters promote more crushing and grinding by increasing impact forces and frequency [149]. The number of lifters affects the impact frequency and particle trajectory [149]. A filling degree above 25% is recommended, as it helps prevent lifter breakage and limit liner wear [149]. However, higher filling degrees and slurry concentrations can dampen impact forces by absorbing ball and ore energy [162]. These parameters should be optimized in order to maximize size reduction while controlling wear.

Size reduction is correlated with energy metrics in both dry and wet milling. Specific energy relates energy input to size reduction, and impact energy is uniquely correlated with grinding rate for each particular material [157, 82]. Collision energy between particles is directly linked to breakage, and the energy spectra shift towards higher specific collision energies as particle size decreases [179, 36]. Lifter height, mill speed, ball size, and density also influence the energy distribution and breakage rates [34, 50, 159, 90]. However, only a small fraction of the energy input to a ball mill is utilized for particle breakage. The remaining energy is dissipated as heat, sound, and wear [173, 84].

Force ratio, which is the ratio of tangential to normal forces, indicates the dominant forces during the milling process. Tangential forces result mainly from abrasion and attrition, while normal forces are primarily due to impact. Tangential force dominance is a metric of importance for achieving finer particle sizes in dry milling. At high mill speeds, smaller balls tend to remain near the mill shell periphery, where tangential velocities are highest. This arrangement leads to increased collision frequency and high impact energies which facilitate the generation of finer, rounded particles with rough surfaces [163, 117, 93, 17].

Mill diameter, mass of ore and balls, and filling degree positively correlate with tangential force dominance. Larger mill diameters show higher tangential forces and more cataracting of the charge, as particles are lifted to higher positions and have greater kinetic energy at impacts [100, 35, 46].

Rotational speed, the number of balls per working area, and lifter height negatively impact tangential force dominance. An increase in the rotational speed leads to higher impact forces and collision energies, with more cataracting and higher impact frequencies [162, 185]. Higher lifters translate into increased height of the impact toe and more intensive cataracting motion, leading to higher collision energies and impact forces [25, 33, 149].

However, excessive speeds or lifter heights can cause particles to hit the mill shell directly, causing accelerated wear [162, 11]. As lifter height decreases due to wear, cataracting is reduced, and bulk charge shear is increased. As a result, the energy distribution is shifted from normal impacts to shear, impact breakage is reduced, and attrition grinding is intensified [34].

The maintaining of tangential force dominance requires more energy but may increase the energy efficiency of the grinding process. Tangential forces originate from frictional sliding between particles and the mill shell or other particles when the frictional limit is exceeded. As a result, more energy is dissipated than in normal collisions [12]. The increased energy dissipation due to tangential forces and sliding reduces energy efficiency because energy is lost in non-productive friction rather than being used for size reduction [36, 173]. This observation does not align well with the results of this study, as the dominance of tangential forces was here found to increase energy efficiency, indicating a possible threshold value, beyond which tangential force dominance is excessive.

In wet milling, an increase in slurry density results in a decrease of the force ratio across all scales. Higher slurry density or solids concentration tends to decrease the impact forces and energy due to viscous dampening and resistance to ball motion [162, 187, 43]. An increase in the density and viscosity of the slurry increases its influence on charge trajectory and dynamics. Interestingly, the reduction in tangential forces was greater than the reduction in normal forces This phenomenon indicates that the slurry acted either as grease, reducing friction, or as an adhesive, gluing the grinding media together with cohesive forces and reducing the movement between balls.

The optimal force ratio depends on the desired outcome of the milling process. Mill speed, lifter design, ball size, and filling degree interact with each other, affecting the impact and abrasion forces in the mill. Balanced in models and experiments, these factors can optimize the breakage rates and energy efficiency for a particular feed material and target product size [33, 46]. Mechanistic models and DEM simulations are valuable in the predictions and optimization of force ratio and charge motion for specific milling applications [116, 179].

In summary, this study provides insights into the factors influencing size reduction and force dynamics in ball milling. The findings demonstrate the importance of mill diameter, slurry density, filling degree, lifter height, and their relationships required for achieving the desired milling outcomes. The results also emphasize the significance of force ratio as a tool for determining the dominant breakage mechanisms and ensuring energy efficiency. By integrating these findings with existing knowledge and by employing advanced modeling techniques it is possible to optimize milling performance and energy utilization for various applications.

7.3 Implications for Ball Mill Scaling and Optimization

The findings of this study have significant implications for ball mill scale-up and optimization in both dry and wet milling operations. The insights gained from investigating charge motion, torque, energy consumption, size reduction, and force dynamics across different scales and operating conditions have a potential to inform the design and operation of more efficient and sustainable milling systems.

One of the main implications is the importance of lifter design in maintaining consistent charge motion and grinding performance across scales. The study found that an increase in the number of lifters can stabilize the type of charge movement in both dry and wet

milling, while a lower height and number of lifters, lower filling degree, and higher speed can increase the scale effect and cause shifts in charge motion. This finding suggests that optimized lifter configuration is one of the most important factors influencing successful scale-up and can help maintain the desired grinding mechanisms and energy efficiency at a consistent level.

The study also demonstrates the significance of slurry density in wet milling, and notably that its higher density translates into lower mean torque and specific energy. This finding emphasizes the need for the careful control and optimization of slurry density, so that energy consumption and operational costs can be minimized. The relationship between slurry density and filling degree is another important factor, particularly in the case of larger mill diameters, as it can significantly impact energy utilization and grinding efficiency.

The scaling constant developed as part of this research offers a novel approach to maintaining consistent performance across scales. Although the scaling constant was found to work more efficiently in wet milling conditions, its direct correlation with rotational speed and its ability to maintain specific energy and specific energy per rotation across scales confirm its potential as a tool for industrial applications. Further improvement and validation of the scaling constant in computational simulations and pilot-scale tests is expected to aid scale-up strategies and more predictable milling performance.

The study also provides insights into the factors influencing size reduction and force dynamics in ball milling. The dominance of tangential forces was found to be advantageous in achieving finer particle sizes in dry milling. On the other hand, an increase in slurry density decreased the force ratio across all scales in wet milling. These findings can inform the selection of such operating parameters and mill designs that result in the desired product characteristics and energy efficiency.

Furthermore, the correlations between the energy metrics, size reduction, and force ratio point to the importance of a holistic approach to mill optimization. By considering the relationship between mill diameter, filling degree, rotational speed, slurry density, and lifter design, mill operators can identify the optimal combination of parameters and maximize grinding efficiency while minimizing energy consumption for a particular application.

In conclusion, the findings of this study are believed to have significant implications for ball mill scale-up and optimization, and thus to inform the design and operation of more efficient and sustainable milling systems. An integration of the findings from this research with advanced modeling techniques, e.g. of Discrete Element Method (DEM) with Population Balance Models (PBM), may allow even more accurate predictions of milling performance and facilitate the development of scale-up strategies.

7.4 Limitations and Future Research Directions

One of the main limitations identified in this study as an area requiring further research is the limited range of the analyzed mill diameters (300, 400, and 500 mm). Although these scales are suitable for laboratory and pilot-scale testing, they may not provide a complete representation of the complexities and problems related to industrial-scale milling operations. Future research should involve larger mill diameters and include validations of the findings in full-scale industrial mills.

Another limitation results from the focus on a single ore type and grinding media. The relationships between ore properties, grinding media characteristics, and mill operating conditions can significantly influence milling performance and energy efficiency. Therefore,

future studies should focus on a wider range of ore types, particle size distributions, and grinding media materials in order to offer more general insights and optimization strategies.

The discrepancies between the experimental and the simulated data in this study demonstrate the need for further improvement of numerical models. While the Discrete Element Method (DEM) and Smoothed Particle Hydrodynamics (SPH) serve as promising tools for simulating charge motion and fluid dynamics, their accuracy depends on the quality of input parameters and model assumptions. Future research should focus on both increasing the resolution of the existing computational methods and developing new, improved computational methods, so that the complex interactions and power losses in industrial mills can be represented more accurately.

The scaling constant developed in this study appears to be a promising solution. However, its performance was found to be better in wet milling conditions than in dry milling. Future research should investigate the factors contributing to this difference and focus on methods to improve the predictive capabilities of the scaling constant in dry milling. Additionally, the integration of the scaling constant with computational simulations and its validation in pilot-scale tests may provide more practical and reliable scale-up strategies.

The study also demonstrates the importance of lifter design, slurry density, and filling degree in optimizing mill performance and energy efficiency. Future research should be aimed at optimizing these parameters with the use of advanced experimental designs, such as response surface methodology, and multi-objective optimization techniques so as to identify the optimal combinations for specific applications. The integration of these optimization approaches with mechanistic models and DEM simulations is expected to result in more efficient and targeted optimization strategies.

Another potential direction for future research is to investigate advanced control strategies for ball mills. The insights gained from this study,e.g. the correlations between torque, charge motion, and energy efficiency, could be used to develop real-time monitoring and control systems. Such systems could adjust mill operating conditions based on real-time measurements and predictions for improved process stability, energy efficiency, and product quality.

Another area for future research lies in the environmental and economic aspects of ball mill optimization. The development of more energy-efficient and sustainable milling technologies is important for reducing the carbon footprint and operating costs of mineral-processing operations. Life Cycle Assessment (LCA) and Techno-Economic Analysis (TEA) could be employed in the evaluations of the long-term environmental and economic impacts of different optimization strategies and inform the development of more sustainable milling practices.

7.5 Concluding Remarks

This research aimed to investigate the scale-up process of ball milling operations from laboratory to industrial scale by analyzing the influence of operational parameters on milling performance and energy efficiency across selected mill diameters. The study was motivated by the need for a more systematic and scientific approach to the fundamental principles governing ball milling across different scales, as the current approach relies on empirical knowledge and trial-and-error methods, which often result in suboptimal performance, excessive energy consumption, and increased operational costs.

In order to achieve this research goal, a series of objectives were established and systematically addressed throughout the study. A systematic methodology for calibrating a digital twin of a laboratory ball mill was developed by integrating advanced modeling techniques (DEM-SPH simulations) with experimental methods (video recordings and sensor measurements). This digital twin served as a reliable and accurate virtual representation of the ball mill, providing a basis for further investigations and analyses.

Also, a scaling constant was developed and evaluated as a potential parameter for maintaining similar milling performance across different mill scales. The study tested whether maintaining the scaling constant at the same level resulted in a consistent size reduction degree, similar specific energy, and comparable specific energy per rotation under both dry and wet milling conditions. The findings show that the scaling constant is directly correlated with rotational speed for both dry and wet milling, and that it performs better in wet milling conditions. However, size reduction in dry milling was not consistent across scales, particularly between the 300 mm and 500 mm mill diameters. This fact points to the need for further improvement of the scaling constant approach.

The calibrated digital twin was applied to a multivariate analysis of copper ore milling, and the simulations provided additional insights into load dynamics and the dominant types of forces within the mill. The study investigated the impact of operational parameters such as mill diameter, filling degree, rotational speed, lifter size, lifter numbers, and slurry properties on the main performance indicators, including size reduction, energy consumption, and force distribution within the mill. The findings identify the factors which most influence ball mill performance and efficiency, pointing inter alia to the importance of lifter design in maintaining consistent charge motion and grinding performance across scales, and to the significance of slurry density in wet milling.

The study also identified and quantified correlations between mill diameter, operational parameters, and performance metrics in dry and wet milling environments with an aim to inform the development of scale-up strategies. It established transparent relationships between mill size and performance, which can be applied in the design and operation of ball mills across different scales.

The observed limitations and the resulting opportunities for future research include the following ideas: to extend research to larger mill diameters, to investigate a wider range of ore types and grinding media, to improve numerical models and the predictive capabilities of the scaling constant, to optimize the main parameters with the use of advanced experimental designs, to develop advanced control strategies, and to consider environmental and economic aspects. It is expected that addressing these limitations and pursuing these research directions can result in more efficient, sustainable, and cost-effective ball milling operations.

Bibliography

[1] M. Akhondizadeh, M. Fooladi Mahani, M. Rezaeizadeh, and S. H. Mansouri. Load behavior prediction in a tumbling mill. *Applied Mechanics and Materials*, 315:394–398, 2013.

[2] C. Altomare, A.J.C. Crespo, B.D. Rogers, et al. Numerical modelling of armour block sea breakwater with smoothed particle hydrodynamics. *Computers & Structures*, 130:34–45, 2014.

[3] Vibeke Andersson and Jón Steinar Gudmundsson. Flow properties of hydrate-in-water slurries. *Annals of the New York Academy of Sciences*, 912(1):322–329, 2000.

[4] M. Antuono, A. Colagrossi, and S. Marrone. Numerical diffusive terms in weakly-compressible sph schemes. *Computer Physics Communications*, 183:2570–2580, 2012.

[5] Sebastian Avalos, Willy Kracht, and Julian M. Ortiz. Machine learning and deep learning methods in mining operations: a data-driven sag mill energy consumption prediction application. *Mining, Metallurgy & Exploration*, 37:1197–1212, 8 2020.

[6] N. J. Balmforth and J. N. McElwaine. From episodic avalanching to continuous flow in a granular drum. *Granular Matter*, 20, 8 2018.

[7] G.K. Batchelor. *An Introduction to Fluid Dynamics*. Cambridge University Press, Cambridge, 2000.

[8] Lawrence Sidney Bbosa, Indresan Govender, and Aubrey Mainza. Development of a novel methodology to determine mill power draw. *International Journal of Mineral Processing*, 149:94–103, 4 2016.

[9] L.S. Bbosa, I. Govender, A.N. Mainza, and M.S. Powell. Power draw estimations in experimental tumbling mills using pept. *Minerals Engineering*, 24:319–324, 2 2011.

[10] B. Behera, B.K. Mishra, and C.V.R. Murty. Experimental analysis of charge dynamics in tumbling mills by vibration signature technique. *Minerals Engineering*, 20:84–91, 1 2007.

[11] Xiaolei Bian, Guoqiang Wang, Hongdi Wang, Shuai Wang, and Weidong Lv. Effect of lifters and mill speed on particle behaviour, torque, and power consumption of a tumbling ball mill: Experimental study and dem simulation. *Minerals Engineering*, 105:22–35, 5 2017.

[12] Dominik Boemer and Jean Philippe Ponthot. A generic wear prediction procedure based on the discrete element method for ball mill liners in the cement industry. *Minerals Engineering*, 109:55–79, 8 2017.

[13] F.C. Bond. *Crushing and Grinding Calculations*. Allis-Chalmers Manufacturing, Milwaukee, WI, 1961.

[14] J. Bonet and T.-S.L. Lok. Variational and momentum preservation aspects of smooth particle hydrodynamic formulations. *Computer Methods in Applied Mechanics and Engineering*, 180:97–115, 1999.

[15] P. Bortnowski, L. Gładysiewicz, R. Król, and M. Ozdoba. Energy efficiency analysis of copper ore ball mill drive systems. *Energies*, 14, 2021.

[16] N.V. Brilliantov and T. Pöschel. Granular gases with impact-velocity-dependent restitution coefficient. In *Granular Gases*, pages 100–124. Springer, 2001.

[17] Xiangning Bu, Yuran Chen, Guangxi Ma, Yujin Sun, Chao Ni, and Guangyuan Xie. Differences in dry and wet grinding with a high solid concentration of coking coal using a laboratory conical ball mill: Breakage rate, morphological characterization, and induction time. *Advanced Powder Technology*, 30:2703–2711, 11 2019.

[18] Christine Friederike Burmeister, Moritz Hofer, Palanivel Molaiyan, Peter Michalowski, and Arno Kwade. Characterization of stressing conditions in a high energy ball mill by discrete element simulations. *Processes*, 10, 4 2022.

[19] M. H. Buszko and A. K. Krella. An influence of factors of flow condition, particle and material properties on slurry erosion resistance. *Advances in Materials Science*, 19(2):28–53, 2019.

[20] M.M. Bwalya, M.H. Moys, G.J. Finnie, and F.K. Mulenga. Exploring ball size distribution in coal grinding mills. *Powder Technology*, 257:68–73, 5 2014.

[21] J. J. Campbell, R. J. Holmes, S. J. Spencer, P. L. Phillips, D. G. Barker, and K. J. Davey. An on-line surface vibration monitoring system for ag/sag mills. In *IMPC 2006 - Proceedings of 23rd International Mineral Processing Congress*, pages 1747–1752, 9 2006.

[22] R.B. Canelas, A.J.C. Crespo, J.M. Domínguez, et al. Sph–dcdem model for arbitrary geometries in free surface solid–fluid flows. *Computer Physics Communications*, 202:131–140, 2016.

[23] Ricardo B Canelas, Jose M Domínguez, Alejandro JC Crespo, Moncho Gómez-Gesteira, and Rui ML Ferreira. A smooth particle hydrodynamics discretization for the modelling of free surface flows and rigid body dynamics. *International Journal for Numerical Methods in Fluids*, 78(9):581–593, 2015.

[24] S. Cayirli. Influences of operating parameters on dry ball mill performance. *Physicochemical Problems of Mineral Processing*, 54:751–762, 2018.

[25] Mohammad Jahani Chegeni and Sajad Kolahi. Determining an appropriate range for the number of cuboid lifters in ball mills using dem. *Journal of Mining and Environment*, 12:845–862, 6 2021.

[26] Ngonidzashe Chimwani, François K. Mulenga, Diane Hildebrandt, David Glasser, and Murray M. Bwalya. Use of the attainable region method to simulate a full-scale ball mill with a realistic transport model. *Minerals Engineering*, 73:116–123, 3 2015.

[27] Heechan Cho, Jihoe Kwon, Kihong Kim, and Myoungwook Mun. Optimum choice of the make-up ball sizes for maximum throughput in tumbling ball mills. *Powder Technology*, 246:625–634, 9 2013.

[28] Paul W. Cleary. Effect of rock shape representation in dem on flow and energy utilisation in a pilot sag mill. *Computational Particle Mechanics*, 6:461–477, 7 2019.

[29] Paul W. Cleary, Gary W. Delaney, Matt D. Sinnott, and Rob D. Morrison. Inclusion of incremental damage breakage of particles and slurry rheology into a particle scale multiphase model of a sag mill. *Minerals Engineering*, 128:92–105, 11 2018.

[30] Paul W. Cleary and Rob D. Morrison. Understanding fine ore breakage in a laboratory scale ball mill using dem. *Minerals Engineering*, 24:352–366, 2 2011.

[31] Paul W. Cleary and Rob D. Morrison. Prediction of 3d slurry flow within the grinding chamber and discharge from a pilot scale sag mill. *Minerals Engineering*, 39:184–195, 12 2012.

[32] Paul W. Cleary, Rob D. Morrison, and Matt D. Sinnott. Prediction of slurry grinding due to media and coarse rock interactions in a 3d pilot sag mill using a coupled dem + sph model. *Minerals Engineering*, 159:106614, 12 2020.

[33] Paul W. Cleary and Phil Owen. Development of models relating charge shape and power draw to sag mill operating parameters and their use in devising mill operating strategies to account for liner wear. *Minerals Engineering*, 117:42–62, 3 2018.

[34] Paul W. Cleary and Phil Owen. Effect of operating condition changes on the collisional environment in a sag mill. *Minerals Engineering*, 132:297–315, 3 2019.

[35] Paul W. Cleary and Phil Owen. Effect of particle shape on structure of the charge and nature of energy utilisation in a sag mill. *Minerals Engineering*, 132:48–68, 3 2019.

[36] P.W. Cleary and R.D. Morrison. Comminution mechanisms, particle shape evolution and collision energy partitioning in tumbling mills. *Minerals Engineering*, 86:75–95, 2 2016.

[37] A. Colagrossi, M. Antuono, A. Souto-Iglesias, and D. Le Touzé. Theoretical analysis and numerical verification of the consistency of viscous smoothed-particle-hydrodynamics formulations in simulating free-surface flows. *Physical Review E: Statistical, Nonlinear, and Soft Matter Physics*, 84:026705, 2011.

[38] Andrea Colagrossi and Maurizio Landrini. Numerical simulation of interfacial flows by smoothed particle hydrodynamics. *Journal of Computational Physics*, 191(2):448–475, 2003.

[39] A.J.C. Crespo, M. Gómez-Gesteira, and R.A. Dalrymple. Boundary conditions generated by dynamic particles in sph methods. *Computational Materials Continua*, 5:173–184, 2007.

[40] S.J. Cummins and P.W. Cleary. Using distributed contacts in dem. *Applied Mathematical Modelling*, 35:1904–1914, 2011.

[41] R.A. Dalrymple and B.D. Rogers. Numerical modeling of water waves with the sph method. *Coastal Engineering*, 53:141–147, 2006.

[42] M J Daniel. The modelling of scrubbers and ag mills, when to use them. In *IMPC 2016: XXVIII International Mineral Processing Congress*. Canadian Institute of Mining, Metallurgy and Petroleum, 5 2016.

[43] Sarada Prasad Das, Debi Prasad Das, Santosh Kumar Behera, and Barada Kanta Mishra. Interpretation of mill vibration signal via wireless sensing. *Minerals Engineering*, 24:245–251, 2 2011.

[44] Eduardo Nozawa Caetano de Araujo and Homero Delboni Jr. Development of a method to measure charges in tumbling mills. *Rem: Revista Escola de Minas*, 67:311–316, 9 2014.

[45] Rodrigo M. de Carvalho, Tulio M. Campos, Patricia M. Faria, and Luís Marcelo Tavares. Mechanistic modeling and simulation of grinding iron ore pellet feed in pilot and industrial-scale ball mills. *Powder Technology*, 392:489–502, 11 2021.

[46] Rodrigo M. de Carvalho and Luís Marcelo Tavares. Predicting the effect of operating and design variables on breakage rates using the mechanistic ball mill model. *Minerals Engineering*, 43-44:91–101, 4 2013.

[47] Walter Dehnen and Hossam Aly. Improving convergence in smoothed particle hydrodynamics simulations without pairing instability. *Monthly Notices of the Royal Astronomical Society*, 425(2):1068–1082, 09 2012.

[48] Kateryna Deineka and Yurii Naumenko. Revealing the effect of decreased energy intensity of grinding in a tumbling mill during selfexcitation of autooscillations of the intrachamber fill. *Eastern-European Journal of Enterprise Technologies*, 1:6–15, 2019.

[49] G.W. Delaney, P.W. Cleary, R.D. Morrison, S. Cummins, and B. Loveday. Predicting breakage and the evolution of rock size and shape distributions in ag and sag mills using dem. *Minerals Engineering*, 50-51:132–139, 9 2013.

[50] N. Djordjevic. Discrete element modelling of the influence of lifters on power draw of tumbling mills. *Minerals Engineering*, 16:331–336, 4 2003.

[51] J. M. Domínguez, A. J. C. Crespo, M. Gómez-Gesteira, and J. C. Marongiu. Neighbour lists in smoothed particle hydrodynamics. *International Journal for Numerical Methods in Fluids*, 67(12):2026–2042, 2011.

[52] J. M. Domínguez, G. Fourtakas, C. Altomare, R. B. Canelas, A. Tafuni, O. García-Feal, I. Martínez-Estévez, A. Mokos, R. Vacondio, A. J. C. Crespo, B. D. Rogers, P. K. Stansby, and M. Gómez-Gesteira. Dualsphysics: from fluid dynamics to multiphysics problems. *Computational Particle Mechanics*, 9(5):867–895, mar 2021.

[53] Jose M. Domínguez, Alejandro J.C. Crespo, and Moncho Gómez-Gesteira. Optimization strategies for cpu and gpu implementations of a smoothed particle hydrodynamics method. *Computer Physics Communications*, 184(3):617–627, 2013.

[54] Ali Dorkhah, Alireza Arab Solghar, and Masoud Rezaeizadeh. Experimental analysis of semi-autogenous grinding mill characteristics under different working conditions. *Iranian Journal of Science and Technology - Transactions of Mechanical Engineering*, 44:1103–1114, 12 2020.

[55] Robert C. Dunnie, S. Komar Kawatara, and Courtney A. Young, editors. *Comminution: Grinding Circuit Design*, pages 465–483. SOCIETY FOR MINING, METALLURGY & EXPLORATION (SME), 2019.

[56] A. Ebadnejad, G.R. Karimi, and H. Dehghani. Application of response surface methodology for modeling of ball mills in copper sulphide ore grinding. *Powder Technology*, 245:292–296, 9 2013.

[57] A. English, J.M. Domínguez, R. Vacondio, et al. Modified dynamic boundary conditions (mdbc) for general purpose smoothed particle hydrodynamics (sph): application to tank sloshing, dam break and fish pass problems. *Computational Particle Mechanics*, 2021.

[58] P. Español and M. Revenga. Smoothed dissipative particle dynamics. *Physical Review E*, 67(2):026705, 2003.

[59] Patricia M.C. Faria, Raj K. Rajamani, and Luís M. Tavares. Optimization of solids concentration in iron ore ball milling through modeling and simulation. *Minerals*, 9, 2019.

[60] G. Fourtakas, J.M. Dominguez, R. Vacondio, and B.D. Rogers. Local uniform stencil (lust) boundary condition for arbitrary 3-d boundaries in parallel smoothed particle hydrodynamics (sph) models. *Computers & Fluids*, 190:346–361, 2019.

[61] Peng Gao, Wentao Zhou, Yuexin Han, Yanjun Li, and Wenli Ren. Enhancing the capacity of large-scale ball mill through process and equipment optimization: An industrial test verification. *Advanced Powder Technology*, 31:2079–2091, 5 2020.

[62] Fan Geng, Luo Gang, Yingchao Wang, Yimin Li, and Zhulin Yuan. Numerical investigation on particle mixing in a ball mill. *Powder Technology*, 292:64–73, 5 2016.

[63] A.R. Ghasemi, E. Razi, and S. Banisi. Determining a lower boundary of elasticity modulus used in the discrete element method (dem) in simulation of tumbling mills. *Advanced Powder Technology*, 31:1365–1371, 4 2020.

[64] Randall G Gillies and Clifton A Shook. Modelling high concentration settling slurry flows. *The Canadian journal of chemical Engineering*, 78(4):709–716, 2000.

[65] Mohammad Hasan Golpayegani and Bahram Rezai. Modelling the power draw of tumbling mills: A comprehensive review. *Physicochemical Problems of Mineral Processing*, 58, 6 2022.

[66] H. Gotoh, T. Shibahara, and T. Sakai. Sub-particle-scale turbulence model for the mps method: Lagrangian flow model for hydraulic engineering, 2001.

[67] Hitoshi Gotoh and Abbas Khayyer. On the state-of-the-art of particle methods for coastal and ocean engineering. *Coastal Engineering Journal*, 60(1):79–103, 2018.

[68] Indresan Govender. Granular flows in rotating drums: A rheological perspective, 6 2016.

[69] F. Guerrero, J. Bouchard, Poulin, and D. Sbarbaro. Real-time simulation and control of a sag mill. *IFAC-PapersOnLine*, 49:61–66, 2016.

[70] Ashok Gupta and Denis Yan. *Tubular Ball Mills*, pages 189–240. Elsevier, 2nd edition, 2016.

[71] V.K. Gupta. Population balance modeling approach to determining the mill diameter scale-up factor: Consideration of size distributions of the ball and particulate contents of the mill. *Powder Technology*, 395:412–423, 1 2022.

[72] V.K. Gupta and Shivani Sharma. Analysis of ball mill grinding operation using mill power specific kinetic parameters. *Advanced Powder Technology*, 25:625–634, 3 2014.

[73] M. Góralczyk, P. Krot, R. Zimroz, and S. Ogonowski. Increasing energy efficiency and productivity of the comminution process in tumbling mills by indirect measurements of internal dynamics—an overview. *Energies*, 13, 2020.

[74] M. Hadizadeh, A. Farzanegan, and M. Noaparast. A plant-scale validated matlab-based fuzzy expert system to control sag mill circuits. *Journal of Process Control*, 70:1–11, 10 2018.

[75] Maruf Hasan, Sam Palaniandy, Marko Hilden, and Malcolm Powell. Simulating product size distribution of an industrial scale vertimill® using a time-based population balance model. *Minerals Engineering*, 127:312–317, 10 2018.

[76] A.R. Hasankhoei, M. Maleki-Moghaddam, A. Haji-Zadeh, M.E. Barzgar, and S. Banisi. On dry sag mills end liners: Physical modeling, dem-based characterization and industrial outcomes of a new design. *Minerals Engineering*, 141:105835, 9 2019.

[77] N. Hlabangana, G. Danha, and E. Muzenda. Effect of ball and feed particle size distribution on the milling efficiency of a ball mill: An attainable region approach. *South African Journal of Chemical Engineering*, 25:79–84, 6 2018.

[78] D Hodouin, S.-L Jämsä-Jounela, M.T Carvalho, and L Bergh. State of the art and challenges in mineral processing control. *Control Engineering Practice*, 9:995–1005, 9 2001.

[79] B. Hoomans. *Granular dynamics of gas-solid two-phase flows*. PhD thesis, University of Twente, Enschede, 2000.

[80] Poorya Hosseini, Sudarshan Martins, Tristan Martin, Peter Radziszewski, and Francois-Raymond Boyer. Acoustic emissions simulation of tumbling mills using charge dynamics. *Minerals Engineering*, 24:1440–1447, 10 2011.

[81] Peng Huang, Min ping Jia, and Bing lin Zhong. Investigation on measuring the fill level of an industrial ball mill based on the vibration characteristics of the mill shell. *Minerals Engineering*, 22:1200–1208, 11 2009.

[82] C. T. Jayasundara and H. P. Zhu. Impact energy of particles in ball mills based on dem simulations and data-driven approach. *Powder Technology*, 395:226–234, 1 2022.

[83] C. T. Jayasundara and H. P. Zhu. Predicting liner wear of ball mills using discrete element method and artificial neural network. *Chemical Engineering Research and Design*, 182:438–447, 6 2022.

[84] Jack Jeswiet and Alex Szekeres. Energy consumption in mining comminution. *Procedia CIRP*, 48:140–145, 2016.

[85] Shengqiang Jiang, Yixuan Ye, Yuanqiang Tan, Sisi Liu, Jingang Liu, Hao Zhang, and Dongmin Yang. Discrete element simulation of particle motion in ball mills based on similarity. *Powder Technology*, 335:91–102, 7 2018.

[86] P. Jonsén, B.I. Pålsson, J.F. Stener, and H.-Å. Häggblad. A novel method for modelling of interactions between pulp, charge and mill structure in tumbling mills. *Minerals Engineering*, 63:65–72, 2014.

[87] Pär Jonsén, Samuel Hammarberg, Bertil I. Pålsson, and Göran Lindkvist. Preliminary validation of a new way to model physical interactions between pulp, charge and mill structure in tumbling mills. *Minerals Engineering*, 130:76–84, 1 2019.

[88] Pär Jonsén, Jan F. Stener, Bertil I. Pålsson, and Hans Åke Häggblad. Validation of a model for physical interactions between pulp, charge and mill structure in tumbling mills. *Minerals Engineering*, 73:77–84, 3 2015.

[89] Pratish Keshav, Bernard de Haas, Benoit Clermont, Aubrey Mainza, and Michael Moys. Optimisation of the secondary ball mill using an on-line ball and pulp load sensor – the sensomag. *Minerals Engineering*, 24:325–334, 2 2011.

[90] Hyun Na Kim, Jin Woo Kim, Min Sik Kim, Bum Han Lee, and Jin Cheul Kim. Effects of ball size on the grinding behavior of talc using a high-energy ball mill. *Minerals*, 9:668, 10 2019.

[91] Alexander Kirillov, Eric Mintun, Nikhila Ravi, Hanzi Mao, Chloe Rolland, Laura Gustafson, Tete Xiao, Spencer Whitehead, Alexander C. Berg, Wan-Yen Lo, Piotr Dollár, and Ross Girshick. Segment anything, 2023.

[92] Seiichi Koshizuka, Atsushi Nobe, and Yoshiaki Oka. Numerical analysis of breaking waves using the moving particle semi-implicit method. *International journal for numerical methods in fluids*, 26(7):751–769, 1998.

[93] Naoya Kotake, Mitsuyuki Kuboki, Shinichi Kiya, and Yoshiteru Kanda. Influence of dry and wet grinding conditions on fineness and shape of particle size distribution of product in a ball mill. *Advanced Powder Technology*, 22:86–92, 1 2011.

[94] Harald Kruggel-Emden, Erdem Simsek, Stefan Rickelt, Siegmar Wirtz, and Viktor Scherer. Review and extension of normal force models for the discrete element method. *Powder Technology*, 171(3):157–173, 2007.

[95] Goro Kuwabara and Kimitoshi Kono. Restitution coefficient in a collision between two spheres. *Japanese journal of applied physics*, 26(8R):1230, 1987.

[96] El Mahdi Lakhdissi, Afshin Fallahi, Christophe Guy, and Jamal Chaouki. Effect of solid particles on the volumetric gas liquid mass transfer coefficient in slurry bubble column reactors. *Chemical Engineering Science*, 227:115912, 2020.

[97] Hansol Lee, Kwanho Kim, and Hoon Lee. Analysis of grinding kinetics in a laboratory ball mill using population-balance-model and discrete-element-method. *Advanced Powder Technology*, 30:2517–2526, 11 2019.

[98] B. Leimkuhler and C. Matthews. *Introduction*, pages 1–51. Springer, 2015.

[99] M Lemieux, G Léonard, Jocelyn Doucet, L-A Leclaire, F Viens, Jamal Chaouki, and François Bertrand. Large-scale numerical investigation of solids mixing in a v-blender using the discrete element method. *Powder Technology*, 181(2):205–216, 2008.

[100] Y. Li, Y. You, D. Gou, A. Yu, and R. Yang. A dem based scale-up model for tumbling ball mills. *Powder Technology*, 409, 2022.

[101] S.J. Lind, R. Xu, P.K. Stansby, and B.D. Rogers. Incompressible smoothed particle hydrodynamics for free-surface flows: A generalised diffusion-based algorithm for stability and validations for impulsive flows and propagating waves. *Journal of Computational Physics*, 231:1499–1523, 2012.

[102] M.B. Liu, G.R. Liu, and K.Y. Lam. Constructing smoothing functions in smoothed particle hydrodynamics with applications. *Journal of Computational and Applied Mathematics*, 155(2):263–284, 2003.

[103] Zhengbin Liu, Guoqiang Wang, Wei Guan, Jianbo Guo, Gang Sun, and Zeren Chen. Research on performance of a laboratory-scale sag mill based on dem-embd. *Powder Technology*, 406:117581, 7 2022.

[104] Y.M. Lo and S. Shao. Simulation of near-shore solitary wave mechanics by an incompressible sph method. *Applied Ocean Research*, 24:275–286, 2002.

[105] Shaowen Lu, Ping Zhou, Tianyou Chai, and Wei Dai. Modeling and simulation of whole ball mill grinding plant for integrated control. *IEEE Transactions on Automation Science and Engineering*, 11:1004–1019, 10 2014.

[106] Weidong Lv, Guoqiang Wang, and He Tian. Electromechanical dynamic behaviour and start-up evaluation of tumbling ball mills. *Mathematical Problems in Engineering*, 2018, 2018.

[107] Alban J. Lynch and Chester A. Rowland. *Tumbling Mills*, pages 95–131. Society for Mining, Metallurgy, and Exploration, Inc. (SME), 2005.

[108] Marcela V. C. Machado, Dyrney A. Santos, Marcos A. S. Barrozo, and Claudio R. Duarte. Experimental and numerical study of grinding media flow in a ball mill. *Chemical Engineering & Technology*, 40:1835–1843, 10 2017.

[109] Augustine B. Makokha, Michael H. Moys, Murray M. Bwalya, and Kiangi Kimera. A new approach to optimising the life and performance of worn liners in ball mills: Experimental study and dem simulation. *International Journal of Mineral Processing*, 84:221–227, 10 2007.

[110] M. Maleki-Moghaddam, M. Yahyaei, and S. Banisi. Converting ag to sag mills: The gol-e-gohar iron ore company case. *Powder Technology*, 217:100–106, 2 2012.

[111] Sauro Manenti, Dong Wang, José M. Domínguez, Shaowu Li, Andrea Amicarelli, and Raffaele Albano. Sph modeling of water-related natural hazards. *Water*, 11(9), 2019.

[112] Sudarshan Martins, Wei Li, Peter Radziszewski, Sylvain Caron, Marc Aguanno, Michael Bakhos, and Emma Lee Petch. Validating the instrumented ball outputs with simple trajectories. *Minerals Engineering*, 21:782–788, 10 2008.

[113] Edward Mavhungu, Túlio M. Campos, Brena Karolyne N. Rocha, Nomonde Solomon, Carl Bergmann, Luís Marcelo Tavares, and Jens Lichter. Simulating large-diameter industrial ball mills from batch-grinding tests. *Minerals Engineering*, 206, 1 2024.

[114] K. Mayank, M. Malahe, I. Govender, and N. Mangadoddy. Coupled dem-cfd model to predict the tumbling mill dynamics. *Procedia IUTAM*, 15:139–149, 2015.

[115] J Mellmann. The transverse motion of solids in rotating cylinders—forms of motion and transition behavior. *Powder Technology*, 118:251–270, 8 2001.

[116] B.K. Mishra and Raj K. Rajamani. The discrete element method for the simulation of ball mills. *Applied Mathematical Modelling*, 16:598–604, 11 1992.

[117] Aman Mittal, Mayank Kumar, and Narasimha Mangadoddy. A coupled cfd–dem model for tumbling mill dynamics—effect of lifter profile. *Powder Technology*, 433, 1 2024.

[118] S.R. Carberry Mogan, D. Chen, J.W. Hartwig, I. Sahin, and A. Tafuni. Hydrodynamic analysis and optimization of the titan submarine via the sph and finite–volume methods. *Computers & Fluids*, 174:271–282, 2018.

[119] Satish Mohanty, Karunesh K. Gupta, and Kota Solomon Raju. Vibration feature extraction and analysis of industrial ball mill using mems accelerometer sensor and synchronized data analysis technique. *Procedia Computer Science*, 58:217–224, 2015.

[120] D. Molteni and A. Colagrossi. A simple procedure to improve the pressure evaluation in hydrodynamic context using the sph. *Computer Physics Communications*, 180:861–872, 2009.

[121] J. Monaghan and R. Gingold. Shock simulation by the particle method sph. *Journal of Computational Physics*, 52:374–389, 1983.

[122] J. J. Monaghan. Smoothed particle hydrodynamics. *Annual Review of Astronomy and Astrophysics*, 30(1):543–574, 1992.

[123] J.J. Monaghan. Simulating free surface flows with sph. *Journal of Computational Physics*, 110:399–406, 1994.

[124] J.J. Monaghan. Smoothed particle hydrodynamics. *Reports on Progress in Physics*, 68:1703–1759, 2005.

[125] J.J. Monaghan and A. Kos. Solitary waves on a cretan beach. *Journal of Waterway, Port, Coastal, and Ocean Engineering*, 125:145–155, 1999.

[126] Farhad Moosakazemi, M.R. Tavakoli Mohammadi, M. Mohseni, M. Karamoozian, and M. Zakeri. Effect of design and operational parameters on particle morphology in ball mills. *International Journal of Mineral Processing*, 165:41–49, 8 2017.

[127] S. Morrell. Modelling the influence on power draw of the slurry phase in autogenous (ag), semi-autogenous (sag) and ball mills. *Minerals Engineering*, 89:148–156, 4 2016.

[128] A. J. Morrison, I. Govender, A. N. Mainza, and D. J. Parker. The shape and behaviour of a granular bed in a rotating drum using eulerian flow fields obtained from pept. *Chemical Engineering Science*, 152:186–198, 10 2016.

[129] Nontawat Muanpaopong, Rajesh Davé, and Ecevit Bilgili. A comparative analysis of steel and alumina balls in fine milling of cement clinker via pbm and dem. *Powder Technology*, page 118454, 5 2023.

[130] François K. Mulenga. Sensitivity analysis of austin's scale-up model for tumbling ball mills — part 2. effects of full-scale milling parameters. *Powder Technology*, 317:6–12, 7 2017.

[131] François K. Mulenga and Ngonidzashe Chimwani. Introduction to the use of the attainable region method in determining the optimal residence time of a ball mill. *International Journal of Mineral Processing*, 125:39–50, 12 2013.

[132] François K. Mulenga and Michael H. Moys. Effects of slurry filling and mill speed on the net power draw of a tumbling ball mill. *Minerals Engineering*, 56:45–56, 2 2014.

[133] Dilip Kumar Nayak, Debi Prasad Das, Santosh Kumar Behera, and Sarada Prasad Das. Monitoring the fill level of a ball mill using vibration sensing and artificial neural network. *Neural Computing and Applications*, 32:1501–1511, 3 2020.

[134] S.M Olhero and J.M.F Ferreira. Influence of particle size distribution on rheology and particle packing of silica-based suspensions. *Powder Technology*, 139(1):69–75, 2004.

[135] Phil Owen and Paul W. Cleary. The relationship between charge shape characteristics and fill level and lifter height for a sag mill. *Minerals Engineering*, 83:19–32, 11 2015.

[136] Kwaku Boateng Owusu, Massimiliano Zanin, William Skinner, and Richmond K. Asamoah. Ag/sag mill acoustic emissions characterisation under different operating conditions. *Minerals Engineering*, 171, 9 2021.

[137] R. Panjipour and K. Barani. The effect of ball size distribution on power draw, charge motion and breakage mechanism of tumbling ball mill by discrete element method (dem) simulation. *Physicochemical Problems of Mineral Processing*, 54:258–269, 2018.

[138] A.N. Parshikov, S.A. Medin, I.I. Loukashenko, and V.A. Milekhin. Improvements in sph method by means of interparticle contact algorithm and analysis of perforation tests at moderate projectile velocities. *International Journal of Impact Engineering*, 24:779–796, 2000.

[139] Francisco Pedrayes, Joaquín G. Norniella, Manuel G. Melero, Juan M. Menéndez-Aguado, and Juan J. del Coz-Díaz. Frequency domain characterization of torque in tumbling ball mills using dem modelling: Application to filling level monitoring. *Powder Technology*, 323:433–444, 1 2018.

[140] Yuxing Peng, Tongqing Li, Zhencai Zhu, Shengyong Zou, and Zixin Yin. Discrete element method simulations of load behavior with mono-sized iron ore particles in a ball mill. *Advances in Mechanical Engineering*, 9:168781401770559, 5 2017.

[141] Malcolm Powell, Ian Emit, Peter Radziszewski, Paul Cleary, Bruce Rattray, Klas Erikssont, Goran, and Leon Schaeffer. Selection and design of mill liners. In *2006 SME Annual Conference - Advances in Comminution*, pages 331–376. Society for Mining, metallurgy, and exploration, Inc., 2006.

[142] M.S. Powell, N.S. Weerasekara, S. Cole, R.D. LaRoche, and J. Favier. Dem modelling of liner evolution and its influence on grinding rate in ball mills. *Minerals Engineering*, 24:341–351, 2 2011.

[143] Daniel J Price. Modelling discontinuities and kelvin–helmholtz instabilities in sph. *Journal of Computational Physics*, 227(24):10040–10057, 2008.

[144] Alberto M. Puga, Nicolin Govender, and Raj K. Rajamani. Verification of polyhedral dem with laboratory grinding mill experiments†. *KONA Powder and Particle Journal*, 39:208–218, 2022.

[145] Jose Venegas Pulgar, M. Anibal Valenzuela, and Cristian Molina Vicuna. Correlation between power and lifters forces in grinding mills. *IEEE Transactions on Industry Applications*, 55:4417–4427, 7 2019.

[146] P. Radziszewski and S. Tarasiewicz. Simulation of ball charge and liner wear. *Wear*, 169:77–85, 10 1993.

[147] Peter Radziszewski. Predictive model for ball mill wear. *Canadian Metallurgical Quarterly*, 36:87–93, 4 1997.

[148] Sripriya Rajendran, Teja Reddy Vakamalla, and Narasimha Mangadoddy. *Numerical methods in mineral processing: an overview*, pages 251–285. Elsevier, 1 2023.

[149] M. Rezaeizadeh, M. Fooladi, M.S. Powell, and S.H. Mansouri. Experimental observations of lifter parameters and mill operation on power draw and liner impact loading. *Minerals Engineering*, 23:1182–1191, 12 2010.

[150] M.J. Robinson. *Turbulence and viscous mixing using smoothed particle hydrodynamics*. PhD thesis, Monash University, Clayton, 2010.

[151] MC Roco and CA Shook. Modeling of slurry flow: The effect of particle size. *The Canadian Journal of Chemical Engineering*, 61(4):494–503, 1983.

[152] Victor A. Rodriguez, Rodrigo M. de Carvalho, and Luís Marcelo Tavares. Insights into advanced ball mill modelling through discrete element simulations. *Minerals Engineering*, 127:48–60, 10 2018.

[153] Takayuki R Saitoh and Junichiro Makino. A density-independent formulation of smoothed particle hydrodynamics. *The Astrophysical Journal*, 768(1):44, 2013.

[154] P.K. Senapati, B.K. Mishra, and A. Parida. Modeling of viscosity for power plant ash slurry at higher concentrations: Effect of solids volume fraction, particle size and hydrodynamic interactions. *Powder Technology*, 197(1):1–8, 2010.

[155] Pradipta Kumar Senapati, Dibakar Panda, Ashutosh Parida, et al. Predicting viscosity of limestone–water slurry. *Journal of minerals and materials characterization and Engineering*, 8(03):203, 2009.

[156] M.S. Shadloo, G. Oger, and D. Le Touzé. Smoothed particle hydrodynamics method for fluid flows, towards industrial applications: Motivations, current state, and challenges. *Computers & Fluids*, 136:11–34, 2016.

[157] Fengnian Shi and Weiguo Xie. A specific energy-based ball mill model: From batch grinding to continuous operation. *Minerals Engineering*, 86:66–74, 2 2016.

[158] Frank Shi. Grinding mills. In Barry A. Wills and Tim J. Napier-Munn, editors, *Mineral Processing Technology An Introduction to the Practical Aspects of Ore Treatment and Mineral*, pages 146–185. Elsevier Science & Technology Books, 7th edition, 10 2006.

[159] Hyunho Shin, Sangwook Lee, Hyun Suk Jung, and Jong-Bong Kim. Effect of ball size and powder loading on the milling efficiency of a laboratory-scale wet ball mill. *Ceramics International*, 39:8963–8968, 12 2013.

[160] M.D. Sinnott, P.W. Cleary, and R.D. Morrison. Combined dem and sph simulation of overflow ball mill discharge and trommel flow. *Minerals Engineering*, 108:93–108, 7 2017.

[161] A. Skillen, S. Lind, P.K. Stansby, and B.D. Rogers. Incompressible smoothed particle hydrodynamics (sph) with reduced temporal noise and generalised fickian smoothing applied to body–water slam and efficient wave–body interaction. *Computer Methods in Applied Mechanics and Engineering*, 265:163–173, 2013.

[162] M. M. Soleymani, M. Fooladi, and M. Rezaeizadeh. Effect of slurry pool formation on the load orientation, power draw, and impact force in tumbling mills. *Powder Technology*, 287:160–168, 1 2016.

[163] Rahul K. Soni and B. K. Mishra. *Understanding Size Segregation in Tumbling Mills*, volume 188, pages 1153–1168. Springer Science and Business Media, LLC, 2017.

[164] J. Tang, T. Chai, W. Yu, Z. Liu, and X. Zhou. A comparative study that measures ball mill load parameters through different single-scale and multiscale frequency spectra-based approaches. *IEEE Transactions on Industrial Informatics*, 12:2008–2019, 2016.

[165] Jian Tang, Tianyou Chai, Wen Yu, and Lijie Zhao. Feature extraction and selection based on vibration spectrum with application to estimating the load parameters of ball mill in grinding process. *Control Engineering Practice*, 20:991–1004, 10 2012.

[166] Jian Tang, Tianyou Chai, Wen Yu, and Lijie Zhao. Modeling load parameters of ball mill in grinding process based on selective ensemble multisensor information. *IEEE Transactions on Automation Science and Engineering*, 10:726–740, 7 2013.

[167] Jian Tang, Tianyou Chai, Lijie Zhao, Wen Yu, and Heng Yue. Soft sensor for parameters of mill load based on multi-spectral segments pls sub-models and on-line adaptive weighted fusion algorithm. *Neurocomputing*, 78:38–47, 2 2012.

[168] Jian Tang, Junfei Qiao, Zhuo Liu, Xiaojie Zhou, Gang Yu, and Jianjun Zhao. Mechanism characteristic analysis and soft measuring method review for ball mill load based on mechanical vibration and acoustic signals in the grinding process. *Minerals Engineering*, 128:294–311, 11 2018.

[169] Jian Tang, Gaowei Yan, Zhuo Liu, Yefeng Liu, Gang Yu, and Ning Sheng. Experimental analysis of wet mill load parameter based on multiple channel mechanical signals under multiple grinding conditions. *Minerals Engineering*, 159, 12 2020.

[170] Jian Tang, Wen Yu, Tianyou Chai, Zhuo Liu, and Xiaojie Zhou. Selective ensemble modeling load parameters of ball mill based on multi-scale frequency spectral features and sphere criterion. *Mechanical Systems and Signal Processing*, 66-67:485–504, 1 2016.

[171] Kent T. Tano, Bertil I. Pålsson, and Anders Sellgren. On-line lifter deflection measurements showing flow resistance effects in grinding mills. *Minerals Engineering*, 18:1077–1085, 9 2005.

[172] L.M. Tavares. A review of advanced ball mill modelling. *KONA Powder and Particle Journal*, 2017:106–124, 2017.

[173] Desmond Tromans. Mineral comminution: Energy efficiency considerations. *Minerals Engineering*, 21:613–620, 7 2008.

[174] TADEUSZ Tumidajski, EWELINA Kasińska-Pilut, TOMASZ Gawenda, ZDZISŁAW Naziemiec, and RADOSŁAW Pilut. Badania energochłonności procesu mielenia oraz podatności na rozdrabnianie składników litologicznych polskich rud miedzi. *Gospodarka Surowcami Mineralnymi*, 26:61–72, 2010.

[175] L. Verlet. Computer 'experiments' on classical fluids. i. thermodynamical properties of lennard-jones molecules. *Physical Review*, 159:98–103, 1967.

[176] D. Vetsch. *Numerical simulation of sediment transport with meshfree methods*. PhD thesis, ETH Zurich, 2011.

[177] D. Violeau. *Fluid mechanics and the SPH method*. Oxford University Press, Oxford, 2012.

[178] D. Violeau and B.D. Rogers. Smoothed particle hydrodynamics (sph) for free-surface flows: past, present and future. *Journal of Hydraulic Research*, 54:1–26, 2016.

[179] M.H. Wang, R.Y. Yang, and A.B. Yu. Dem investigation of energy distribution and particle breakage in tumbling ball mills. *Powder Technology*, 223:83–91, 6 2012.

[180] Ting Wang, Wenjie Zou, Ruijing Xu, Huaibing Xu, Le Tao, Jianjun Zhao, and Yi He. Assessing load in ball mill using instrumented grinding media. *Minerals Engineering*, 173:107198, 11 2021.

[181] N. S. Weerasekara, M. S. Powell, P. W. Cleary, L. M. Tavares, M. Evertsson, R. D. Morrison, J. Quist, and R. M. Carvalho. The contribution of dem to the science of comminution, 2013.

[182] H. Wendland. Piecewise polynomial, positive definite and compactly supported radial functions of minimal degree. *Advances in Computational Mathematics*, 4:389–396, 1995.

[183] Changhua Xie, Yuan Zhao, Tao Song, and Yongzhi Zhao. Investigation of the effect of filling level on the wear and vibration of a sag mill by dem. *Particuology*, 63:24–34, 4 2022.

[184] Yu xing Peng, Xu Ni, Zhen cai Zhu, Zhang fa Yu, Zi xin Yin, Tong qing Li, Song yong Liu, La la Zhao, and Jie Xu. Friction and wear of liner and grinding ball in iron ore ball mill. *Tribology International*, 115:506–517, 11 2017.

[185] Lei Xu, Kun Luo, and Yongzhi Zhao. Numerical prediction of wear in sag mills based on dem simulations. *Powder Technology*, 329:353–363, 4 2018.

[186] Lei Xu, Kun Luo, Yongzhi Zhao, Jianren Fan, and Kefa Cen. Influence of particle shape on liner wear in tumbling mills: A dem study. *Powder Technology*, 350:26–35, 5 2019.

[187] Zixin Yin, Yuxing Peng, Zhencai Zhu, Chenbo Ma, Zhangfa Yu, and Guiyi Wu. Effect of mill speed and slurry filling on the charge dynamics by an instrumented ball. *Advanced Powder Technology*, 30:1611–1616, 8 2019.

[188] Zixin Yin, Nan Wang, Tongqing Li, and Yuxing Peng. Experimental investigation of the impact breakage characteristics between grinding media and iron ore particle in ball mills. *Advanced Powder Technology*, 34, 4 2023.

[189] T. Yoshida, F. Kuratani, T. Ito, and K. Taniguchi. Vibration characteristics of an operating ball mill. *Journal of Physics: Conference Series*, 1264, 7 2019.

[190] Jianwen Yu, Yonghong Qin, Peng Gao, Yuexin Han, and Yanjun Li. An innovative approach for determining the grinding media system of ball mill based on grinding kinetics and linear superposition principle. *Powder Technology*, 378:172–181, 1 2021.

[191] F. Zhang, A. Crespo, C. Altomare, et al. Dualsphysics: a numerical tool to simulate real breakwaters. *Journal of Hydrodynamics*, 30:95–105, 2018.

[192] Jie Zhang, Hui Zhao, Chunyu Wang, Weifeng Li, Jianliang Xu, and Haifeng Liu. The influence of pre-absorbing water in coal on the viscosity of coal water slurry. *Fuel*, 177:19–27, 2016.

[193] Xinyu Zhang and Goodarz Ahmadi. Eulerian–lagrangian simulations of liquid–gas–solid flows in three-phase slurry reactors. *Chemical Engineering Science*, 60(18):5089–5104, 2005.

[194] Bilge Öksüzoğlu and Metin Uçurum. An experimental study on the ultra-fine grinding of gypsum ore in a dry ball mill. *Powder Technology*, 291:186–192, 4 2016.